Beamforming for OFDM based Hybrid Terrestrial-Satellite Mobile System

Ammar Hussain Khan

Submitted for the Degree of
Doctor of Philosophy
from the
University of Surrey

Centre for Communication Systems Research
Faculty of Engineering and Physical Sciences
University of Surrey
Guildford, Surrey GU2 7XH, U.K.

January 2011

Abstract

The thesis research concerns an integrated framework of terrestrial and satellite networks based on Orthogonal Frequency Division Multiple Access (OFDM) air interface which we call Hybrid Terrestrial-Satellite Mobile System (HTSMS). HTSMS which enables frequency reuse amongst the two networks serves users in urban areas via terrestrial Base Stations whilst satellite links provide service in rural areas in a transparent and seamless manner. The thesis focuses on mitigation of Co-Channel Interference on the uplink of the satellite using Least Mean Squares beamforming onboard the satellite.

We propose a preamble transmission strategy based on pilot re-allocation for superior Co-Channel Interference mitigation, specific to HTSMS. Within the preamble framework, we further propose Fully-Dense Preamble, Partially-Dense Preamble and Reduced-Length Preamble as possible schemes and analyse their performance as compared to receiver side alternatives such as Variable Step Size-Least Mean Squares and Normalised-Least Mean Squares beamforming. Results show that the approach not only gives superior convergence but it enables better system performance with less pilot transmissions.

Exploiting the susceptibility of the beamforming process to pilots, we further propose Novel Iterative Turbo Beamforming for the HTSMS with a Bit Interleaved Coded Modulation-OFDM. The proposed technique is based on improving *a priori* information of the soft decoded data and uses both soft data and pilots to perform adaptive beamforming in a turbo-like recursive manner. Results show that proposed approach exhibits significant bit error rate gains with only 1 iteration.

Finally, to reduce the associated complexity of onboard beamforming, we first quantify performance advantages of adaptive beamforming against non-adaptive. For the non-adaptive case, we propose onboard based semi-static beamforming where the required beam orientation computed at the ground is transmitted to the satellite at which beamforming weights are calculated. The proposed mechanism is a practical and attractive alternative to existing non-adaptive beamforming approaches, especially for satellite systems offering broadcasting/fixed services. On comparison, results show that adaptive beamforming is superior, however semi-static has comparable performance in specific scenarios. In light of this, we propose a novel-semi adaptive beamformer. The proposed technique is a switch-type beamforming, where a novel switching mechanism enables adaptive and non-adaptive processing to coexist. The algorithm is also robust to both spurious switching as well as other disturbances in the system. For HTSMS, results show that semi-adaptive beamformer can save up to 98% of the filtering computing power without degradation to system performance.

Key words: OFDM, Beamforming, Hybrid Terrestrial-Satellite Mobile System.

Email: A.H.Khan@surrey.ac.uk

WWW: http://www.ee.surrey.ac.uk/profiles?s_id=3083

۷۸۶-۱۱۰

Dedicated to my parents

فرحت حسین خان ، مسرت رباب

to my siblings

مقدَاد حسین خان ، جزَاء زینب ، شھوَار حسین

and to my lovely wife

مومنہ عمار

Declaration of Originality

I hereby declare that the research recorded in this thesis and the thesis itself was composed and originated by myself in the Centre for Communication Systems Research (CCSR), University of Surrey UK.

Acknowledgements

First of all, I am grateful to my Creator who made me capable of thinking and acquiring knowledge.

I find myself highly obliged to my supervisor, Professor Barry Evans for providing me with an opportunity to work under his kind supervision. Indeed his generous guidance, support and vision has played a pivotal role towards the formation of this thesis. It was a life time experience and a great honour to work with him.

I am also highly indebted to Dr. Muhammad Ali Imran for his continuous technical guidance, encouragement, support and for being an excellent critic. His cooperation at all times has been really inspirational and motivating. He always had a very tight schedule but somehow always managed to find ample time for me. I wish him all the happiness and success in his life.

I am also thankful to the Centre for Communication Systems Research (CCSR) and Overseas Research Studentship Award Scheme for supporting me financially during the course of work.

I also owe a great deal of gratitude to National University of Sciences and Technology, Pakistan for providing me the opportunity to study at the University of Surrey. I also want to take this opportunity to pay my regards to all the faculty at College of Aeronautical Engineering (CAE), Pakistan where I did my undergraduate. CAE is where it all started and indeed it was instructors like Professor Ahmad Ejaz Nadeem and Associate Professor Tahir Butt who inspired me to work and peruse a PhD degree. Also would like to thank my batch mates in G-61 course for being wondrous and supportive throughout the course of my degree.

All my colleagues and friends at CCSR who provided me with an opportunity to learn in a highly intellectual environment and provided an opportunity to discuss problems and derive motivation. Specifically, bundle of thanks to my colleague Ali

Imran for being an excellent critic of my work and providing me ample guidance and time. He has been a great friend on as well as off the campus.

I am also grateful to centre administrator Liz James, Alison and Safay Sway for the continuous support and help in administration issues. Especially Liz and Alison who I admire due to their work and I would always feel their absence.

I am also very grateful to a very close and dear friend Farrukh Soofian Ahmed for being my moral boaster at all stages. He has been alongside me since we did our Masters together at the University of Surrey. Also a big thanks to Muhammad Ali for being a wonderful and supportive friend. I would always miss his company over lunch which was a consistent feature throughout my PhD.

I will always fall short of words to thank my parents and my family in Pakistan for their prayers and support without which I would not have made it to this point. They endured a long separation from me and let me complete my work and they are the reason why I am what I am.

And last but definitely not the least, my lovely wife who was affected the most by my decision to pursue this path. I duly acknowledge her patience at times when I had to concentrate on my work and she suffered loneliness.

Contents

List of Figures

List of Tables

Nomenclature

General Notation

$\bar{a}$	Mean of a
$\hat{a}$	Estimate of a
$\mathbf{a}$	Vector $\mathbf{a}$
a	Scalar a
$[\mathbf{A}]_{n,m}$	n^{th} row and m^{th} column of matrix $\mathbf{A}$
$\mathbf{A}$	$\mathbf{A}$ in the time-domain
$\widetilde{\mathbf{A}}$	$\mathbf{A}$ in the frequency-domain
$\approx$	Approximately equal to
$\mathrm{diag}\{\cdot\}$	Diagonal of a matrix with 0's at all off-diagonal entries
exp	Exponential function
$\mathrm{E}\{a\}$	Expectancy of a
filt	Interpolation filter
$(\cdot)^H$	Hermitian transpose operator
tanh	Hyperbolic tangent function
lim	Limit operator
ln	Natural logarithmic
log	Logarithmic

$\| A \|$	Length of A
$\vert A \vert$	Magnitude of A
max	Maximum function
min	Minimum function
sin	Sine function
$\sum$	Summation operator
$(\cdot)^T$	Transpose operator
$\otimes$	Time convolution operator
tr	Trace of a matrix
Var	Variance operator

Superscripts/Subscripts

d	Desired user denotation
i	Number of iterations in ITBF
j	Indexing of mobile users in the system
J	Total mobile users in the system under consideration
κ	Indexing of decoding stages
l	OFDM symbol index
L	Window of OFDM symbols
n	Indexing of sub-carriers in an OFDM symbol
p	Denotation of information at pilots sub-carriers
q	Denotation of information at data sub-carriers
s	Indexing of antenna elements in the ULA
t	Indexing of message bits
u	u^{th} bit of a constellation set
v	v^{th} bit of a constellation set

Greek Symbols

$\Delta\varpi$	Bandwidth of each sub-carrier
Λ	Bit triggering flag
$\nabla\Psi$	Beamforming Switching Metric
$\mathcal{CN}$	Complex Noise
Δ	Delta function
θ_j	DOA of the j^{th} user
δ	Error floor in LMS
τ	Excess delay spread of the channel
Γ^κ	*extrinsic* information about the set of message bits generated by encoder κ
ϖ	Frequency of operation
∇	Slope
∞	Infinity
$\mu^{'}$	Intermediate adaptive step size in case of VSS-LMS
$\widetilde{\Gamma}^\kappa$	*intrinsic* information about the set of message bits generated by encoder κ
ρ	Length of MMW
μ_{max}	Maximum step size possible for LMS
μ_{min}	Minimum step size for LMS
ω	Mean Squared Error for the LMS
τ_{mac}	Maximum delay spread of the channel
ζ^κ	Noisy parity-check bits generated by encoder κ
π	Pi
ϱ	PRBS sequence
ε	Random error in LMS
$\mathcal{I}$	Set representing pilot sub-carrier locations
μ	Step size in case of FSS-LMS

Ω	Variance of the mean of $\nabla\Psi$
Ψ	Variance of the MSE for the LMS
$\acute{\delta}$	Variance floor due to disturbance in the system
σ^2	Variance of complex Gaussian noise
α	VSS-LMS forgetting factor
γ	VSS-LMS instantaneous contributing factor
λ	Wavelength of the carrier

Roman Symbols

$[\mathbf{A}]_{s,j}$	ULA response of the s^{th} antenna element for the j^{th} user
B	Bandwidth
B_c	Coherence bandwidth of the channel
$[\mathbf{B}]_{s,n}$	Complex Gaussian noise at the s^{th} antenna element and n^{th} sub-carrier
$\mathbf{c}$	Interleaved bits
d	Desired user signal
d_a	Inter-element spacing in the ULA
$\widetilde{\mathbf{e}}$	Error between transmitted and received pilot sequence in the frequency-domain
$\mathbf{e}$	Error vector in the time-domain
$e[k]$	Instantaneous error at time instant k
f	Number of consecutive MMWs combined to form a MMB
$\mathbf{F}$	FFT matrix
g	Number of OFDM symbols by which MMB slides
g_m	Rectangular pulse shaping
G	Length of Cyclic Prefix
$\widetilde{\mathbf{h}}^p$	Channel estimates at pilot sub-carriers
$\mathbf{h}$	Time-domain representation of channel

$\widetilde{\mathbf{h}}$	Channel estimates at all the sub-carriers
k	Indexing of time
K	Total symbol duration
K_s	Presentation of delays in each of the element
K_{GI}	Duration of Guard Interval
l	Indexing of OFDM symbols
$\widetilde{L}$	The number of initial OFDM symbols not considered in BER computation
L	Total OFDM symbols transmitted
L_{min}	Minimum number of OFDM symbol for which adaptive BF will take place
L_s	OFDM symbol number when BSM triggers a switch
$L^{'}$	Preamble length in terms of OFDM symbols
M	Multiplication Operations
n	Indexing of sub-carriers in an OFDM symbol
N	Total sub-carriers in an OFDM symbol
N_p	Total number of pilots in conventional OFDM transmitter
$N_{p'}$	Total number of pilots in an OFDM symbol transmitted during DP of proposed preamble based beamformer
N_{pp}	Total number of pilots in an OFDM symbol transmitted during PP of proposed preamble based beamformer
$\mathbf{o}$	Information bits transmitted
P	Addition Operations
$\widetilde{\mathbf{r}}$	OFDM symbol at the input of QPSK demapper
$\mathbf{R}$	Covariance matrix
s	Indexing of antenna elements in the ULA at the receiver side
S	Total number of antenna elements in the ULA

$\mathbf{t}$	Encoded bits
U^{+}	Constellation set constituting of 1's
U^{-}	Constellation set constituting of 0's
$[\mathbf{V}]_{s,n}$	Array output at the s^{th} antenna element of the ULA and n^{th} sub-carrier
$\mathbf{w}$	Applied complex BF weights/coefficients at the receiver
$\bar{\mathbf{x}}_j$	Time-domain OFDM signal of the j^{th} user after CP insertion at the transmitter side
$\widetilde{\mathbf{x}}_j$	Frequency-domain OFDM symbol the j^{th} user at the transmitter side
$\widehat{\widetilde{\mathbf{x}}}$	Estimates of the desired user transmitted sequence
$\widetilde{\mathbf{x}}_j^p$	Pilots corresponding to the j^{th} user at the transmitter side
$\widetilde{\mathbf{x}}_j^q$	Modulated data sequence corresponding to the j^{th} user
$\mathbf{x}_j$	Time-domain OFDM signal of the j^{th} user
$\bar{\mathbf{y}}_j[k]$	Transmitted OFDM signal of the j^{th} user
$[\mathbf{Y}]_{s,j}$	Received signal at s^{th} antenna element of the ULA for the j^{th} user
$\widetilde{\mathbf{z}}$	Frequency-domain weighted output of the beamformer
$\mathbf{z}$	Time-domain weighted output of the beamformer

Units

dB	Decibel
dBW	Decibel Watt
GHz	Gigahertz
kbps	Kilo bits per second
km	Kilometer
km/hr	Kilometer per hour
μ	Microsecond
MHz	Megahertz

ns	Nanosecond

Acronyms

3GPP	3rd Generation Partnership Project
4G	4th Generation
AIAA	American Institute of Aeronautics and Astronautics
APP	*a posteriori* probability
ATC	Ancillary Terrestrial Component
AWGN	Additive White Gaussian Noise
BCC	Beamforming Coefficient Calculator
BER	Bit Error Rate
BERG	Bit Error Rate Gain
BF	Beamforming
BFG	Beamforming Gain
BICM	Bit Interleaved Coded Modulation
BLAST	Bell Labs Layered Space-Time
BSM	Beamforming Switching Metric
BTF	Beamforming Triggering Flag
BTS	Base Station
CE_f	Combined Error in the frequency-domain for the case of ITBF
CBFW	Cumulative Beamforming Weights
CCI	Co-Channel Interference
CDMA	Code Division Multiple Access
CE	Channel Estimation
CGC	Complimentary Ground Component
CMA	Constant Modulus Algorithm
CMSE	Cumulative Mean Squared Error

CP	Cyclic Prefix
DFT	Discrete Fourier Transform
DOA	Direction-of-Arrival
DP	Data Phase
DVB	Digital Video Broadcasting
DVB-SH	Digital Video Broadcasting - Satellite to Handheld
E_b/N_o	Energy per bit to noise power spectral density ratio
EU	European Union
FDM	Frequency Division Multiplexing
FDP	Fully-Dense Preamble
FFT	Fast Fourier Transform
FIR	Finite Impulse-Response
FS	False Switching
FSS-LMS	Fixed Step Size - Least Mean Squares
GBBF	Ground Based Beamforming
GBBF-A	Ground Based Beamforming-Adaptive
GBBF-S	Ground Based Beamforming-Static
GEO	Geostationary
GI	Guard Interval
GT	Guard Time
HTSMS	Hybrid Terrestrial-Satellite Mobile System
i.i.d.	independent and identically Distributed
IBS	Iterative Beamforming Stage
ICI	Inter Carrier Interference
IDFT	Inverse Discrete Fourier Transform
IEEE	Institute of Electrical & Electronics Engineers

IFFT	Inverse Fast Fourier Transform
IMT	International Mobile Telecommunications
Inmarsat	International Maritime Satellite
ISI	Inter Symbol Interference
ITBF	Iterative Turbo Beamformer
LLR	Log-Likelihood Ratio
LMS	Least Mean Squares
LS	Least Squares
LTE	Long Term Evolution
MAESTRO	Mobile Applications & sErvices based on Satellite & Terrestrial inteRwOrking
MAP	*maximum a posteriori* probability
MIMO	Multiple Input Multiple Output
MMB	Moving Monitoring Block
MMW	Moving Monitoring Window
MSB	Multi-Stage Beamformer
MSE	Mean Squared Error
MSS	Mobile Satellite Service
MSV	Mobile Satellite Ventures
MW	Monitoring Window
NLMS	Normalised - Least Mean Squares
OBBF	Onboard Based Beamforming
OBBF-A	Onboard Based Beamforming-Adaptive
OBBF-ERC	Onboard Based Beamforming-Equal Ratio Combining
OBBF-SA	Onboard Based Beamforming-Semi Adaptive
OBBF-SS	Onboard Based Beamforming-Semi Static

OFDM	Orthogonal Frequency Division Multiple Access
P/S	Parallel-to-Serial
PDP	Partially-Dense Preamble
PG	Precision Gain
PP	Preamble Phase
QPSK	Quadrature Phase Shift Keying
RBFW	Real-time Beamforming Weights
RBS	Rudimentary Beamforming Stage
RLP	Reduced-Length Preamble
RLS	Recursive Least Squares
S/P	Serial-to-Parallel
SIMO	Single Input Multiple Output
SINR	Signal-to-Interference plus Noise Ratio
SISO	Soft-Input Soft-Output
SMI	Sample Matrix Inversion
SNR	Signal-to-Noise Ratio
STICS	Satellite/Terrestrial Integrated mobile Communication System
TBS	Termination Beamforming Stage
TR	Terrestrial Repeater
ULA	Uniform Linear Array
UMTS	Universal Mobile Telecommunications System
VSS-LMS	Variable Step Size - Least Mean Squares
WCDMA	Wideband Code Division Multiple Access
WiMAX	Worldwide Interoperability for Microwave Access
WLAN	Wireless Local Area Network

Chapter 1

Introduction

1.1 Background

Wireless communications has seen enormous growth over the past decade or so. The huge take up of mobile technology and exponential growth of the internet has resulted in an increased demand for high capacity wireless systems. This has lead to the evolution of 4G [1] networks which will employ Orthogonal Frequency Division Multiplexing (OFDM) [2] at the physical layer. Similarly in parallel, Multiple Input Multiple Output (MIMO) [3–5] technology has emerged as the most significant breakthrough in modern communication providing higher capacity by utilising multiple antenna arrangements at both the transmitter and receiver side. The combination of OFDM with advanced antenna systems thus forms an intuitive and formidable solution towards higher capacity communication systems and has already been adopted by standards such as 3GPP-LTE, LTE Advanced and IEEE802.11a/g/n WLAN.

Success of a communication network does not only depend on provisioning of high data rates, but also on the coverage it can offer. Future networks also need to incorporate global connectivity to ensure a rich customer base. Standalone, existing terrestrial mobile networks are unable to provide such coverage due to lack of infrastructure in rural areas. This is where satellite networks are favoured as they have the potential to offer true global coverage as well as rapid network deployment. However satellite links suffer from reduced signal penetration and capacity/coverage issues in urban areas as well as at lower elevation angles.

The respective disadvantages of satellite and terrestrial networks motivates the existence of hybrid architectures. In pursuit of global coverage, the Digital Video Broadcasting (DVB) group has developed a standard called DVB-SH for delivery of mobile TV from satellite to hand-held devices using OFDM air interface. DVB-SH is a hybrid system developed for TV broadcast service to mobile users. In rural areas, service is provided by the satellite links whereas in urban areas users are served via the Complimentary Ground Component (CGC) or Terrestrial Repeater (TR).

As similar hybrid topology has been pursued in the U.S. by SkyTerra, formerly known as Mobile Satellite Ventures (MSV) [6]. MSV proposed a hybrid architecture [7] to offer two-way communication services to rural areas via satellite links and to users in urban areas via an Ancillary Terrestrial Component (ATC). MSV employs Code Division Multiple Access (CDMA) in the physical layer combined with a multiple antenna system to enhance system performance. The MSV design is based on the concept of frequency reuse where ATCs and satellite users reuse the spectrum dedicated to each other enabling higher system capacities. However frequency reuse induces Co-Channel Interference (CCI) from the terrestrial terminals at the uplink of satellite. MSV incorporates CDMA based adaptive Beamforming (BF) [8, 9]. BF [10] is a spatial filtering technique that cancels interference by forming nulls towards interference sources while providing high gain in the desired directions.

Recently in Japan a project named Satellite/Terrestrial Integrated mobile Communication System (STICS) [11] has been proposed. It aims to integrate the satellite and existing terrestrial mobile networks to full fill the aim of global connectivity. The STICS design is also based on a frequency reuse concept similar to MSV and its choice of air interface is CDMA. However for the uplink CCI scenario, they have not considered any interference mitigation approach. Their study so far is focused towards estimation of uplink CCI induced by the terrestrial users and the use of spatial guard-bands to mitigate it [12].

Traditionally satellite systems have been used as independent service platforms with access to dedicated frequency bands. Hence interference from terrestrial users has not been an issue. The inter-satellite system interference is managed via having a minimum orbital distance between two adjacent satellite in space. Satellite systems such as Inmarsat [13] have used interference avoidance as compare to interference mitigation. However with the evolution of hybrid systems as well as two-way communication between satellite networks and Mobile Satellite System (MSS), interference mitigation on an adaptive basis becomes imperative [8]. Two-way communication systems such as ICO [14] and MSV [6] have proposed full-adaptive BF on the gateway [7, 8, 15, 16] to mitigate interference. This approach is preferable to Onboard Based Beamforming (OBBF) since there are substantial overheads associated with onboard BF networks such as hardware mass, cost, power consumption and thermal control requirements.

Despite the benefits of the ground based approach, payload complexity is a sensitive function to the number of feed elements transmitted from the satellite gateway [17] which is significantly higher in the case of Ground Based Beamforming (GBBF). Furthermore, redundant transmit and receive processing channels are required for each feed signal in order to compensate for imperfect feed characteristics. Recently hybrid BF approaches have been proposed [18, 19] that address the trade-off between ground and onboard BF. However a BF capable satellite system inherits instabilities due to payload/gateway component changes over temperature and life time, and propagation amplitude and phase dispersion effects on the gateway link. These impact significantly on the system performance and must be compensated by a complex calibration system [20]. The complexity of this system depends on where the BF is implemented with the calibration system being most complex for GBBF.

With advancement of technology as predicted by Moore's law, BF can potentially be implemented onboard the satellite by having onboard digital processing [21]. In the case of OBBF, all the processing related to forming of beams can be done onboard the satellite by using solar energy. Apart from providing more flexibility onboard the satellite, this would also result in significant reduction of power consumption at the gateway hence enabling a shift towards more eco-friendly 'green satellite' systems.

OBBF greatly reduces the number of feed elements transmitted from the satellite to the gateway which not only reduces the feeder link bandwidth requirement, but also leads to a far less complex calibration system. Moreover the onboard digital payload design gives more flexibility in the case of variation in traffic dynamics and also if beam patterns need to be changed more frequently. Illustrated in Fig. 1.1(b) is onboard, ground and hybrid BF employed to mitigate inter-cell interference at the uplink of a satellite in a MSS. Fig. 1.1(a) depicts the general trade-off between satellite payload complexity, complexity at the gateway and feed signal space (bandwidth requirement) for onboard, ground and hybrid BF.

1.2 Motivation and Scope

The MSV system proposed a hybrid architecture of satellite and terrestrial networks. However as the coverage in urban areas is provided by ATCs, it inevitably leads to additional set up and operational costs for the satellite operator. As the system fails to exploit the existing terrestrial mobile infrastructure, the frequency reuse between satellite and ATCs offers global connectivity but does not increase

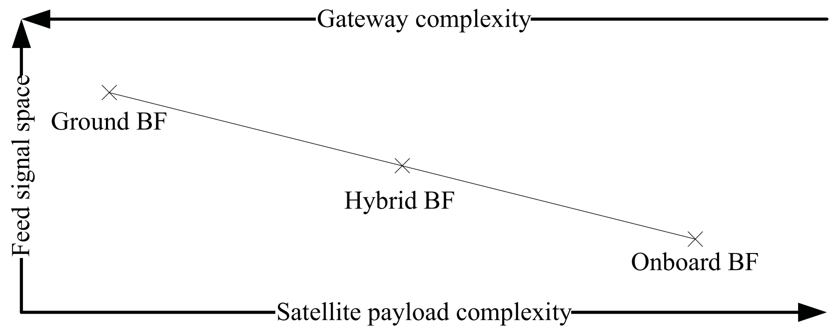

(a) Trade-off between complexity and feed signal space

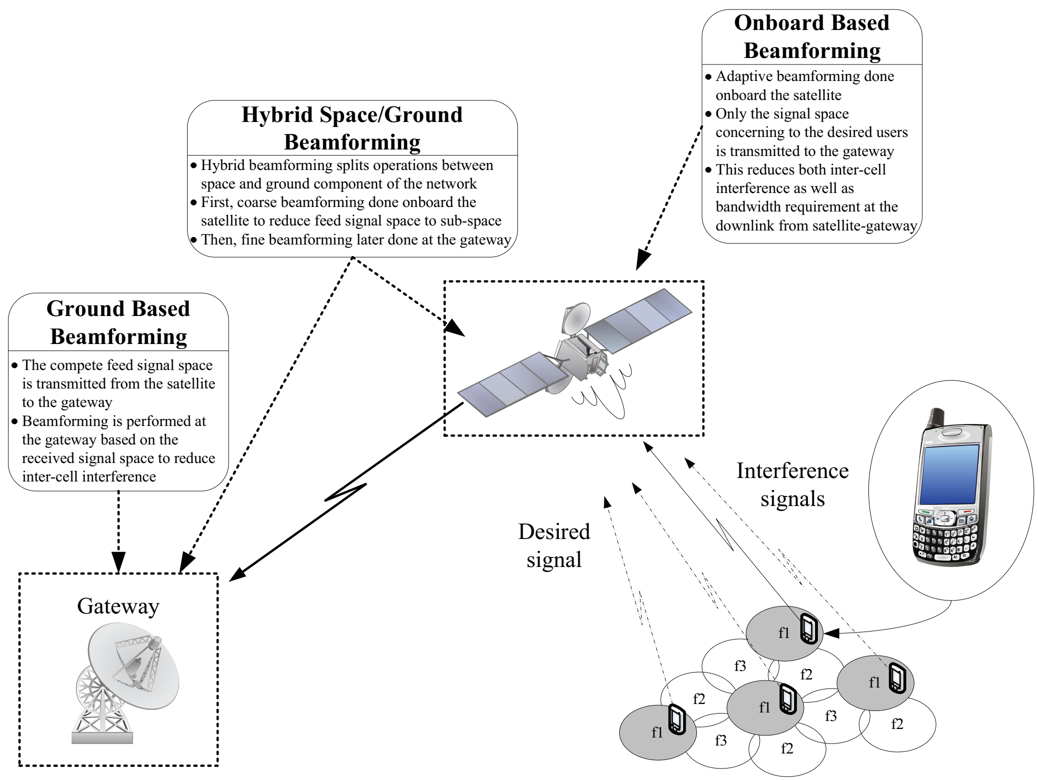

(b) Onboard, ground and hybrid beamforming in a Mobile Satellite System

Figure 1.1: Concept illustration of beamforming and complexity trade-off

the overall spectrum available. Moreover, as MSV uses a CDMA based approach it cannot function homogeneously with future 4G terrestrial networks that are based on OFDM. While DVB-SH offers an OFDM air interface, it again fails to offer an integrated platform for satellite and terrestrial networks. STICS proposes an integrated framework of service via Base Stations (BTSs) and satellite. However its architecture is again based on CDMA and hence will not be compatible with future 4G terrestrial networks.

Thus we conclude that an OFDM based hybrid architecture with complimentary service from existing terrestrial mobile BTSs and satellite links will be needed in future. A system where urban users are served via existing BTSs and rural users by satellite links and with both systems are able to reuse spectrum dedicated to each other. This would enable global coverage and rapid deployment of services via the satellite network in rural areas.

In essence just as in the MSV design, the OFDM based hybrid system will also suffer from interference. Here OFDM based BF can be employed which allows more flexibility due to the narrow band sub-carrier architecture of OFDM. Moreover, while adaptive BF for OFDM based systems has been extensively studied, its specific implications to satellite systems is yet to be explored. Moreover, where ground BF is traditionally used in satellite systems such as MSV [8] and ICO [15], research needs to be done towards OBBF for future hybrid system architectures.

In real hybrid systems, interference would be induced both at the uplink as well as the downlink. In the uplink, satellite is faced with interference while at the downlink terrestrial systems are faced with interference from satellite. However, we only consider adaptive BF for the uplink case following the MSV design [8] [1]. The downlink scenario on the other hand is very distinct to uplink scenario in

[1]MSV design only considers ground based adaptive BF for the uplink and assumes fixed beams for the downlink.

terms of BF. In the uplink, the feedback loop of the spatial filtering is "local" [2]. However for the downlink scenario, satellite would require feedback to perform BF. This effectively translates to 1-round trip delay for the satellite which is $\approx$ 500 ms. Therefore tracking in the case of downlink can not be done as fast as for the case of uplink. Having said that, adaptive BF can be utilised in the downlink to "shape" the beams and form nulls in order to reduce the interference caused to terrestrial systems. Downlink BF can optimized for the downlink as proposed in [22–24] or done jointly with uplink BF as described for instance in [25]. Due the distinct challenges for downlink BF, our work is focused towards uplink BF [3].

1.3 Objectives

Following the above motivation, we define the following objectives for this work:

- To envision and develop a hybrid architecture of satellite and terrestrial networks that is based on an OFDM air interface and employs frequency reuse.

- To investigate the applicability of BF for mitigating CCI induced by terrestrial users on the satellite uplink and its application onboard the satellite.

- To study the impact of BF convergence on system performance of a hybrid architecture and propose solutions to enhance system performance. Furthermore, investigate the interaction and interplay of BF and Channel Estimation (CE) processes and how they effect each other in the presence of a wireless channel.

[2] The reference and received signals are both available at the satellite for processing.

[3] We further discuss downlink BF in Chapter 8.

- Incorporation of Bit Interleaved Coded Modulation-OFDM (BICM-OFDM) in the hybrid architecture and work towards proposing an approach that uses both pilots as well as data for performing BF.
- Investigate the performance impact of adaptive and non-adaptive BF in a hybrid scenario. As resources are scarce onboard the satellite, hence explore the possibility of a semi-adaptive BF approach that could save on resources without significantly compromising system performance.

1.4 Major Contributions

The original achievements of the work can be summarised as follows:

- Development of an OFDM based Hybrid Terrestrial-Satellite Mobile System (HTSMS) architecture in which satellite and existing terrestrial networks integrate to provide seamless service to users. A system where users in urban areas can be served via BTSs and in rural areas to be served by satellite links. As their regions of operation are spatially separated, both systems should be able to use spectrum dedicated to each other thus enhancing the overall capacity. The hybrid topology should be transparent to the end user in the sense that similar mobile terminals would be utilised for both satellite and terrestrial coverage areas.

  Sharing of frequency induces CCI by terrestrial users and we employ Onboard Based Beamforming - Adaptive (OBBF-A) at the satellite end to mitigate the CCI. We aim to focus on the uplink scenario considering interference generated by terrestrial users to the satellite and investigate the system performance in a realistic mobile-satellite channel.
- We then investigate the impact of beamformer convergence on system performance as well as the interplay between BF and CE. We find that the

transient state of BF has significant impact on system performance. In addition we note that during BF convergence, CE is performed on pilot sub-carriers that are not interference free. To address these issues, we propose a preamble based BF approach based on pilot-reallocation at the transmitter side. Three distinctive schemes within a preamble based framework are proposed, namely Fully-Dense Preamble (FDP), Partially-Dense Preamble (PDP) and Reduced-Length Preamble (RLP). The advantage of the proposed approach are twofold 1) More reference signals are available for the BF during the convergence phase which reduces its transient state time while maintaining the overall data throughput and 2) with FDP and RLP schemes, we de-couple the BF and CE processes during the convergence phase which enhances the BF performance. To establish the advantages of a preamble based approach, its performance is compared to alternatives such as Nomalised-Least Mean Squares (NLMS) and Variable Step Size-Least Mean Squares (VSS-LMS) algorithms.

- We then introduce BICM to our OFDM based HTSMS architecture to improve system performance. From our work on preamble based approach, we found that the BF performance is extremely sensitive to OFDM pilot signals. If we increase the number of pilot sub-carriers per symbol, this would result in superior BF performance. However this would compromise the data throughput. Using the soft data from the decoding stage in conjunction with pilots, we propose a novel Iterative Turbo Beamforming (ITBF) approach. The ITBF is a distinctive three stage beamformer that works on turbo-like principles and exhibits significant gain in terms of Bit Error Rate (BER) over conventional non-iterative BF approaches.

- Shifting our focus to complexity constraint onboard the satellite, we investigate the applicability of onboard based, ground based and hybrid BF approaches. We then compare the performance of adaptive and non-adaptive

BF for the MSS scenario. For the non-adaptive case, as opposed to conventional architectures, we propose OBBF-Semi Static (OBBF-SS). OBBF-SS is based on transmission of beam orientation from the gateway to the satellite where a Beamforming Coefficient Calculator (BCC) computes BF weights which are then applied at the satellite. The BCC enables this via simple circuitry without any need of signal processing. As the process does not involve transmission of actual weights from ground to satellite, the BF becomes less prone to signal distortions as well as consuming less bandwidth. We then compare performance of OBBF-SS against OBBF-A and OBBF-Equal Ratio Combining (OBBF-ERC) approach and find the adaptive BF to be superior to others due to recursive CCI mitigation. However at lower E_b/N_o, their performances are comparable. Furthermore, as compared to existing static BF approaches, OBBF-SS offers a practical and attractive alternative to ground BF for satellite systems offering broadcast services.

- Irrespective of whether adaptive BF is implemented onboard the satellite, on the gateway or in a hybrid form, it has associated complexities and issues due to its recursive nature. Results of OBBF-SS indicate that there is some possibility for semi-adaptive solutions. In the light of this, we propose a switch-style novel semi-adaptive beamformer for the HTSMS scenario. The beamformer is based on a novel switching mechanism that is both robust to disturbance in the system as well as False Switching (FS). The novel approach enables co-existence of adaptive and non-adaptive BF approaches driven by the input signal characteristics. On comparison with full-adaptive BF in HTSMS scenario, we find the proposed algorithm enables up to 98% filter computing power reduction without any compromise in system performance.

1.5 List of Publications

The outcomes of this study have been disseminated in the form of following publications.

Journal

- A. H. Khan, M. A. Imran, B. G. Evans, “Semi-adaptive beamforming for OFDM based hybrid terrestrial-satellite mobile system,” *Wireless Communications, IEEE Transactions on,* (**proposal under review**).
- A. H. Khan, M. A. Imran, B. G. Evans, “Iterative turbo beamforming for OFDM based hybrid terrestrial-satellite mobile system,” *Communications, IET* (**proposal under review**).

Conferences

- A. H. Khan, M. A. Imran, B. G. Evans, “Ground based and onboard based beamforming for hybrid terrestrial-satellite mobile system,” in *28th ICSSC 2010 American Institute of Aeronautics and Astronautics*, California, USA, Sep. 2010.
- A. H. Khan, M. A. Imran, B. G. Evans, “Preamble based adaptive beamformer for hybrid terrestrial-satellite mobile system,” in *28th ICSSC 2010, American Institute of Aeronautics and Astronautics*, California, USA, Sep. 2010.
- A. H. Khan, M. A. Imran, B. G. Evans, “OFDM based adaptive beamforming for hybrid terrestrial-satellite mobile system with pilot reallocation,” *Satellite and Space Communications, 2009. IWSSC 2009. IEEE International Workshop on*, Siena, Italy, pp. $201-205$, Sep. 2009.

- A. H. Khan, M. A. Imran, B. G. Evans, "Adaptive beamforming for OFDM based hybrid mobile satellite system," in *27th ICSSC 2009, American Institute of Aeronautics and Astronautics*, Edinburgh, UK, April 2009.

The two contributions published in *28th ICSSC 2010, American Institute of Aeronautics and Astronautics*, California, USA, Sep. 2010 together were awarded the **Best Student Technical Paper Award** by the conference technical committee.

1.6 Thesis Organisation

The rest of this thesis is structured as follows. Chapter 2 presents the fundamental concepts of OFDM and BF. We further describe how CCI is induced in mobile communication system in both uplink and downlink scenarios and elaborate how BF can be employed to mitigate it. In Chapter 3 we present an overview of satellite systems and hybrid MSS architectures. We then present our proposed OFDM based Hybrid Terrestrial-Satellite Mobile System (HTSMS) and show how the concept of adaptive BF can be exploited to mitigate terrestrially induced CCI on the uplink of the satellite. In Chapter 4 we introduce our proposed preamble based BF with pilot reallocation at the transmitter end. Chapter 5 introduces BICM-OFDM for HTSMS and our proposed novel Iterative Turbo Beamforming (ITBF) algorithm that uses both pilots and data to perform BF. In Chapter 6 we discuss the applicability of onboard, ground and hybrid BF approaches in a MSS scenario and present our proposed OBBF-Semi Static BF approach and its performance as compared to OBBF-A. Chapter 7 presents our proposed novel semi-adaptive BF algorithm that is based on a novel switching mechanism that enables co-existence of adaptive and non-adaptive BF while maintaining robustness towards both spurious switching and noise in the system. Finally Chapter 8 concludes the thesis by summarising the major findings of the study as well as highlighting some potential areas for further research.

Chapter 2

Beamforming in OFDM based Systems

In this chapter we introduce basic concepts related to Orthogonal Frequency Division Multiplex (OFDM) and OFDM based communication systems. We further introduce interference scenarios and elaborate how Beamforming (BF) can be employed to mitigate interference in a multiple antenna system.

2.1 Introduction

Demand for high data rates has pushed researchers to develop new physical layer technologies that are both cost effective and robust. In light of this, OFDM has attracted much attention as it is robust to distortion induced by frequency selective wireless channels. Moreover, due to narrowband sub-carrier architecture, OFDM enables simpler equalisation resulting in less complex as well as cost effective receiver design. Having profound benefits over other technologies, OFDM has been adopted by many high data rate wireless communication systems and standards. In the terrestrial arena, OFDM is specified in Digital Video Broadcasting (DVB) [26] such as DVB-T and DVB-H standards for fixed and mobile digital multimedia broadcasting. OFDM has also penetrated in the internet world with technologies such as Wireless Local Area Network (WLAN) and Metropolitan Area Network (MAN) standards IEEE 802.11a/g/n, IEEE 802.16 [27]. Within the framework of mobile-telephony, OFDM is also due to replace Wideband Code Division Multiple Access (WCDMA) in the Long Term Evolution (LTE) of Universal Mobile Telecommunications System (UMTS) called 3GPP-LTE [28]. OFDM has also been employed extensively in satellite systems. Standards such as DVB-S and DVB-S2 are based on OFDM technology. For Mobile Satellite Service (MSS), DVB has developed the DVB-SH standard which is specific to video broadcasting to hand-held devises.

In the quest for higher capacity systems, development of Multiple Input Multiple Output (MIMO) systems is also without doubt one of the most significant breakthroughs of the last decade [3–5]. Having multiple antenna elements at the transmitter and/or receiver enables higher capacity and improved system performance. Hence advanced array processing and OFDM forms an intuitive and comprehensive solution towards future high capacity systems. This is already visible in standards such as Worldwide Interoperability for Microwave Access (WiMAX) [29, 30] and 3GPP-LTE that have OFDM as the choice of air-interface combined with multiple antenna systems.

All aforementioned activities are indications that OFDM will continue its domination as an air-interface option within the coming years. Moreover multiple antenna system are bound to combine with OFDM technology paving the way for higher capacity and higher performance systems.

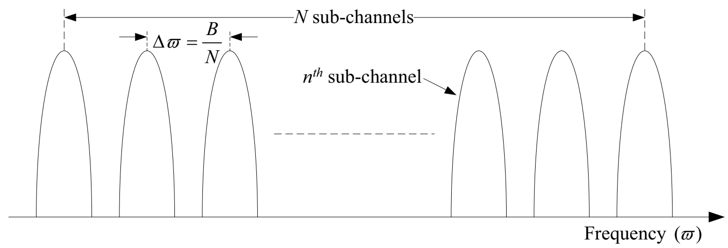

Figure 2.1: Concept illustration of sub-channels in FDM

2.2 Basic concepts of OFDM

2.2.1 Multi-carrier Systems

The concept of multi-carrier transmission or parallel data transmission, referred to as Frequency Division Multiplexing (FDM), was first proposed in the 1950s [31]. In such a system, the total signal bandwidth B is divided equally into N non-overlapping sub-channels as shown in Fig. 2.1. Each sub-channel is modulated with independently generated narrow-band signals followed by their frequency multiplexing. A Guard Interval (GI) is employed to avoid spectral overlapping which eliminates Inter-Carrier Interference (ICI). At the receiver side, filters are used to separate the signals arriving from different sub-carriers [32].

In a conventional single-carrier system, the symbols are sequentially transmitted with each symbol occupying the entire bandwidth B. A deep fade in the channel for such a system can cause the entire link to fail [33]. On the contrary, in a multi-carrier system a deep fade can only affect a small percentage of the sub-channel. Moreover, the erroneous errors can be corrected by using error control coding. Moreover, the multi-carrier system has symbol duration relatively greater than the multipath excess delay spread. This solves the inherent problem of Inter-Symbol Interference (ISI) confronted in high-rate single carrier systems.

2.2.2 OFDM

In FDM, use of non-overlapping sub-channels leads to poor spectral efficiency and thus use of multi-carriers is not an attractive solution to solve the multi-path self-interference problem. This is solved by OFDM, where the property of sub-channel orthogonality allows overlapping of sub-channels without causing ICI [32]. Hence in OFDM, unlike FDM, orthogonal overlapping sub-channels, also referred to as sub-carriers, are used which provide a better means of avoiding equalisation problems, combating impulsive noise and increasing the utilisation of the available bandwidth [34]. The OFDM data can be visualised as a multi-tone data which can be implemented using sinusoidal generators and coherent demodulators. Alternatively, multi-tone data is effectively the Fourier transform of the original serial data and the coherent demodulators are effectively the Inverse Fourier transform, which is much more viable. Fig. 2.2 illustrates usage of bandwidth in an OFDM system as compared to FDM and by transmitting overlapping sub-carriers saves $\approx 50\%$ of the bandwidth. The figure also illustrates how frequency synchronisation is crucial in the case of OFDM systems. Inability to perform very accurate carrier synchronisation will result into sub-carriers not being sampled at their peak energy points. This will result in interference energy from adjacent sub-carriers as well as degraded useful signal energies.

Several flavours of OFDM system are to be found in the literature [35]. This thesis focuses on OFDM based on the Cyclic Prefix (CP) [1] which has been adopted by most OFDM based terrestrial and satellite standards: IEEE 802.11a/g/n, IEEE 802.16, DVB-T/H/S/S2/SH, WiMAX, among others.

[1] See Section 2.2.2.1

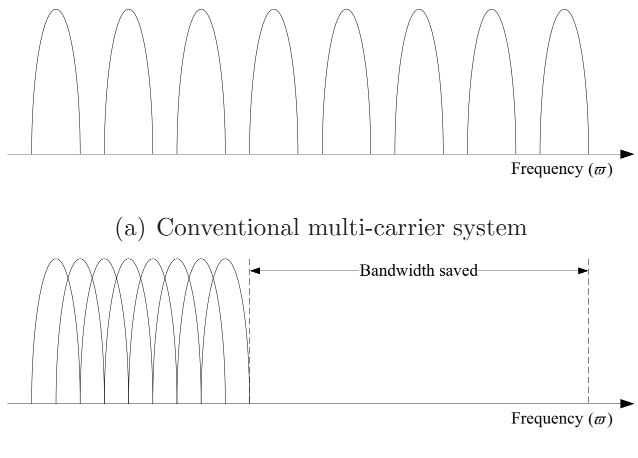

(a) Conventional multi-carrier system

(b) Orthogonal multi-carrier approach

Figure 2.2: Illustration of multi-carrier transmission in FDM and OFDM

2.2.2.1 OFDM Signal Model

Prior to introducing the complete OFDM system architecture, it is imperative to introduce the signal model of OFDM and some of the terminologies related to OFDM. The OFDM signal without the CP insertion is made up of a sum of N complex orthogonal sub-carriers. Each of these sub-carriers is independently modulated with complex symbol $\widetilde{x}_{l,n}$ where l is the OFDM symbol index and n is the sub-carrier index. Within the symbol duration K, the l^{th} OFDM symbol can be represented as:

$$x_l(k) = \frac{1}{\sqrt{N}} \sum_{n=0}^{N-1} \widetilde{x}_{l,n} e^{j2\pi n \Delta\varpi k} g_m(k - lK) \ , \tag{2.1}$$

where $g_m(k)$ is a rectangular pulse shaping applied to each sub-carrier [27]. $\Delta\varpi$ is the inter-carrier spacing. Subdividing the bandwidth into a large number of individual sub-bands makes the bandwidth of these sub-bands much smaller than the overall bandwidth. If the number of sub-bands are large enough, $\Delta\varpi$ can be made much smaller than the coherence bandwidth of the channel.

$$\Delta\varpi \ll B_c = \Delta\varpi \ll \frac{1}{\tau} \tag{2.2}$$

Where B_c is the coherence bandwidth and τ is the excess delay spread of the channel. $x_l(k)$ in (2.1) is referred to as the 'useful OFDM symbol' as it does not include the CP. The total continuous time signal consisting of all OFDM symbols is given by:

$$x(k) = \frac{1}{\sqrt{N}} \sum_{l=0}^{\infty} \sum_{n=0}^{N-1} \widetilde{x}_{l,n} e^{j2\pi n\Delta\varpi k} g_m(k - lK) \ . \tag{2.3}$$

As consecutive OFDM symbol do not overlap, without loss of generality we can consider a single OFDM symbol $x(k)$ where $l = 0$. Since the bandwidth of a symbol $B = N\Delta\varpi$, the signal can be completely determined by its samples if the sampling time $\Delta k = \frac{1}{B} = \frac{1}{N\Delta\varpi}$. The samples of the signal can be presented mathematically as:

$$x_m = \frac{1}{\sqrt{N}} \sum_{n=0}^{N-1} \widetilde{x}_n e^{\frac{j2\pi nm}{N}} \ . \qquad m = 0, 1, \ldots, N-1 \ . \tag{2.4}$$

Equation (2.4) presents exactly the N-point Inverse Discrete Fourier Transform (IDFT). The sequence $x(k)$ can be recovered from its IDFT using DFT:

$$\widetilde{x}_n = \frac{1}{\sqrt{N}} \sum_{m=0}^{N-1} x_m e^{\frac{j2\pi nm}{N}} \ . \qquad n = 0, 1, \ldots, N-1 \ . \tag{2.5}$$

IDFT and DFT are usually implemented in hardware using the Inverse Fast Fourier Transform (IFFT) and Fast Fourier Transform (FFT).

2.2.2.2 Guard Time and Cyclic Prefix

One of the main attributes of OFDM is its computational efficiency due to low complexity equalisation especially for high data rate transmission. In most OFDM systems, a GI is inserted between consecutive OFDM symbols. This GI is chosen to be larger than the maximum delay spread so that multipath components from one symbol do not interfere with the next one. This can be presented as:

$$K_{GI} \geq \tau_{max} \tag{2.6}$$

If the GI is composed of a 'silent period' in the time-domain according to (2.6), the system will be free from ISI due to the sufficient inter-symbol distance. However, the system may suffer from ICI causing the sub-carriers to loose orthogonality. Hence to overcome the ICI problem as well as ISI, the OFDM symbol is cyclically extended in the time-domain, so that any sub-carrier arising from direct or delayed replicas of the signal will continue to have an integer number of cycles with an FFT interval. This ensures orthogonality among the different sub-carriers as long as GI remains larger than the delay spread. The process of extending CP and ISI in an OFDM system is illustrated in Fig. 2.3. As depicted in Fig. 2.3(a), the CP extension is done by copying the last G samples from the end of the useful symbol. The benefits of adding a CP come at a cost. As G samples are added to the data blocks, there is an overhead of G/N, resulting in a data rate reduction of $N/(G+N)$. The transmit power associated with sending the CP is also wasted since this prefix consists of redundant data. However, it is clear from Fig. 2.3(b) that any prefix of length G appended to input blocks of size N eliminates ISI between OFDM data blocks if the first G samples of the block are discarded. To maximise throughput, the symbol duration should be much larger than the CP. Hence,

$$K \gg K_{GI} \tag{2.7}$$

On the contrary, the larger the K, the more the system is susceptible to fast temporal fading, especially if the symbol period is larger than the channel coherence time. In such a case, the orthogonality of sub-carriers will not be preserved resulting in degraded performance [36].

2.2.2.3 OFDM System Model

Presented in Fig. 2.4 is the OFDM baseband system model. At the transmitter end (Fig. 2.4(a)), first random data is generated and modulated to complex symbols using the desired modulation scheme. The output is converted to parallel

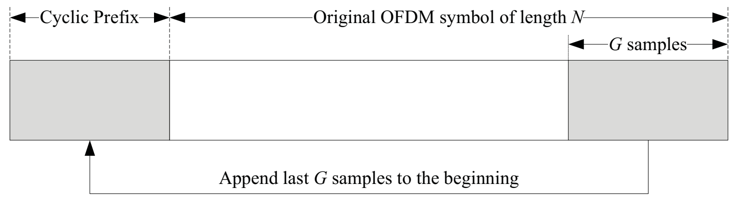

(a) Cyclic Prefix of length G

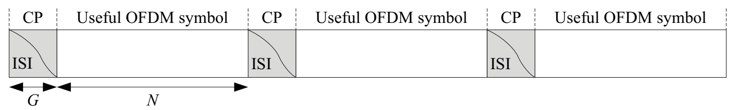

(b) ISI between OFDM symbols

Figure 2.3: Illustration of CP and ISI

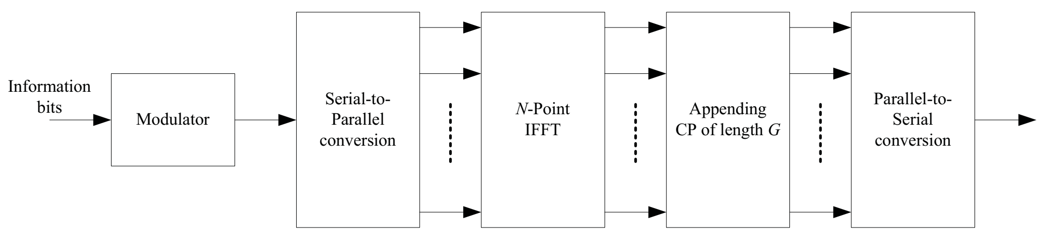

(a) Transmitter

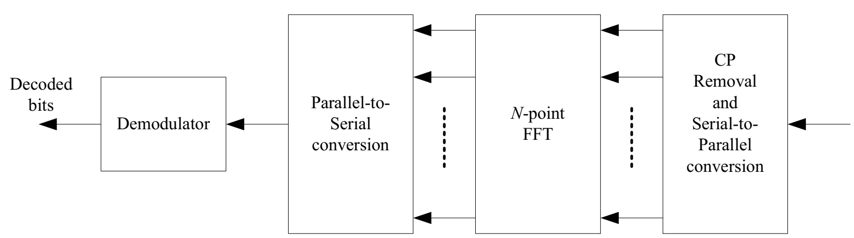

(b) Receiver

Figure 2.4: OFDM baseband system model

form by a Serial-to-Parallel (S/P) converter which is followed by N-point IFFT. Now a CP of length G is appended at the start of each OFDM symbol. Finally, the output of CP processing is transmitted serially into the wireless channel. At the receiver end (Fig. 2.4(b)), the CP is discarded and the output is converted to parallel form and passed to the FFT block. This block performs N-point FFT to convert the OFDM data to the frequency-domain. Now the OFDM symbol is converted back to serial form by Parallel-to-Serial (P/S) conversion which then is finally followed by demodulation to yield the estimates of transmitted bits.

2.3 Temporal Interference and its Mitigation

2.3.1 Co-Channel Interference

One of the main resources of wireless communication is the frequency spectrum. OFDM gives the advantage of high data rates with relatively less complex receiver design and saves valuable bandwidth. In multi-user systems, such as terrestrial cellular, frequency bands are used spatially. In such a scenario, interference occurs when multiple users use the same frequency band. This is referred to as Co-Channel Interference (CCI) and is the major impediment in the realisation of high capacity communication systems. In cellular systems, CCI is introduced due to the frequency reuse of neighbouring cells. CCI is inversely proportional to distance and is the performance driving factor in communication systems rather than Gaussian noise. CCI has different impacts for uplink and downlink and hence there are different solutions applicable to both of these. Specific to region **A**, Fig. 2.5 illustrates the CCI scenarios for both links. In the downlink the transmitter sends orthogonal signals (time, frequency, code, space or hybrid) to all users which belong to the particular system. The target user receives interference from Base Stations (BTSs) of other cells. In the uplink the situation

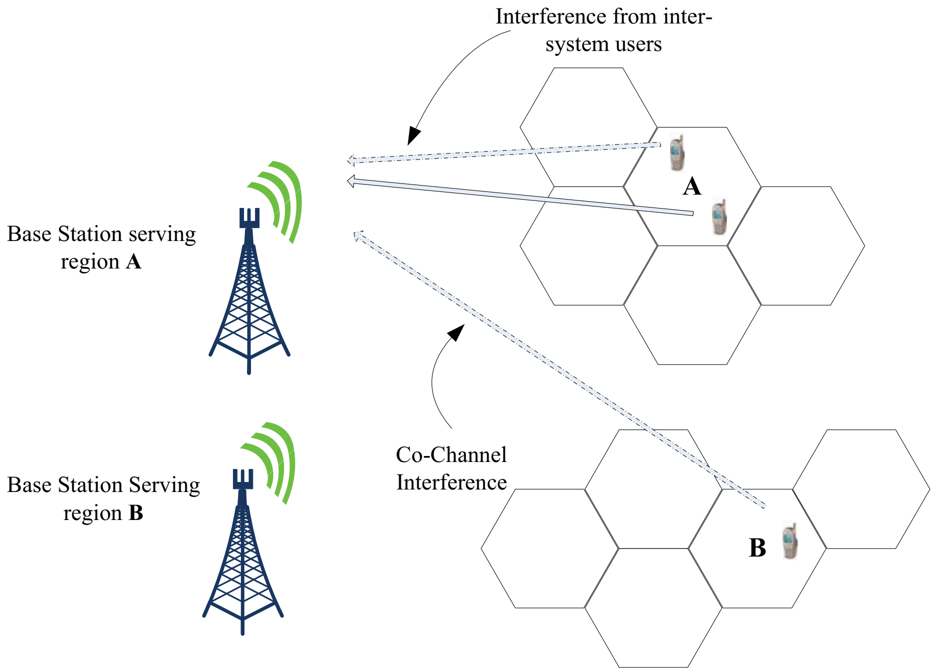

(a) Uplink

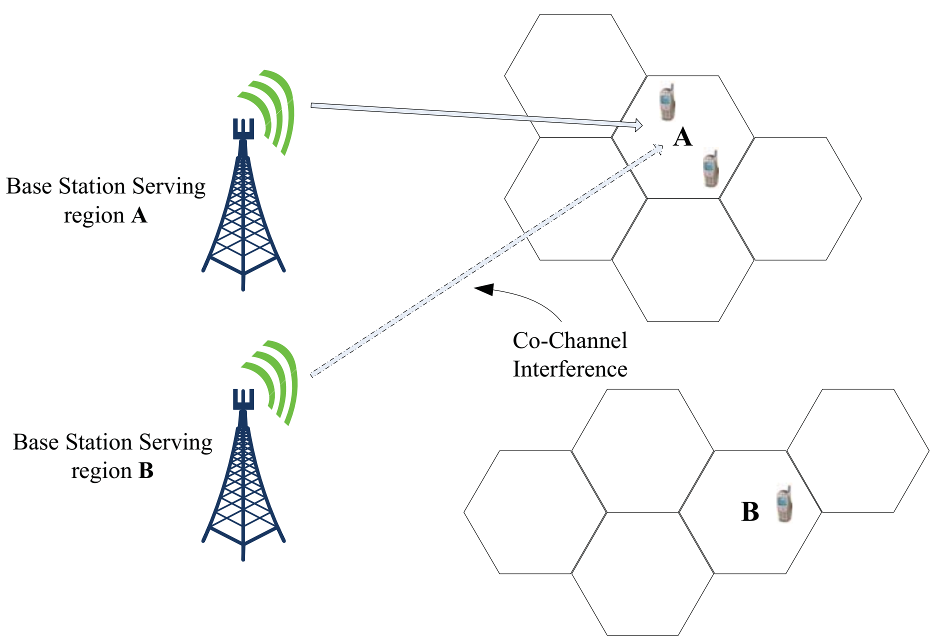

(b) Downlink

Figure 2.5: Uplink and downlink scenarios of Co-Channel Interference

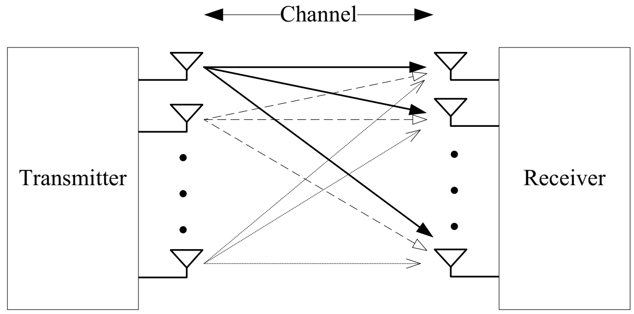

Figure 2.6: Concept illustration of MIMO

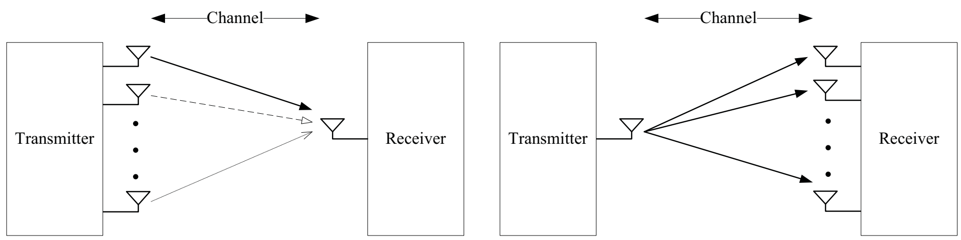

(a) MISO (b) SIMO

Figure 2.7: MISO and SIMO configurations

is more complex and severe. The concerned BTS needs to detect all users in its system and also faces interference from other co-channel cells. Nevertheless, in both the scenarios, interference mitigation is essential for proper functioning of the system.

2.3.2 Beamforming for Interference Mitigation in Multiple Antenna Systems

As mentioned in Section 2.1, OFDM and advanced array processing form an intuitive and formidable solution towards future high capacity systems. With addition of multiple antennas, spatial filtering comes into play which is extremely beneficial for interference mitigation. In this regard, Multiple Input Multiple Output (MIMO) technology has emerged as the most significant breakthrough in modern communications [3–5]. MIMO is a multiple antenna arrangement which uses more than one antenna both at the transmitter and the receiver. An illustration of a MIMO system is depicted in Fig. 2.6. Other configurations in multiple antenna system are Multiple Input Single Output (MISO) and Single input Multiple Output (SIMO), illustrated in Fig. 2.7. With multiple transmit/receiver antennas offer increased capacity [5], this comes at the cost of more complexity. Specially implementing more than 1 antenna at a mobile terminal compromises on weight and cost effectiveness. However when considering BTSs or satellites, implementation of multiple antennas becomes feasible and is a common practise in today's state-of-the-art communication system. Considering the uplink scenario in Fig. 2.5(a), the BTS **A** can have multiple antennas and in such a case, spatial filtering can be used to mitigate CCI. For the downlink scenario in Fig. 2.5(b), multiple antennas can be used to transmit in the desired direction. Similar scenarios can be envisioned for a satellite system where interference in general can be mitigated based on the direction of the desired and interference source.

2.4 Beamforming

As discussed in the previous section, having an array of antenna elements to provide spatial filtering is a way of mitigation interference. BF is a type of spatial filtering and the term Beamforming comes from the fact that spatial filters earlier were designed to form 'pencil' beams. These pencil beams were formed to receive a desired signal from a specific direction and reject signal generated by unwanted sources.

In general, communication systems are designed so as to receive signals from a wide range of locations. With such design, if the wanted as well as unwanted signals use the same frequency band for communication, then this causes interference at the receiver. Referring to Fig. 2.5, we can see that CCI is generated in both uplink and downlink by transmitters due to operation in the same frequency. Focusing on the uplink scenario in Fig. 2.5(a), user terminals in region **B** cause interference to BTS serving region **A**. However, the interference signal is generated from different locations as compared to signals coming from region **A**. This spatial separation can be exploited in a way that BTS serving **A** forms a beam to accept signals coming from the desired users in region **A** and simultaneously suppress signals coming from interference sources in region **B**. Use of such BF approaches for spatial filtering is not only applicable to communication system problems. It has also been successfully employed in other applications such as for RADAR [37, 38], SONAR [39], Imaging [40], Astrophysical exploration [41], Biomedical [42], to name a few.

Use of spatial filtering with array of antenna elements offers two principle advantages: 1) An array of antenna elements or sensors is able to synthesise a much larger spatial aperture as compared to a single physical antenna. Specific to the CCI problem, the capability of interference mitigation is directly proportional to the size (or length) of the spatial aperture. However, the physical size is not relevant, rather its length in terms of wavelength is the crucial parameter. 2) The second and more important advantage is that BF gives the ability to perform active signal suppression. This can be done by adaptively changing the spatial filtering functions to effectively track the desired user and mitigate the interference. Revisiting Fig. 2.5(a), if the desired user in region **A** or/and interference source in region **B** starts moving, then BF parameters can be adapted in accordance to the change in their respective spatial locations. This feature is highly desirable in mobile environments and the process is analogous to adaptive filtering.

Typically, beamformers can be classified into two difference types: narrowband and wideband.

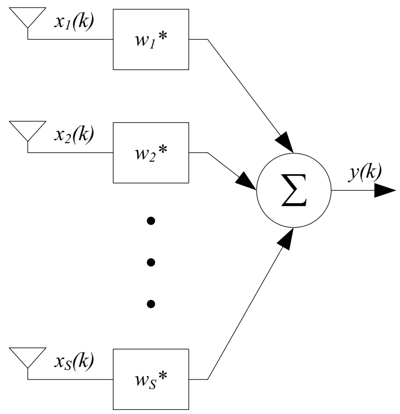

Figure 2.8: Narrowband beamformer

2.4.1 Narrowband Beamformers

Fig. 2.8 illustrates the architecture of a narrowband beamformer. The technique is typically used when signals at the input of antenna elements have narrowband characteristics and a single steering vector $\mathbf{w}$ is applied to the entire received sample. The key advantage of this approach is its reduced complexity: if the number of antenna elements are S, then the size of steering vector $\mid \mathbf{w} \mid= S$. This however comes at the cost of performance degradation in the case when signals at the input are wideband. The output of an S element configuration at time k can be presented as:

$$y(k) = \sum_{s=1}^{S} w_s^* x_s(k) \quad , \tag{2.8}$$

where * represents the complex conjugate, and data as well as weights are assumed to be of complex in nature.

2.4.2 Wideband Beamformers

The wideband beamformer is depicted in Fig. 2.9. This approach is employed in the case of filtering of wideband signals and more than one weight per antenna

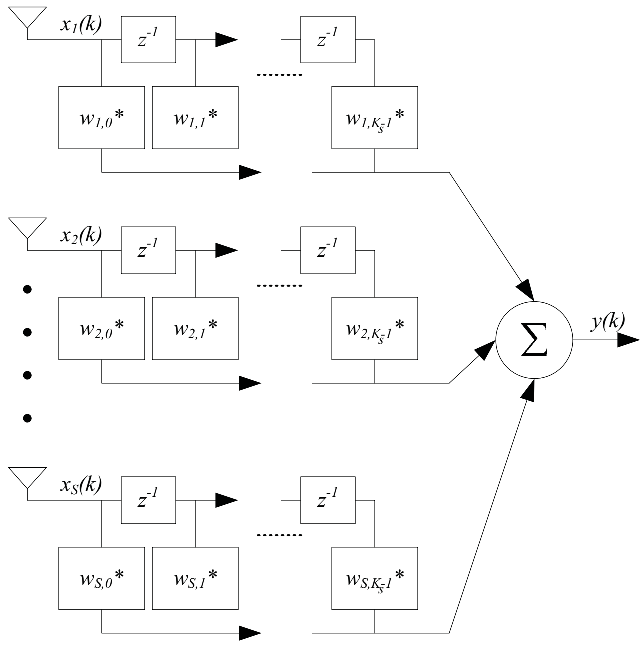

Figure 2.9: Wideband beamformer

element is utilised. The output with wideband beamforming can be presented mathematically as:

$$y(k) = \sum_{s=1}^{S} \sum_{k_s=0}^{K_s-1} w_{s,k}^{*} x_s(k - k_s) \ , \tag{2.9}$$

where $K_s - 1$ is the number of delays in each of the element. Without loss of generality, both the narrowband and wideband beamformers can be presented as:

$$\mathbf{y} = \mathbf{w}^H \mathbf{x} \ . \tag{2.10}$$

2.4.3 Beamformer Response

A beamformer is analogous to an FIR filter in the sense that an FIR filter linearly combines temporally sampled data whereas a beamformer linearly combines spatially sampled data. Therefore, beamformer response can be defined as a function of location and frequency. Fig. 2.10 depicts how a spatially propagating complex

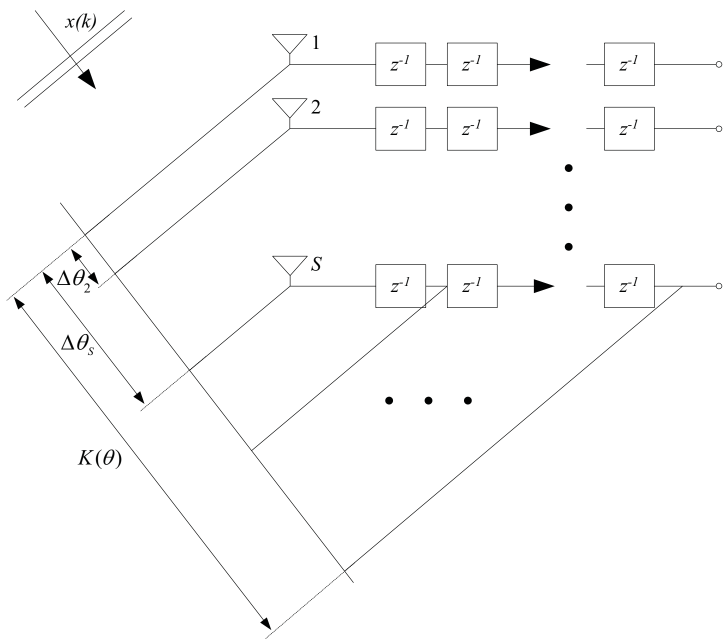

Figure 2.10: Sampling of propagation signal by array of elements

plane wave with Direction-of-Arrival (DOA) θ and frequency ϖ is sampled by the array of antenna elements. Taking the first element as the reference, $x_1(k) = e^{j\varpi k}$ as $\Delta_1(\theta) = 0$ and considering all the elements:

$$x_s(k) = e^{j\varpi[k-\Delta_s(\theta)]} \quad . \qquad s = 1, 2, \ldots, S \ . \tag{2.11}$$

Using (2.9) and (2.11) results in beamformer output:

$$\begin{aligned} y(k) &= e^{j\varpi k} \sum_{s=1}^{S} \sum_{k=0}^{K_s-1} w_{s,k}^* e^{-j\varpi[\Delta_s(\theta)+k_s]} \\ &= e^{j\varpi k} a(\theta, \varpi) \end{aligned} \quad , \tag{2.12}$$

where $\Delta_1(\theta) = 0$ and $a(\theta, \varpi)$ is the beamformer response.

2.5 Adaptive Beamforming

The $\mathbf{w}$ of the beamformer can only be considered as a constant value if the statistics of the signal at the input of the beamformer remain unchanged. In wireless communication systems, as depicted in Fig. 2.5, the users are bound to move causing a constant change in θ. Moreover, users can be present in any location within the service region and hence weights cannot be hard-wired. The beamformer should have the capability of changing its weights depending on the DOA of desired and interference signals. This requires computation of weights at frequent intervals and the subsequent class of BF is referred to as adaptive BF. The BF process is recursive in nature and can generally be based on any of the following criteria:

1. Minimum Mean Squared Error
2. Maximum Signal-to-Interference Ratio
3. Minimum Variance

Interestingly, whichever criterion is followed, the resulting solution of optimum weights is the same. The theoretical results of optimum weights are all given by the Wiener solution [2] which forms the basics of adaptive BF [43]. The optimum weights for the beamformer are given as:

$$\mathbf{w}_{opt} = \mathbf{R}^{-1}\mathbf{r} \ , \tag{2.13}$$

where

$$\mathbf{r} = \mathrm{E}\{d(k)\,\mathbf{x}(k)\} \qquad \mathbf{R} = \mathrm{E}\{\mathbf{x}(k)\,\mathbf{x}^{H}(k)\} \ . \tag{2.14}$$

d is the reference signal and $\mathbf{R}$ is the covariance matrix of the received signal. As different weight criteria have the same optimum weights, this results in the same SIR. Hence the choice of criteria is not critical, however the choice of adaptive algorithm for weight adaptation is pivotal. The choice of algorithm would determine the complexity of the BF process, convergence behaviour, ease of practical implementation and associated hardware complexities. A brief introduction of

[2] Also known as Wiener-Hopf equation

the well known and widely used algorithms is given here, for further details the reader is referred to [43].

2.5.1 Least Mean Squares

This is a well known technique for computation of filter weights adaptation. Apart from BF, it also finds applications in other communication problems such as Multi User Detection [44], Channel estimation [45], to name a few. It is based on the steepest-descent method and needs *a prior* knowledge of the desired signal. Least Mean Squares (LMS) is widely adopted due to its simplicity and reduced complexity. However, the pit fall comes when the signal confronts propagation environments which are statistically variant. This leads to larger spread of the eigenvalues of the covariance matrix $\mathbf{R}$, and thus slow convergence of the algorithm.

2.5.2 Direct Sample Matrix Inversion

One of the methodologies to overcome the convergence problem of the LMS algorithm is to directly invert $\mathbf{R}$. This can be done if both desired and interference signals are known but such knowledge eliminates the need for having a beamformer in the first place. Hence in practical scenarios, $\mathbf{R}$ and $\mathbf{r}$ are estimated in a finite observation interval which depends on the statistics of the propagation conditions. Theoretically the Direct Sample Matrix Inversion (SMI) algorithm can converge more rapidly than LMS, but there are two major problems. One is computation complexity which makes it less favourable for practical implementation. The second is numerical instability due to finite-precision arithmetic and need for inverting of a large matrix [43].

2.5.3 Recursive Least Squares

Recursive Least Squares (RLS) estimates $\mathbf{R}$ and $\mathbf{r}$ using weighted sum rather than using intervals as is the case with SMI. These estimates are taken at each sample of the received signal and are used to compute BF weights. The convergence of RLS is an order faster than LMS, but at the cost of complexity. For the LMS algorithm $2M$ multiples take place per update whereas for RLS, the figure is $4M^2 + 4M + 2$ multiples per update [10]. The second issue is that even with this complexity, the convergence is still slow when SNR is low.

2.5.4 Constant Modulus Algorithm

The Constant Modulus Algorithm (CMA) follows an altogether different approach. It adapts the weights without any reference signal and hence can be referred to as a blind beamformer. It does BF by exploiting the nearly-constant amplitude properties of most modulation formats. Hence, by forcing the received signal to have constant amplitude, the CMA extracts the desired signal. The approach looks attractive but has some short comings. Theoretically the convergence of CMA is not guaranteed [43]. Another problem is that if the interference source is strong enough, the algorithm will end up converging to the undesired signal. This is highly likely in communication scenarios where the desired user signal gets blocked and interference becomes dominant in the received signal.

2.6 Beamforming in OFDM systems

BF can effectively be used as an interference mitigation technique which lends itself well to OFDM systems. This is attributed to OFDM's simpler equalisation due to its narrowband sub-carrier architecture as compared to the broadband single carrier architectures. Moreover, the sub-carrier architecture of OFDM allows

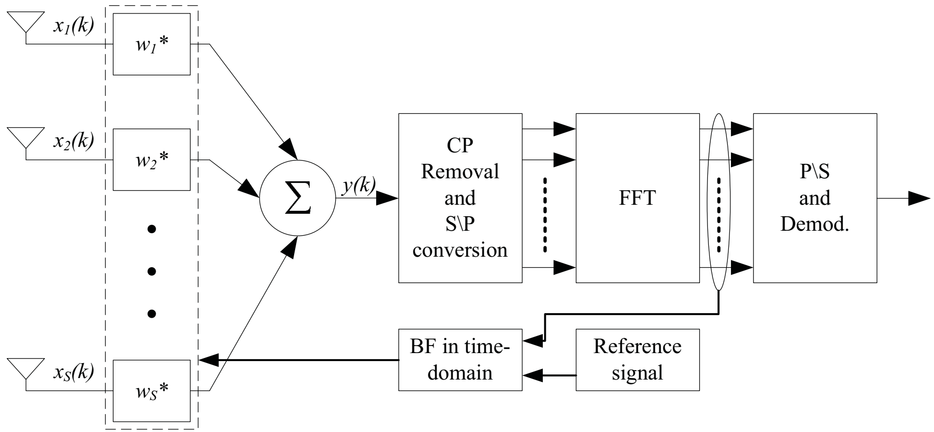

Figure 2.11: Pre-FFT beamforming in OFDM system

the flexibility of having two different classes of BF: Pre-Fast Fourier Transform (Pre-FFT) [46, 47] or symbol level BF and Post-Fast Fourier Transform (Post-FFT) [48] or sub-carrier level BF.

2.6.1 Pre-FFT Beamforming

Symbol-level BF is one way of approaching interference mitigation in OFDM systems. In this case, a single complex weight per antenna element is used, just as was the case with the narrowband beamformer, and hence the total number of weights adapted at each recursion is equal to the number of antenna elements. These BF weights are typically adapted every OFDM symbol. Fig. 2.11 illustrates the general architecture for such a beamformer. Weights are applied to the received OFDM signal and the output of this process is summed up and converted to the frequency domain by the FFT operation. Finally the OFDM symbol being processed, corresponding to the desired signal, is demodulated. The demodulation is normally followed with weights adaptation in the time domain and used for next the OFDM sample. The algorithms found in the literature for BF differ on how they adapt the weights. In [46, 49], an LMS based Pre-FFT beam-

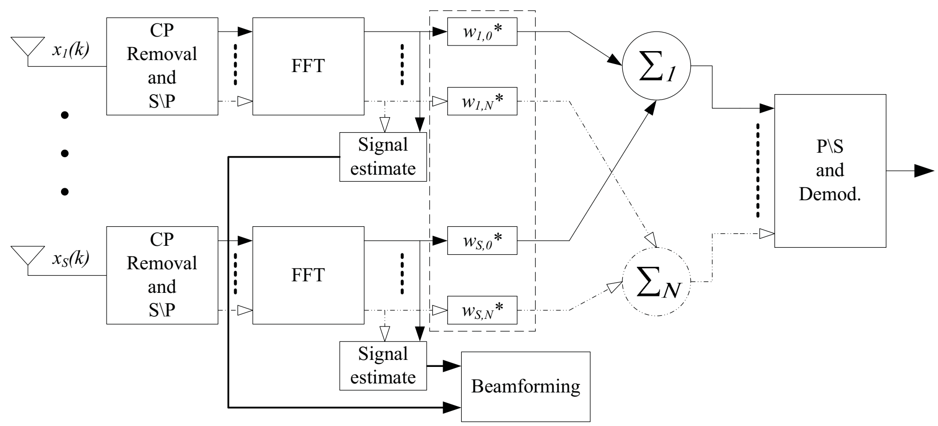

Figure 2.12: Post-FFT beamforming in OFDM system

former is implemented and investigated in AWGN conditions. This architecture is extended in [50] to include frequency-domain adaptive loading. An SMI based beamformer is proposed for an OFDM system in [51] but has high complexity. In [52,53] both LMS and SMI techniques have been employed and studied. In [52] only the convergence behaviour comparison is established whereas in [53] system performance has also been analysed in an AWGN channel.

2.6.2 Post-FFT Beamforming

Fig. 2.12 illustrates the architecture of a sub-carrier level beamformer. Serial-to-Parallel (S/P) conversion is performed on the received signal for each antenna element. This is followed by FFT, signal estimation and application of beamformer weights. These signal estimates are used to update the weights in the frequency-domain for the next OFDM symbol. It is evident that in the time-domain beamformer in Fig. 2.11 the number of weights are equal to the number of antenna elements. However, in Post-FFT BF, total weights to be updated at each recursion are equal to the number of antenna elements $\times$ number of sub-carriers ($S \times N$). Therefore the beamformer complexity greatly increases. However, this yields better performance [48]. This kind of architecture is specifically beneficial in multi-path channels. Apart from traditional LMS, SMI, the BF can also be performed blindly [54–58]. This is not only applicable to Post-FFT BF but also for symbol level BF [59]. In such a case no reference signals are required and hence system dependency on pilots decreased. Although for such approaches, the algorithms convergence is not guaranteed [43].

In this thesis we employ an OFDM system in conjunction with Pre-FFT receiver side BF for mitigation of CCI. The communication scenario under consideration and system model is explained in the next chapter.

2.7 Conclusions

In this chapter we have presented some basic concepts related to OFDM and its advantages. We then elaborated the problem of Co-Channel Interference (CCI) in communication systems and how BF in a multiple antenna system can be employed to mitigate this CCI. We then describe BF, its types and different algorithms as presented in the literature for adaptive BF. Finally we present and describe the model of an OFDM system which employs adaptive BF at the receiver side.

Chapter 3

Hybrid Terrestrial-Satellite Mobile System

This chapter provides a brief overview of satellite systems and the hybrid terrestrial-satellite architectures is presented. We then present our proposed Hybrid Terrestrial-Satellite Mobile System (HTSMS) with adaptive Beamforming (BF) at the satellite end to mitigate uplink CCI. We incorporate realistic satellite channel models and study the interaction between BF and Channel Estimation (CE) specific to the satellite scenario. Part of the work presented here has been published in *Proc. AIAA on 27th ICSSC* 2009 [60].

3.1 Introduction

Success of a communication network not only depends on provisioning of high data rates, but also on the coverage it can offer. Future networks also need to incorporate global connectivity to ensure a rich customer base as customer satisfaction and loyalty are positively affected by service quality. The task of providing service "wherever needed" and "whenever needed" puts significant pressure on communication systems. Standalone existing terrestrial mobile networks fail to provide this due to lack of infrastructure in rural areas. This is where satellite networks are favoured as they have the potential to offer true global coverage as well as rapid network deployment. However satellite links suffer from reduced signal penetration and capacity coverage issues in urban areas as well as at lower elevation angles. This motivates the consideration of location/demand-based hybrid networks, where terminals can enjoy terrestrial coverage in urban areas and be served by satellite links in rural areas.

3.2 Related Work

Arthur Clarke proposed in 1945 that a man-made earth satellite could be used for communication by radio microwaves between distant locations in earth. Following up the idea, the first true communication satellite was launched in 1962 by American Telephone and Telegraph (AT & T) [61]. Since then, an enormous number of communication satellites have been launched into the earth's orbit. The satellite payload capability with each generation has been growing in sophistication and capability.

As envisioned by *Arthur Clarke*, satellite systems have been traditionally used for broadcasting (one-way) services such as Television (TV) broadcasting to fixed locations. However, Mobile Satellite Systems (MSS) have been around since the 1980's, in a similar time frame to terrestrial cellular communications. Systems such as THURAYA started in early 2000 to provide GSM like service covering ASIA and much of Europe [62]. Terrestrial cellular systems on the other hand have shown enormous growth due to their cost-effectiveness. However satellite systems offer some key advantages such as effective service in rural areas with the capability of rapid network deployment. Moreover services to aeronautical and maritime is only viable via satellite networks. Satellite systems have also found application in disaster management where services are deployed within a short frame of time to calamity hit areas.

Satellite service offers key advantages such as wider area of coverage, rapid network deployment, efficient delivery of multicast and broadcast services. However satellite systems suffer in heavily build up areas due to signal penetration issues, especially in areas at low elevation. Terrestrial networks aim to provide users with excellent service within urban areas. However, standalone they cannot guarantee 100% coverage even in urban areas, let alone rural areas. This is due to the cost of infrastructure that is required to guarantee such global coverage. Due to their respective advantages, satellite systems can complement well with terrestrial cellular communications in this respect via an integrated terrestrial-satellite network approach.

In the quest for global coverage and to exploit the advantages of both satellite and terrestrial components, an OFDM based standard for delivery of mobile TV to hand-held devices has been developed by Digital Video Broadcasting (DVB) standard groupd [26], and called DVB-SH [63–65]. The DVB group has also developed several other standards related to video broadcasting [66]. DVB-SH is a hybrid system where service to rural areas is provided by the satellites. In urban areas where satellite suffers from signal penetration and coverage issues, users are served via Complimentary Ground Component (CGC) or Terrestrial Repeater (TR). However incorporation of CGC in rural areas translate to additional cost for the network operator. Moreover, as the system fails to exploit the existing terrestrial mobile infrastructure, the frequency reuse between satellite and CCG offers global connectivity but does not increase the overall spectrum available.

Similar hybrid topology which combines terrestrial and satellite advantages has been perused by SkyTerra, formerly known as Mobile Satellite Ventures (MSV) [6]. The MSV proposed hybrid architecture [7] offers service to rural areas via satellite links and to users in urban areas via Ancillary Terrestrial Components (ATCs).

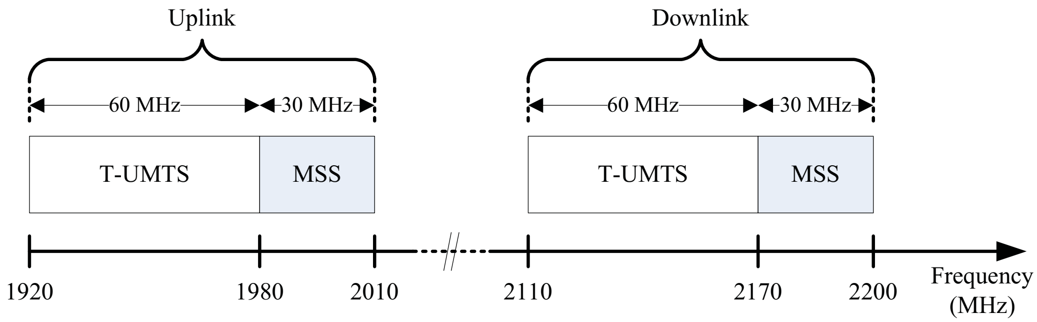

Figure 3.1: IMT-2000 spectrum allocation

MSV employs CDMA in the physical layer combined with multiple antenna system to enhance system performance. Moreover, the service provisioning by the MSV architecture is transparent to the end-user enabling the use of similar terminals for both networks. This is achieved by deploying two satellites and exploiting space diversity to ensure required link margin [9]. However just as in DVB-SH, the MSV design aims to work in isolation of existing terrestrial infrastructure. Furthermore, MSV physical layer is CDMA based and hence cannot function homogeneously with future 4G terrestrial networks.

In a bid to bridge the gap between terrestrial and satellite networks, recently a project named Satellite/Terrestrial Integrated Mobile Communication System (STICS) [11] has been launched in Japan. STICS possesses both satellite and existing terrestrial mobile communication systems and aims to provide service to satellite-terrestrial dual-mode terminals depending on the positions of users in the service area and status of the system (e.g. disaster scene). Moreover to enable higher spectral efficiency, terrestrial and satellite share IMT-2000 Mobile Satellite Service (MSS) band. The International Telecommunication Union (ITU) has defined the global requirement for 3G networks in IMT-2000 standard. The spectrum allocation for MSS band and Terrestrial-UMTS (T-UMTS) within IMT-2000 standard is illustrated in Fig. 3.1. Unlike MSV and DVB-SH, STICS combines existing terrestrial infrastructure and satellite networks in the

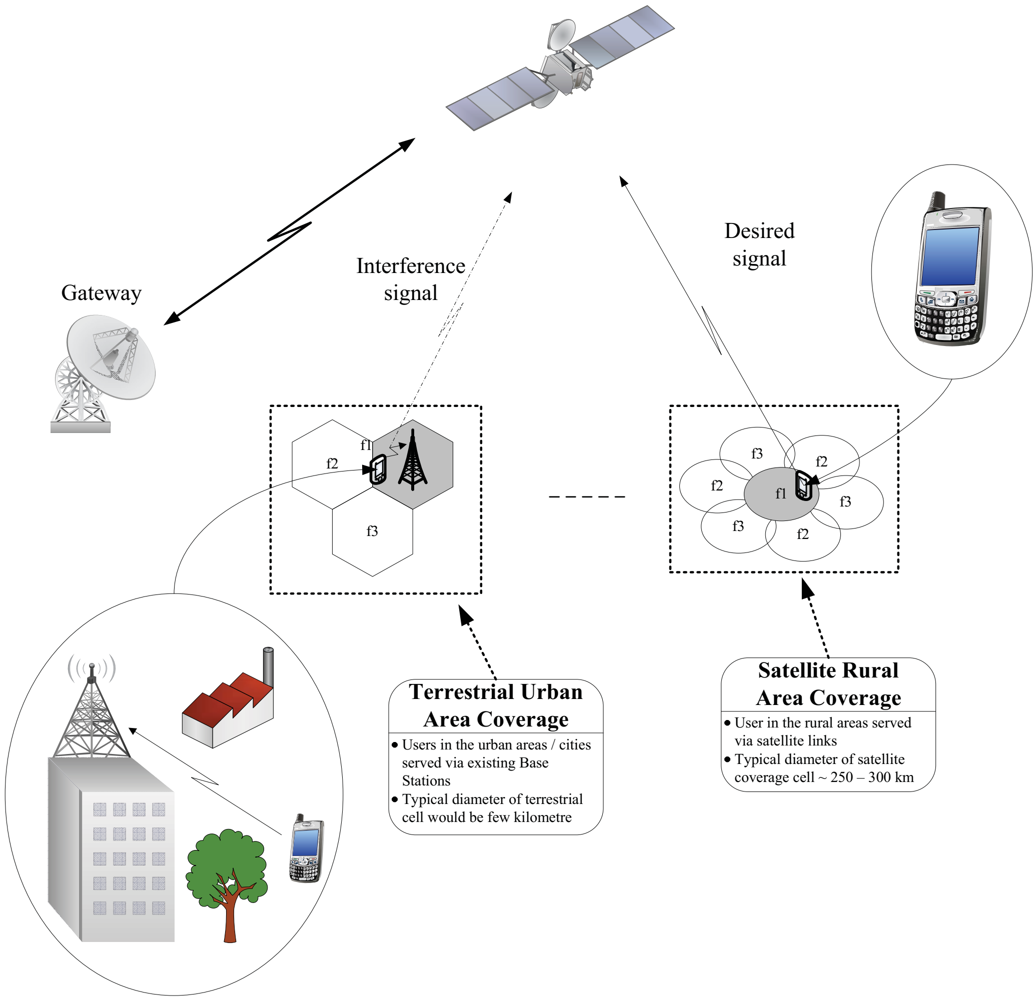

Figure 3.2: Hybrid Terrestrial-Satellite Mobile System

pursuit of integrating satellite and terrestrial mobile systems, reducing the over all costs and enhancing system capacity. However like MSV, STICS is based on CDMA and hence will be less adaptable w.r.t. 4G. Furthermore, the frequency reuse of MSS band introduces interference. STICS study so far focuses on estimation of the uplink interference levels as well as its reduction by using spatial guard-bands [12].

3.3 Hybrid Terrestrial-Satellite Mobile System

In the light of the hybrid architectures existing in the literature, it is clear that a new hybrid framework needs to be devised which offers 1) OFDM technology at the physical layer to enable higher spectrum efficiency, reduced ISI and most importantly enables homogeneous operations amongst future 4G terrestrial mobile system, 2) offers integrated satellite and terrestrial services by combining the existing infrastructures of the respective networks.

Fig. 3.2 depicts the envisioned OFDM based HTSMS which we propose in [60]. Users in the urban areas are served via the existing terrestrial BTSs whereas users in rural areas are served via satellite links. In this system, terrestrial and satellite networks will reuse the common spectrum and hence increase the overall capacity. The service provisioning by two different technologies should be transparent to the end-user, in the sense that the same mobile terminals should work with both terrestrial as well as satellite networks. HTSMS being a transparent and a complimentary architecture is low cost, provides higher data rates and increased overall capacity. Furthermore, HTSMS enables global coverage and rapid network deployment.

The frequency reuse amongst the two networks induces severe CCI which is the main impediment to the realisation of high capacity communication systems. In such a scenario, adaptive interference mitigation becomes imperative [8]. MSV hybrid design incorporates CDMA based adaptive BF [43] to mitigate CCI by forming nulls towards interference sources whilst providing high gains towards the desired locations [8, 9].

3.3.1 Adaptive Beamforming in HTSMS

In relation to our system, the nature of the hybrid architecture causes a considerable increase in CCI on the uplink to the satellite. For such a scenario, we employ an OFDM based Least Mean Squares (LMS) [46] beamformer onboard the satellite to mitigate CCI. BF lends itself well due to OFDM systems due OFDM's simpler equalisation. This is attributed to its narrowband sub-carrier architecture as compared to a broadband single carrier architectures. Moreover, OFDM gives the flexibility of having two different classes of BF; Pre-Fast Fourier Transform (Pre-FFT) [46, 47] or symbol level BF and Post-Fast Fourier Transform (Post-FFT) [48] or sub-carrier level BF. Pre-FFT array processing has low complexity because only one FFT and subsequent demodulation chain is required whereas in Post-FFT spatial processing at sub-carrier level exhibits optimal performance but with much higher complexity [48]. A sub-carrier clustering based BF [67] approach is also found in the literature aiming to minimise the complexity of Post-FFT approach. Recently a Multi-Stage Beamformer (MSB) [68] has been proposed which employs both symbol level and sub-carrier level BF to trade-off system performance and complexity amongst the two approaches. However due to complexity constraints onboard the satellite payload, we only consider the Pre-FFT approach for HTSMS.

With regards to BF, most of the work in the literature is focused on terrestrial systems as mentioned earlier. There is some work for satellite scenarios [7–9] but it is focused on CDMA based system. Moreover, considerable work relating to terrestrial scenarios assumes just AWGN channel conditions. Others considering practical channel models neither relate to the terrestrial-satellite mobile scenario [51, 54, 56, 58] nor to moderate or high user mobility. In the case of frequency selective channel models, there is an interplay between BF and CE and their interrelation which is an area yet to be explored.

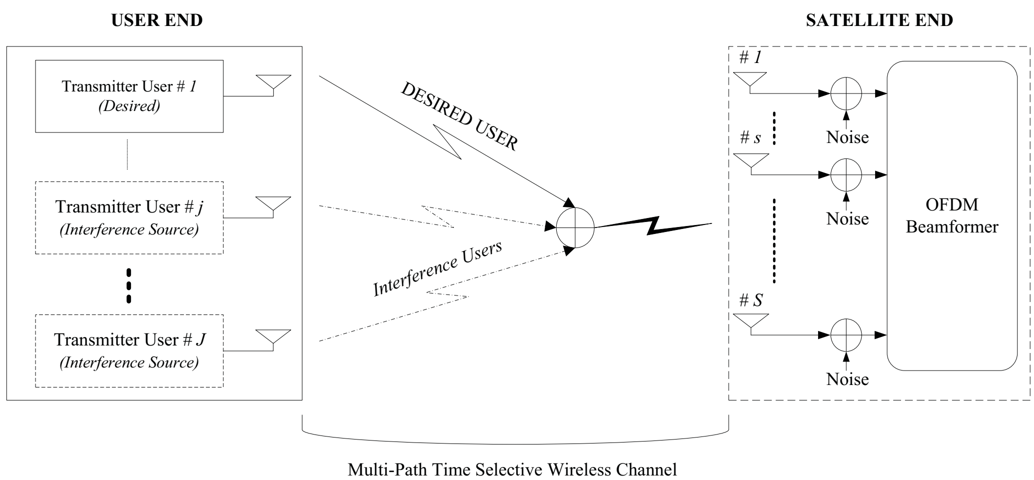

Figure 3.3: HTSMS Scenario

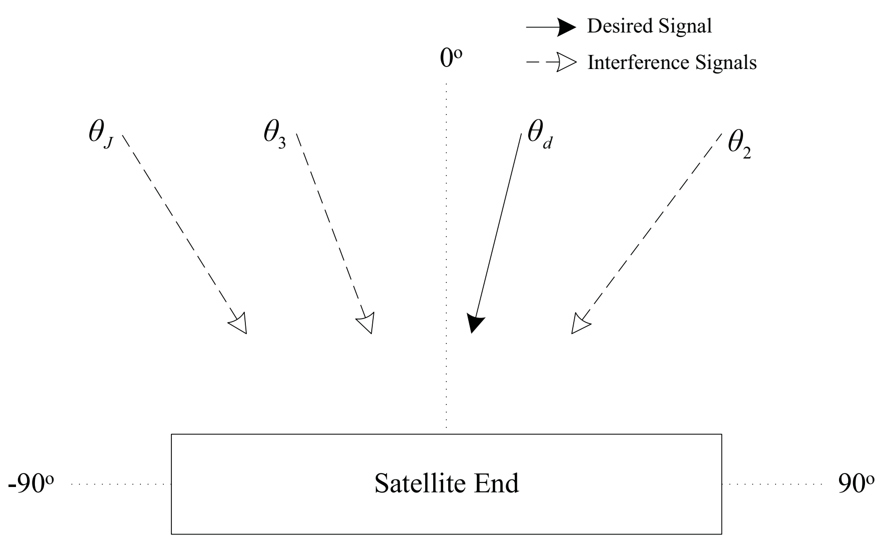

Figure 3.4: Interference Model

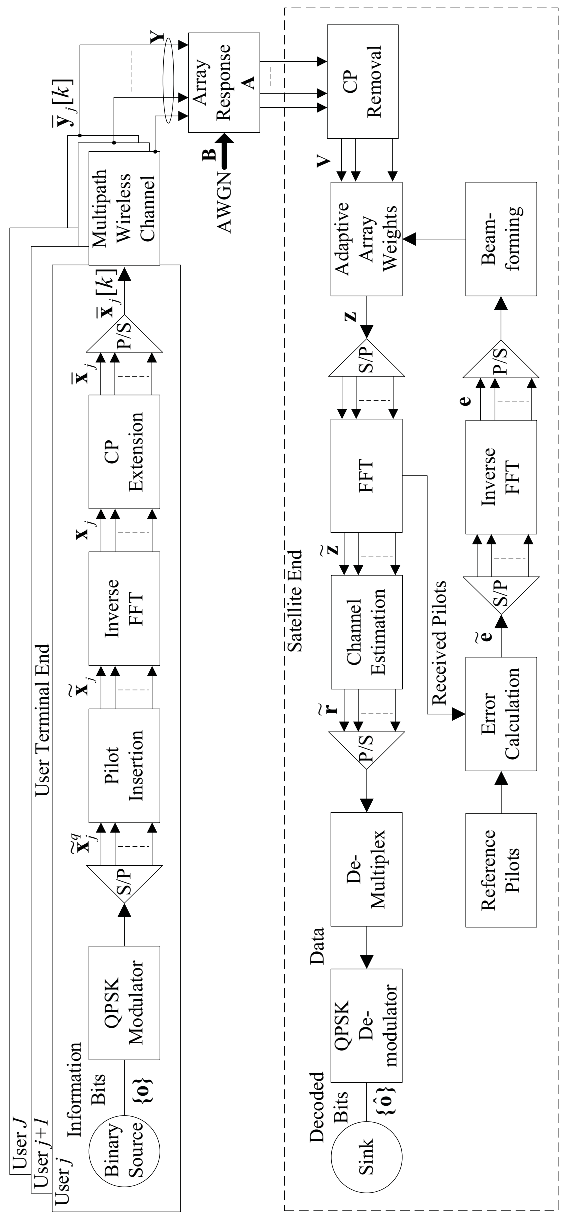

Figure 3.5: OFDM system model for HTSMS

3.4 System Model

HTSMS is envisioned to offer global coverage by operating terrestrial and satellite networks in an integrated framework. Fig. 3.3 depicts the devised system scenario under study with a hybrid framework. We focus on the mitigation of CCI induced by terrestrial mobile users from the perspective of a Geostationary (GEO) satellite. With respect to the system, a link between mobile and satellite is modelled as Single Input Multiple Output (SIMO). Total J users are considered in the system, with one desired user denoted as d being served by the satellite while the rest being served by terrestrial BTSs. After the signal passes through the wireless channel, BF is applied at the satellite end to mitigate interference induced by terrestrial users. The interference geometry corresponding to the desired and interference signals and their respective Direction-of-Arrival (DOA) is illustrated in Fig. 3.4. Due to onboard implementation constraints and less severe satellite channel environment, we employ less complex time-domain symbol level BF (Pre-FFT). We also assume no time or frequency offsets exist in the system.

3.4.1 OFDM Transmitter Model

Fig. 3.5 illustrates the block diagram of the OFDM system with BF at the satellite end and will be referred to throughout the chapter to follow the information flow in the system. At the transmitter end of the j^{th} user ($j = 1, ..., J$), random source data $\{\mathbf{o}\}$ is QPSK modulated and then Serial-to-Parallel (S/P) converted to $\{\widetilde{\mathbf{x}}^q\}$. Pilots $\{\widetilde{\mathbf{x}}^p\}$ are interspersed into data sequence $\{\widetilde{\mathbf{x}}^q\}$ at known pilot sub-carriers $\{\mathcal{I}\}$ to form an N sub-carriers OFDM symbol $\widetilde{\mathbf{x}} = [\widetilde{x}(0), \widetilde{x}(1), \ldots, \widetilde{x}(N-1)]^T$. The values of pilot information are derived from a Pseudo Random Binary Sequence (PRBS), which is a series of values, one for each transmitted sub-carrier. The pilots are modulated according to PRBS sequence, $\varrho(n)$, corresponding to their respective carrier index n. The PRBS is initialised so that the first output bit from the PRBS coincides with the first active carrier. A new value is generated by the PRBS on every carrier (whether or not it is a pilot). The polynomial for the PRBS generator is:

$$X^{11} + X^2 + 1 \ . \tag{3.1}$$

Reference information, taken from the reference sequence, is transmitted in pilot sub-carriers for every OFDM symbol. Pilot cells are always transmitted at the "boosted" power level and the corresponding modulation is given by:

$$\widetilde{x}(\mathcal{I}) = \frac{4}{3} \times 2 \left(\frac{1}{2} - \varrho(\mathcal{I}) \right) \ . \tag{3.2}$$

The amalgamation of pilots and QPSK data to form $\widetilde{\mathbf{x}}$ is followed by N-point IFFT, resulting in $\mathbf{x}$. This can be presented mathematically as:

$$\mathbf{x} = \mathbf{F}^H \widetilde{\mathbf{x}} \ , \tag{3.3}$$

where

$$\mathbf{F} = \begin{bmatrix} 1 & 1 & \cdots & 1 \\ 1 & e^{-j2\pi(1)(1)/N} & \cdots & e^{-j2\pi(1)(N-1)/N} \\ \vdots & \vdots & \ddots & \vdots \\ 1 & e^{-j2\pi(N-1)(1)/N} & \cdots & e^{-j2\pi(N-1)(N-1)/N} \end{bmatrix} \ . \tag{3.4}$$

A Cyclic Prefix (CP) of length G is appended at the start of the OFDM symbol and the output $\bar{\mathbf{x}} = [x(-G), x(-G+1), \ldots, x(N-1)]^T$ is serially transmitted over multi-tap time selective wireless channel, whose effect can be presented as:

$$\bar{\mathbf{y}}[k] = \bar{\mathbf{x}}[k] \otimes \mathbf{h}[k] \ , \tag{3.5}$$

where k and $\otimes$ denote the time index and time convolution operation respectively.

3.4.2 Joint Adaptive Beamforming and Channel Estimation

At the satellite, we model a Uniform Linear Array (ULA) whose output after CP removal for the l^{th} OFDM symbol ($l = 1, \ldots, L$) for all the users can be represented as:

$$\mathbf{V} = \mathbf{A}\mathbf{Y}^H + \mathbf{B} \ , \tag{3.6}$$

where $[\mathbf{Y}]_{n,j}$ represents the received n^{th} sub-carrier for the j^{th} user. Similarly $[\mathbf{B}]_{s,n}$ and $[\mathbf{V}]_{s,n}$ represents the independent and identically distributed (i.i.d) complex Gaussian noise $\sim \mathcal{CN}(0, \sigma^2)$ and ULA output at the s^{th} antenna element and n^{th} sub-carrier respectively where $s = 1, \ldots, S$ is the array element index of the ULA. $\mathbf{A}$ is the ULA response, where $[\mathbf{A}]_{s,j}$ can be be presented mathematically as:

$$a(s,j) = e^{(-j2\pi(s-1)d_a \sin(\theta_j)/\lambda)} \ , \tag{3.7}$$

where d_a is the inter-antenna element spacing in the ULA, θ_j is the DOA of the j^{th} user and λ is the carrier wavelength. We model a ULA with $d_a = \lambda/2$. The output of the ULA is processed by the beamformer to mitigate CCI, which can be expressed as:

$$\mathbf{z} = \mathbf{w}^H \mathbf{V} \ , \tag{3.8}$$

$$\mathbf{z} = [z(0), z(1), \ldots, z(N-1)] \ ,$$

$$\mathbf{w} = [w(1), w(2), \ldots, w(S)]^T \ ,$$

where $\mathbf{z}$ is the weighted output of the beamformer and $\mathbf{w}$ are the applied complex weights. This is followed by S/P conversion and transformation of $\mathbf{z}$ to the frequency-domain, which can be expressed mathematically as:

$$\widetilde{\mathbf{z}} = \mathbf{F}\mathbf{z}^H \ . \tag{3.9}$$

The proposed architecture utilises one weight per antenna element in a multi-path fading environment. CE thus becomes essential before $\widetilde{\mathbf{z}}$ is decoded since different fading exists across OFDM sub-carriers. Several CE techniques can be employed [69], however we employ the Least Squares (LS) algorithm. Representing the channel transfer function at pilot positions, we get:

$$\widetilde{\mathbf{h}}^p = (\mathrm{diag}\{\widetilde{\mathbf{x}}_d^p\}^{-1})\widetilde{\mathbf{z}}^p \ . \tag{3.10}$$

$\widetilde{\mathbf{h}}^p$ represents the channel estimates at pilot sub-carriers $\mathcal{I}$ for the desired user and diag$\{\cdot\}$ represents a matrix formed by placing elements of a vector at the diagonal entries of the matrix with zeros at all off-diagonal entries. Estimates $\widetilde{\mathbf{h}}^p$ are then linearly interpolated and the output can be expressed as $\widetilde{\mathbf{h}}$. The interpolation process can be expressed as:

$$\widetilde{\mathbf{h}} = \text{filt}(\widetilde{\mathbf{h}}^p) \ . \tag{3.11}$$

Estimates $\widetilde{\mathbf{h}}$ are then used to reduce the channel effect, which can be expressed as:

$$\widetilde{\mathbf{r}} = (\text{diag}\{\widetilde{\mathbf{h}}\}^{-1})\widetilde{\mathbf{z}} \ . \tag{3.12}$$

The data sub-carriers in $\widetilde{\mathbf{r}}$ are passed to the QPSK demodulator where they are decoded into $\{\hat{\mathbf{o}}\}$.

3.4.2.1 LMS Adaptive BF

For the subsequent OFDM symbol, computation of new complex weights is required. This computation is performed using a Mean Squared Error (MSE) based adaptive algorithm which takes the error between the transmitted and received pilot sequence of the desired user as an input. This error vector (prediction error) in the frequency-domain at the pilot locations can then be expressed as:

$$\widetilde{\mathbf{e}} = \widetilde{\mathbf{z}}^p - \widetilde{\mathbf{x}}_d^p \ . \tag{3.13}$$

The error vector in (3.13) is a sparse matrix, i.e. locations corresponding to data sub-carriers are all zero. This has the advantage that it ensures better normalisation within an FFT window. As we employ Pre-FFT based BF, the weight adaptation takes place in the time-domain. Hence a frequency-to-time transform is used to convert the error vector for the l^{th} OFDM symbol to the time-domain, which can be presented as:

$$\mathbf{e} = \mathbf{F}^H\widetilde{\mathbf{e}} \ . \tag{3.14}$$

After the computation of error the vector in (3.14), we implement the widely used complex LMS algorithm to update the complex weights of the beamformer following [46]. As the LMS adaptation aims to mitigate interference, it can be referred to as interference aware BF. The LMS adaptation is given by:

$$\mathbf{w}[l+1] = \mathbf{w}[l] + 2\mu\mathbf{V}[l]\mathbf{e}[l] \ . \tag{3.15}$$

Substituting (3.14) into (3.15), we get:

$$\mathbf{w}[l+1] = \mathbf{w}[l] + 2\mu\mathbf{V}[l]\mathbf{F}^{H}\widetilde{\mathbf{e}}[l] \ . \tag{3.16}$$

Here $\mathbf{w}[l]$ and $\mathbf{w}[l+1]$ represent the beamformer's complex weights for (l) and $(l+1)$ OFDM symbols. μ represents the positive step size which controls the rate of convergence. The algorithm only converges [70] if:

$$\mu_{min} \leq \mu \leq \mu_{max} \ , \tag{3.17}$$

with

$$\mu_{max} \leq \frac{2}{3\,\mathrm{tr}\,(\mathbf{R})} \ , \tag{3.18}$$

where μ_{max} is chosen to bound the MSE of the algorithm and depends on the maximum eigenvalue of the received signal covariance matrix $\mathbf{R}$. Whereas μ_{min} is chosen to provide minimum tracking capability to the algorithm. When constant μ (FSS)[1] is employed with LMS, μ will usually be close to μ_{min} [70]. LMS with optimised μ can be employed that adapts at each iteration according to (3.18). In this chapter we employ FSS-LMS having a fixed μ.

In terms of complexity of the full-adaptive beamformer, the computation process for (3.15) in terms of addition and multiplication can be presented as:

$$LS(M + N(M+P)) \qquad \forall L \ , \tag{3.19}$$

where M and P represent multiplication and addition operations respectively. As M operations are far more complex than P, hence ignoring adder operations

[1]Fixed Step Size.

simplifies (3.19) to:

$$LSM(1+N) \qquad \forall L \ , \tag{3.20}$$

3.4.2.2 Optimum BF

Optimum BF (OBF) does not aim to minimise interference but maximise the gain towards a particular direction. Hence OBF can be referred to as orientation aware BF. To calculate the BF complex weights in the case of OBF, we reformulate (3.8) by incorporating (3.6).

$$\mathbf{z} = \mathbf{w}^H(\mathbf{A}\mathbf{Y}^H + \mathbf{B}) \ . \tag{3.21}$$

By examining (3.21) it is clear that in order to maximize the gain in a particular direction, complex weights $\mathbf{w}$ should be equal to the array response of the antenna elements. If θ_d is the desired beam direction, the BF weights calculation process can be written as:

$$\mathbf{w} = [w(1), w(2), \ldots, w(S)]^T \ , \tag{3.22}$$

where

$$w(s) = \exp^{(-j2\pi(s-1)d_a \sin(\theta_d)/\lambda)} \ , \tag{3.23}$$

and the relation between consecutive weights of l and $l+1$ OFDM symbols can be expressed as:

$$\mathbf{w}[l+1] = \mathbf{w}[l] \ . \tag{3.24}$$

We can see in (3.23) and (3.24) that no adaptation of weights takes place. This can also be referred to as a static BF approach. These weights calculated at the beginning for θ_d are continuously applied by the beamformer until all data is decoded. Therefore compared to the full-adaptive beamformer, complexity is greatly reduced as the optimum weights in (3.23) need to be calculated only once.

3.5 Simulation and Discussions

3.5.1 Channel Model

We model a multi-path time selective channel model with parameters specific to the terrestrial-satellite mobile scenario in order to analyse the system performance. The multi-path phenomenon is modelled as a linear Finite Impulse-Response (FIR) filter with multiple taps and time selectivity of the channel is modelled using Jakes model [71]. The channel parameters considered are specific to a terrestrial-satellite mobile scenario and were measured as part of the EU project Mobile Applications & sErvices based on Satellite & Terrestrial inteRwOrking (MAESTRO) [72]. In this study we consider two of the MAESTRO cases, namely Outdoor Rural (case 1) and Outdoor Urban (case 2). The channel parameters for the two cases are presented in Table 3.1 while the respective power delay profiles are plotted in Fig. 3.6. The rural case has Rician factor (K-factor) = 10 dB whereas urban has K-factor = 7 dB.

	Outdoor Rural		**Outdoor Urban**	
Tap Index	Delay [ns]	Power Loss [dB]	Delay [ns]	Power Loss [dB]
1	0	91.9	0	91.8
2	195.3	106.3	130.2	100
3	260.4	110.1		
4	846.3	112.5		
5	1171.9	110.2		
6	1953.1	112.5		
7	2734.3	112.5		

Table 3.1: MAESTRO channel parameters

While we incorporate time-selectivity in our channel model using Jakes model [71], we however assume that the angle of arrival difference is very small for a GEO

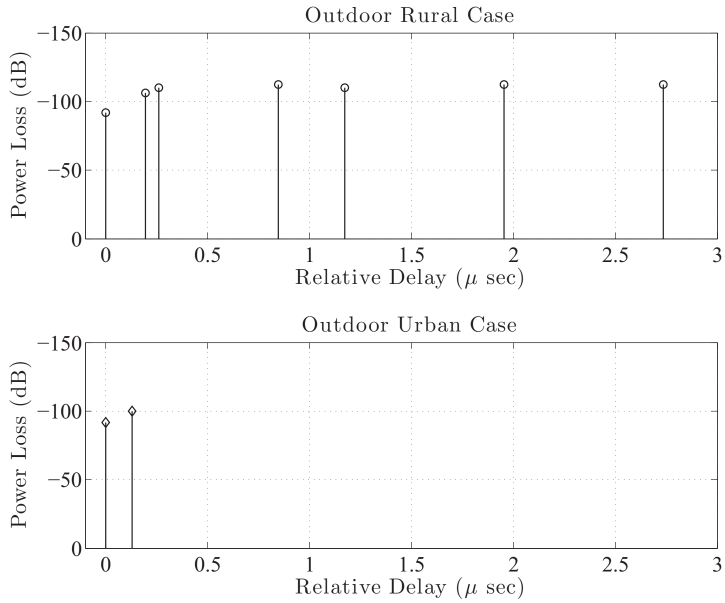

Figure 3.6: Power delay profiles

satellite system as compared to terrestrial systems. To justify this assumption, let us assume d as the distance between a user and satellite with the user directly under the satellite. If the user moves from here in a straight line with a velocity v for time t, then the difference in DOA with respect to the satellite for such a scenario can be expressed as:

$$\Delta\theta = \tan^{-1}\left(\frac{vt}{d}\right) \quad . \tag{3.25}$$

For a typical GEO satellite, $d \approx 35786$ km. This effectively means $d \ll vt$ resulting $\Delta\theta$ in (3.25) to be very small. For instance, with $v = 60$ km/hr and $t = 1$ hr, $\Delta\theta = 0.096°$ and on a per minute basis this change is $0.0016°$/min. In comparison, if we assume the same user moving in circular motion at the cell edge of a cellular base station having cell radius r, the rate of change of $\Delta\theta$ with respect to the base station can be presented as:

$$\frac{\Delta\theta}{t} = \frac{v}{2\pi r} \times 360 \quad . \tag{3.26}$$

Using the same velocity and time and assuming a typical terrestrial cellular cell of $r = 3$ km, on a per minute basis is $\frac{\Delta\theta}{t} = 19.1°/\text{min}$. Hence we can clearly see that the DOA spread for a GEO satellite is extremely small as compared to the terrestrial case.

3.5.2 Parameters

A SIMO OFDM system with per link, one transmit and multiple receive antenna elements $S = \{3, 9\}$ is modelled. However, actual number of antenna elements in a satellite will be much more. For instance in the MSV system, the satellite has total of 88 antenna elements covering whole of North America. However 9 is a realistic value because 1) we are considering 1 desired user and several interferes but the total users in the system $J < 9$ throughout the thesis, 2) Having more antenna elements causes slower BF convergence and higher latency issues [2] and 3) This arrangement can be considered as a subset of the total antenna elements which is selected as function of the interference sources. Hence if we have lesser interference, we do not need to perform BF using all the elements but a subset of them.

The power per interference user at the satellite end is set to -10 dBW. It must be noted that we follow random distribution while modelling the Direction-of-Arrivals of the users. This is done deliberately to verify the capability of beamformer for a wide spread of Direction-of-Arrivals. The LMS step size for the beamformer is $\mu = 0.0007$.

3.5.3 Performance

Prior to presenting the results, we pause to investigate the way in which BF convergence could be studied. In literature, the convention of presenting BF

[2] We discuss this in Chapter 8

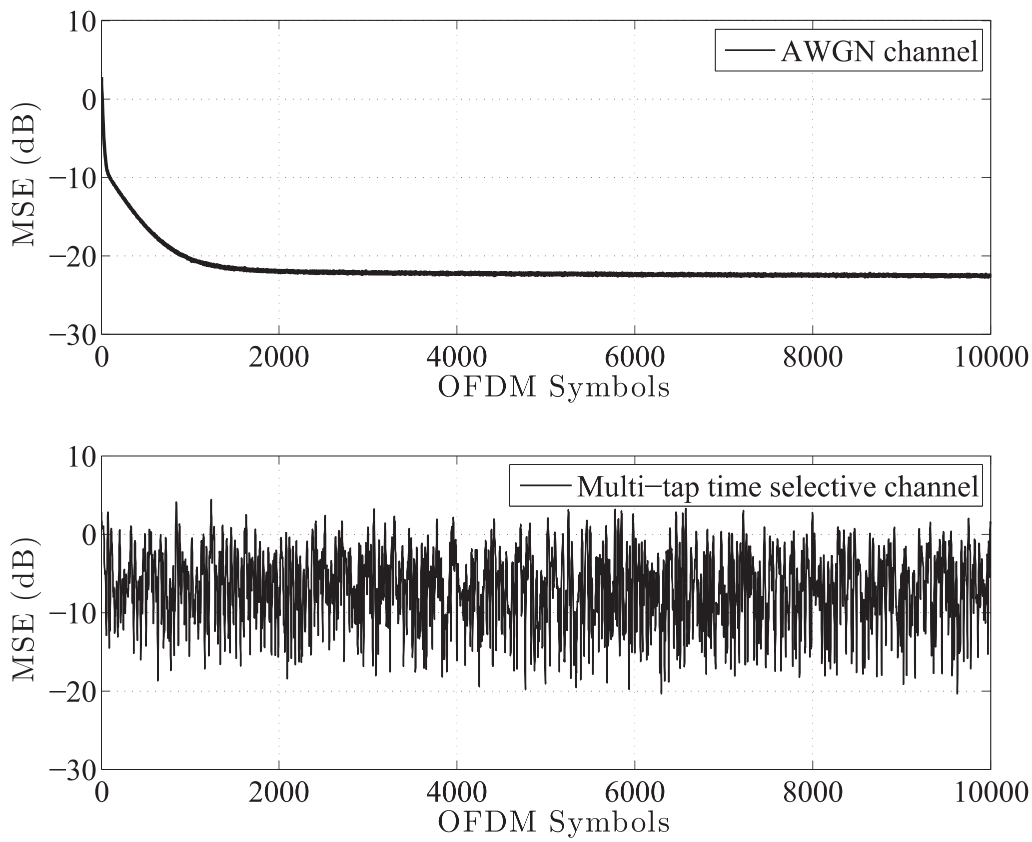

Figure 3.7: Beamforming convergence in terms of Mean Squared Error vs OFDM symbols, antenna elements = 3 and SNR = 20 dB.

convergence is in terms of MSE (dB) against number of iterations passed (or in our case OFDM symbols), for instance in [46]. MSE is the instantaneous mean error of the beamformer. With the parameters defined in Section 3.5.2, the convergence of beamformer in terms of MSE against OFDM symbols for both AWGN and wireless multi-tap time selective channel scenario [3] is depicted in Fig. 3.7 with results similar to as presented in [46]. Another way of presenting the mean of any data in statistical theory is the Cumulative Moving Average or Running Average. Running average (or running mean) is a valuable tool and has been used in

[3]Outdoor Rural case, mobile speed = 3 km/hr

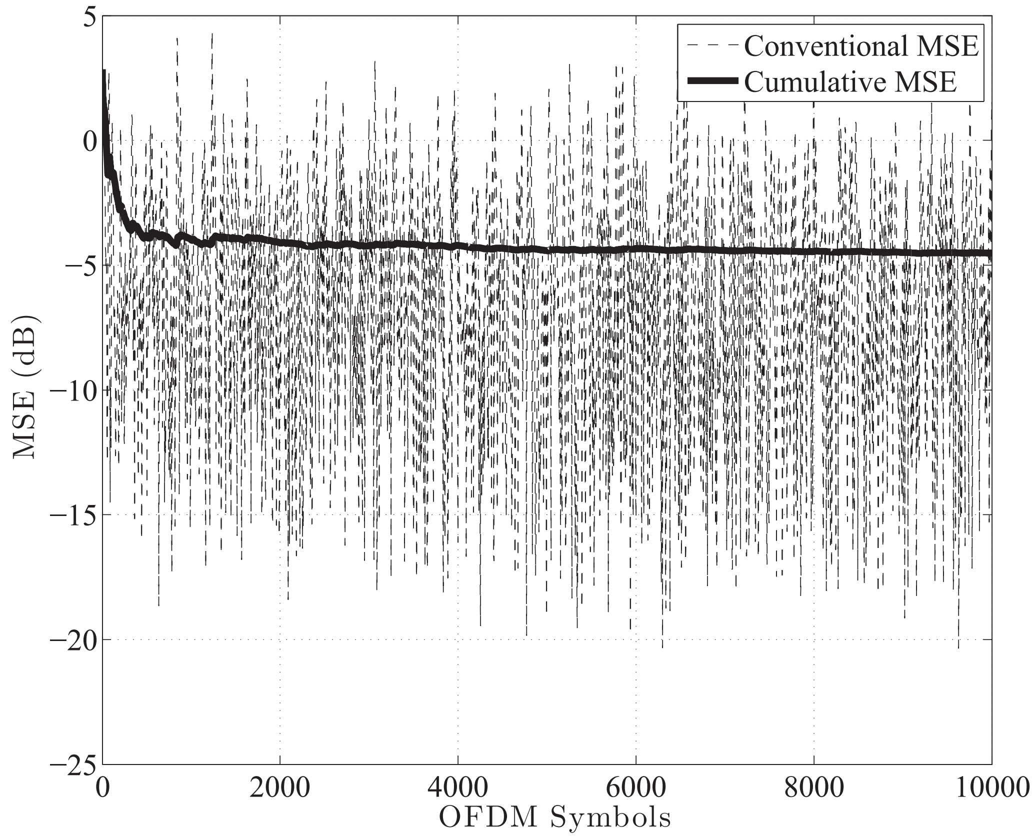

Figure 3.8: Beamforming convergence in terms of Cumulative MSE and conventional MSE vs OFDM symbols in rural environment with mobile speed = 3 km/hr, antenna elements = 3 and SNR = 20 dB.

several disciplines, like digital circuits [73], economics and sociology [74], motion detection [75], adaptive traffic control [76] to measure "learning processes". It presents the running average of the data rather than the instantaneous mean. In case of beamforming, if ω_l is the MSE of the l^{th} OFDM symbol, then the running average (or we call it the Cumulative MSE) for L OFDM symbols can be presented as:

$$\mathrm{CMSE}_L = \left[\omega_1, \frac{\omega_1+\omega_2}{2}, \frac{\omega_1+\omega_2+\omega_3}{3}, \cdots, \frac{\sum_l^L \omega_l}{L}\right] . \tag{3.27}$$

Now using the running mean as defined in 3.27, we present the CMSE and MSE results for the same wireless channel scenario in Fig. 3.8. From the figure we can clearly see that CMSE is a running average representation of the mean of the same data and hence both of these could be used interchangeably to analyse mean of statistical data against time [4].

3.5.3.1 Results

In the first scenario, we present the results for a rural environment with mobile speed = 3 km/hr. Fig. 3.9 presents a snap shot of the short term BF prediction error in terms of Cumulative MSE (CMSE) in dB against OFDM symbols. In other words this figure presents the transient and the steady state behaviour of BF in terms of prediction error for a specific SNR level. The error is presented in cumulative form so as to average the MSE over time and effectively shows how BF MSE converges to its steady state. For both $S = 3$ and $S = 9$ configuration, we assume the same channel conditions and Fixed LMS step size (μ) [5]. By fixing these parameters, we ensure that the convergence speed for both the cases is same and hence we only analyse the performance in terms "which achieves lower CMSE". We observe that with $S = 9$, the BF shows superior performance (by achieving lower CMSE) as compared to the case with $S = 3$. Moreover we also note that CMSE reduces with OFDM symbol numbers for both antenna element configuration and then becomes more or less constant indicating convergence. The minimum CMSE achieved for $S = 3$ is ≈ -6.5 dB while for the case of $S = 9$ is ≈ -7.5 dB.

Fig. 3.10 depicts the long term BF prediction error at the pilot sub-carriers in terms of Mean Squared Error (MSE) in dB. The MSE at any instant can be

[4] In our case BF prediction error against OFDM symbols

[5] This is done to ensure that channel or the step size does not affect convergence. Thus $S = 9$ does not converge faster to the $S = 3$ case even though it may appear to.

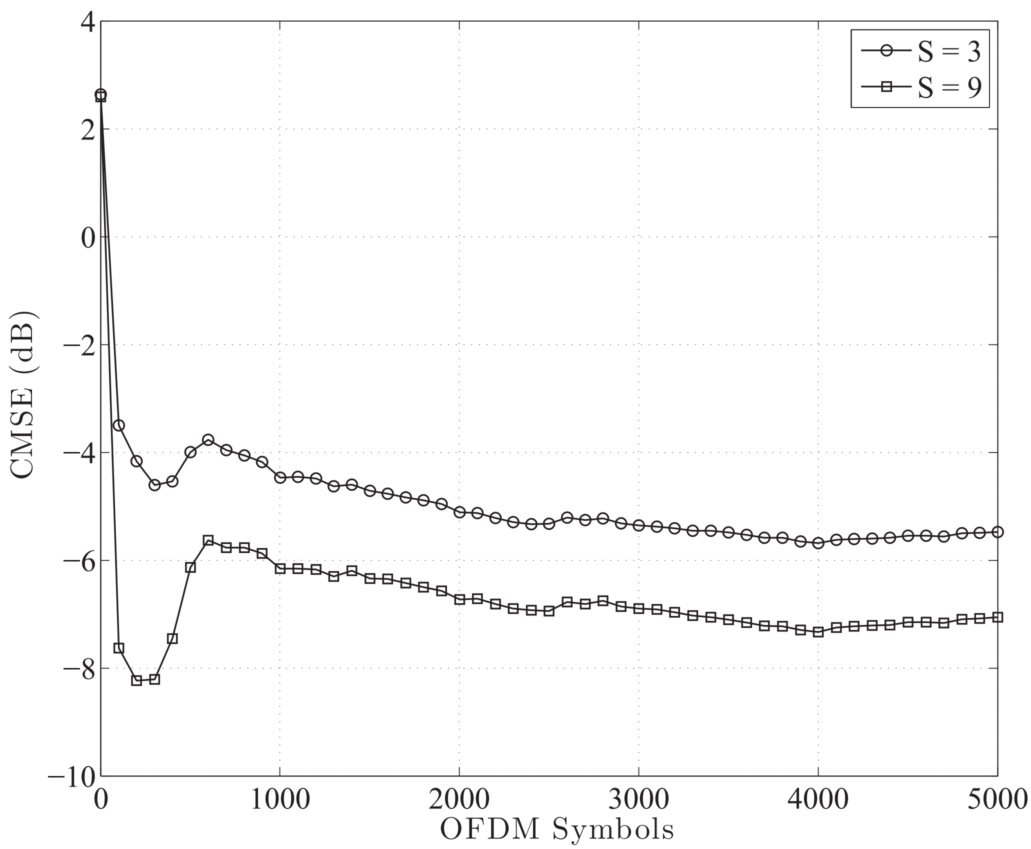

Figure 3.9: Beamforming convergence in terms of Cumulative Mean Squared Error vs OFDM symbols in rural environment with mobile speed = 3 km/hr, antenna elements = 3 & 9 and SNR = 20 dB.

derived from (3.13) and is plotted vs desired user Signal-to-Noise Ratio (SNR). We can note that as the available SNR increases, the MSE reduces indicating reduced difference between received and transmitted pilots of the desired user. In other words, at higher SNR, disturbances in the system are low and hence improved BF is observed. We can also observe that 9 antenna element configuration onboard the satellite yields far superior interference mitigation as compare to the case of 3. This is attributed to better CCI mitigation by the beamformer due to a higher degree of freedom available by having ULA with increased antenna elements.

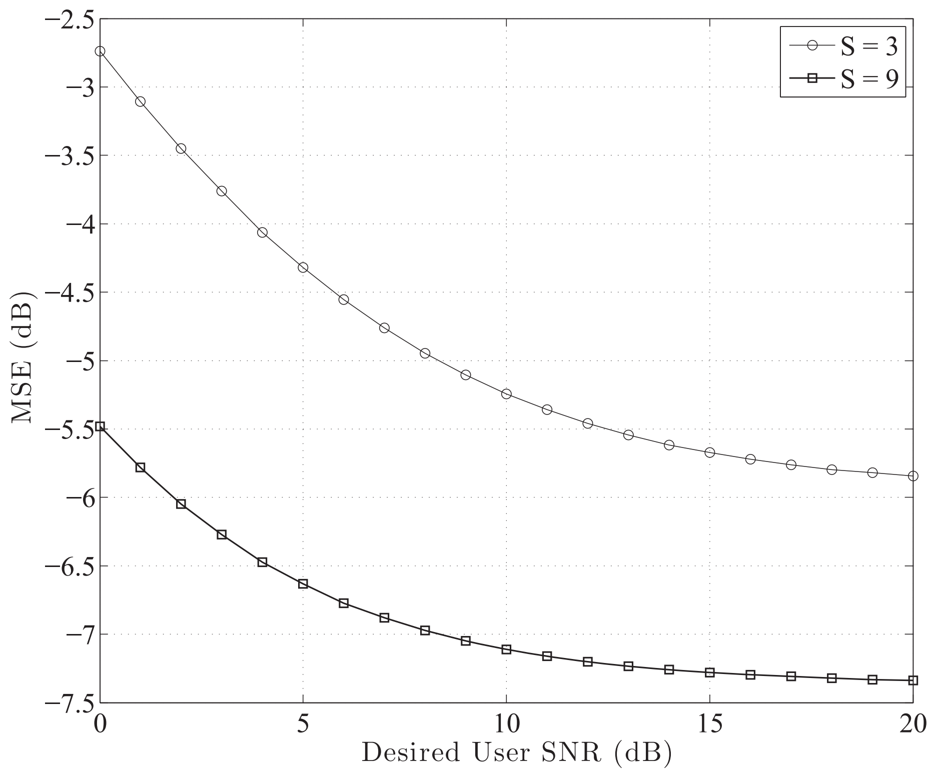

Figure 3.10: Beamforming prediction error in terms of Mean Squared Error vs desired user SNR in rural environment with mobile speed = 3 km/hr and antenna elements = 3 & 9.

The MSE achieved at SNR = 20 dB for both antenna element configuration is consistent with results presented in 3.9.

The main aim of BF is to reduce the interference in the system caused by the undesired sources. Hence to have further insight as well as validate beamformer's performance, we analyse the beam patterns in Fig. 3.11. We can observe that for both antenna element configurations, a high gain is projected towards the desired DOA whereas low gain is provided towards the direction of interferes. We also note that with the $S = 9$ case, gains projected towards interference source are lower as compared to when $S = 3$. This effectively means suprior interference mitigation with more antenna element. To quantify how much interference is

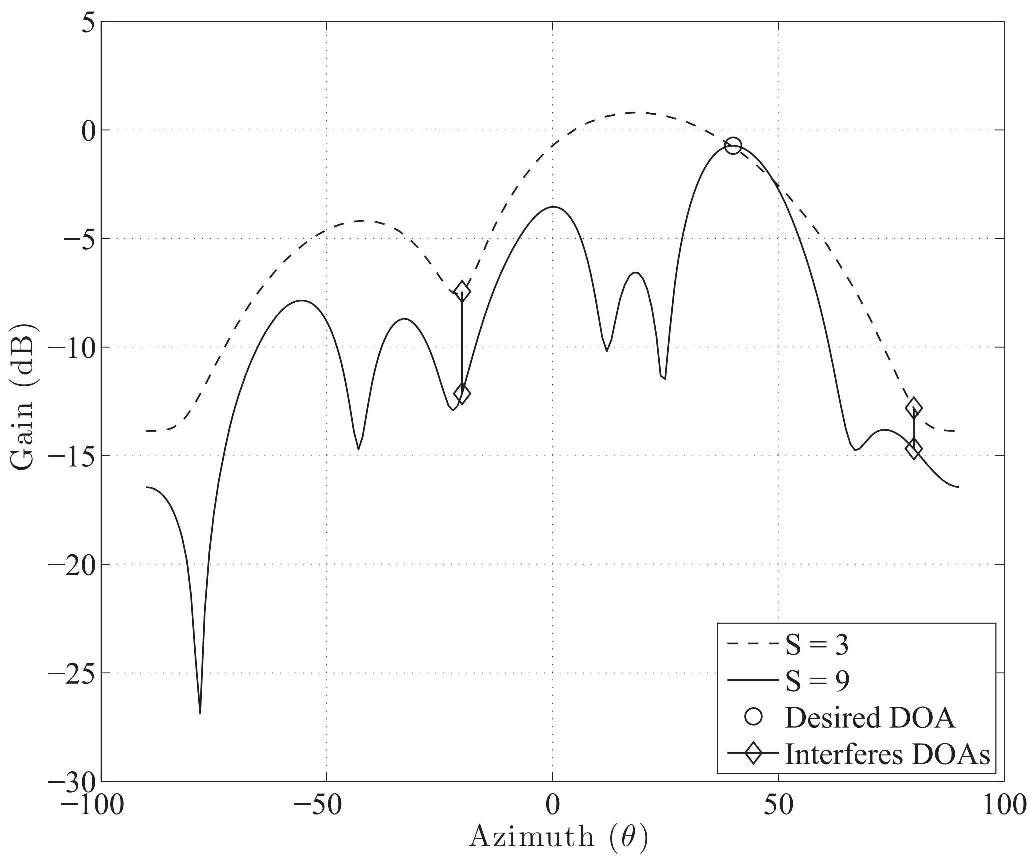

Figure 3.11: Beam patter in rural environment with mobile speed = 3 km/hr, antenna elements = 3 & 9 and SNR = 20 dB.

mitigated, we define a metric - Beamforming Gain (BFG) - as the gain projected towards the desired direction relative to the direction of interference sources. BFG corresponding to Fig. 3.11 is depicted in Fig. 3.12. We can see that for $S = 3$ configuration, the interference from the user at $-20°$ is suppressed by 8.24 dB whereas from the user at 80° is suppressed by 13.6 dB. The suppression improves with the $S = 9$ case, as user at $-20°$ is suppressed by 11.4 dB whereas the user at 80° is suppressed by 14 dB.

Fig. 3.13 shows the system performance in terms of Bit Error Rate (BER) versus desired user SNR with different antenna element configurations. We again note

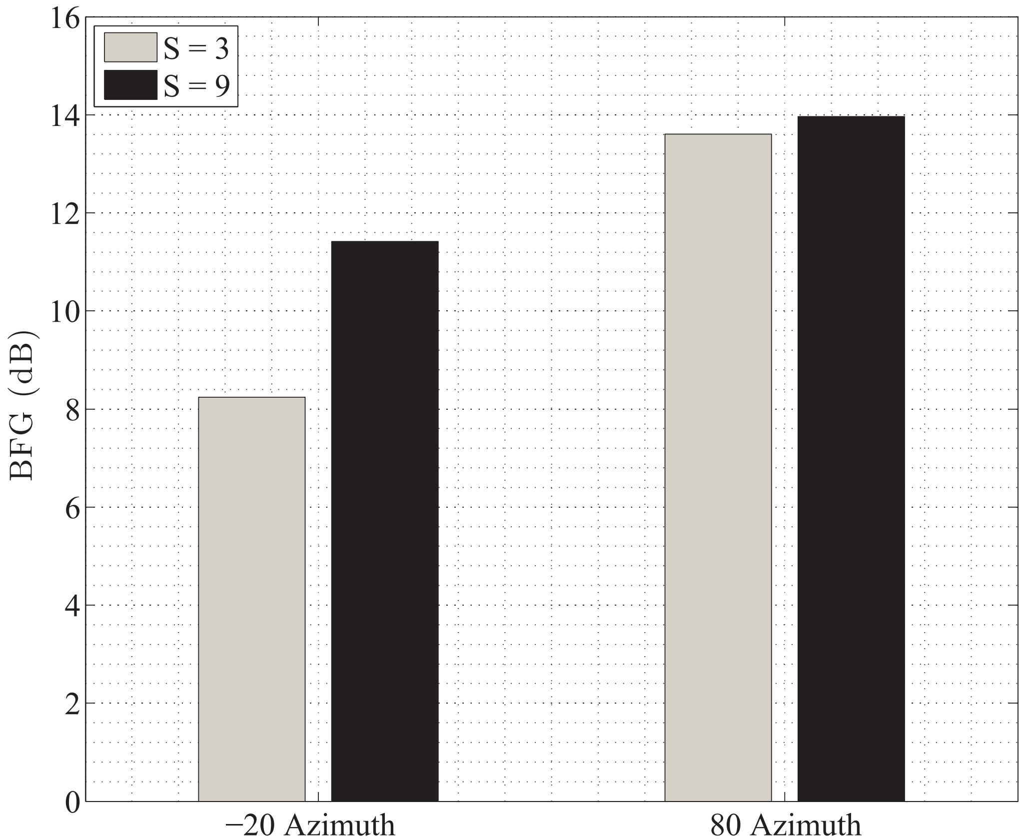

Figure 3.12: Beamforming Gain in rural environment with mobile speed = 3 km/hr, antenna elements = 3 & 9 and SNR = 20 dB.

that the BER improves for higher SNR. We can also observe that with increased number of antenna elements, the BER performance is superior. Both of these observations are consistent with the results presented earlier. To put the result in perspective, we quantify the BER Gain (BERG) provided for two extreme scenarios: Scenario 1 - SNR = 0 dB and Scenario 2 - SNR = 20 dB. For Scenario 1, $S = 9$ configuration provides a BER gain of $\approx$ 7 dB against the $S = 3$ case whereas for Scenario 2, the gain increases to $\approx$ 16 dB. This highlights the performance advantages available by increasing the number of antenna elements as it paves the way for better BF due to superior CCI mitigation.

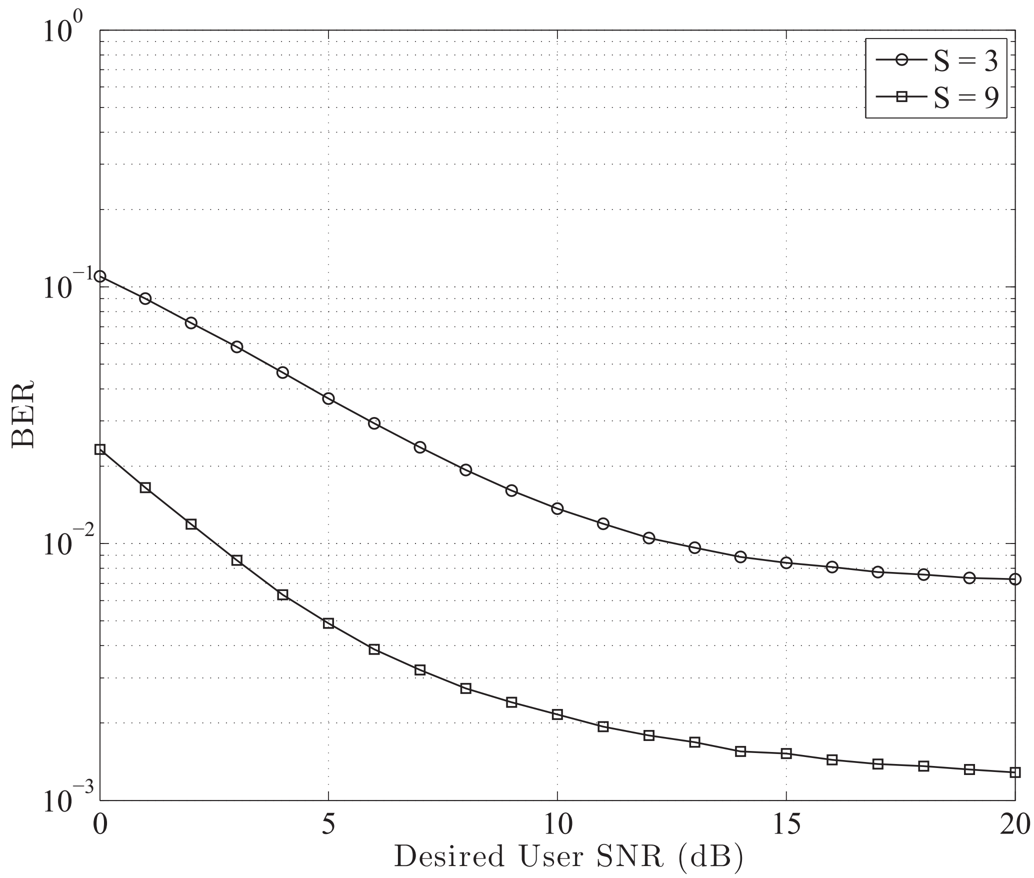

Figure 3.13: Bit Error Rate vs desired user SNR in rural environment with mobile speed = 3 km/hr and antenna elements = 3 & 9.

3.5.4 Impact of Environment and Mobility

In Section 3.5.3, we analysed BF as well as system performance in a rural environment. Now we investigate the impact in an urban environment on the system and compare it to the rural case. Moreover, we consider a mobile speed of up to 60 km/hr. In the first scenario, we choose pedestrian mobile speed of 3 km/hr with both MAESTRO channel cases to study the effect of environment. Fig. 3.14 presents the MSE results for these scenarios. It can be seen that over all possible SNR values tested, the BF process performs better in the rural case. This is at-

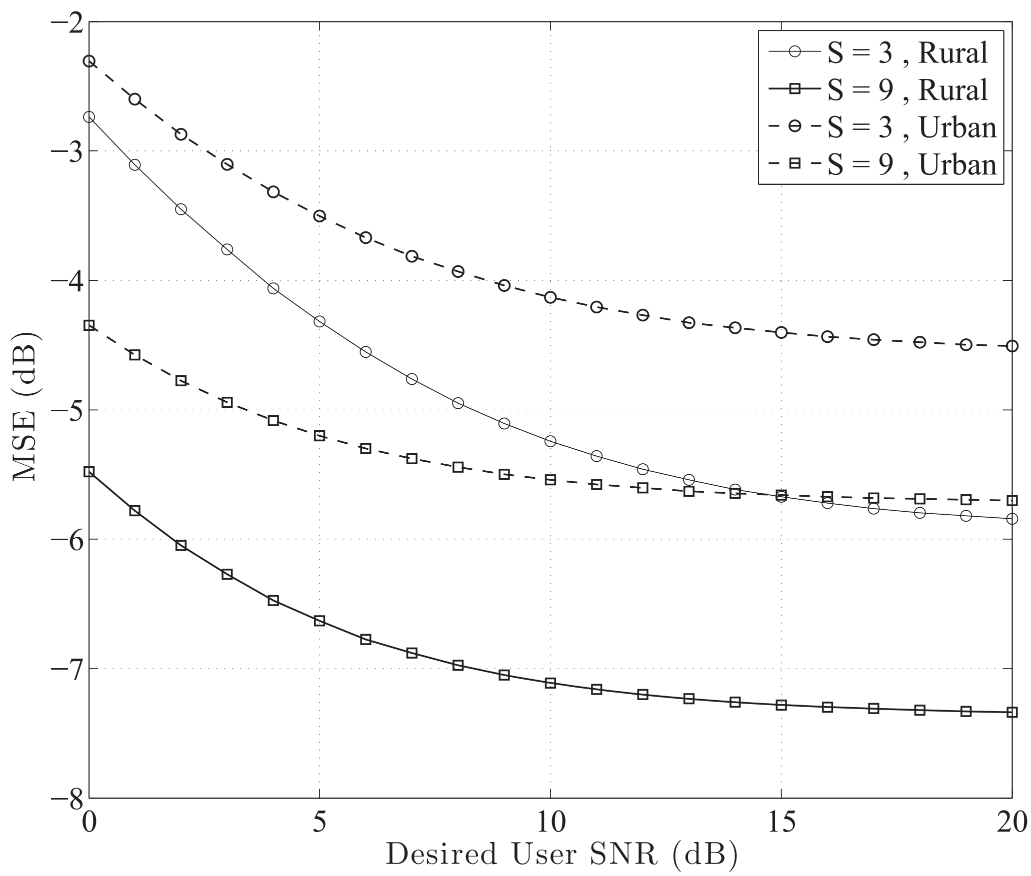

Figure 3.14: Beamforming prediction error in terms of Mean Squared Error vs desired user SNR in rural and urban environment with mobile speed = 3 km/hr and antenna elements = 3 & 9.

tributed to a lower Rician K-factor as well as a more frequency selective channel corresponding to the urban area. We also observe a performance improvement in terms of MSE when either the SNR or number of antenna elements are increased. To better analyse the result, we define a generic Precision Gain (PG) as the improvement achieved by the superior case in terms of MSE as compared to the inferior case(s) at a specific SNR value. In this chapter, PG is defined as the improvement in MSE for the case of rural environment as compared to urban. We reconsider the two extreme scenarios earlier described in Section 3.5.3. In

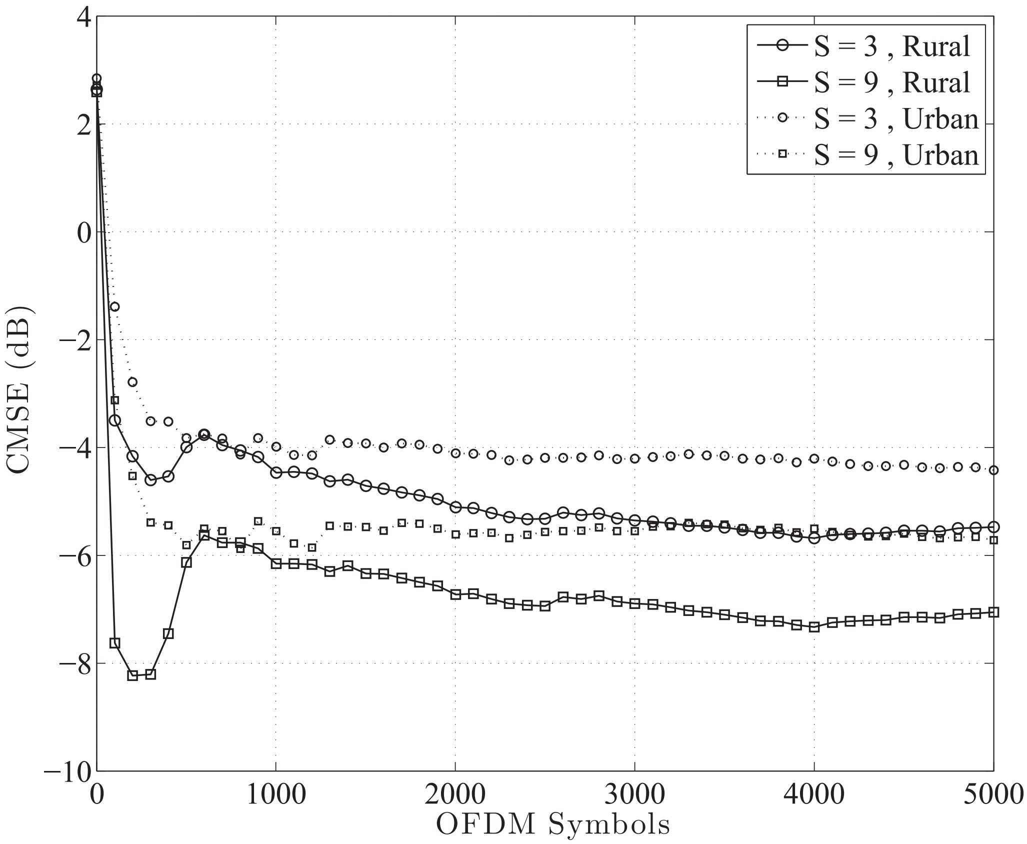

Figure 3.15: Beamforming convergence in terms of Cumulative Mean Squared Error vs OFDM symbols in rural and urban environment with mobile speed = 3 km/hr, antenna elements = 3 & 9 and SNR = 20 dB.

Scenario 1, the $S = 3$ configuration provides a PG of 0.43 dB, which increases to 1.04 dB with $S = 9$ configuration. In Scenario 2, the PG increases to 1.33 dB from 0.43 dB for the $S = 3$ case while for the $S = 9$ configuration, PG provided by BF process is 1.63 dB as opposed to the earlier 1.04. Hence we can see that PG increases when either SNR or antenna elements increase and is always higher in the rural environmental. This effectively translates to better BF in rural areas and at high SNR values.

In Fig. 3.15 we show a snap shot of the short term BF prediction error in terms

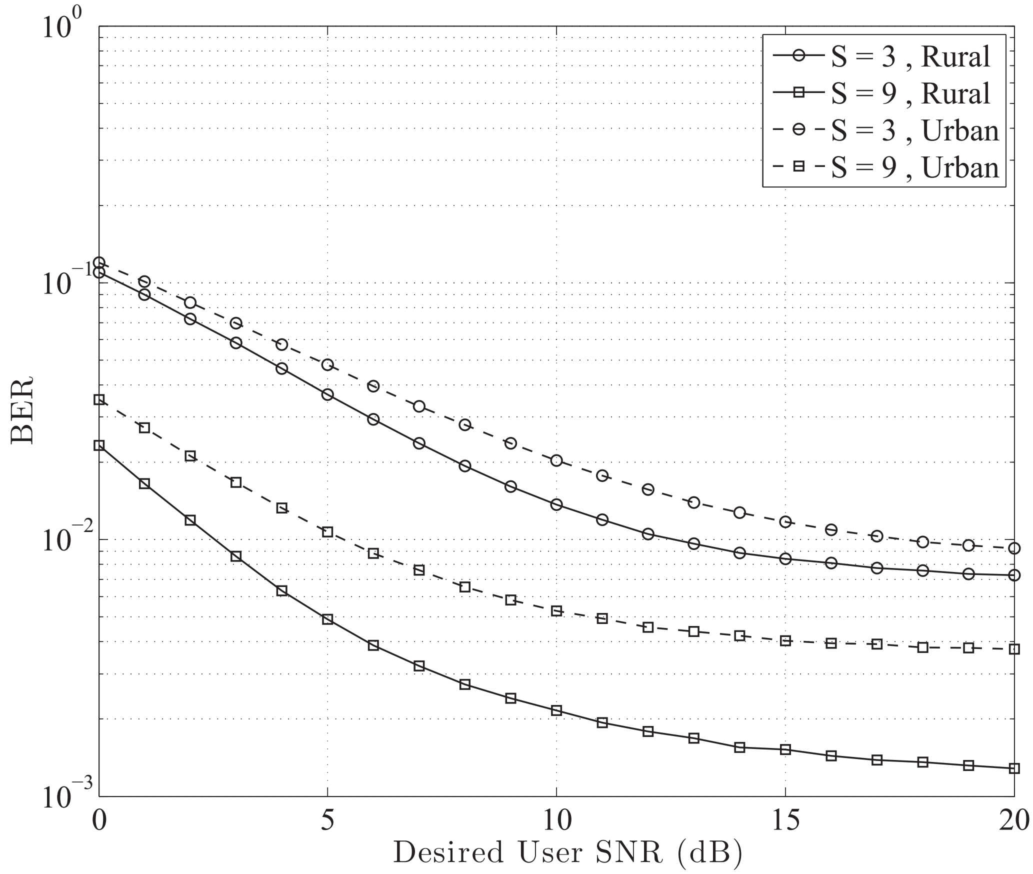

Figure 3.16: Bit Error Rate vs desired user SNR in rural and urban environment with mobile speed = 3 km/hr and antenna elements = 3 & 9.

of CMSE over a period of time for the same scenario. We can again observe that BF performs better for the rural case as compare to urban case and the performance improves as we increase the number of antenna elements. Moreover we also note that at first, MSE reduces with the number of OFDM symbols for both antenna element configurations and environments and then becomes more or less flat indicating convergence. The minimum CMSE achieved is consistent with the results presented in Fig. 3.14.

The overall system performance is presented in Fig. 3.16 which compares BER

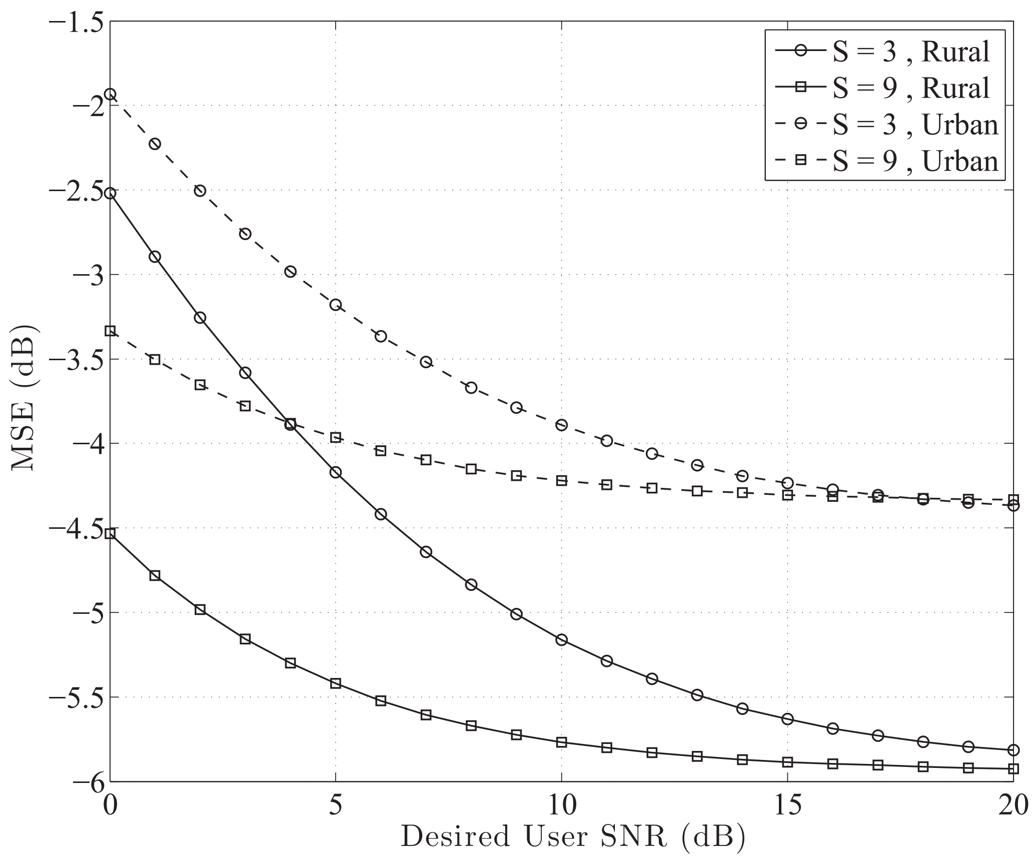

Figure 3.17: Beamforming prediction error in terms of Mean Squared Error vs desired user SNR in rural and urban environment with mobile speed = 60 km/hr and antenna elements = 3 & 9.

vs the desired user SNR. Irrespective of the environment and number of antenna elements, we note that an increase in SNR improves the BER which is attributed to the reduction in complex Gaussian noise. Moreover, in the case of 3 antenna elements, as the user moves from an urban to a rural area we observe improvement in system performance due to the milder channel conditions. Moreover, if the number of antenna elements are increased from 3 to 9 in the same scenario, significant improvement in BER is observed.

In practice, user speeds are much higher and evaluation of performance in such

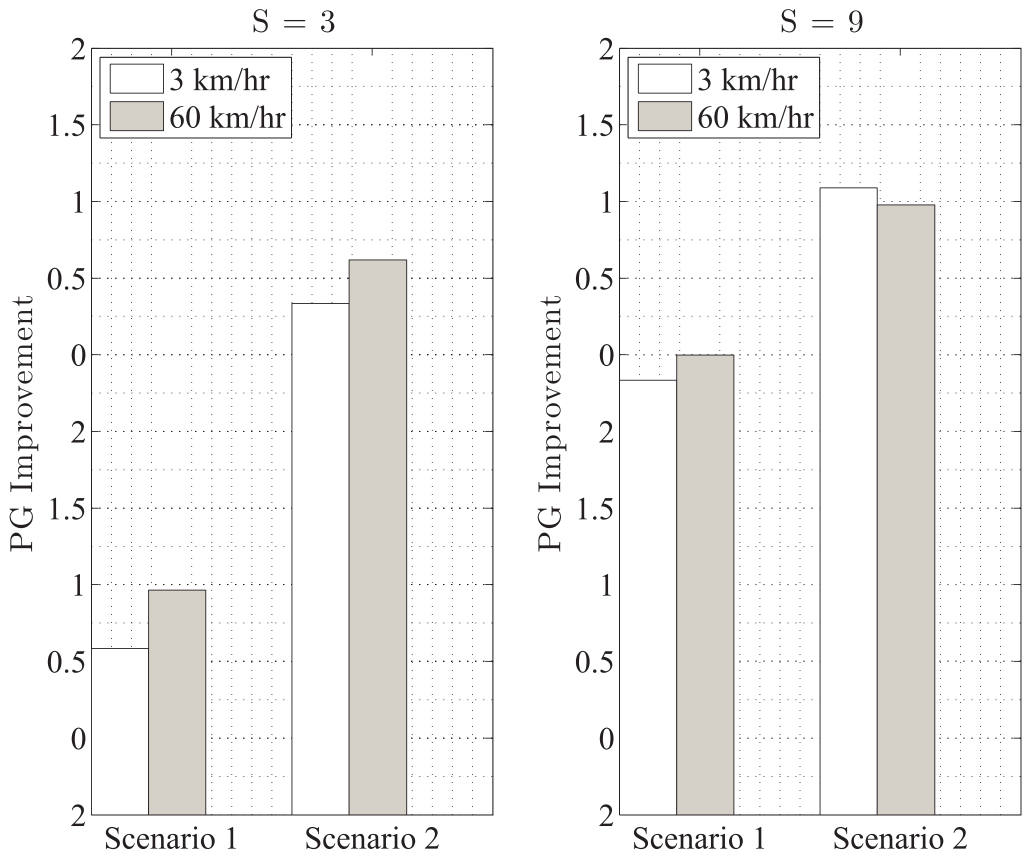

Figure 3.18: Precision Gain improvement for two scenarios relative to urban environment with mobile speed = 3 & 60 km/hr and antenna elements = 3 & 9.

scenarios is necessary. Hence we now study the BF performance for the case of higher user speed in rural as well as urban environment. Fig. 3.17 shows the MSE of BF for user speed of 60 km/hr for both the MAESTRO cases. Congruent with earlier results, we note that increase in either the SNR or number of antenna elements results in improved performance. However for the scenario under study, we can also observe degradation in MSE due to higher mobile speed as compared to the case of 3 km/hr. Higher speed translates to increased time selectivity in the channel and higher ICI, which in turn results in poor CE. Furthermore, we observe degradation in MSE as compared to the case of 3 km/hr in Fig. 3.14

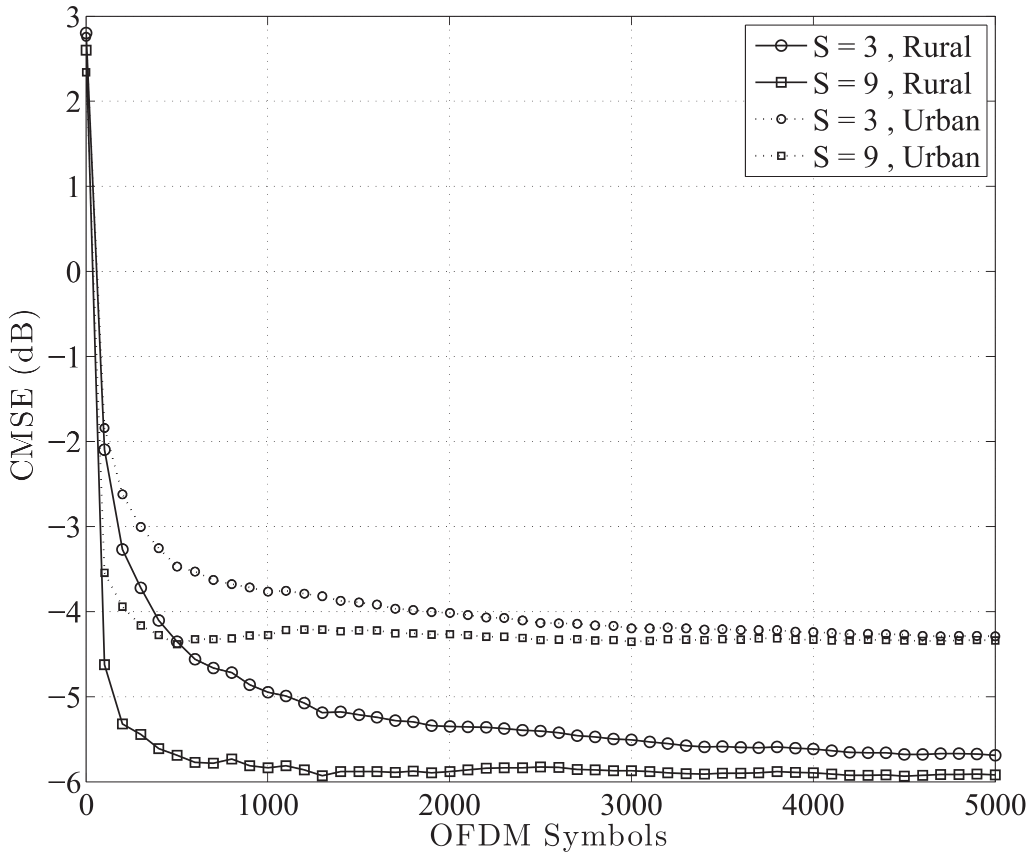

Figure 3.19: Beamforming convergence in terms of Cumulative Mean Squared Error vs OFDM symbols in rural and urban environment with mobile speed = 60 km/hr and antenna elements = 3 & 9.

when users in rural areas move to urban areas. To highlight this observation, in Fig. 3.18 we compare the improvement in PG as the user moves from urban to rural environments for the two mobile speeds in the extreme scenarios described in Section 3.5.3. It is clear from the results that in general, a higher PG is observed as the user moves from urban to rural environments. Moreover, improvement is noted for the case of 9 antenna elements as compare to 3 antenna elements. As the interference scenario remains unchanged, performance degradation in MSE depicted in Fig. 3.17 and Fig. 3.18 at higher mobile speed is dominated by poor

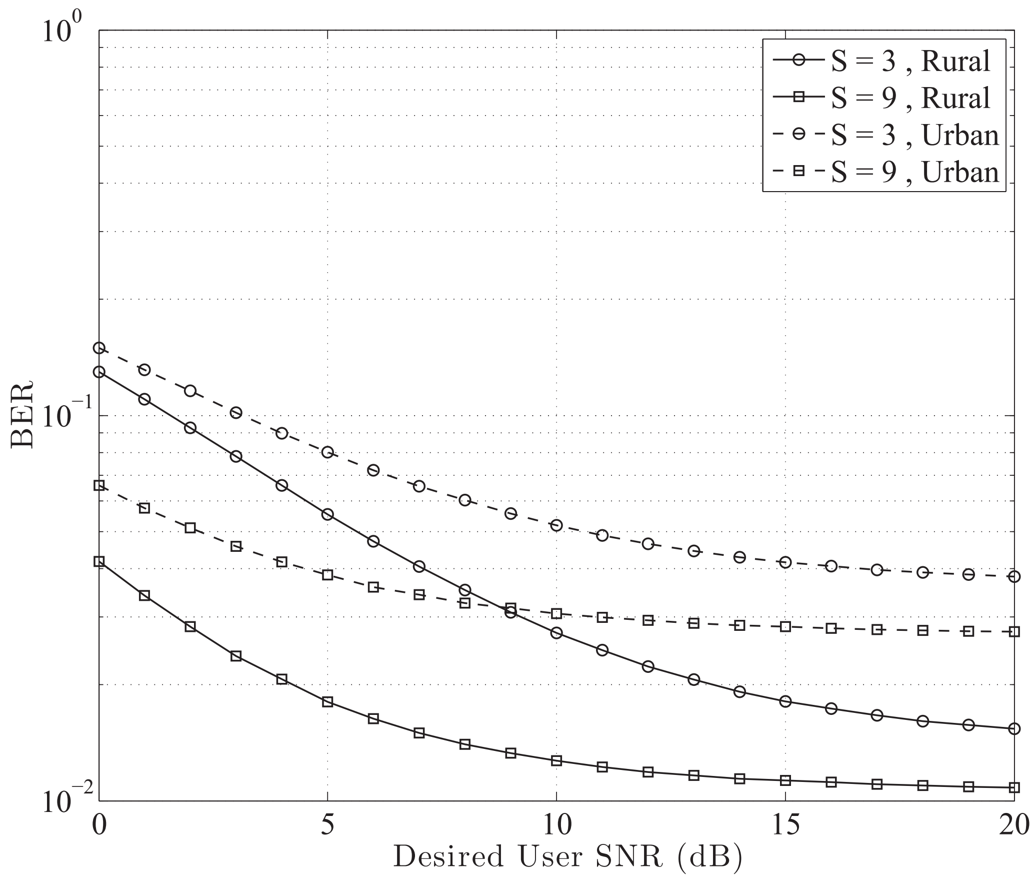

Figure 3.20: Bit Error Rate vs desired user SNR in rural and urban environment with mobile speed = 60 km/hr and antenna elements = 3 & 9.

CE rather than BF. This also highlights the importance of CE and whilst BF tries to mitigate interference, it is unable to compensate the channel effect.

For the high mobility case, we now discuss how the short term CMSE is affected. Fig. 3.19 shows the comparison of CMSE against number of OFDM symbols for a similar scenario. We again note the consistent trend of improved CMSE as number of OFDM symbols or receive antenna elements increases. Moreover, the performance in rural case is superior when compared to the urban case. We can also observe a much higher minimum CMSE value irrespective of the antenna

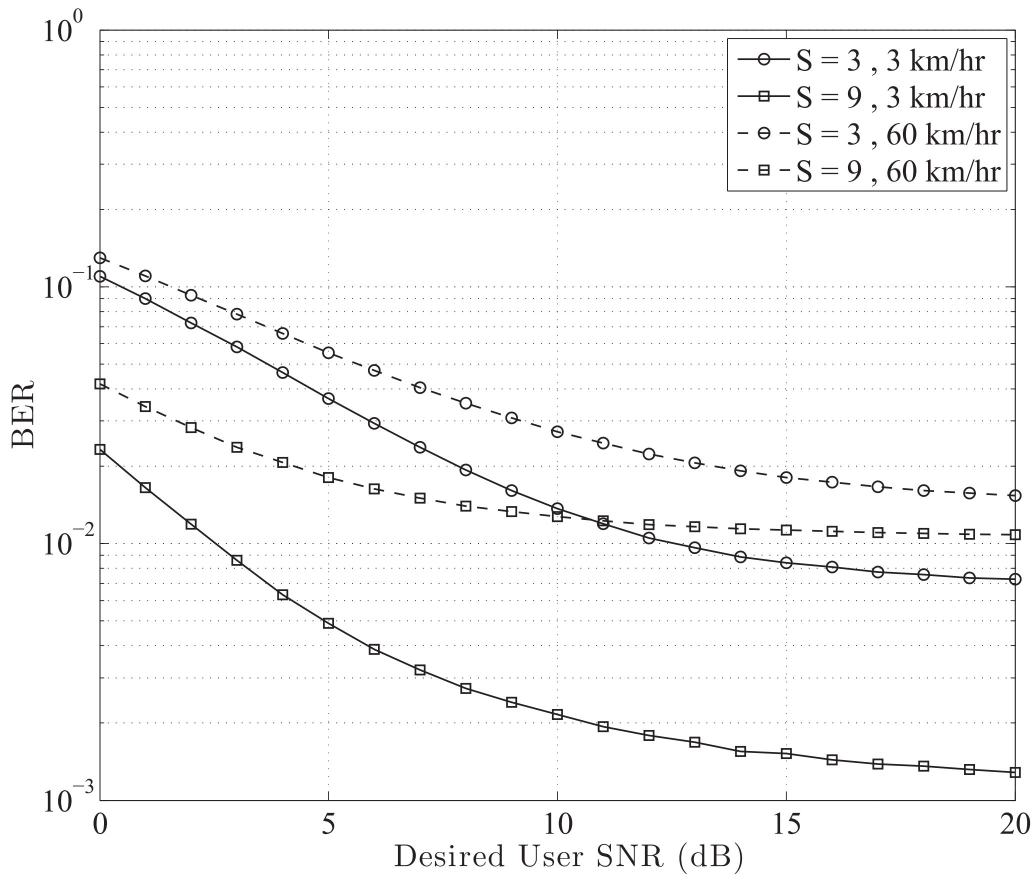

Figure 3.21: Bit Error Rate vs desired user SNR in rural environment with mobile speed = 3 & 60 km/hr and antenna elements = 3 & 9.

elements as compare to the 3 km/hr case in Fig. 3.15. This is consistent with our results discussed in Fig. 3.17 and Fig. 3.18.

The main metric for analysis of system performance of our model is BER. Fig. 3.20 presents the results for the 60 km/hr scenario. We observe again that as noise reduces in the system, a superior BER is achieved. Moreover, improved BER is observed with increase in antenna elements for the rural case as compared to the urban case. To gain further insight into system performance, we compare the BER results for the rural case only at two speeds. These are depicted in Fig. 3.21.

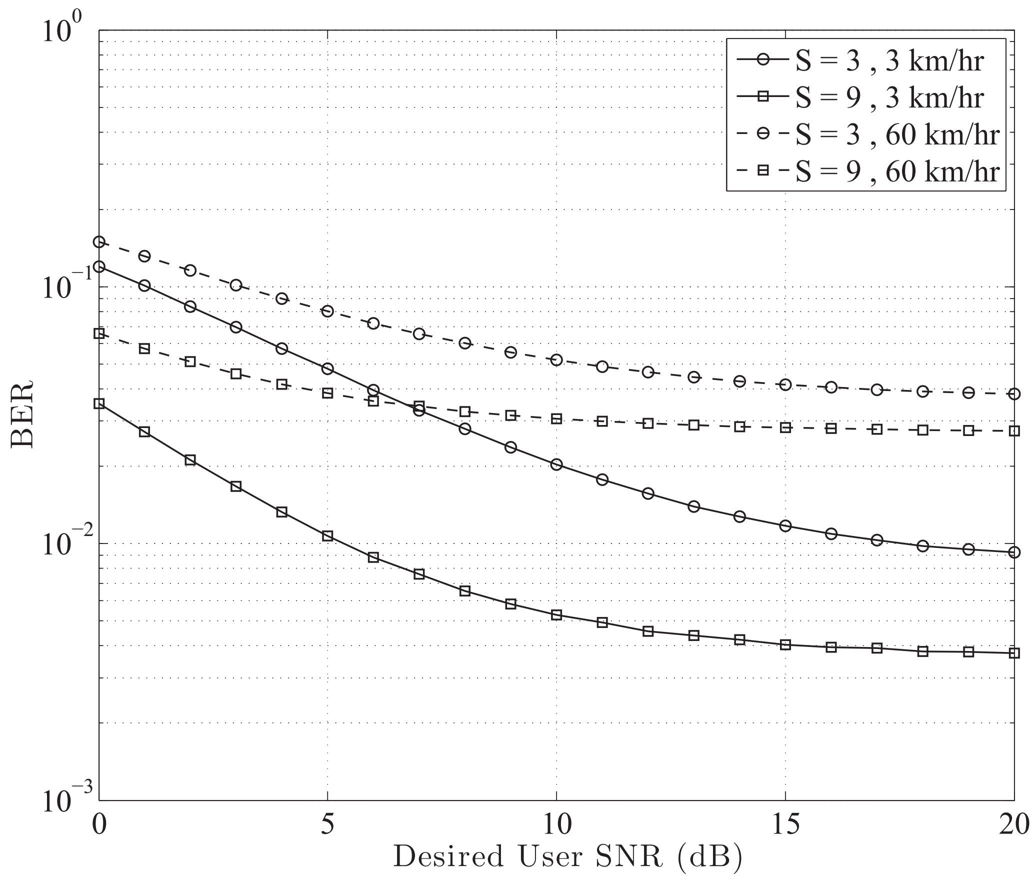

Figure 3.22: Bit Error Rate vs desired user SNR in urban environment with mobile speed = 3 & 60 km/hr and antenna elements = 3 & 9.

We can clearly see the effect of speed when the environment remains constant. Severe degradation is observed when the speed increases from 3 to 60 km/hr irrespective of the SNR value or number of antenna elements. The impact is so large that the performance of the 9 antenna case with 60 km/hr is worse than the case with 3 antenna elements at 3 km/hr. This magnifies the importance of CE in the system and shows that BF alone cannot yield acceptable system performance. A similar result is presented for the urban environment in Fig. 3.22. The general tend observed is the same, however the BER degrades further as compared to Fig. 3.21 due to worse channel conditions in the urban environment as was also

Scheme	**Attributes**
INC	Interference sources are considered in the system BER computation considers all OFDM symbols received
NINC	No Interference is considered in the system BER computation considers all OFDM symbols received
IC	Interference sources are considered in the system. BER computation ignores first $\widetilde{L}$ OFDM symbols
NIC	No Interference is considered in the system. BER computation ignores first $\widetilde{L}$ OFDM symbols
NINC-OBF	No Interference is considered in the system. BER computation considers all OFDM symbols received Optimum BF is performed (Section 3.4.2.2)

Table 3.2: Modelled schemes to investigate error floor and convergence behaviour observed in Fig. 3.20.

3.5.5 Convergence Issue and Concurrent BF & CE Problem

A comprehensive analysis of system performance for the proposed HTSMS was presented in Section 3.5.3 and Section 3.5.4. From the BER results we can clearly observe that there is an error floor irrespective of the antenna elements configuration, rural/urban environment or the mobility scenario. To have a complete insight into the system behaviour, we de-couple the BF and CE processes by operating the system in an AWGN only scenario. Hence only the BF processing is performed with Gaussian noise as the only disturbance in the system. Tabulated in Table 3.2 are five distinctive schemes that we define to analyse the error floor and its impact on convergence behaviour of the system. Fig. 3.23 presents the

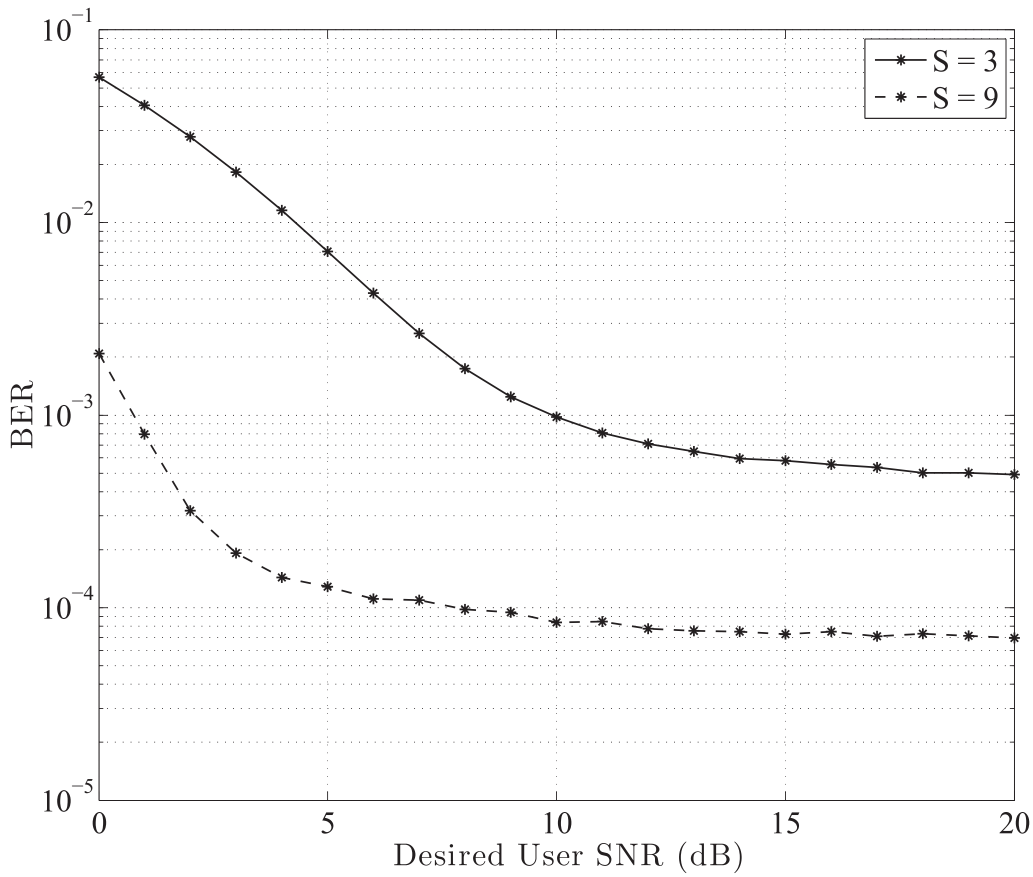

Figure 3.23: Bit Error Rate vs desired user SNR for INC scheme, antenna elements = 3 & 9.

BER results for INC scheme. We note that BER reaches $\approx 10^{-4}$ which is lower than in the case of the wireless channel ($\approx 10^{-3}$). However, interestingly the error floor still exists in the absence of the wireless channel.

Now to get a picture of system behaviour in the absence of interference as well as the channel, we investigate performance of the NINC scheme and compare it to INC. The BER for the INC and NINC is plotted in Fig. 3.24. We observe that BER performance further improves, however the error floor still exists. This effectively means that the error floor is least affected due to the channel state, mobile speed or the interference in the system.

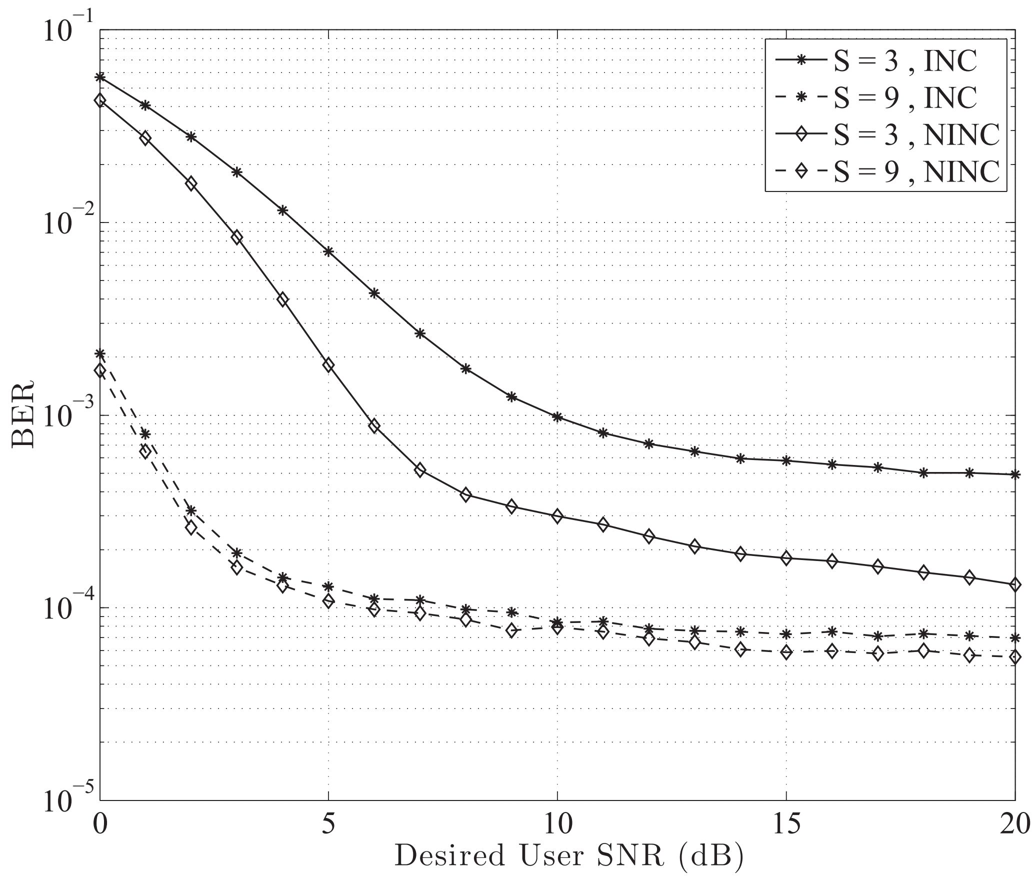

Figure 3.24: Bit Error Rate vs desired user SNR for INC and NINC scheme, antenna elements = 3 & 9.

As adaptive BF starts, some OFDM symbols are consumed by the BF process for the purpose of convergence of the weights. This behaviour was observed in Section 3.5.3 and Section 3.5.4. BF is an adaptive process that tries to adapt its weights so as to accept the desired signal and reject signals from interference sources. Even if there is no interference in the system, BF still takes some time for weights convergence so as to accept the signal from the desired direction. To get an idea of how the performance is affected if we don't include the convergence phase in BER computation, we ignore (clip) $\widetilde{L}$ initial OFDM symbols. For the interference and interference fee scenario, these are referred to as IC and NIC

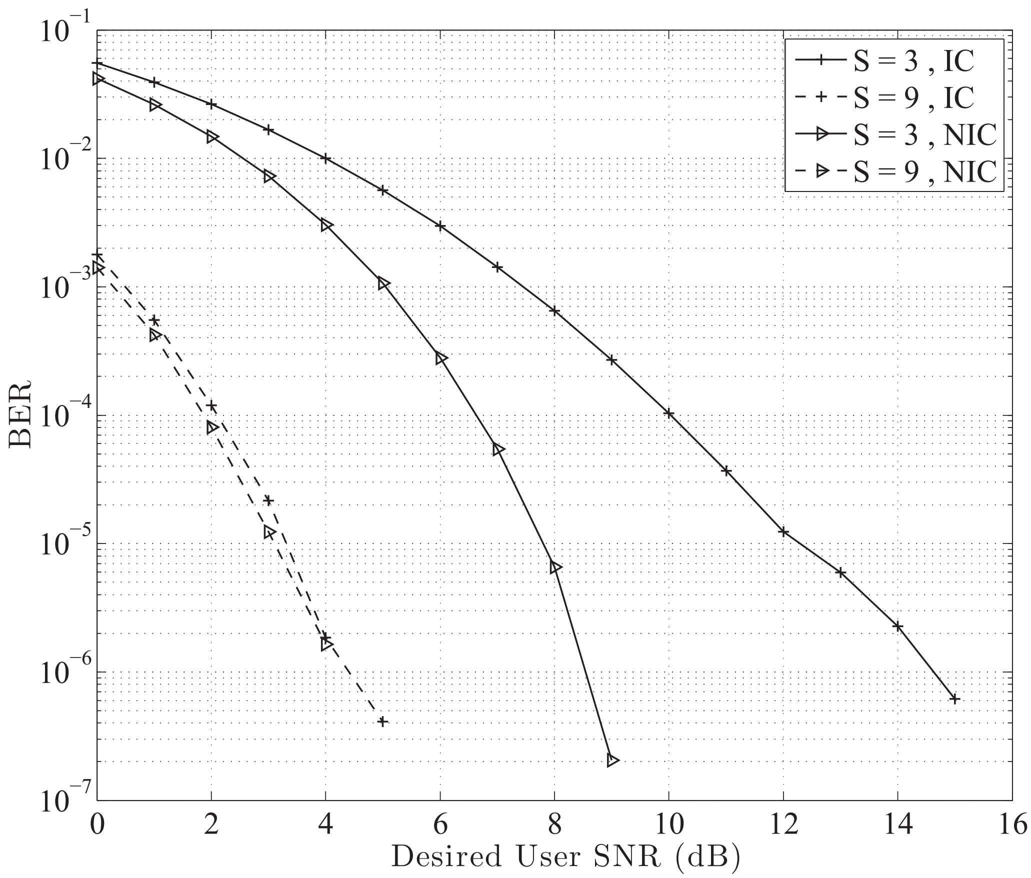

Figure 3.25: Bit Error Rate vs desired user SNR for IC and NIC scheme, $\widetilde{L} = 1000$ and antenna elements $= 3$ & 9.

schemes respectively, we ignore the first 1000 OFDM symbols to see the impact on the error floor as well as the BER performance. Fig. 3.25 presents the BER and it can be seen that no error floor at all persists in the system, irrespective of whether interference is present or absent. We also note that with the 9 antenna elements configuration, the performance of interference and interference free cases are almost identical. Furthermore, this elaborates that having more antenna elements can improve system performance. This magnifies the importance of BF convergence and its impact on system performance. This motivates us to devise techniques that can improve BF convergence. Furthermore, the result in Fig. 3.25

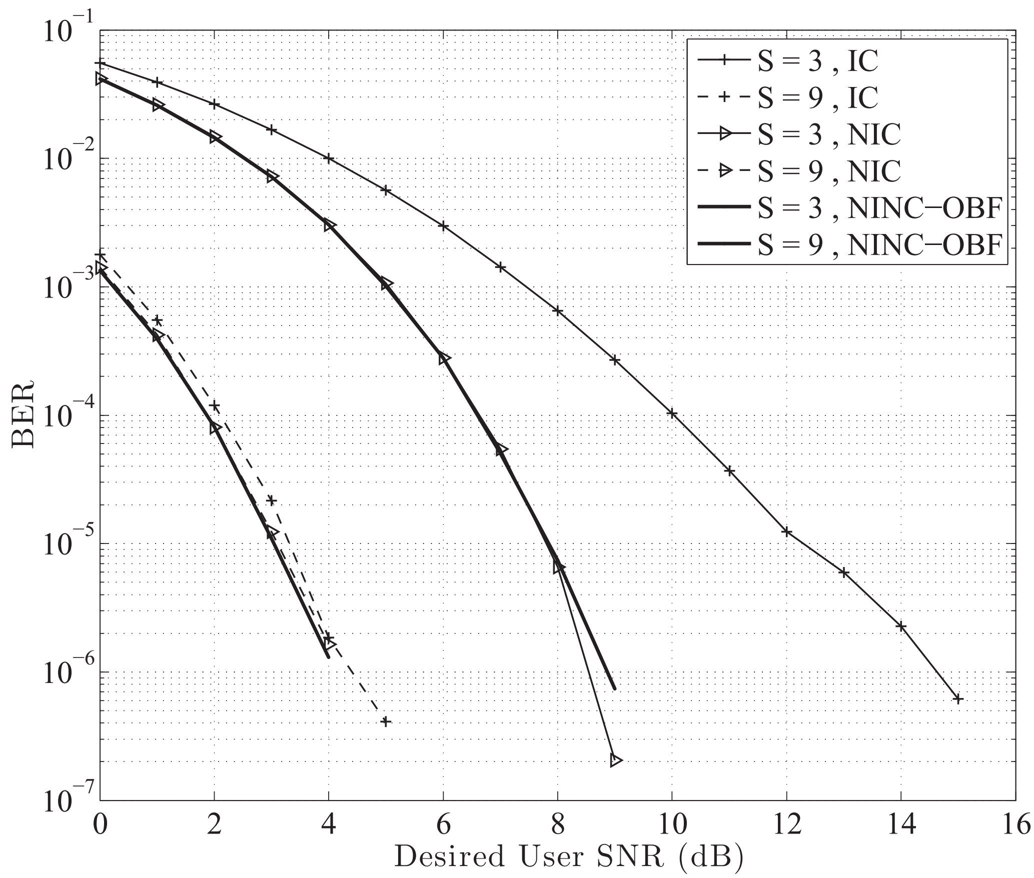

Figure 3.26: Bit Error Rate vs desired user SNR for IC, NIC and NINC-OBF schemes, antenna elements = 3 & 9.

validates our system model as the BER is comparable to the other results found in literature [46].

To further validate our work, we compare the results in Fig. 3.25 to the case when OBF is performed, presented in (3.21)−(3.24). We employ the scheme NINC-OBF and the BER results are shows in Fig. 3.26. We can clearly see that BER curves for NIC and NINC-OBF exactly overlap each other. This means the performance of BF with clipping the initial $\widetilde{L}$ is the same as OBF in the absence of interference. This further validates our implemented BF capable OFDM transceiver architecture.

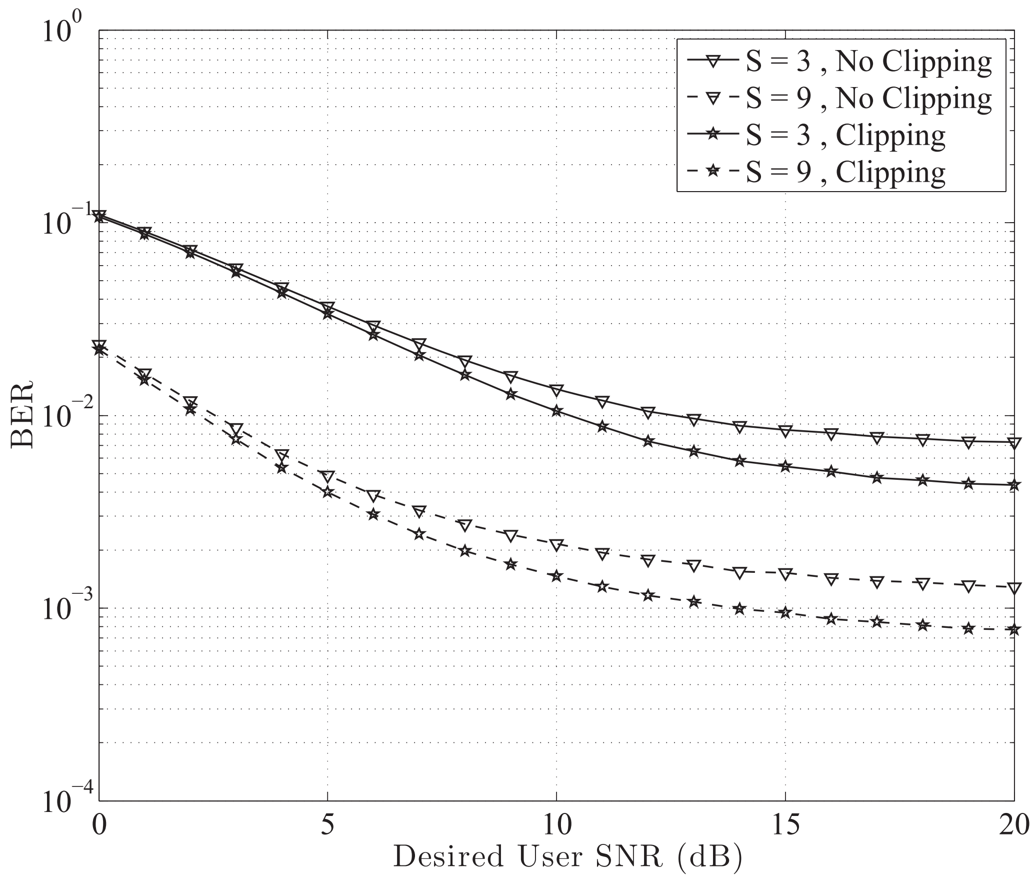

Figure 3.27: Bit Error Rate vs desired user SNR with and without clipping in rural environment with mobile speed = 3 km/hr, antenna elements = 3 & 9 and $\widetilde{L} = 1000$.

Finally we investigate how the clipping impacts system performance in the presence of channel fading and time selectivity. Hence we revisit the scenario in Section 3.5.4 and present the BER results in Fig. 3.27 for the rural environment with user speed of 3 km/hr with and without clipping. We can observe that ignoring the first 1000 symbols produces a performance improvement in BER, however the improvement is not as drastic as was seen in the case of the AWGN channel scenario. The reason for this is related to CE while BF is converging. From results presented earlier, we know that CE has significant impact on system performance. During the transient state of the BF process when it is trying to converge the CE block is also operating in parallel. We refer to this problem as the concurrent processing of BF and CE. During the BF transient state, CE is carried out on pilot sub-carriers which are not interference free. Hence in the presence of the interference, CE cannot yield accurate results. While accurate estimation requires the signal at the output of the beamformer to be interference free, this is not available to the CE block until the beamformer converges.

3.6 Conclusions

In this chapter we proposed an OFDM based HTSMS where satellite and existing mobile terrestrial networks amalgamate in a transparent fashion. Adaptive BF onboard the satellite is then utilised to mitigate uplink CCI arising due to frequency reuse. We have investigated this system in rural and urban environments with different schemes and mobile speeds and evaluated system performance. The simulation results show an improved system performance with increase in antenna elements. This was expected since more elements translate to better interference mitigation. In addition, as the user travels from a rural to an urban area, degradation in performance is observed. We also investigate the existence of the error floor in BER results due the BF. We devise schemes namely INC, NINC, IC, NIC to investigate the problem and find that the floor primarily exists due to the convergence time. We also present the results with Optimum BF in the absence of interference (NINC-OBF) which validate our system model. We have further investigated the interplay between BF and CE. We find that even though the beamformer tries to converge to the desired user, it is not able to cancel the channel effect. Thus the channel estimator is essential and the beamformer alone cannot produce acceptable performance. We also identify that concurrent operations of BF and CE can lead to poor performance in the presence of interference.

We address this problem in the next chapter and propose a preamble based BF approach to solve the problem.

Chapter 4

Preamble based Beamforming for HTSMS

This chapter provides an overview of the approaches that can improve BF convergence. We then propose a preamble incorporated beamformer based on pilot reallocation for the HTSMS. Subsequently, we compare the proposed approach with several existing algorithms to establish its performance advantages. Part of the work presented here has been published in *Proc. IEEE on IWSSC 2009* [77] and in *Proc. AIAA on 28th ICSSC 2010* [78].

4.1 Introduction

In Chapter 3 we proposed an OFDM based HTSMS architecture which combines the advantages of satellite and terrestrial networks. HTSMS, based on frequency reuse between satellite and terrestrial networks, offers true global coverage in an integrated framework. However frequency reuse induces CCI to the satellite from terrestrial users for which we employed an LMS based Pre-FFT adaptive BF. We then studied the system performance in satellite channel scenarios and investigated the interplay between BF and CE. Concurrent processing of BF and CE was identified as problematic in the presence of interference. In this chapter we first discuss factors that influence the performance of LMS based OFDM BF and then based on the discussion propose a preamble based BF approach as a potential solution to the aforementioned problem. Advantages of using the preamble based approach are twofold, 1) Reduction of convergence time which in-turn translates to faster BF and hence better system performance and 2) De-coupling the BF and CE processes during transient state enabling CE on interference mitigated sub-carriers. Simulation results show that preamble based transmission methodologies outperform alternative receiver side strategies such as NLMS, VSS-LMS.

4.2 Related Work and Problem Formulation

BF or any adaptive filtration based process aims to approach the scenario specific optimal solution. This phase of reaching an optimal point is referred to as the transient state. Once reached, the phase thereafter is referred to as the steady state. Specific to BF, the transient state defines the convergence behaviour of the beamformer and is critical to overall system performance as shown in Chapter 3. Within the domain of LMS BF, factors that influence the convergence behaviour are 1) numbers of BF weights, 2) LMS step size μ, 3) number of reference signals and 4) design of reference signals or OFDM frame structure.

To improve performance of an OFDM beamformer, the number of complex weights can be increased by employing a Post-FFT [79] approach where the total number of weights per antenna element are greater than one. However this makes the BF process more complex [48]. An alternative approach to improve performance is to employ a larger array of antenna elements. This would contribute to superior interference mitigation. However this not only increases the hardware costs but also increases BF convergence time.

Another approach to enhance the convergence performance of the BF is to optimise the LMS step size μ. In conventional LMS, μ is considered constant and independent of the received signal characteristics and algorithm's convergence behaviour. This is referred to as Fixed Step Size-LMS (FSS-LMS) as we employed in Chapter 3. Deviation from this convention is Variable Step Size-LMS (VSS-LMS) [70, 80] that adaptively changes μ to achieve the objective of faster conversion and minimum misadjustment. Another variant of LMS is the Normalised-LMS (NLMS) [81, 82] that offers faster convergence for both correlated and whitened data input [83]. VSS-LMS and NLMS can offer faster convergence while having slightly higher complexity as compared to FSS-LMS but is much simpler as compared to employing Post-FFT or increasing the number of antenna elements.

Yet another aspect that influences the beamformer's convergence is the design of pilots [53], which are responsible for coherence detection. The impact of pilots has been studied extensively for OFDM systems with focus on CE [45, 69, 84–86]. In the OFDM based Worldwide Interoperability for Microwave Access (WiMAX) [29, 30] system, the uplink frame structure constitutes of preamble symbols which are formed of pilots. Traditionally preambles are not transmitted in the uplink [87] due to the presence of interference. But with BF mitigating interference, preamble transmission on the uplink becomes viable for improved detection performance [88].

In non-blind OFDM based BF, the resources utilised to reach the steady state impact the overall data throughput. Irrespective of the LMS beamformer, using a preamble based transmission can significantly reduce the transient state time thus enabling faster detection and better performance. However, preamble transmission would consume power as well as bandwidth. While the use of preamble incorporated transmission is found in the literature, its applicability and optimisation specific to BF is to the best of our knowledge not studied. In light of this we propose an adaptive beamformer based on pilot reallocation [77,78]. The main idea is to disperse the pilots from OFDM symbols and reposition them to form a preamble at the transmitter side. This preamble, transmitted prior to data OFDM symbols, guarantees faster convergence without affecting data throughput. Within it also lies the solution of the concurrent BF and CE processing problem. During preamble transmission, the receiver initiates BF whilst CE as well as decoding of the desired user data only begins after this preamble phase. This decouples CE from BF as CE only takes place after interference is mitigated by BF.

We also study the impact of pilot density in the preamble and its length on the beamformer's convergence, throughput and overall system performance. Schemes studied include Fully-Dense Preamble (FDP), Partially-Dense Preamble (PDP) and Reduced-Length Preamble (RLP). The preamble in FDP and PDP schemes are 100% and 50% constituted of pilot sub-carriers respectively. In case of the FDP, due to its predetermined preamble length, some of the pilots are still transmitted even after the beamformer converges, thus wasting valuable throughput. In this regard we propose RLP, a scenario tailored preamble length that saves on resources. For the scenario observed in the given simulation, RLP is 35% shorter than FDP in terms of preamble length. However as mentioned earlier, pilot design is not the only solution to improve beamformer convergence. Application of VSS-LMS, NLMS or other variants of LMS algorithm would also effect the transient behaviour of the beamformer. Employing a Pre-FFT beamformer due to complexity constraints onboard the satellite, we compare the performance of the proposed schemes with FSS-LMS, NLMS and VSS-LMS. Our results show that the preamble based approach provides far better convergence than FSS-LMS, NLMS and VSS-LMS in a terrestrial-satellite scenario.

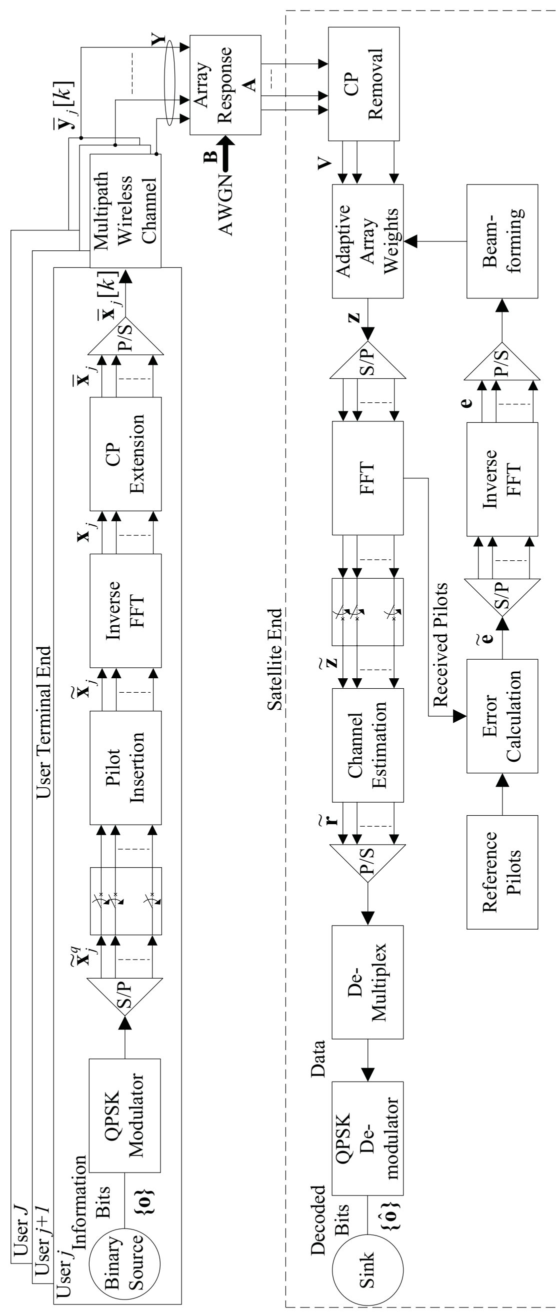

Figure 4.1: OFDM system for HTSMS with preamble based transmission strategies

4.3 System Model

The HTSMS uplink scenario and the interference model is the same as depicted in Chapter 3, Fig. 3.3 and Fig. 3.4 respectively. A link between mobile and satellite is modelled as SIMO with one desired user and $J-1$ interference users. Preamble based transmission is employed at the user terminal end whilst communicating with the satellite network. After the signal passes through the wireless channel, Pre-FFT BF is applied at the satellite end to mitigate interference. We also assume that no time or frequency offsets exist in the system.

4.3.1 OFDM Transmitter Model with Pilot Reallocation

Fig. 4.1 illustrates the transceiver architecture of the proposed OFDM based HTSMS and will be referred to throughout the remainder of the chapter in order to follow the information flow in the system. In conventional OFDM transmission, pilots are uniformly interspersed at known locations over all OFDM symbols. However in the presence of interference this results in poor CE during the transient BF state. To address this problem we propose a pilot reallocation scheme where predefined numbers of pilots from every symbol are dispersed to form a preamble. This enables the beamformer at the receiver to converge prior to any CE processing.

In the proposed preamble based architecture, transmission takes place in two phases, namely Preamble Phase (PP) and Data Phase (DP). If in the conventional scheme a total of N_p pilots are uniformly distributed and $N_{p'}$ pilots per OFDM symbol are transmitted during DP of the proposed scheme, then the preamble length can be presented mathematically as:

$$L^{'} = \left\lfloor \frac{(N_p - N_{p'}) \times L}{N - N_{p'}} \right\rfloor \qquad (N_p - N_{p'}) \geq 0 \ , \tag{4.1}$$

where N and L represent the total number of sub-carriers in an OFDM symbol and total number of OFDM symbols transmitted respectively. We formulate three distinctive preamble based transmission strategies; namely Fully-Dense Preamble (FDP), Partially-Dense Preamble (PDP) and Reduced-Length Preamble (RLP). They differ in their structure and how the reallocated pilots are derived from (4.1) to form the preamble. If a total of N_{pp} pilots per OFDM symbol are transmitted during the PP, then for the different transmission strategies this can be presented mathematically as:

$$N_{pp} = \begin{cases} N & l \leq L^{'} \;\; (\mathrm{FDP, RLP}) \\ \frac{N}{2} & l \leq L^{'} \;\; (\mathrm{PDP}) \end{cases} , \tag{4.2}$$

where $l = 1, 2, \ldots, L^{'}, L^{'} + 1, \ldots, L$ is the indexing of OFDM symbols. It is clear from (4.2) that for the FDP and RLP cases, all the dispersed pilots form the preamble. However for RLP the preamble length is 35% shorter than for FDP. During the PP phase of PDP, half of the sub-carriers are pilots and half are data. The OFDM frame structure for the FDP, RLP and PDP transmission strategies is depicted in Fig. 4.2.

During DP of all the schemes and PP for the case of PDP only, random source data $\{\mathbf{o}\}$ for the j^{th} user ($j = 1, ..., J$), is QPSK modulated and then S/P converted to $\{\widetilde{\mathbf{x}}^{q}\}$. Pilots $\{\widetilde{\mathbf{x}}^{p}\}$ are inserted into data sequence $\{\widetilde{\mathbf{x}}^{q}\}$ at known pilot sub-carrier locations $\mathcal{I}$ to form an OFDM symbol $\widetilde{\mathbf{x}} = [\widetilde{x}(0), \widetilde{x}(1), \ldots, \widetilde{x}(N-1)]^{T}$ with N sub-carriers. For the case of FDP and RLP, $\widetilde{\mathbf{x}}$ consists of only pilots during PP whereas for PDP, $\widetilde{\mathbf{x}}$ is formed of both pilots and data throughout the transmission. Irrespective of the transmission strategy and phase, $\widetilde{\mathbf{x}}$ is then converted to the time-domain by N-point IFFT that can be presented mathematically as:

$$\mathbf{x} = \mathbf{F}^{H}\widetilde{\mathbf{x}} \ , \tag{4.3}$$

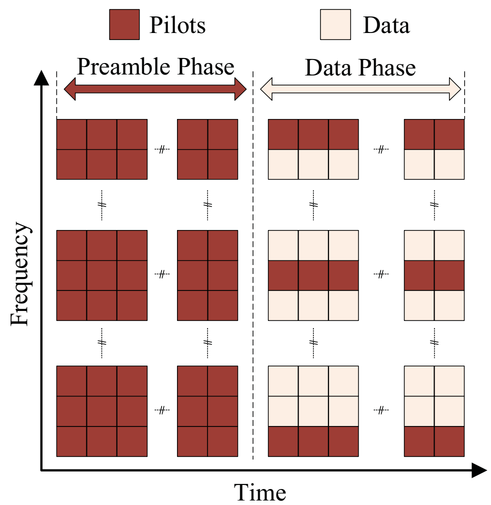

(a) Frame structure for FDP and RLP schemes

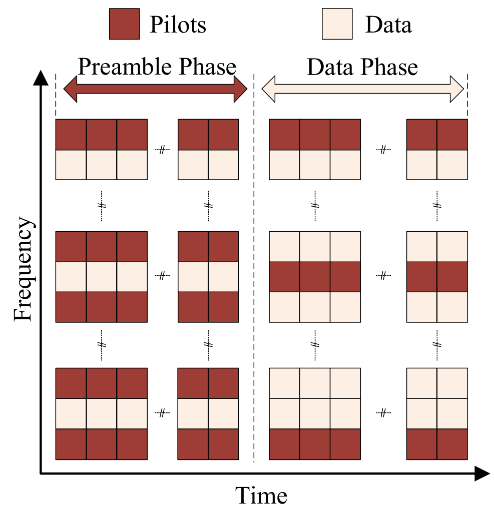

(b) Frame structure for PDP scheme

Figure 4.2: OFDM frame structure for proposed preamble based transmission strategies

where

$$\mathbf{F} = \begin{bmatrix} 1 & 1 & \cdots & 1 \\ 1 & e^{-j2\pi(1)(1)/N} & \cdots & e^{-j2\pi(1)(N-1)/N} \\ \vdots & \vdots & \ddots & \vdots \\ 1 & e^{-j2\pi(N-1)(1)/N} & \cdots & e^{-j2\pi(N-1)(N-1)/N} \end{bmatrix} . \tag{4.4}$$

A CP of length G is appended at the start of the OFDM symbol and the output $\bar{\mathbf{x}} = [x(-G), x(-G+1), \ldots, x(N-1)]^T$ is serially transmitted over a multi-tap time selective wireless channel, whose effect can be represented as:

$$\bar{\mathbf{y}}[k] = \bar{\mathbf{x}}[k] \otimes \mathbf{h}[k] \ , \tag{4.5}$$

where k and $\otimes$ denote the time index and time convolution operation respectively.

4.3.2 Joint Adaptive Beamforming and Channel Estimation

At the satellite end, the ULA output for the l^{th} OFDM symbol ($l = 1, \ldots, L$) for all the users after CP removal can be represented as:

$$\mathbf{V} = \mathbf{A}\mathbf{Y}^H + \mathbf{B} \ , \tag{4.6}$$

where $\mathbf{Y}$, $\mathbf{B}$ and $\mathbf{V}$ represents the received signal, i.i.d complex Gaussian noise and ULA output respectively as defined earlier in Chapter 3, page 46. $\mathbf{A}$ is the ULA response, where $[\mathbf{A}]_{s,j}$ can be presented mathematically as:

$$a(s, j) = e^{(-j2\pi(s-1)d_a \sin(\theta_j)/\lambda)} \ . \tag{4.7}$$

The output of the ULA is processed by the beamformer to mitigate CCI. This is given by:

$$\mathbf{z} = \mathbf{w}^H\mathbf{V} \ , \tag{4.8}$$

$$\mathbf{z} = [z(0), z(1), \ldots, z(N-1)] \ ,$$

$$\mathbf{w} = [w(1), w(2), \ldots, w(S)]^T \ ,$$

where $\mathbf{z}$ is the weighted output of beamformer and $\mathbf{w}$ are the applied BF complex weights. This is followed by S/P conversion and transformation of $\mathbf{z}$ to the frequency-domain, which can be mathematically expressed as:

$$\widetilde{\mathbf{z}} = \mathbf{F}\mathbf{z}^H \ . \tag{4.9}$$

$\widetilde{\mathbf{z}}$ in (4.9) is now processed by the CE block. For FDP and RLP schemes CE is not performed during PP ($l \leq L^{'}$) and solely BF processing takes place. However during DP as well as throughout the PDP scheme, both CE and BF processes take place concurrently. Fig. 4.3 illustrates receiver behaviour under proposed transmission strategies during PP and DP. Now employing the LS algorithm [69]

	Preamble Phase	Data Phase
FDP , RLP	Beamforming Only	Beamforming and Channel Estimation
PDP	Beamforming and Channel Estimation	Beamforming and Channel Estimation

Figure 4.3: Receiver behaviour against proposed schemes

in accordance with Fig. 4.3 for CE, the channel transfer function at pilot locations is given by:

$$\widetilde{\mathbf{h}}^p = (\mathrm{diag}\{\widetilde{\mathbf{x}}_d^p\}^{-1})\widetilde{\mathbf{z}}^p \ . \tag{4.10}$$

Estimates $\widetilde{\mathbf{h}}^p$ are then linearly interpolated to obtain estimates across all sub-carriers. This can be represented as:

$$\widetilde{\mathbf{h}} = \mathrm{filt}(\widetilde{\mathbf{h}}^p) \tag{4.11}$$

Estimates obtained in (4.11) are then used to reduce the channel effect, which can be expressed as:

$$\widetilde{\mathbf{r}} = (\mathrm{diag}\{\widetilde{\mathbf{h}}\}^{-1})\widetilde{\mathbf{z}} \ . \tag{4.12}$$

The data sub-carriers in $\widetilde{\mathbf{r}}$ are passed to the QPSK demodulator where they are decoded into $\{\hat{\mathbf{o}}\}$. For the next OFDM symbol, new complex weights are computed using a MSE based adaptive beamforming algorithm as described in Chapter 3, page 47. This error vector at the input of the beamformer in the frequency-domain can be expressed as:

$$\widetilde{\mathbf{e}} = \widetilde{\mathbf{z}}^p - \widetilde{\mathbf{x}}_d^p \ . \tag{4.13}$$

As the weight adaptation takes place in the time-domain, hence a frequency-to-time transform is used to convert the error vector to the time-domain, which can be represented as:

$$\mathbf{e} = \mathbf{F}^H\widetilde{\mathbf{e}} \ . \tag{4.14}$$

The time-domain error vector obtained in (4.14) is then used to perform adaptive BF.

4.3.3 LMS and FSS-LMS Beamformer

We employ the LMS algorithm to adapt BF complex weights until all OFDM symbols have been decoded. The LMS adaptation is given by:

$$\mathbf{w}[l+1] = \mathbf{w}[l] + 2\mu\mathbf{V}[l]\mathbf{e}[l] \quad . \tag{4.15}$$

Substituting (4.14) in (4.15), we obtain:

$$\mathbf{w}[l+1] = \mathbf{w}[l] + 2\mu\mathbf{V}[l]\mathbf{F}^H\widetilde{\mathbf{e}}[l] \quad . \tag{4.16}$$

Here $\mathbf{w}[l]$ and $\mathbf{w}[l+1]$ represent the beamformer's complex weights for $[l]$ and $[l+1]$ OFDM symbols. μ represents the positive step size which controls the rate of convergence such that [70]:

$$\mu_{min} \leq \mu \leq \mu_{max} \quad , \tag{4.17}$$

with

$$\mu_{max} \leq \frac{2}{3\,\mathrm{tr}\,(\mathbf{R})} \quad . \tag{4.18}$$

When constant μ (FSS)[1] is employed with LMS, μ will usually be close to μ_{min} [70]. For the HTSMS in this chapter, we employ LMS with optimised μ that adapts at each iteration according to (4.18). FSS-LMS is the same as LMS with μ satisfying (4.17). However it uses FSS and hence μ is not optimised at every iteration. The complexity of FSS-LMS is described in Chapter 3, page 48. As compared to it, the optimised LMS requires one additional step corresponding to (4.18).

[1]Fixed Step Size.

4.3.4 NLMS Beamformer

The NLMS algorithm whilst having potentially faster convergence also exhibits stable behaviour for a known range of μ, independent of the input data correlation statistics [83]. The NLMS filter update is given by:

$$\mathbf{w}[l+1] = \mathbf{w}[l] + \frac{2\mu \mathbf{V}[l]\mathbf{F}^H \widetilde{\mathbf{e}}[l]}{\|\mathbf{V}[l]\|^2} \ . \tag{4.19}$$

As compared to optimised LMS, one additional step of normalisation is required as indicated in (4.19).

4.3.5 VSS-LMS Beamformer

The choice of μ in LMS adaptation reflects a trade-off between misadjustment and the speed of adaptation. VSS-LMS aims to optimise μ as a function of the prediction error. A large prediction error increases μ to enable faster adaptation towards the optimal solution. When the algorithm is near to an optimal solution, μ is reduced resulting in smaller misadjustment, thus yielding overall improved performance. The VSS-LMS adaptation is of the following form:

$$\mathbf{w}[l+1] = \mathbf{w}[l] + 2\mu[l]\mathbf{V}[l]\mathbf{F}^H \widetilde{\mathbf{e}}[l] \ , \tag{4.20}$$

where

$$\mu[l+1] = \begin{cases} \mu_{max} & \mu^{'}[l+1] > \mu_{max} \\ \mu_{min} & \mu^{'}[l+1] < \mu_{min} \\ \mu^{'}[l+1] & \text{otherwise} \end{cases} \ , \tag{4.21}$$

and

$$\mu^{'}[l+1] = \alpha\mu[l] + \gamma \mathbf{F}^H \widetilde{\mathbf{e}}[l] \ . \qquad 0 < \alpha < 1 \ . \qquad \gamma > 0 \ . \tag{4.22}$$

The step size μ is controlled by the parameters α and γ. α is referred to as the forgetting factor and is chosen in the range of $(0, 1)$. The parameter γ is usually small and is chosen in conjunction with α to meet the misadjustment requirements. More details can be found in [70]. The additional overhead over the optimised LMS algorithm is essentially one more weight update at each time step reflected in (4.21).

4.4 Simulation and Discussions

4.4.1 Performance

A SIMO OFDM system with per link one transmit and multiple receive antenna elements $S = \{2 - 6\}$ was modelled. Total sub-carriers in an OFDM symbol are 32. For all transmission schemes, we take L as $10,000$. A conventional scheme (no preamble) has $\mathcal{I} = \{1, 8, 16, 24, 32\}$ hence a total of 5 pilots (N_p) per OFDM symbol are transmitted. On the other hand, preamble based transmission schemes have $\mathcal{I} = \{1, 11, 22, 32\}$ and hence 4 pilots ($N_{p'}$) per OFDM symbol during DP. In the proposed FDP, using (4.1) yields preamble size ($L^{'}$) as 357 OFDM symbols. For the RLP transmission scheme, $L^{'}$ is 35% shorter than FDP which comes out as 200 symbols. In the PDP case, since the preamble is not all pilots but 50% of both data and pilots, $L^{'}$ is twice the size of FDP which results in 714 symbols. Moreover, we employ several BF algorithms[2] with the proposed and conventional transmission schemes. Table 4.1 shows the transmission strategies and the BF algorithm applied to each of them. For all schemes, signal bandwidth was taken as 5 MHz with centre frequency being 3 GHz. In this study we consider both MAESTRO configurations, namely Outdoor Rural and Outdoor Urban. The channel model we follow was given in Chapter 3 while the parameters are the same as tabulated in Table 3.1.

[2]As stated in Section 4.3.2.

Transmission Strategy	**Beamforming Algorithm**
Conventional	FSS-LMS
	NLMS
	VSS-LMS
FDP, PDP	LMS
RLP	LMS

Table 4.1: Transmission strategies and the corresponding BF employed

4.4.2 Stability and Convergence

The discussion in this section considers one desired user at 40° azimuth while interference users are located at −70°, −35° and 30° azimuth in accordance with Fig. 3.4 (Chapter 3, page 42). The power per interference user at the satellite end is set to −10 dBW. We first analyse the convergence behaviour of the schemes. Fig 4.4 depicts the convergence of different transmission strategies in terms of CMSE against OFDM symbols with 6 antenna elements configuration onboard the satellite. We observe that FDP and RLP schemes converge to a low CMSE much faster as compared to PDP, which is then followed by VSS-LMS, NLMS and FSS-LMS. Furthermore the converged CMSE of FDP and RLP is the lowest which is followed by PDP and then the non-preamble approaches. This clearly highlights the potential advantage of using preamble based schemes for BF as compared to conventional approaches. Not only does it provide faster convergence, the MSE achieved is far lower than non-preamble approaches. Moreover, as the performance of RLP and FDP are similar, implementation of RLP in this case increases the throughput to 86% whereas for the conventional approaches throughput is 84%.

In Fig. 4.5 we show the results of changes in the variance of the MSE, thus reflecting the fluctuation of the BF with different schemes against desired user SNR. The

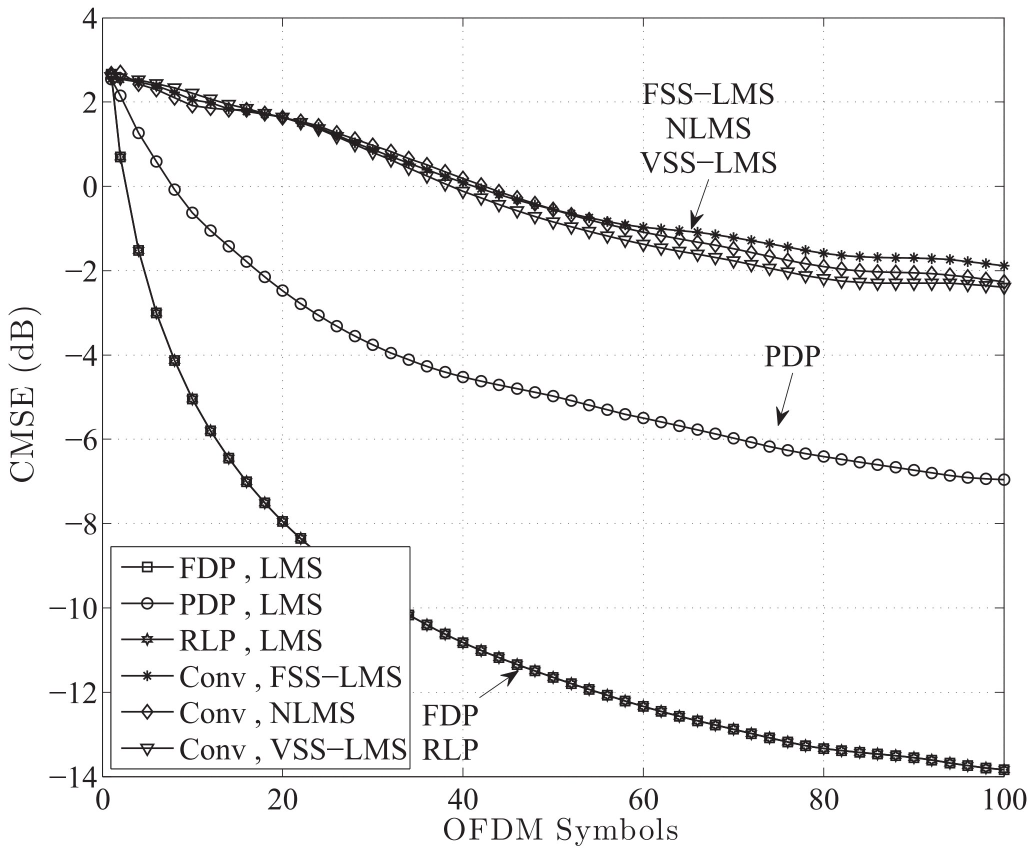

Figure 4.4: Beamforming convergence in terms of Cumulative Mean Squared Error vs OFDM symbols in rural environment with mobile speed = 3 km/hr, antenna elements = 6 and desired user SNR = 20 dB.

result indicate reduced variance of FDP, PDP and RLP versus FSS-LMS, NLMS and VSS-LMS with the 4 antenna elements configuration. RLP and PDP perform better than others with similar performance, followed by PDP and then the non-preamble approaches. This metric shows how the weights computation process of a preamble beamformer is more robust as compared to the non-preamble approach. The variance of the MSE of the proposed schemes exhibit further reduction with an increase in antenna elements to 6. Hence the proposed schemes have the potential of more stable BF as compared to the conventional strategies.

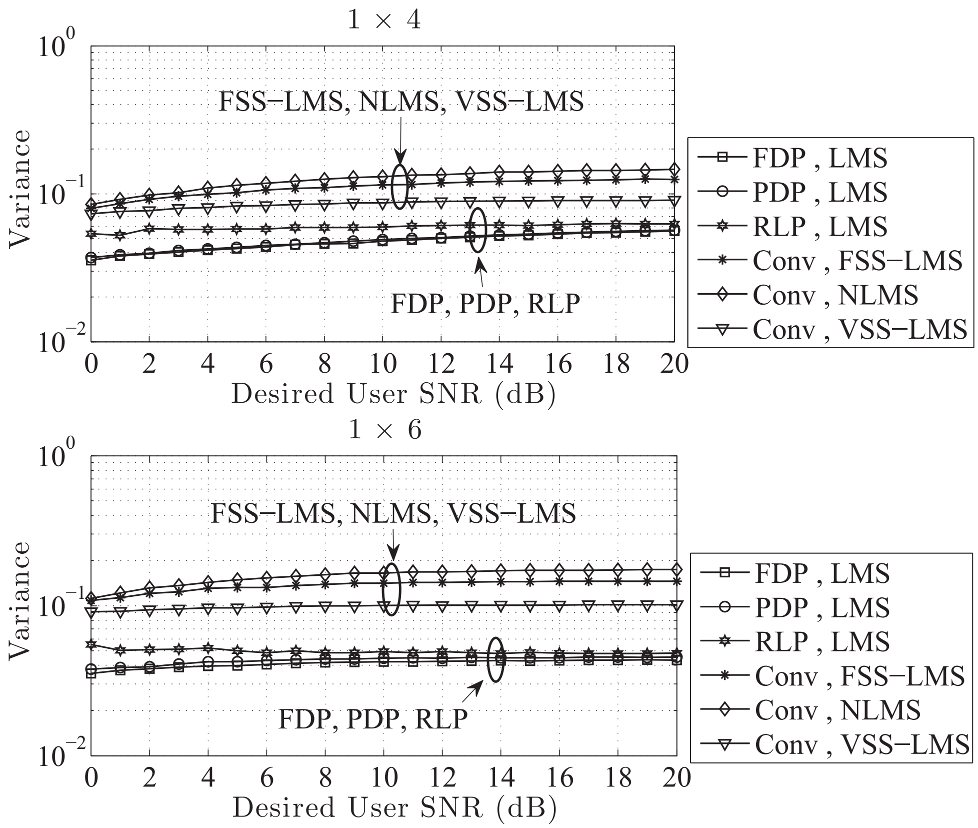

Figure 4.5: Variance of Mean Squared Error vs desired user SNR in rural environment with mobile speed = 3 km/hr and antenna elements = 4 & 6.

In the Fig. 4.4 we observed the short term BF performance for the first 100 OFDM symbols. This corresponds to the PP phase of the proposed strategies during which the density of pilots for the preamble based approaches is higher as compare to the conventional cases. Hence for fair comparison, we must analyse BF performance in terms of its long term precision to establish the performance advantages of the proposed preamble approach. Therefore we evaluate BF prediction error in terms of MSE of the studied schemes against desired user SNR in Fig. 4.6. It is evident from the figure that the preamble based approaches

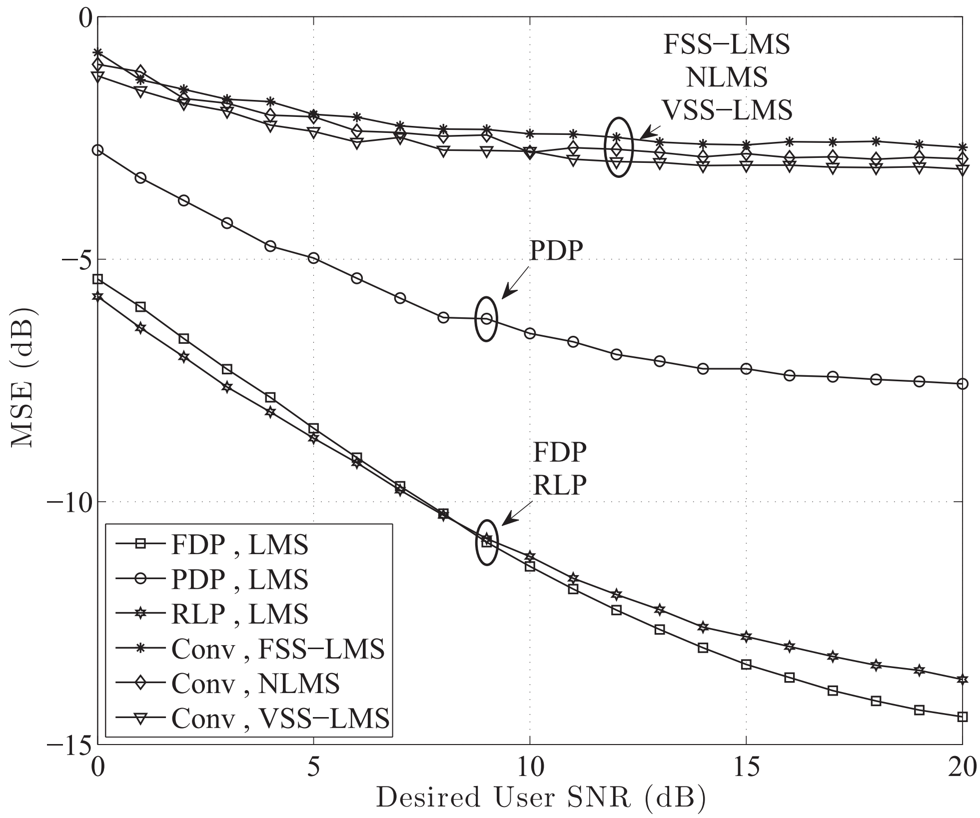

Figure 4.6: Beamforming prediction error in terms of Mean Squared Error vs desired user SNR in rural environment with mobile speed = 3 km/hr and antenna elements = 6.

exhibit much lower MSE as compare to the conventional cases irrespective of the SNR. Moreover, the minimum MSE obtained for all the schemes studied is consistent with the CMSE results in Fig. 4.4. To put this result in perspective, lets consider two extreme scenarios: Scenario 1 - SNR = 0 dB and Scenario 2 - SNR = 20 dB. We define the Precision Gain (PG) metric which is a measure of BF prediction error of schemes under study relative to FSS-LMS. PG for the two scenarios under observation is presented in Fig. 4.7. For Scenario 1, FDP and RLP provide around 4.7 and 5 dB PG respectively which is followed by PDP

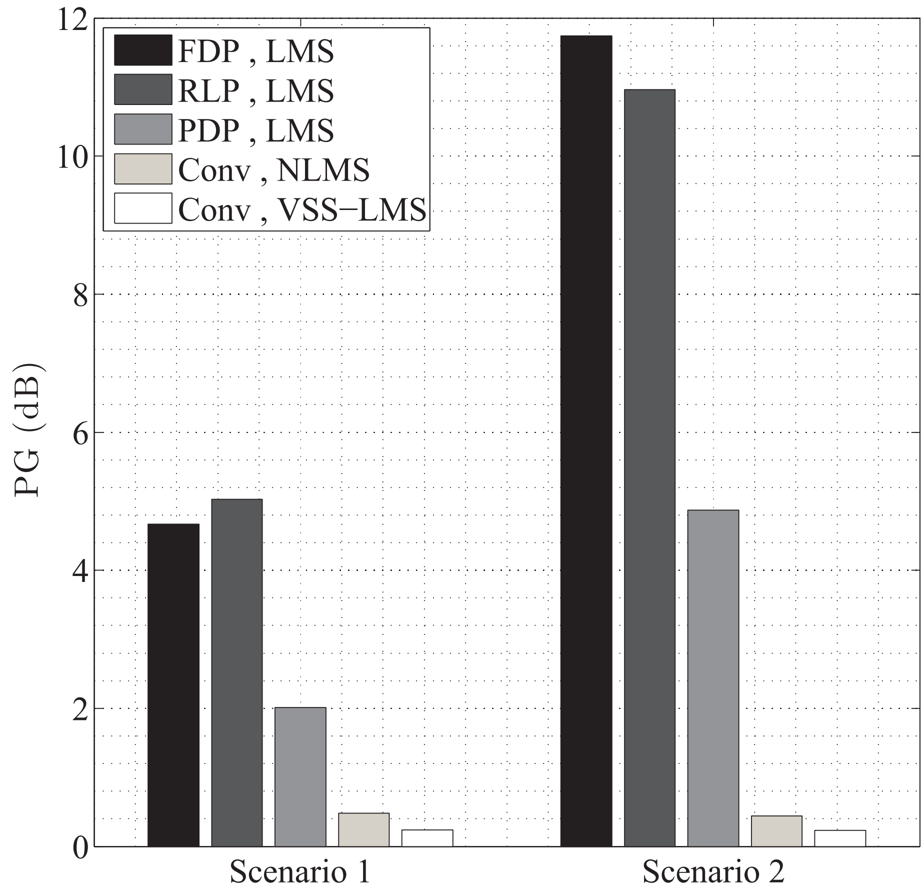

Figure 4.7: Precision Gain for the two scenarios.

which provides around 2 dB PG. NLMS and VSS-LMS offer only 0.5 and 0.25 dB PG respectively. Whereas for Scenario 2 where SNR is high, FDP, RLP and PDP provide around 11.7, 10.9 and 4.9 dB PG respectively. On the other hand NLMS and VSS-LMS offer 0.5 and 0.2 dB PG. Hence clearly not only does the preamble based approach improve convergence, it also displays superior MSE performance even through it uses one less pilot during DP.

Fig. 4.8 shows the system performance in terms of BER versus desired user SNR with different antenna element configuration. For the 2 antenna elements case, none of the schemes is able to mitigate interference as the number of interference

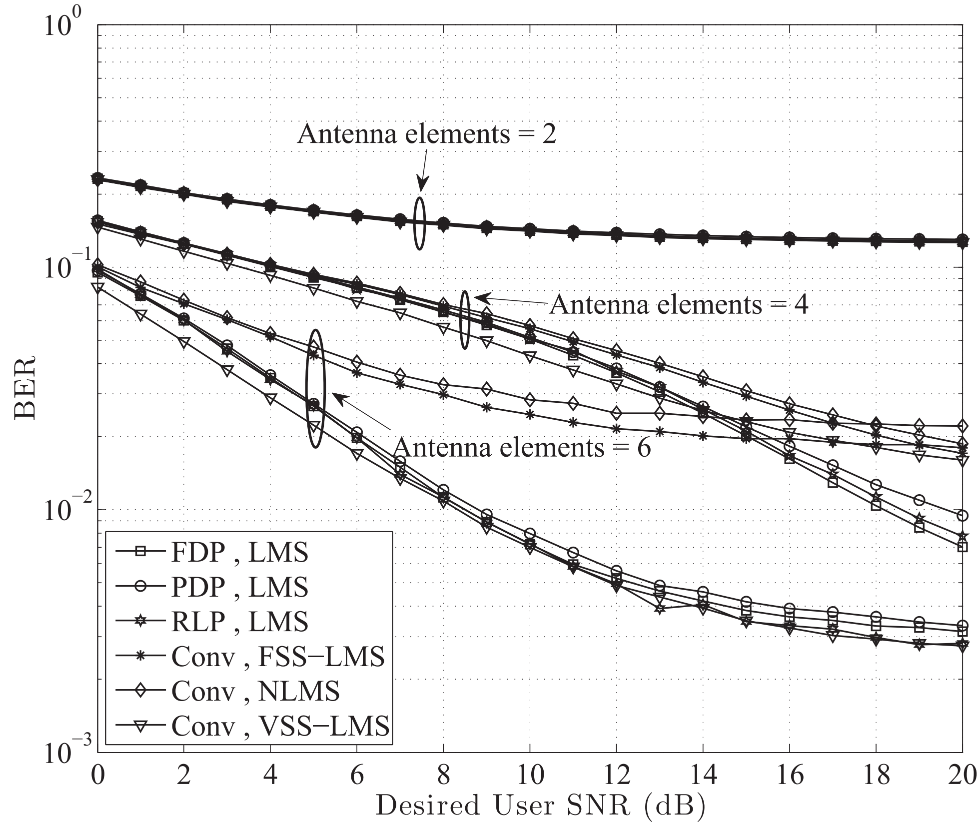

Figure 4.8: Bit Error Rate vs desired user SNR in rural environment with mobile speed = 3 km/hr and antenna elements = $2-6$.

users is more than the antenna elements. For the 4 antenna elements configuration, the proposed schemes exhibit superior BER performance as compared to conventional approaches, especially at high SNR's. It is worth highlighting here that even though the proposed schemes have less effective CE due to one less pilot in each OFDM data symbol, the overall system performance is still superior as it is dominated by CCI mitigation. In the 6 antenna elements case, VSS-LMS performance is quite similar to the proposed schemes. This is attributed to the combination of increase in antenna elements and one additional reference signal per OFDM symbol. However with RLP, we not only achieve the objective of interference mitigation but do it whilst having higher data throughput. The FSS-LMS and NLMS show inferior performance as compared to the others due to non-optimisation of the adaptation step size μ. This result also highlights the importance of the step size in the performance of LMS based signal processing.

4.4.3 Impact of Interference, Channel and Mobility

Having established that the preamble based beamformer outperforms the conventional schemes in Section 4.4.2, we now shift our focus to how the preamble based strategies perform in high mobility scenarios. We will also investigate how increased numbers of interference users impact the system performance. While studying the preamble approaches in Section 4.4.2 we assumed the environment to be outdoor rural. Therefore in this section we also quantify the performance of the beamformer with preamble based approach in an urban environment.

The transceiver parameters remain unchanged except for the number of interference users that are increased from 3 to 4 located at $-70°$, $-35°$, $65°$ and $80°$ azimuth while antenna elements onboard the satellite are reduced to 3. Therefore we increase the interference subjected to the satellite by terrestrial users. We compare PDP against conventional OFDM transmission without any preamble. It should be noted that we assume a wide range of interference locations for the purpose of analysis.

Fig. 4.9 presents the results in terms of achieved BER. We observe a significant difference in performance amongst proposed and conventional schemes. It is however clear that as compared to results in Section 4.4.2, the system performance degrades. This is attributed to increased numbers of interference users as well as fewer antenna elements onboard the satellite. However even in these severe conditions, the preamble approach having one less pilot per OFDM symbol shows superior performance when compared to the conventional case. It is also inter-

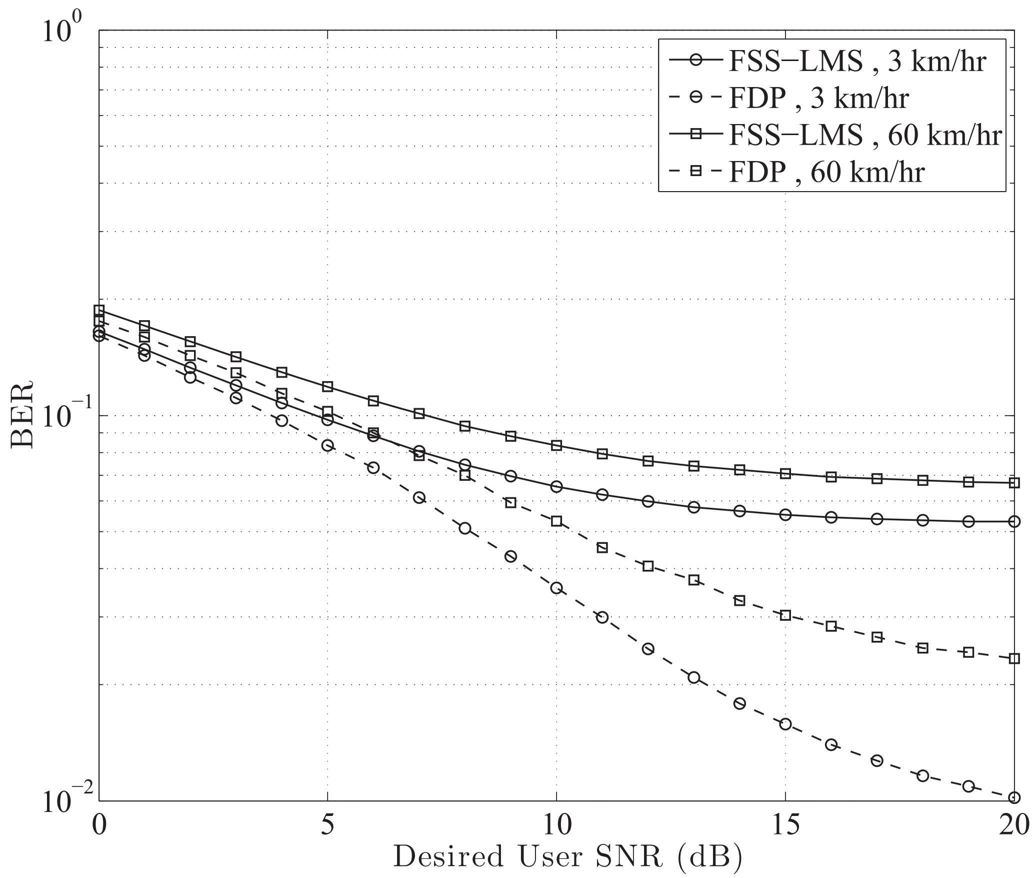

Figure 4.9: Bit Error Rate vs desired user SNR for two schemes in rural environment with mobile speed = 3 & 60 km/hr and antenna elements = 3.

esting to note that even at 60 km/hr mobile speed, the preamble based approach outperforms the conventional case. One would expect that with fewer pilots during DP and more Inter Carrier Interference (ICI), the preamble approach would suffer due to inaccurate CE. However, simulation results show that the pilot reallocation scheme still exhibits better performance in terms of BER. This highlights the importance of CCI mitigation and how system performance can be improved if channel estimates are obtained by processing interference mitigated signal.

Fig. 4.10 represents the results for both schemes in rural and urban environments.

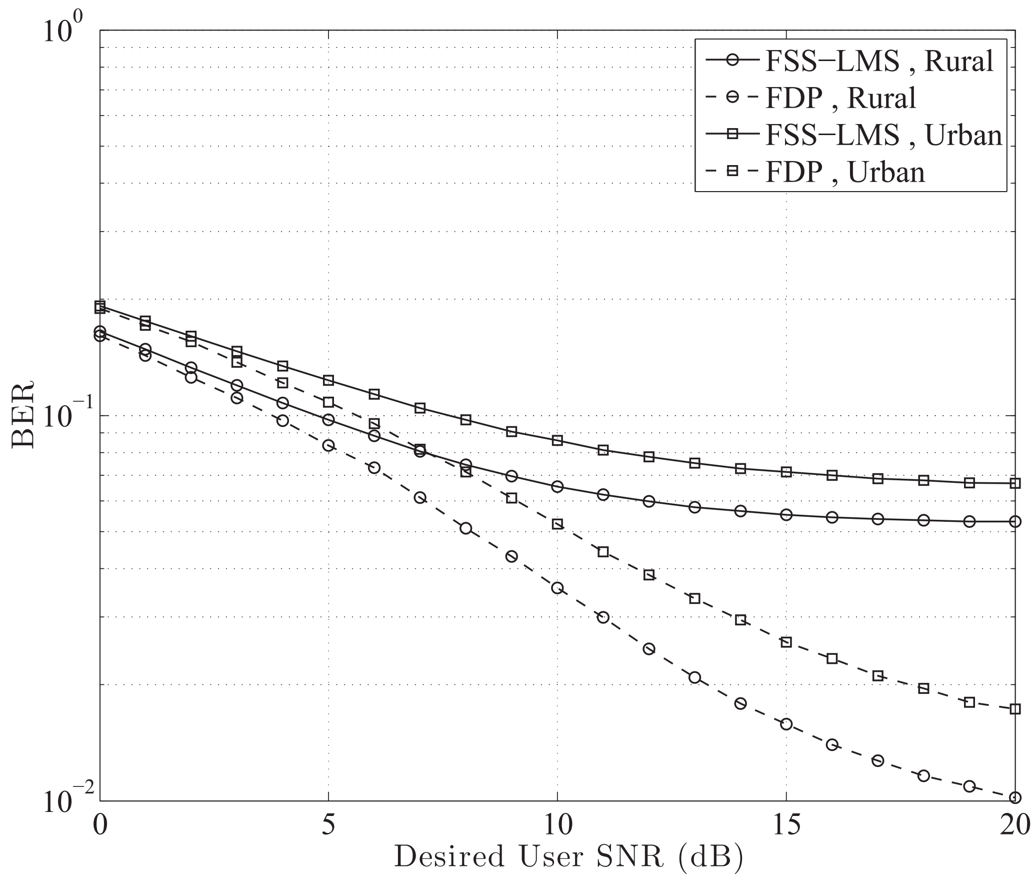

Figure 4.10: Bit Error Rate vs desired user SNR for two schemes in rural and urban environment with mobile speed = 3 km/hr and antenna elements = 3.

It can be seen that the proposed preamble approach outperforms the conventional case in both rural and urban environment. However, the BER performance gain achieved in urban environments is less than in the rural case which is attributed to the harsher channel conditions associated with the urban scenario.

4.5 Conclusions

In this chapter we have presented our proposed preamble based beamformer. We formulated Fully-Dense Preamble (FDP) and Partially-Dense Preamble (RLP) and investigated their performance in conjunction with LMS based spatial filtering with channel models specific to a mobile satellite scenario. We have shown that the preamble based approach exhibits superior performance by decoupling BF and CE processes enabling CE to be performed on interference mitigated OFDM sub-carriers. We then proposed a Reduced-Length Preamble (RLP) strategy which not only enabled higher throughput, but also exhibited superior CCI mitigation as compared to conventional schemes. The proposed strategies also show more stable BF as compared to the conventional approaches. It was also noted that the VSS approach can significantly boost the capability of LMS based BF by adapting the step size μ based on the prediction error. Simulation results verify that superior BF convergence contributes critically towards obtaining the short term goal of faster convergence and long term objectives of better overall system performance in HTSMS. Finally, we analysed the performance of the PDP scheme against FSS-LMS with higher number of interferes to antenna element ratio in high mobility as well as different environments. Simulation results verify that even at higher speed, the proposed approach shows promising results without increase in total number of transmitted pilots. We also conclude that the BF in OFDM systems are sensitive to pilot sub-carriers as well as OFDM frame structure and will exploit this observation in the next chapter.

Chapter 5

Iterative Beamforming for HTSMS

This chapter provides an overview of iterative processing and its applications to different communication problems. We then formulate our novel Iterative Turbo Beamforming (ITBF) for HTSMS based on Bit Interleaved Coded Modulation-OFDM (BICM-OFDM). Subsequently, we compare the proposed ITBF with non-iterative BF. Part of the work presented here is under review in *IET Communications* 2010 [89].

5.1 Introduction

In the proposed preamble based BF presented in Chapter 4, we observed that the BF performance exhibits a high degree of sensitivity to the number of pilot sub-carriers in an OFDM symbol. During the transient state, as we increased the number of pilots from conventional to PDP and then to FDP, we noted significant improvements both in terms of BF prediction error (short term and long term) as well as in the over all system performance. Therefore, in the context of our model if we increase the number of pilot sub-carriers, we can enhance the interference mitigation process but achieve this at the cost of data throughput. We however

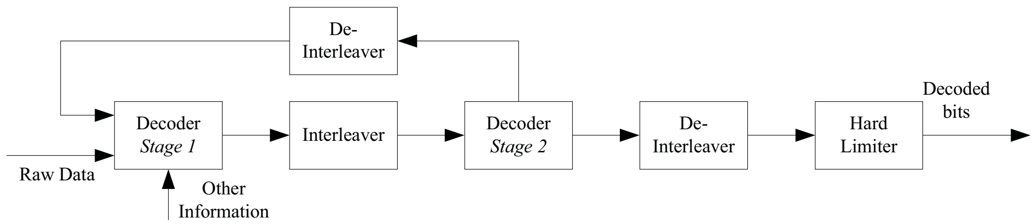

Figure 5.1: Block diagram of turbo decoder

also receive data in conjunction with the pilots in an OFDM receiver. If this data could be used in some way with pilots sub-carriers to perform BF, this may enable superior performance without scarifies of data throughput. In light of this, we propose a novel iterative beamformer which uses both pilots as well as data to do BF. Depending on the reliability of the data received, we formulate a data and pilot driven BF which exhibits significant gains in terms of system performance.

5.2 Related Work and Algorithm Formulation

The innovative iterative turbo receiver proposed by *Berrou et al.* [90] demonstrated that *turbo codes* exhibit near Shannon capacity in an AWGN channel. The receiver is designed in two stages, and turbo processing is referred to as an iterative exchange of soft decisions between these two stages. Specifically, the turbo receiver constitutes of three components namely, *inner decoder*, *outer decoder* and a *de-interleaver* that are connected to each other in the form of a feedback loop. Fig. 5.1 shows the basic structure of the turbo decoder.

Each of the two decoders in Fig. 5.1 is based on a Soft-Input Soft-Output (SISO)[1] decoder to solve a symbol-by-symbol *maximum a posteriori* probability (MAP) detection problem e.g. *BCJR algorithm* [91]. The quantity fed from one SISO decoding stage to the next irrespective of the path followed is referred to as *ex-*

[1] Appendix A

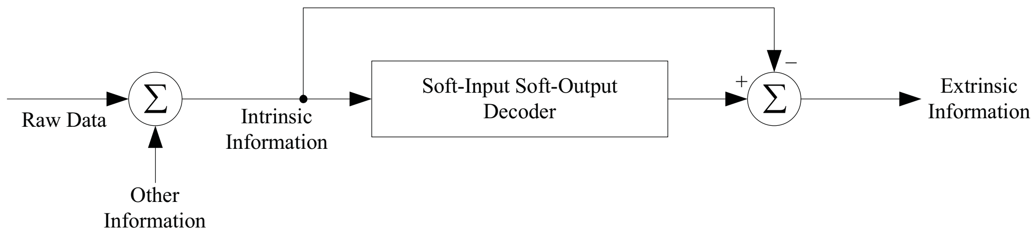

Figure 5.2: Concept illustration of information flow in a SISO decoder

trinsic information which is generally defined in terms of Log-Likelihood Ratio (LLR). LLR is an estimate of the *a posteriori* probability (APP) of a transmission sequence, given an observation of the received sequence. Specifically, *extrinsic* information generated by a decoding stage is defined as the difference between LLR computed for a set of systematic (message) bits at the output of that decoding stage. On the other hand *intrinsic* information, represented by a LLR, is applied to the input of the decoding stage. Illustration of the concept of information flow w.r.t *extrinsic* and *intrinsic* information in a SISO decoder is depicted in Fig. 5.2.

In an iterative process the *extrinsic* LLR from one decoding stage serves as *a priori* information to the next decoding stage. In effect the *extrinsic* information is the incremental information gained by exploiting the dependencies that exist between a message bit of interest and incoming raw data bits processed by the decoder. The magnitude of LLR is associated with the quality of *extrinsic* information which in turn corresponds to the reliability of the decoding decision. This reliability is a measure of the certainty of "what was transmitted" and is referred to as *soft estimates*. Based on this *priori* information, the decoder computes new APPs which are again fed back to the first decoder as *a priori* information and so on. The demodulation stage takes place after the final iteration and takes into account the reliability factor. Based on a two-stage turbo decoder depicted in Fig. 5.1, the flow of information in a turbo-decoder is presented in Fig. 5.3. The first decoding stage uses the SISO decoder to produce soft estimates of systematic

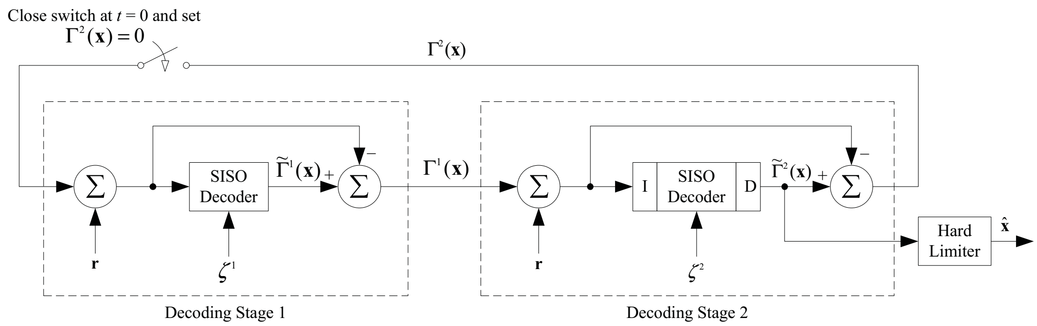

Figure 5.3: Information flow in a turbo decoder

bit x_t, expressed in terms of LLR as:

$$\widetilde{\Gamma}^1(x_t) = \ln \frac{P(x_t = 1|\mathbf{r},\, \zeta^{\mathbf{1}},\, \Gamma^2(\mathbf{x}))}{P(x_t = 0|\mathbf{r},\, \zeta^{\mathbf{1}},\, \Gamma^2(\mathbf{x}))} \ , \qquad t = 1, 2, \ldots, T \ , \tag{5.1}$$

where I and D represents interleaving and de-interleaving operations respectively. $\mathbf{r}$ is the set of noisy systematic bits, $\zeta^{\mathbf{1}}$ is the set of noisy parity-check bits generated by encoder 1, and $\Gamma^2(\mathbf{x})$ is the *extrinsic* information about the set of message bits $\mathbf{x}$ obtained from the decoding stage 2 and fed back to decoding stage 1. The *extrinsic* LLR at the output of the decoding stage 1 can be presented as:

$$\Gamma^1(\mathbf{x}) = \widetilde{\Gamma}^1(\mathbf{x}) - \Gamma^2(\mathbf{x}) \tag{5.2}$$

where

$$\widetilde{\Gamma}^1(\mathbf{x}) = \sum_{t=1}^{T} \widetilde{\Gamma}^1(x_t) \tag{5.3}$$

The iterative turbo receiver design is not limited to decoding of turbo codes. The turbo principle has been successfully applied to other communication problems such as channel estimation, joint source and channel coding, synchronization, multi-user detection. Turbo receiver design also finds its use in interference mitigation applications such as BF. *Sellathurai* and *Haykin* in [92] proposed an iterative beamformer for multi-transmit, multi-receive wireless communication systems. They present a MAP decoder based iterative receiver in conjunction with a soft iterative interference canceller that employs turbo-like processing for

Bell Labs Layered Space-Time (BLAST) architecture [3]. Using similar turbo principles, authors in [93, 94] present iterative BF and multi-user detection for CDMA based systems. *Hunziker et al* in [95] propose a Sample Matrix Inversion (SMI) working in conjunction with MAP working iteratively to mitigate system interference. By employing the iterative BF, authors show effective CCI cancellation in wireless ad-hoc networks with uncoordinated channel access and propose it as an alternative to collision avoidance protocols. The author extended their work for SIMO OFDM wireless ad-hoc system in [96] and showed effective CCI mitigation using similar SMI based iterative beamformer. Authors in [97] propose an iterative symbol-level transmit and receive beamformer with the objective of SINR maximisation whereas authors in [98] propose a smooth beamformer based on orthogonal iterations across sub-carriers. Specific to OFDM, recently *Zhao et al.* [87] proposed a turbo based channel estimator which aims to reduce ICI induced in OFDM systems due to users mobility. Most of the aforementioned iterative receiver designs for BF are non-OFDM systems. Work in [96] is based on OFDM but is related to ad-hoc networks and focuses on collision avoidance. Moreover, authors use SMI based BF which is complex as compared to LMS. Work in [87] is again based on OFDM but focuses towards ICI mitigation through enhanced turbo channel estimation and does not involve BF or CCI mitigation.

In this chapter we propose a novel symbol-level LMS based iterative beamformer that uses a turbo processing approach to mitigate CCI for HTSMS uplink scenario. Compared to conventional non-iterative BF methods, the proposed beamformer uses both pilots and soft decoded data information with the turbo principle to enhance interference mitigation. As compared to the aforementioned iterative approaches, the proposed technique is a three-stage OFDM based LMS beamformer which improves BF and system performance w.r.t the soft data input. More specifically, the beamformer is based on improving the *a priori* information of the soft decoded data and the pilots by adapting BF weights according to

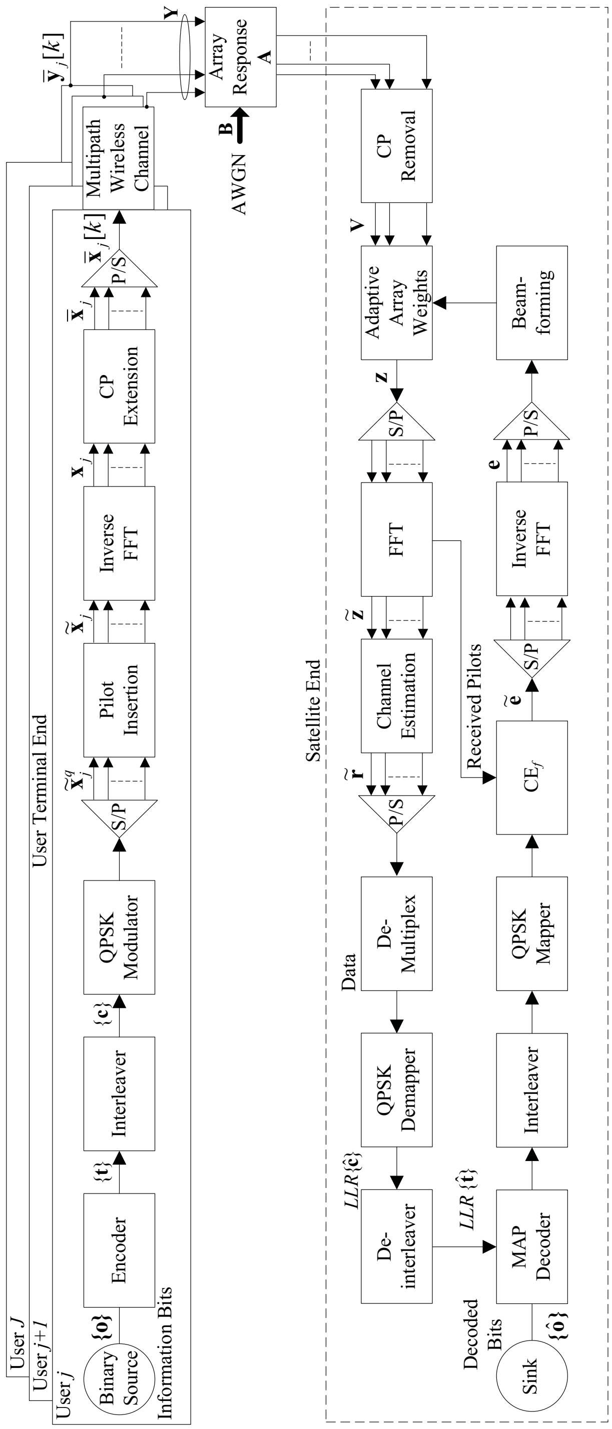

Figure 5.4: BICM-OFDM system for HTSMS with ITBF

the respective levels of reliability. The turbo-like iterative procedure significantly enhances BF performance which in turn leads to improved system performance.

5.3 System Model

The HTSMS scenario and the uplink interference model is the same as depicted in Chapter 3, Fig. 3.3 and Fig. 3.4 respectively. A link between mobile and satellite is modelled as SIMO with one desired user and $J-1$ interference users. After the signal passes through the wireless channel, symbol-level iterative BF is applied at the satellite end to mitigate interference induced by BTS users. Again no time or frequency offsets exist in the system.

5.3.1 BICM-OFDM Model for HTSMS

Transceiver architecture for a BICM-OFDM HTSMS is presented in Fig. 5.4 and will be referred to throughout the chapter to follow the information flow in the system. At the transmitter end, information bits $\{\mathbf{o}\}$ of the j^{th} user ($j = 1, \ldots, J$) are generated. These information bits are encoded into $\{\mathbf{t}\}$ and then interleaved into $\{\mathbf{c}\}$. The Interleaved bits are then mapped into QPSK complex symbols and Serial-to-Parallel (S/P) converted to $\{\widetilde{\mathbf{x}}^q\}$. Pilots for the user considered $\{\widetilde{\mathbf{x}}^p\}$ are interspersed into data sequence $\{\widetilde{\mathbf{x}}^q\}$ at known pilot sub-carriers $\{\mathcal{I}\}$. This process forms an N sub-carriers OFDM symbol that can be expressed as:

$$\widetilde{\mathbf{x}} = [\widetilde{x}(0), \widetilde{x}(1), \ldots, \widetilde{x}(N-1)]^T \quad . \tag{5.4}$$

This is followed by conversion of the OFDM symbol to the time-domain by a N-point IFFT. This can be presented mathematically as:

$$\mathbf{x} = \mathbf{F}^H \widetilde{\mathbf{x}} \ , \tag{5.5}$$

where

$$\mathbf{F} = \begin{bmatrix} 1 & 1 & \cdots & 1 \\ 1 & e^{-j2\pi(1)(1)/N} & \cdots & e^{-j2\pi(1)(N-1)/N} \\ \vdots & \vdots & \ddots & \vdots \\ 1 & e^{-j2\pi(N-1)(1)/N} & \cdots & e^{-j2\pi(N-1)(N-1)/N} \end{bmatrix} . \tag{5.6}$$

At the start of the OFDM symbol, a CP of length G is appended and the output $\bar{\mathbf{x}} = [x(-G), x(-G+1), \ldots, x(N-1)]^T$ is serially transmitted. At the satellite end, the ULA output after CP removal for the l^{th} OFDM symbol $(l = 1, \ldots, L)$ for all the users can be presented as:

$$\mathbf{V} = \mathbf{A}\mathbf{Y}^H + \mathbf{B} \ , \tag{5.7}$$

where $\mathbf{Y}$, $\mathbf{B}$ and $\mathbf{V}$ represents the received signal, i.i.d complex Gaussian noise and ULA output respectively as defined earlier in Chapter 3, page 46. $\mathbf{A}$ is the ULA response, where $[\mathbf{A}]_{s,j}$ can be presented mathematically as:

$$a(s, j) = e^{(-j2\pi(s-1)d_a \sin(\theta_j)/\lambda)} \ . \tag{5.8}$$

5.3.2 Iterative Turbo Beamforming (ITBF)

In the proposed ITBF, a QPSK demapper and a MAP decoder work in an iterative fashion. At each iteration, BF complex weights are computed based on received pilots and soft decoded data from previous iterations. The ITBF comprises of three distinctive stages, namely Rudimentary Beamforming Stage (RBS), Iterative Beamforming Stage (IBS) and Termination Beamforming Stage (TBS).

The ULA output $\mathbf{V}$ for the l^{th} OFDM symbol is processed by the Pre-FFT beamformer. This is expressed as:

$$\mathbf{z}_i = \mathbf{w}_i^H(\mathbf{A}\mathbf{Y}^H + \mathbf{B}) \ , \tag{5.9}$$

where $\mathbf{z}_i = [z_i(0), z_i(1), \ldots, z_i(N-1)]$ is the weighted output of the BF corresponding to the desired user, while $\mathbf{w}_i = [w_i(1), w_i(2), \ldots, w_i(S)]^T$ represents the beamformer's complex weights for the i^{th} iteration. When $i = 0$, this stage is referred to as RBS as BF weights applied correspond to the previous OFDM symbol ($\mathbf{w}_i[l] = \mathbf{w}_I[l-1]$). Now $\mathbf{z}_i$ is S/P converted followed by FFT. This can be presented mathematically as:

$$\widetilde{\mathbf{z}}_i = \mathbf{F}(\mathbf{w}_i^H \mathbf{A}\mathbf{Y}^H + \mathbf{w}_i^H \mathbf{B})^H \quad . \tag{5.10}$$

For the case of an AWGN channel, data sub-carriers in $\widetilde{\mathbf{z}}_i$ are directly de-multiplexed into $\widetilde{\mathbf{r}}_i^q$ which are passed to the QPSK demapper. However for the wireless channel scenario, CE is performed on $\widetilde{\mathbf{z}}_i$ to yield $\widetilde{\mathbf{r}}_i$ which is then followed by de-multiplexing of data-sub-carriers $\widetilde{\mathbf{r}}_i^q$. For the sake of brevity, we define the demapper task as computation of APP's given received vector $\widetilde{\mathbf{r}}_i^q$, channel estimates $\widetilde{\mathbf{h}}_i^q$, and outputs *extrinsic* information, or LLRs Γ_i^1 for the v^{th} coded bit c_v in desired user's transmitted data sequence $\widetilde{\mathbf{x}}^q$. This is given by:

$$\Gamma_i^1(c_v(\widetilde{x}^q(n))) = \ln \frac{\sum_{b \in U_v^+} P(\widetilde{x}^q(n) = b \mid \widetilde{r}_i^q(n), \widetilde{h}_i^q(n), \Gamma_i^2)}{\sum_{b \in U_v^-} P(\widetilde{x}^q(n) = b \mid \widetilde{r}_i^q(n), \widetilde{h}_i^q(n), \Gamma_i^2)} \quad , \tag{5.11}$$

$$\begin{aligned} & P(\widetilde{x}^q(n) = b \mid \widetilde{r}_i^q(n), \widetilde{h}_i^q(n), \Gamma_i^2) = \\ & \frac{1}{2\pi\sigma^2} \exp\left(-\frac{\|\widetilde{r}_i^q(n) - \widetilde{h}_i^q(n)\widetilde{x}^q(n))\|^2}{2\sigma^2} \right) \prod_{u \neq v} P(c_u(\widetilde{x}^q(n)) \quad , \end{aligned} \tag{5.12}$$

where U_v^- and U_v^+ represent the constellation set that contains all the symbols whose v^{th} bit is 0 and 1 respectively. Γ_i^1 is de-interleaved and passed to the MAP decoder. The MAP decoder outputs and feedbacks the *extrinsic* information $\Gamma_i^2(c_v(\widetilde{x}^q(n))$. Γ_i^2 is interleaved and then used to compute the soft data symbols as follows:

$$\hat{\widetilde{x}}_i^q(n) = \sum_{b \in U} b \cdot P(\widetilde{x}^q(n) = b) \quad , \tag{5.13}$$

$$P(\widetilde{x}^q(n) = b) = \prod_{u=1}^{\log_2 |U|} P(c_u(\widetilde{x}^q(n))) \quad , \tag{5.14}$$

where$\mid U \mid$ denotes the cardinality of the set U. The soft data symbols for the

QPSK case can be computed by:

$$\hat{\tilde{x}}_i^q(n) = \frac{1}{\sqrt{2}}(\tanh(\Gamma_i^2(c_0(\tilde{x}^q(n))/2) + j\tanh(\Gamma_i^2(c_1(\tilde{x}^q(n))/2)) \ . \tag{5.15}$$

The conventional LMS beamformer requires the difference between transmitted and received pilots as an input (as described in Chapter 3, page 47). However with the proposed beamformer, soft data symbols and received pilots work in conjunction to perform BF. Hence the error vectors corresponding to soft data and pilots are given by:

$$\tilde{\mathbf{e}}_i^q = \hat{\tilde{\mathbf{x}}}_i^q - \tilde{\mathbf{x}}^q. \tag{5.16}$$

$$\tilde{\mathbf{e}}_i^p = \tilde{\mathbf{z}}_i^p - \tilde{\mathbf{x}}^p \ . \tag{5.17}$$

Error vectors $\tilde{\mathbf{e}}_i^q$ and $\tilde{\mathbf{e}}_i^p$ are mapped to known sub-carrier locations to obtain the frequency-domain Combined Error (CE$_f$) vector $\tilde{\mathbf{e}}_i = [\tilde{e}_i(0), \tilde{e}_i(1), \ldots, \tilde{e}_i(N-1)]^T$. As we employ Pre-FFT BF, CE$_f$ is converted to the time-domain which can be presented mathematically as:

$$\mathbf{e}_i = \mathbf{F}^H \tilde{\mathbf{e}}_i \ . \tag{5.18}$$

$\mathbf{e}_i$ is used to update BF weights for the next iteration. Using (5.18), the LMS adaptation is given by:

$$\mathbf{w}_{i+1}[l] = \mathbf{w}_i[l] + 2\mu\mathbf{V}[l]\mathbf{e}_i[l] \ . \tag{5.19}$$

Substituting (5.18) into (5.19) we get:

$$\mathbf{w}_{i+1}[l] = \mathbf{w}_i[l] + 2\mu\mathbf{V}[l]\mathbf{F}^H\tilde{\mathbf{e}}_i[l] \ . \tag{5.20}$$

The new BF weights $\mathbf{w}_{i+1}$ are used for the next iteration in (5.9). For $1 < i < I$, the process presented in (5.9)−(5.20) is referred to as IBS. The IBS continues for the desired number of iterations. In the final stage ($i = I$) referred to as TBS, the output of the MAP decoder is decoded into $\{\hat{\mathbf{o}}\}$ using hard-decision. Moreover, $\mathbf{w}_{i+1}$ computed during TBS are used for the next OFDM symbol which is given by:

$$\mathbf{w}_I[l+1] = \mathbf{w}_I[l] + 2\mu\mathbf{V}[l]\mathbf{e}_I[l] \ , \tag{5.21}$$

where $[l]$ and $[l+1]$ in (5.21) correspond to complex weights for consecutive OFDM symbols. μ represents the positive step size which controls the rate of convergence such that [70]:

$$\mu_{min} \leq \mu \leq \mu_{max} \quad , \tag{5.22}$$

with

$$\mu_{max} \leq \frac{2}{3\,\mathrm{tr}\,(\mathbf{R})} \quad . \tag{5.23}$$

For the HTSMS, we employ LMS with optimised μ that adapts at each iteration as well as every OFDM symbol l according to (5.23). The complexity of non-iterative optimised LMS has already been described in Chapter 4, page 89. Hence in addition to that, I weight updates per OFDM symbol are performed. Hence ITBF is more complex as compared to conventional LMS BF. However, the technique would become viable if considerable gains can be achieved with minimal iterations. The pseudo-code representation of the proposed ITBF algorithm is presented as Algorithm 1.

5.4 Simulation and Discussions

5.4.1 Coding and Uncoded OFDM Systems

Prior to proceeding to the performance of the ITBF receiver, we pause to verify the performance of the employed coded system in the absence of interference. Until now we have only worked and verified operation of the uncoded OFDM design for HTSMS. Therefore before we consider BICM-OFDM for HTSMS, it is imperative to verify the implementation of BICM-OFDM system and its performance. Fig. 5.5 is the block diagram of the modelled single-link BICM-OFDM systems. Binary data $\{\mathbf{o}\}$ is encoded and interleaved to $\{\mathbf{t}\}$. The interleaved bits $\{\mathbf{t}\}$ are mapped into QPSK complex symbols. The output of the QPSK

Algorithm 1 Iterative Turbo Beamforming

Initialise: (l, s, i, μ)

Require: $\sum_{s=1}^{s=S} w(s) = 1$ for $l = 1$

$\mu_{min} \leq \mu \leq \mu_{max}$ for every l

while $l \leq L$ **do**
  for $i = 1$ to I for every l **do**
    if $i = 1$ **then**
      $\mathbf{w}_i[l] = \mathbf{w}_I[l-1]$
      Apply $\mathbf{w}_i[l]$
      Compute CE_f
      Compute $\mathbf{w}_{i+1}[l]$
    else if $1 < i < I$ **then**
      $\mathbf{w}_i[l] = \mathbf{w}_{i-1}[l]$
      Apply $\mathbf{w}_i[l]$
      Compute CE_f
      Compute $\mathbf{w}_{i+1}[l]$
    else if $i = I$ **then**
      $\mathbf{w}_I[l] = \mathbf{w}_{i-1}[l]$
      Apply $\mathbf{w}_I[l]$
      Compute CE_f
      Compute $\mathbf{w}_I[l+1]$
      Decode data $\{\hat{\mathbf{o}}\}$
    end if
  end for
end while

modulator is S/P converted to $\widetilde{\mathbf{x}}$ and passed to the IFFT block. The IFFT block converts the OFDM signal to the time-domain and outputs $\mathbf{x}$ which is converted to serial form $\mathbf{y}$ and transmitted. At the receiver side i.i.d. complex Gaussian noise $\sim \mathcal{CN}(0, \sigma^2)$ is added to $\mathbf{y}$. The noisy signal $\mathbf{r}$ is S/P converted followed by FFT that converts the signal back into the frequency-domain. The output of FFT operation $\widetilde{\mathbf{r}}$ is converted to serial form and fed to the QPSK demapper. The demapper outputs $\{\widetilde{\mathbf{c}}\}$ which are the LLR or the reliability indicator for the transmitted sequence $\{\mathbf{c}\}$. These are de-interleaved into $\{\widetilde{\mathbf{t}}\}$ and passed to the decoding stage. Based on hard-decision, the decoder outputs $\{\widetilde{\mathbf{o}}\}$ which are estimates of the transmitted information bits.

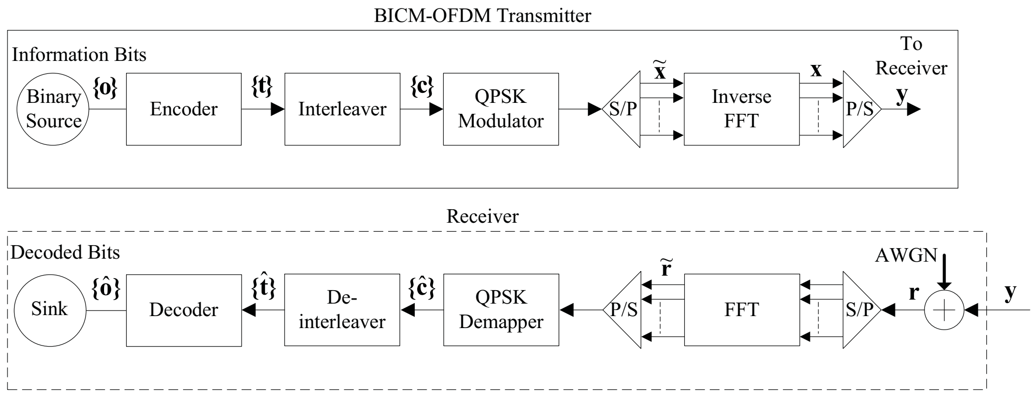

Figure 5.5: Single-link BICM-OFDM system

Performance

32 OFDM sub-carriers per OFDM symbol (N) where considered in the system. A rate-1/2 $(5,7)_8$ convolution encoder combined with random interleaver was employed at the transmitter end. At the receiver side we employ random de-interleaver combined with MAP as well as Viterbi decoding [99]. System performance is analysed in AWGN channel conditions for both coded and uncoded OFDM systems. No interference is considered in the system.

Fig. 5.6 presents the simulated and theoretical BER results for coded and uncoded OFDM system in absence of interference. The result verifies our implementation of the BICM. As BF has already been verified in Chapter 3, we can now move forward and integrate our coded system with HTSMS and employ ITBF at the receiver side.

5.4.2 Performance of ITBF

A SIMO BICM-OFDM system with 32 sub-carriers (N) having 5 pilots per OFDM symbol (N_p) is modelled. 1×2 and 1×4 SIMO configurations are employed. In accordance with Fig. 3.4 (Chapter 3, page 42), one desired user

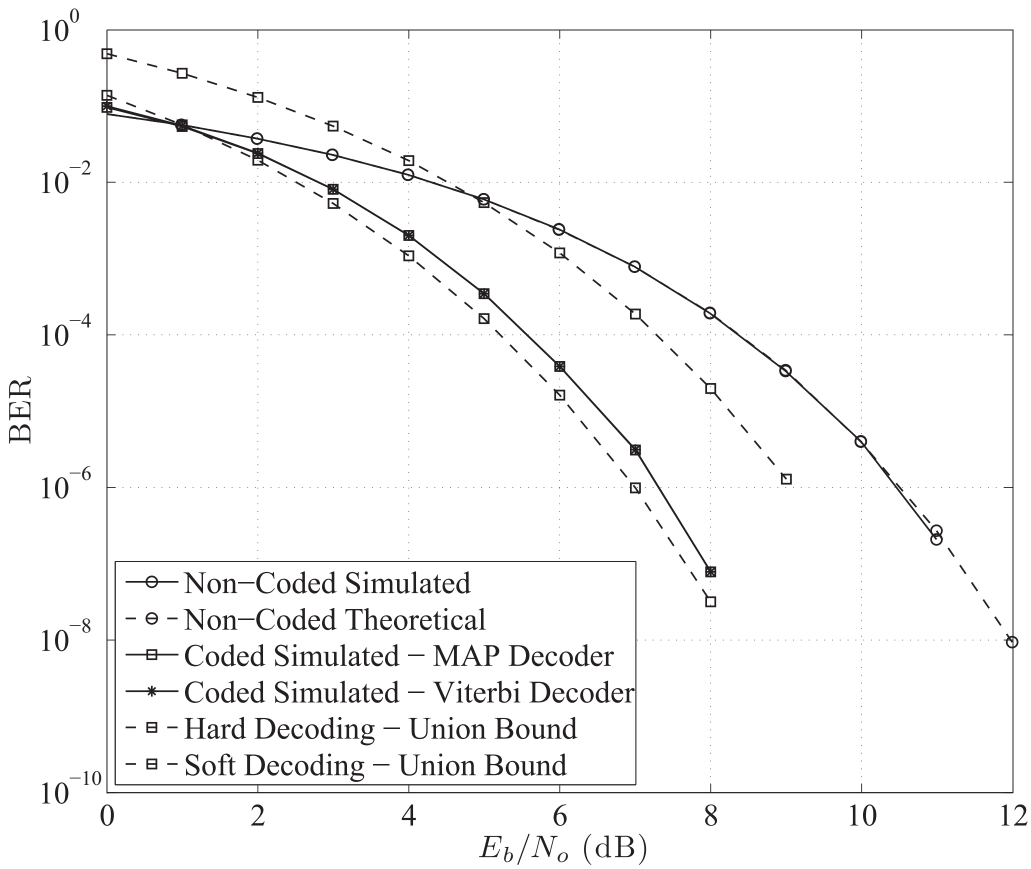

Figure 5.6: Performance of coded and uncoded OFDM systems in AWGN channel.

was modelled at 40° while interference users were located at −70°,−35° and 60° azimuth respectively. A rate-1/2 $(5, 7)_8$ convolution encoder and random interleaver/de-interleaver are employed in an AWGN channel condition. The power per interference user at the satellite end is set to −5 dBW which is higher then the interference level considered in previous chapters. The proposed ITBF is compared with conventional non-iterative adaptive LMS beamformer.

Fig. 5.7 presents a snap shot of the short term BF prediction error in terms of Cumulative MSE (CMSE) in dB against OFDM symbols for the case of 2 antenna element configuration. In other words this figure presents the transient and the steady state behaviour of BF in terms of prediction error for a specific SNR level.

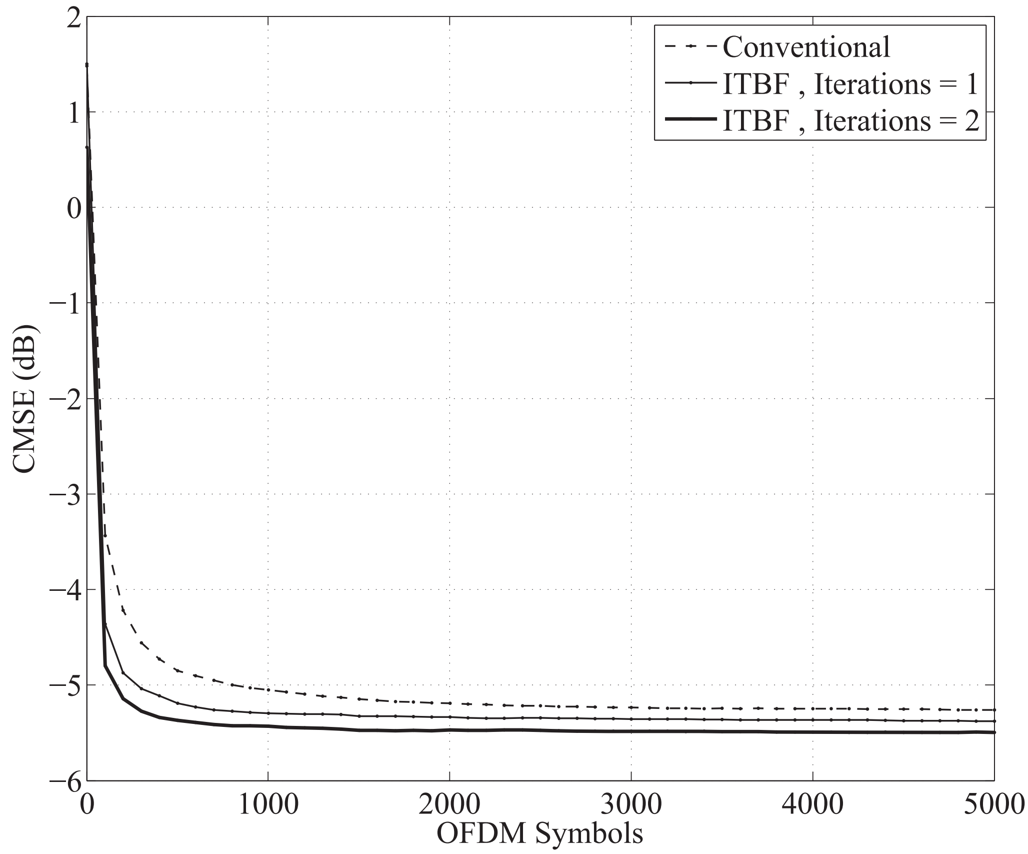

Figure 5.7: Beamforming convergence in terms of Cumulative Mean Squared Error vs OFDM symbols, antenna elements = 2 and $E_b/N_o = 8$ dB.

The error is presented in cumulative form so as to average the MSE over time and effectively shows how BF MSE converges to its steady state. We can see that ITBF converges faster as well as attains a lower CMSE as compared to the conventional case. Moreover, within the ITBF framework, further improvement in the minimum CMSE is achieved as well as speed of convergence is observed with increased number of iterations (i). Effectively, iterative BF translates to better CCI mitigation as well as shorter transient state time.

Now if we increase the number of antenna elements to 4, we can observe in Fig. 5.8 that a much lower CMSE is obtained by all the studied schemes as compared to

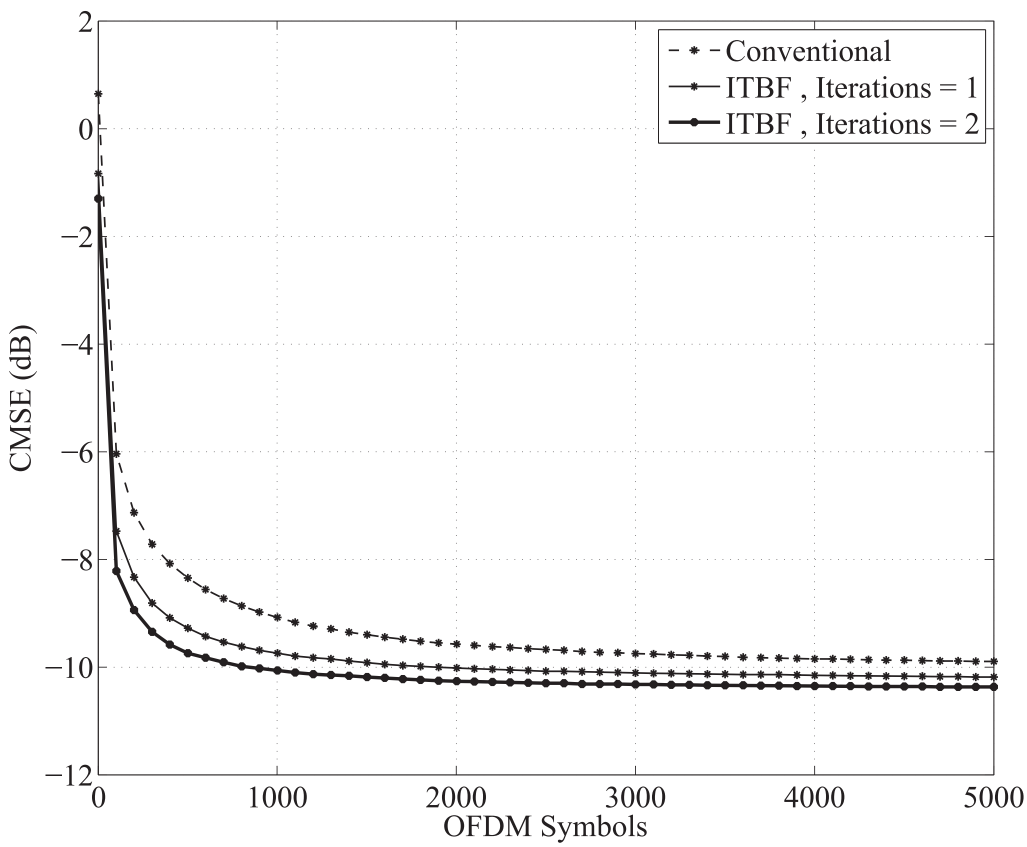

Figure 5.8: Beamforming convergence in terms of Cumulative Mean Squared Error vs OFDM symbols, antenna elements = 4 and $E_b/N_o = 8$ dB.

$S = 2$ case. However, convergence speed in case of proposed ITBF is superior as compared to the conventional case. We can also observe further reduction in minimum CMSE achieved as well transient time with increased number of iterations. To compare the case of 2 and 4 antenna elements, we present a snapshot of the CMSE for the two configurations at $l = 300$ in Fig. 5.9. We can observe an increasing trend of improved CMSE as the iterations increase when BF has processed 300 OFDM symbols irrespective of the number of antenna elements employed. Moreover, we can observe that CMSE reduces for $S = 4$, with ITBF showing superior performance.

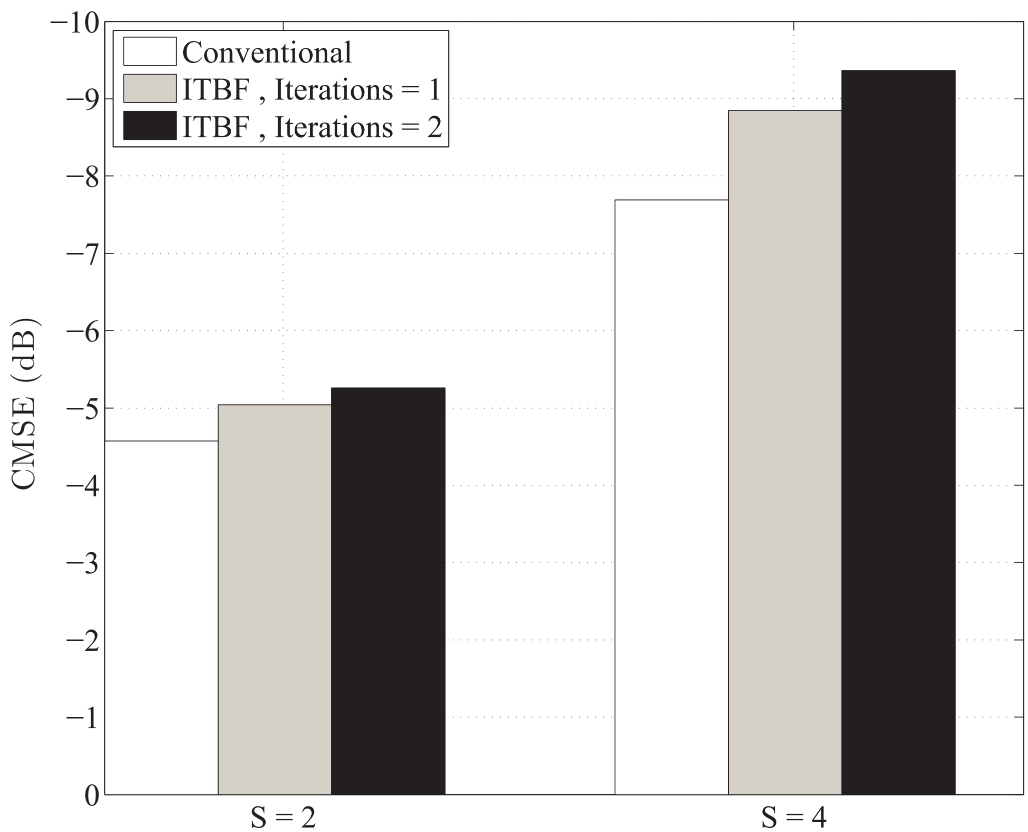

Figure 5.9: Snapshot of Cumulative Mean Squared Error at 300^{th} OFDM symbol, antenna elements = 2 & 4 and $E_b/N_o = 8$ dB.

Another perspective of BF performance is how the BF complex weights adapt w.r.t time. Fig. 5.10 presents the CBFW for the case of $S = 2$. It is evident that BF weights for the conventional case exhibit highest latency in terms of convergence. With one iteration, the weights convergence speed is enhanced which is further improved with 2 iterations. For the case of $S = 4$, the BF weights adaptation is shown in Fig. 5.11. We observe a similar trend to the case with 2 antenna elements. These results further validate CMSE results as well as the performance advantage of the proposed iterative approach.

The CMSE depicted in Fig. 5.7−5.9 give an idea as to how ITBF improves BF

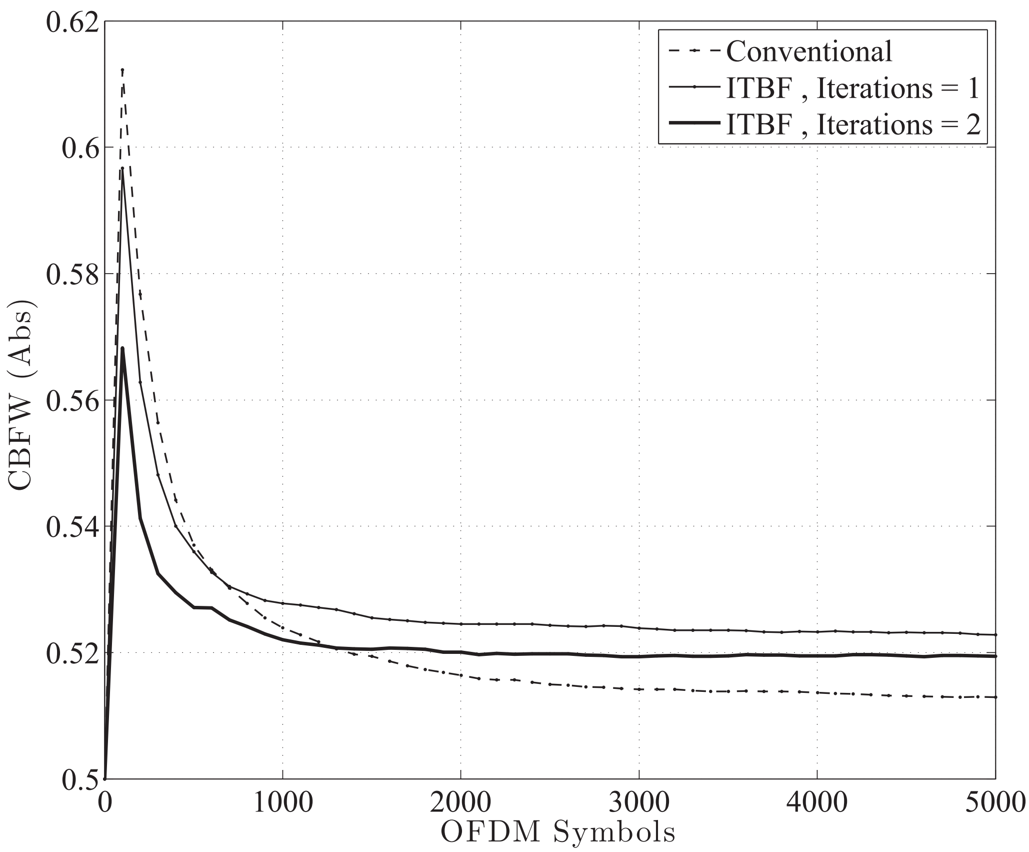

Figure 5.10: Beamforming convergence in terms of Cumulative Beamforming Weights (Abs) of one of the antenna elements vs OFDM symbols, antenna elements = 2 and $E_b/N_o = 8$ dB.

convergence as well as prediction error. However since CMSE is only evaluated at pilot locations, whereas BF takes place using both pilots and data, results do not depict the true performance advantages of the ITBF. Therefore it is imperative to analyse the error rate performance of the ITBF as compared to the conventional non-iterative BF. Hence we look at the BER in Fig. 5.12 to explore the performance advantages of ITBF.

It is evident from the BER result that ITBF outperforms the conventional case irrespective of E_b/N_o. With only one iteration, the ITBF provides a BERG of $\approx$

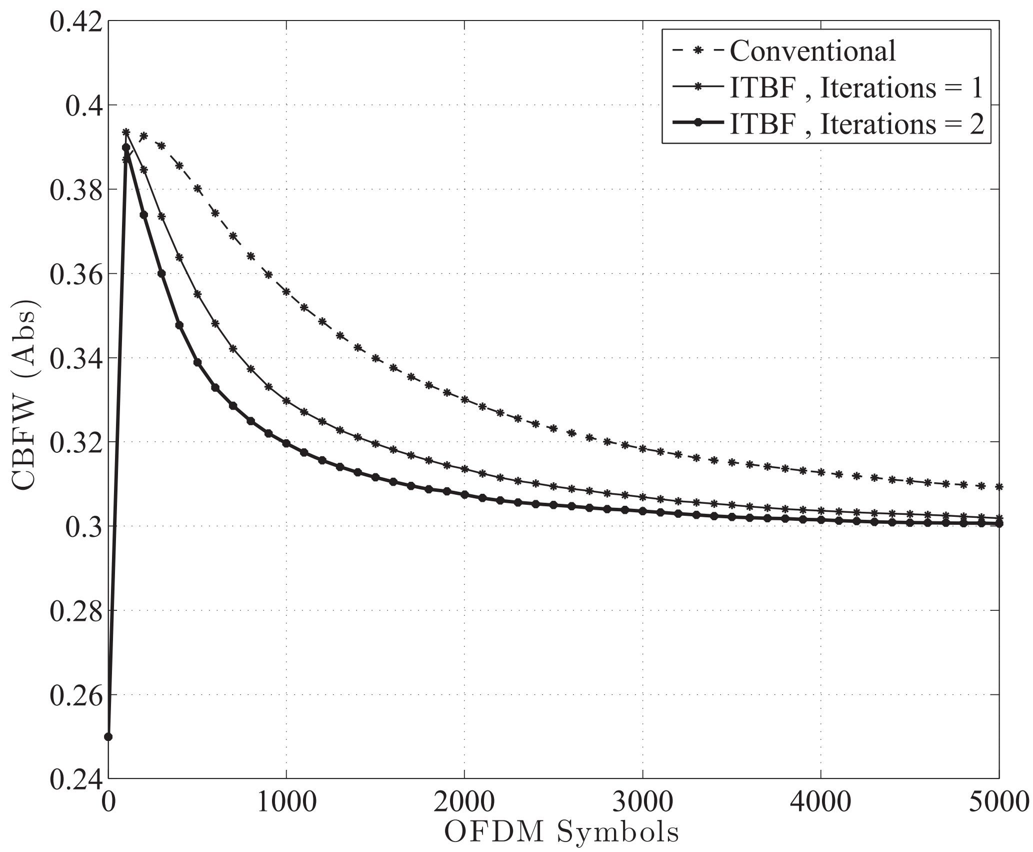

Figure 5.11: Beamforming convergence in terms of Cumulative Beamforming Weights (Abs) of one of the antenna elements vs OFDM symbols, antenna elements = 4 and $E_b/N_o = 8$ dB.

1.5 dB with 2 antenna elements. This gain increases to ≈ 2.5 dB when 4 antenna elements are employed. Furthermore at a worst case scenario of $E_b/N_o = 0$ dB, the proposed approach exhibits far superior performance compared to the conventional case. To quantify the BER improvements, we present the BERG achieved by ITBF as compared to the conventional case in Fig. 5.13 for the two extreme scenarios; Scenario 1 $-$ $E_b/N_o = 0$ dB and Scenario 2 $-$ $E_b/N_o = 7$ dB. We clearly note a consistent increase in gain achieved as we increase the number of iterations for the Scenario 1 case. When we move to Scenario 2 having

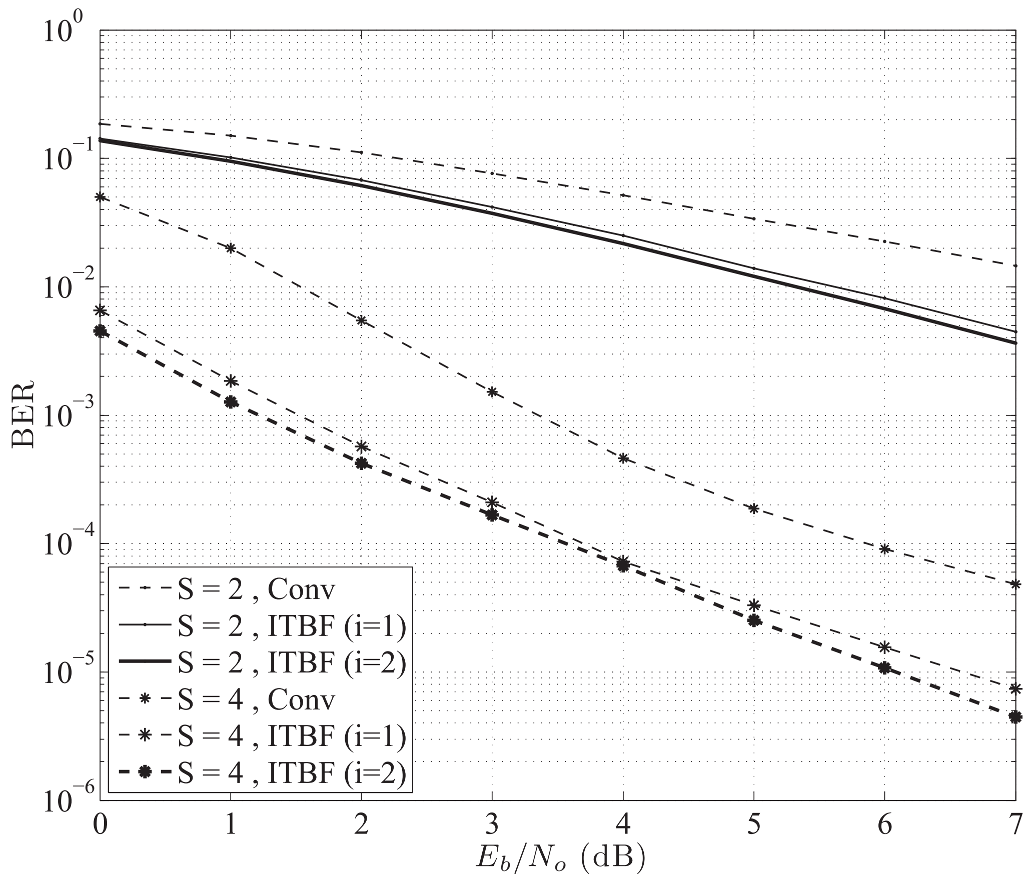

Figure 5.12: Bit Error Rate vs desired user E_b/N_o, antenna elements = 2 & 4.

high E_b/N_o, we can see a further improvement in BER increasing upto 2.6 dB. Irrespective of the scenarios, we can observe increased BERG as we increase S from 2 to 4.

Finally as we observed in Chapter 3 that the convergence period has pronounced impact on the BER. If we ignore some initial OFDM symbols in the BER computation process, BER improves significantly. Fig. 5.14 present the BER performance for the case $S = 2$, if we ignore the first 500 OFDM symbols in BER computation. It is evident that for the case of 2 antenna elements, clipping or no clipping translates to almost similar performance irrespective of non-iterative

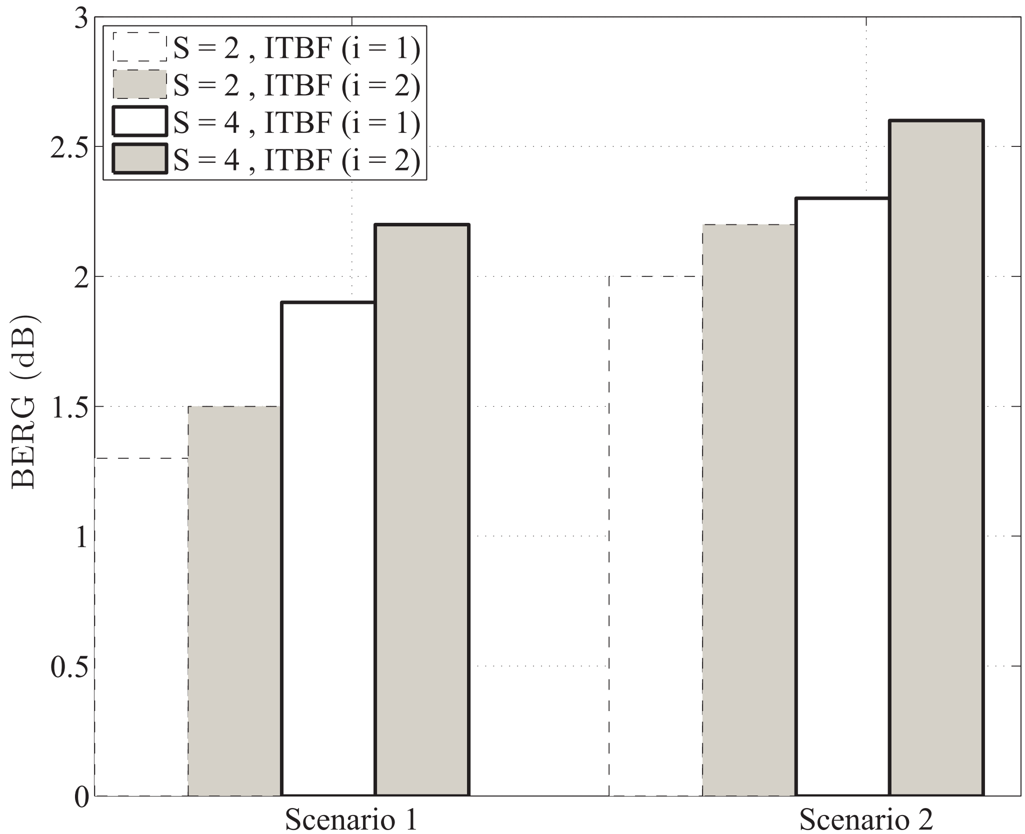

Figure 5.13: Bit Error Rate Gain for the extreme scenarios, antenna elements = 2 & 4.

or ITBF approach. This indicates that channel coding reduces the impact of BF transient state on system performance. As we increase the number of antenna element to $S = 4$, we see in Fig. 5.15 that clipping offers slightly better performance. However the performance gap is not as significant as in Chapter 3. Hence employing channel coding not only provides us with the opportunity of introducing a novel ITBF algorithm, but also enabled us to reduce the impact of BF convergence on system performance as well as eliminating the error floor.

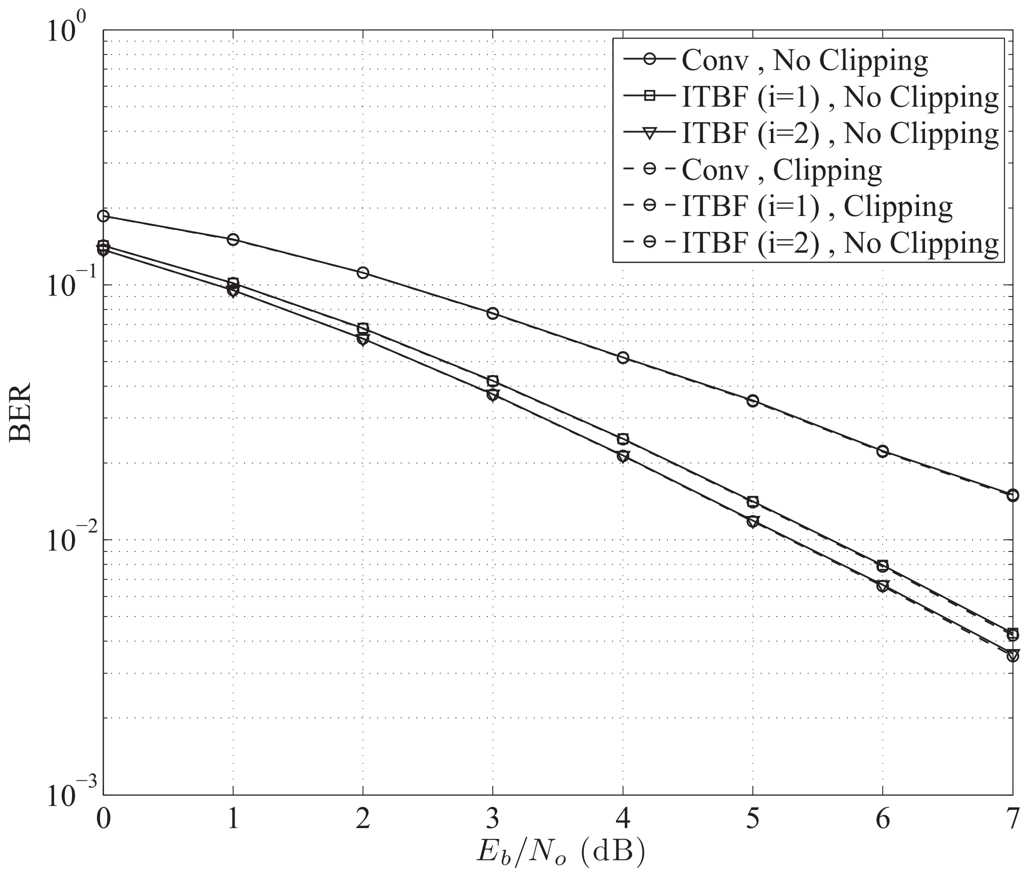

Figure 5.14: Bit Error Rate vs desired user E_b/N_o with and without clipping, antenna elements = 2 and $\widetilde{L} = 500$.

5.5 Conclusions

In this chapter we first introduced channel coding and interleaving / de-interleaving functionality in our OFDM based HTSMS. We then validated the performance of the channel coding by comparing it to the theoretical bounds. Exploiting the coding in the system, we then formulated a novel iterative BF algorithm which uses both pilots as well as data with the turbo principle to perform CCI mitigation. The proposed ITBF comprises three distinctive stages namely; Rudimentary Beamforming Stage (RBS), Iterative Beamforming Stage (IBS) and Termination

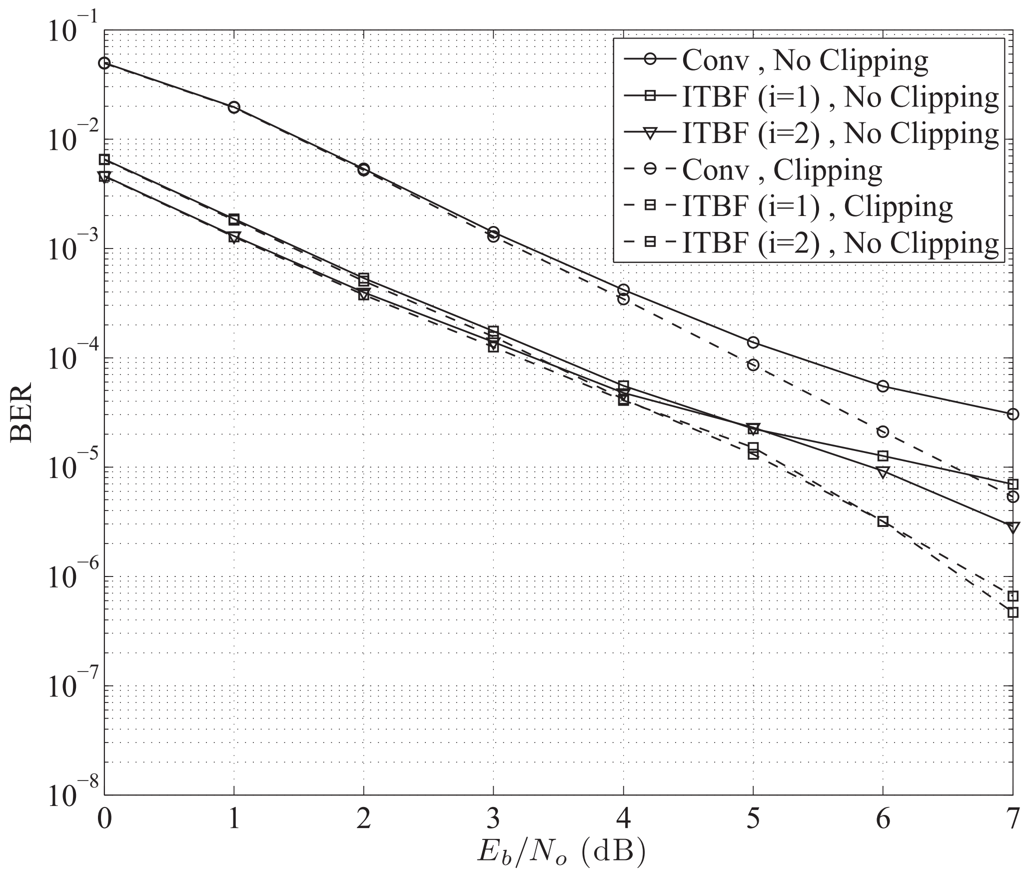

Figure 5.15: Bit Error Rate vs desired user E_b/N_o with and without clipping, antenna elements = 4 and $\widetilde{L} = 500$.

Beamforming Stage (TBS). We then compared the performance of proposed approach to the conventional non-iterative case and report considerable gain in terms of system performance in high interference level scenarios. As we increase the number of iterations for the ITBF, we observe improved system performance. Even in worse case scenarios such as at $E_b/N_o = 0$ dB, the proposed algorithm outperforms the conventional case providing significant gain. Finally we investigate how incorporation of channel coding effects the error floor problem reported in Chapter 3. We find that by introducing channel coding we can largely eliminate the error floor problem.

Chapter 6

Ground vs Onboard Beamforming

In this chapter we present an overview of onboard and ground based BF together with their advantages and associated problems. We then propose a semi-static BF approach which makes beam patterns lesser prone to amplitude and phase distortions. Moreover, it also reduces signalling bandwidth requirement in the uplink from the gateway. We then compare the performance of semi-static and full adaptive BF for the HTSMS scenario. Part of the work presented here has been published in *Proc. AIAA on 28th ICSSC* 2010 [100].

6.1 Introduction

In Chapter 3−5 , we employ full adaptive BF at the satellite end. For brevity, we refer to this as Onboard Based Beamforming-Adaptive (OBBF-A). This topology is suited for Mobile Satellite System (MSS) scenarios, such as HTSMS, where beams need to be adapted more frequently. However in the case of the satellite payload, OBBF-A is currently not cost effective due to higher onboard complexity requirements, power consumption issues and associated costs. The less complex solution is to opt for Ground Based Beamforming (GBBF) saving valuable onboard resources. Despite the benefits of GBBF, high feeder link bandwidth is required to support uplink and downlink transmissions. Moreover with GBBF, the satellite payload complexity is a sensitive function of the feed signals transmitted via gateway uplinks and downlinks. Furthermore, performance of GBBF is highly sensitive to the gateway calibration system which must compensate for instabilities induced due to payload/gateway component changes with temperature and life as well as propagation amplitude and phase dispersion effects. Hence clearly, the choice of BF not only depends on complexity but also on performance. In this chapter we investigate ground based and onboard based BF solutions for a BICM-OFDM architecture in our proposed HTSMS. We also propose a semi static hybrid space/ground BF and show that it is a far less complex solution compared to onboard adaptive BF. We then investigate the applicability of onboard and ground based approaches and quantify their performance advantages for the HTSMS case.

6.2 Related Work

Current generations of satellite system such as ICO [14, 16, 20] and MSV [7] have employed GBBF with full adaptivity with MSS scenario; we refer to this as GBBF-Adaptive (GBBF-A). GBBF-A is the simpler alternative to OBBF-A and is based on the exchange of radiating element feeder signals between satellite and gateway. The BF is realised in the gateway with all the flexibility offered by on-ground digital signal processing. This approach is preferable with respect to OBBF-A since there are substantial overheads associated with onboard BF networks such as hardware mass, cost, power consumption and thermal control requirements. Hence GBBF-A reduces the cost, weight and power consumption issues associated with having complex dynamic BF hardware onboard the satellite by moving this hardware to the ground station.

Despite the benefits, GBBF-A still requires a large amount of transceiver hardware to pass the individual feed signals through gateway uplinks and downlinks, to and from the ground station. The payload complexity is a sensitive function of the number of feed signals transmitted across the satellite's gateway link [17]. For example, a circular coverage region divided into $C^{'}$ cells would require $C = (\sqrt{C'} + \sqrt{F})^2$ feeds, where F equals the number of feeds used in synthesizing each beam. For instance, if $C^{'} = 162$ and $F = 50$ then $C = 392$ feeds. This transmitter and receiver hardware is carried onboard the satellite and is undesirable due to aforementioned problems. Furthermore, redundant transmit and receive processing channels are required for each feed signal in order to compensate for imperfect feed characteristics.

Recently, hybrid onboard/ground BF solutions [18, 19] have been proposed to address the trade-off between ground and space BF. It splits the BF process between the satellite and the gateway. Coarse BF is performed onboard the satellite with the objective of reducing the feed signal space to a subspace, thus decreasing the required feeder link bandwidth. This is followed by fine BF at the gateway thus improving the overall system performance. However both classical GBBF-A as well as the hybrid BF [18, 19] topology have instabilities due to payload/gateway component changes with temperature and life time, and propagation amplitude and phase dispersion effects which have to be compensated by a complex ground based BF calibration system [20]. Moreover with the hybrid BF, primary and redundant feed links are still required, forcing the need for bandwidth resources, onboard complexity as well as a complex calibration system on the ground. With the OBBF-A, feed link requirements as well as complexity of ground based calibration system are greatly reduced. This however is achieved at the cost of complexity and power consumption onboard the satellite. Illustration of ground, onboard and hybrid beamforming in a MSS and their respective trade-off is shown in Chapter 1, page 5.

Irrespective of whether adaptive processing is done onboard the satellite or gateway, both have associated complexities and problems. Inmarsat satellites [101] have used GBBF in a non-adaptive fashion, which can also be referred to as GBBF-Static (GBBF-S). The BF coefficients are realised at the ground and uploaded to the satellite where they remain unchanged. Inmarsat satellites have the capability of uploading new BF coefficients, however this is not done on a frequent basis. The GBBF-S greatly reduces the onboard as well as ground station complexity, feeder link bandwidth requirement and the need of redundant feeds. However, the process of uploading the filter coefficients (weights) requires excessive signalling bandwidth. More importantly, the process is also prone to amplitude and phase distortion during the transmission which potentially translates to inaccurate beam patterns. Moreover in the MSS, the non-adaptive beam pattern may result in performance degradation due to non-adaptive interference cancellation. Hence clearly, the choice of BF not only depends on complexity and resources, but is also a function of performance advantages of the respective approaches. Hence the primary question to answer is how much performance improvement is achieved with adaptive processing in a MSS scenario.

The question above drives the trade-off between complexity and performance and is both scenario as well as system dependent. From the literature, work is found on onboard adaptive BF impact on complexity and the possible solutions, as described earlier. However, performance analysis between adaptive and non-adaptive BF solutions, specifically in an HTSMS architecture is to the best of our knowledge not studied.

To analyse and quantify the performance advantages, we employ adaptive and non-adaptive BF for the HTSMS. For the adaptive case, OBBF-A is implemented onboard the satellite with per symbol BF (Pre-FFT) approach. To avoid uploading of BF coefficients from the gateway for the non-adaptive case, we propose OBBF-Semi Static (OBBF-SS) as opposed to aforementioned GBBF-S for MSS, which is a hybrid of ground and onboard BF. OBBF-SS is referred to as semi static as BF weights are not hard-wired and can be changed when required. In OBBF-SS, based on the coordinates of the required focus point on the earth surface, we calculate the specific direction in which this receive beam should be oriented. In order to point the beam in a specific direction, this required orientation is calculated at the ground station and transmitted to the satellite. The calculation process for BF coefficients is done onboard the satellite without any need of complex signal processing. Addition of simple circuity onboard the satellite enables this capability while the satellite can still have a transparent payload design (analogue or digital). This significantly reduces the signalling bandwidth requirement in the uplink from the gateway as only the orientation is communicated rather than the actual BF coefficients. Moreover the approach makes beam patterns less prone to amplitude and phase distortions.

To establish comparison, we also employ another variant of non-adaptive BF, namely OBBF-Equal Ratio Combining (OBBF-ERC). In OBBF-ERC BF coefficients are set such that signals from all antenna elements are summed up in equal proportion. We investigate and analyse the performance of OBBF-A, OBBF-SS and OBBF-ERC for the BICM-OFDM based HTSMS.

6.3 System Model

We focus on adaptive and non-adaptive CCI mitigation from the perspective of a GEO satellite in the HTSMS scenario. The uplink scenario and interference model is the same as depicted in Chapter 3, Fig. 3.3 and Fig. 3.4 respectively. A link between mobile and satellite is modelled as SIMO with one desired user and $J-1$ interference users. OBBF-A is employed with the Pre-FFT approach as earlier. We also assume no time or frequency offsets exist in the system.

6.3.1 BICM-OFDM Transmitter Model

Fig. 6.1 illustrates the transceiver architecture of the proposed BICM-OFDM based HTSMS and will be referred to throughout the chapter to follow the information flow in the system. At the transmitter end, binary information bits $\{\mathbf{o}\}$ corresponding to the j^{th} user are generated. Bits are encoded into $\{\mathbf{t}\}$ and then interleaved into $\{\mathbf{c}\}$. The Interleaved bits $\{\mathbf{c}\}$ are then mapped into QPSK complex symbols and S/P converted to $\{\widetilde{\mathbf{x}}^q\}$. Pilots for the user considered $\{\widetilde{\mathbf{x}}^p\}$ are interspersed into data sequence $\{\widetilde{\mathbf{x}}^q\}$ at known pilot sub-carriers $\{\mathcal{I}\}$. This process forms an N sub-carriers OFDM symbol that can be expressed as:

$$\widetilde{\mathbf{x}}_j = [\widetilde{x}_j(0), \widetilde{x}_j(1), \ldots, \widetilde{x}_j(N-1)]^T \quad . \qquad j = 1, \ldots, J \ . \tag{6.1}$$

For the sake of brevity, we drop the subscript j that indicates user indexing. After formation of the OFDM symbol, $\widetilde{\mathbf{x}}$ is converted to the time-domain by a N-point IFFT. This can be presented mathematically as:

$$\mathbf{x} = \mathbf{F}^H \widetilde{\mathbf{x}} \ , \tag{6.2}$$

where

$$\mathbf{F} = \begin{bmatrix} 1 & 1 & \cdots & 1 \\ 1 & e^{-j2\pi(1)(1)/N} & \cdots & e^{-j2\pi(1)(N-1)/N} \\ \vdots & \vdots & \ddots & \vdots \\ 1 & e^{-j2\pi(N-1)(1)/N} & \cdots & e^{-j2\pi(N-1)(N-1)/N} \end{bmatrix} \ . \tag{6.3}$$

At the start of the every OFDM symbol, a CP of length G is appended and the output $\bar{\mathbf{x}} = [x(-G), x(-G+1), \ldots, x(N-1)]^T$ is serially transmitted over the wireless channel, whose effect can be represented as:

$$\bar{\mathbf{y}}[k] = \bar{\mathbf{x}}[k] \otimes \mathbf{h}[k] \ . \tag{6.4}$$

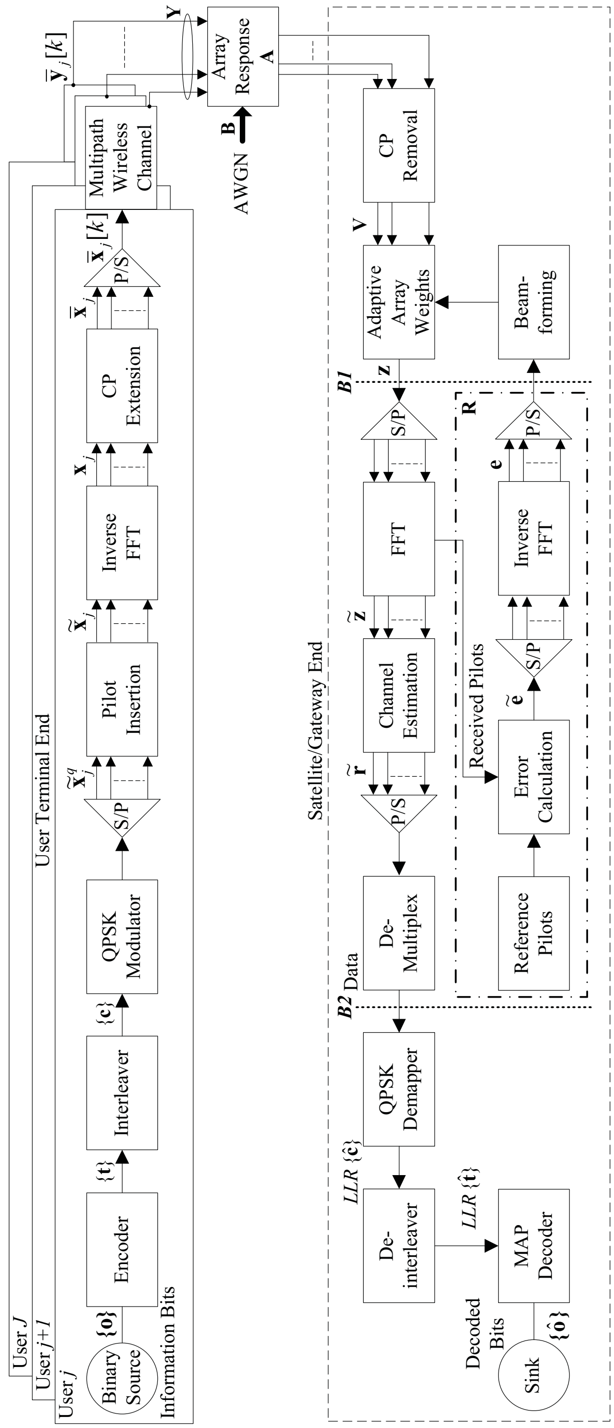

Figure 6.1: BICM-OFDM system model for the HTSMS with OBBF-A and OBBF-SS

6.3.2 Beamforming Capable Receiver

The signals from desired and interference sources are received at the satellite antenna elements (satellite end in Fig. 6.1). The ULA output after CP removal for the l^{th} OFDM symbol ($l = 1, \ldots, L$) for all the users can be represented as:

$$\mathbf{V} = \mathbf{A}\mathbf{Y}^H + \mathbf{B} \ , \tag{6.5}$$

where $\mathbf{Y}$, $\mathbf{B}$ and $\mathbf{V}$ represents the received signal, i.i.d complex Gaussian noise and ULA output respectively as defined earlier in Chapter 3, page 46. $\mathbf{A}$ is the ULA response, where $[\mathbf{A}]_{s,j}$ can be presented mathematically as:

$$a(s,j) = e^{(-j2\pi(s-1)d_a \sin(\theta_j)/\lambda)} \ . \tag{6.6}$$

The output of the ULA is processed by the beamformer to mitigate CCI. This is given by:

$$\mathbf{z} = \mathbf{w}^H\mathbf{V} \ . \tag{6.7}$$

Substituting (6.5) into (6.7), we get:

$$\mathbf{z} = \mathbf{w}^H(\mathbf{A}\mathbf{Y}^H + \mathbf{B}) \ , \tag{6.8}$$

$$\mathbf{z} = [z(0), z(1), \ldots, z(N-1)] \ ,$$

$$\mathbf{w} = [w(1), w(2), \ldots, w(S)]^T \ ,$$

where $\mathbf{z}$ is the weighted output of beamformer and $\mathbf{w}$ are the applied BF complex weights. This is followed by S/P conversion and transformation of $\mathbf{z}$ to the frequency-domain, which can be mathematically expressed as:

$$\widetilde{\mathbf{z}} = \mathbf{F}\mathbf{z}^H \ . \tag{6.9}$$

Using (6.9) and (6.8),

$$\widetilde{\mathbf{z}} = \mathbf{F}(\mathbf{w}^H\mathbf{A}\mathbf{Y}^H + \mathbf{w}^H\mathbf{B})^H \ . \tag{6.10}$$

The data sub-carriers in $\widetilde{\mathbf{z}}$ are de-multiplexed into $\widetilde{\mathbf{r}}^q$ which are then passed to the QPSK demapper as described in Chapter 5, page 111. The demapper outputs LLRs Γ for the v^{th} coded bits c_v in the desired user transmitted data sequence $\widetilde{\mathbf{x}}_d^q$ given received vector $\widetilde{\mathbf{r}}^q$, channel estimates $\widetilde{\mathbf{h}}^q$.

$$\Gamma(c_v(\tilde{x}_d^q(n))) = \ln \frac{\sum_{b\in U_v^+} P(\tilde{x}_d^q(n) = b \mid \tilde{r}^q(n), \tilde{h}^q(n))}{\sum_{b\in U_v^-} P(\tilde{x}_d^q(n) = b \mid \tilde{r}^q(n), \tilde{h}^q(n))} \quad , \tag{6.11}$$

$$P(\tilde{x}_d^q(n) = b \mid \tilde{r}^q(n), \tilde{h}^q(n)) = \frac{1}{2\pi\sigma^2} \exp(-\frac{\|\tilde{r}^q(n) - \tilde{h}^q(n)\tilde{x}_d^q(n))\|^2}{2\sigma^2}) \quad , \tag{6.12}$$

where U_v^- and U_v^+ represent the constellation set that contains all the symbols whose v^{th} bit is 0 and 1 respectively. The conditional probability given in (6.11) is computed using (6.12). The LLRs of the coded bits are de-interleaved and passed to the MAP decoder which outputs the decoded bits $\{\hat{\mathbf{o}}\}$.

6.3.2.1 LMS based OBBF-A

For the next OFDM symbol, computation of new complex BF weights is required. This computation is performed using a MSE based LMS adaptive algorithm as described in Chapter 3, page 47. This error vector at the input of the beamformer in the frequency-domain can be expressed as:

$$\widetilde{\mathbf{e}} = \widetilde{\mathbf{z}}^p - \widetilde{\mathbf{x}}_d^p \quad . \tag{6.13}$$

As we employ Pre-FFT BF, $\widetilde{\mathbf{e}}$ is converted to the time-domain which can be presented mathematically as:

$$\mathbf{e} = \mathbf{F}^H \widetilde{\mathbf{e}} \quad . \tag{6.14}$$

The time-domain error vector obtained in (6.14) is then used in the adaptive beamformer onboard the satellite (OBBF-A). OBBF-A has the objective of interference minimisation and hence can be referred to as interference aware BF. When OBBF-A is pursued as the BF choice, boundary ***B2*** in Fig. 6.1 defines the split between onboard and gateway operations. Moreover region $\mathbf{R}$ in Fig. 6.1

is only implemented with OBBF-A as it constitutes the blocks responsible for adaptive BF. For the case of OBBF-A, we employ LMS algorithm to adapt the complex BF weights until all OFDM symbols have been decoded. The LMS adaptation is given by:

$$\mathbf{w}[l+1] = \mathbf{w}[l] + 2\mu\mathbf{V}[l]\mathbf{e}[l] \ . \tag{6.15}$$

Using (6.14) and (6.15), we get:

$$\mathbf{w}[l+1] = \mathbf{w}[l] + 2\mu\mathbf{V}[l]\mathbf{F}^H\tilde{\mathbf{e}}[l] \ , \tag{6.16}$$

where $\mathbf{w}[l]$ and $\mathbf{w}[l+1]$ represent the beamformer's complex weights for $[l]$ and $[l+1]$ OFDM symbols. μ represents the positive step size which controls the rate of convergence such that [70]:

$$\mu_{min} \leq \mu \leq \mu_{max} \ , \tag{6.17}$$

with

$$\mu_{max} \leq \frac{2}{3\,\mathrm{tr}\,(\mathbf{R})} \ . \tag{6.18}$$

For the HTSMS, we employ LMS with optimised μ that adapts at each iteration according to (6.18). The complexity of beamformer is same as described as described in Chapter 4, page 89.

6.3.2.2 OBBF-SS

OBBF-SS unlike OBBF-A does not aim to minimize interference but maximisation of the gain towards a particular direction. Hence OBBF-SS can be referred to as orientation aware BF. In relation to our HTSMS model in Fig. 6.1, the boundary ***B1*** defines the split between space and ground operations when OBBF-SS is employed. Moreover, blocks in region $\mathbf{R}$ are not implemented as they form the adaptive processing unit. Hence only BF weight application takes place onboard the satellite while remaining operations are transferred to the ground station.

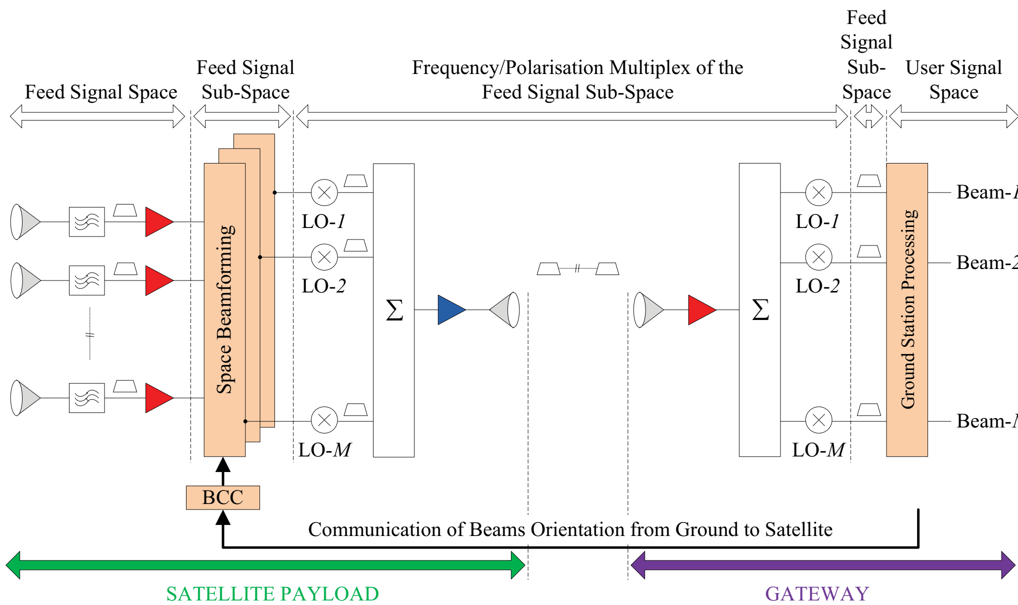

Figure 6.2: OBBF-SS schematic

This significantly reduces onboard complexity, payload mass and the associated costs.

A generalised schematic of OBBF-SS is illustrated in Fig. 6.2. Based on the required beam focus point on the earth surface, the ground processing unit of OBBF-SS calculates the specific direction in which the beam should be oriented. This orientation is transmitted to the satellite where the onboard BF unit calculates the required BF coefficients. The task of weight calculation does not require any signal processing and can be accomplished with simple circuitry which we refer to as Beamforming Coefficient Calculator (BCC) in Fig. 6.2. At the input of BCC are the beam orientations and at the output are the BF coefficients. BCC calculates weights with the objective of maximizing gain towards a specific direction. To calculate these weights, we revisit (6.8).

$$\mathbf{z} = \mathbf{w}^H(\mathbf{A}\mathbf{Y}^H + \mathbf{B}) \ . \tag{6.19}$$

By examining (6.19) it is clear that in order to maximize the gain in a particular direction, complex weights $\mathbf{w}$ should be equal to the array response of the antenna elements. The BCC circuitry enables the weight calculation process via (6.21) – (6.22). These weights are then applied by the space beamformer. If θ_d is the desired beam direction, the BF weights at the output of BCC can be expressed as:

$$\mathbf{w} = [w(1), w(2), \ldots, w(S)]^T \ , \tag{6.20}$$

where

$$w(s) = \exp^{(-j2\pi(s-1)d_a \sin(\theta_d)/\lambda)} \ , \tag{6.21}$$

and

$$\mathbf{w}[l+1] = \mathbf{w}[l] \ . \tag{6.22}$$

After the application of BF weights, the beamformer output is multiplexed and transmitted to the ground station via the feeder links where they are decoded. The complexity of OBBF-SS is same as of optimum BF in Chapter 3, page 49.

6.3.2.3 OBBF-ERC

OBBF-ERC is neither interference aware nor orientation aware BF. It simply sums up signals from all antenna elements in equal proportion. The BF coefficients for the case of OBBF-ERC are the same as (6.20). All the elements of $\mathbf{w}$ are the same and equal to $\frac{1}{S}$ where S are the total number of antenna elements. OBBF-ERC is employed onboard the satellite in the same way as OBBF-SS with minimal complexity. With OBBF-ERC, boundary ***B1*** in Fig. 6.1 defines the split between ground and space operations, while blocks in region $\mathbf{R}$ are not implemented.

6.4 Simulation and Discussions

A SIMO OFDM system with per link one transmit and multiple receive antenna elements S={2,4} was modelled. Total sub-carriers in an OFDM symbol are 32 and L (OFDM symbols) is taken as 40,000. $\mathcal{I} = \{1, 8, 16, 24, 32\}$ hence $N_p = 5$. In accordance with Fig. 3.4 (Chapter 3, page 42), one desired user was modelled at 40° azimuth while interference users were located at −70°, −35° and 60° azimuth. A rate-1/2 $(5, 7)_8$ convolution encoder is employed for channel coding. Random interleaving/de-interleaving is adopted in the simulations with QPSK as the modulation scheme. We compare the performances of OBBF-A, OBBF-SS and OBBF-ERC for BICM-OFDM based HTSMS.

6.4.1 Performance

We first investigate beamformers' performance in terms of their precision (prediction error). This is plotted in Fig. 6.3 in terms of MSE (dB) against desired user E_b/N_o. We note that as the number of antenna elements increases from 2 to 4, reduction in MSE is observed. This is due to superior interference mitigation as a result of more antenna elements onboard the satellite. We can also observe that as available E_b/N_o increases, the performance of all studied BF schemes improve. This is attributed towards reduced Gaussian noise in the system. Specific to the studied schemes, we observe that irrespective of the number of antenna elements, OBBF-ERC shows poor performance as its MSE is non-negative for all values of E_b/N_o. For all antenna elements configurations and E_b/N_o levels tested, OBBF-A provides superior precision which is followed by OBBF-SS. This is because OBBF-A is trying to provide high gain in the direction of the desired user as well as simultaneously minimise gain towards the direction of interference users. However when E_b/N_o is low, the performance of OBBF-A and OBBF-SS are similar. To put this result in perspective, lets consider two extreme scenarios

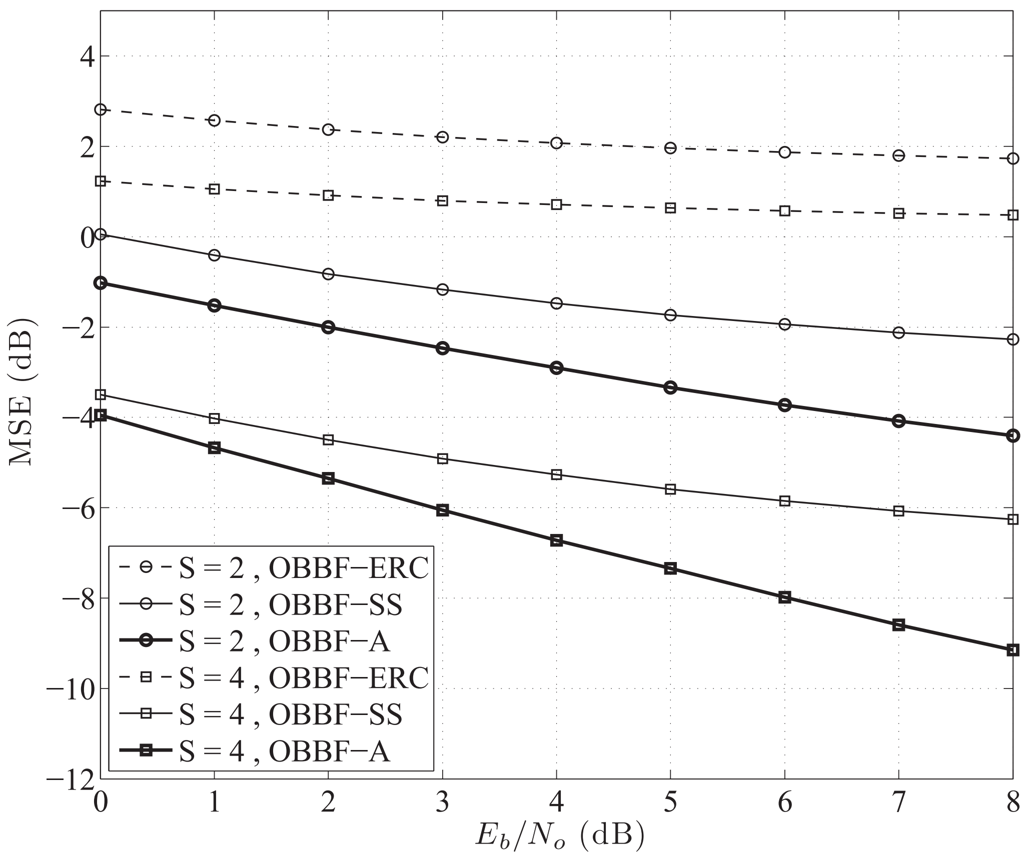

Figure 6.3: Beamforming prediction error in terms of Mean Squared Error vs desired user E_b/N_o, antenna elements = 2 & 4.

that were simulated: Scenario 1 – E_b/N_o = 0 dB and Scenario 2 – E_b/N_o = 8 dB. We define the Precision Gain (PG) metric as a measure of BF prediction error of the respective schemes as compared to OBBF-ERC. PG for the two mentioned scenarios is presented in Fig. 6.4. It is evident from the figure that in the low E_b/N_o regime irrespective of the number of antenna elements, the PGs for OBBF-A and OBBF-SS are comparable. However as the available E_b/N_o increases, PG improves. Furthermore, with higher number of antenna elements, adaptive processing provides a much higher PG as compared to the semi static approach.

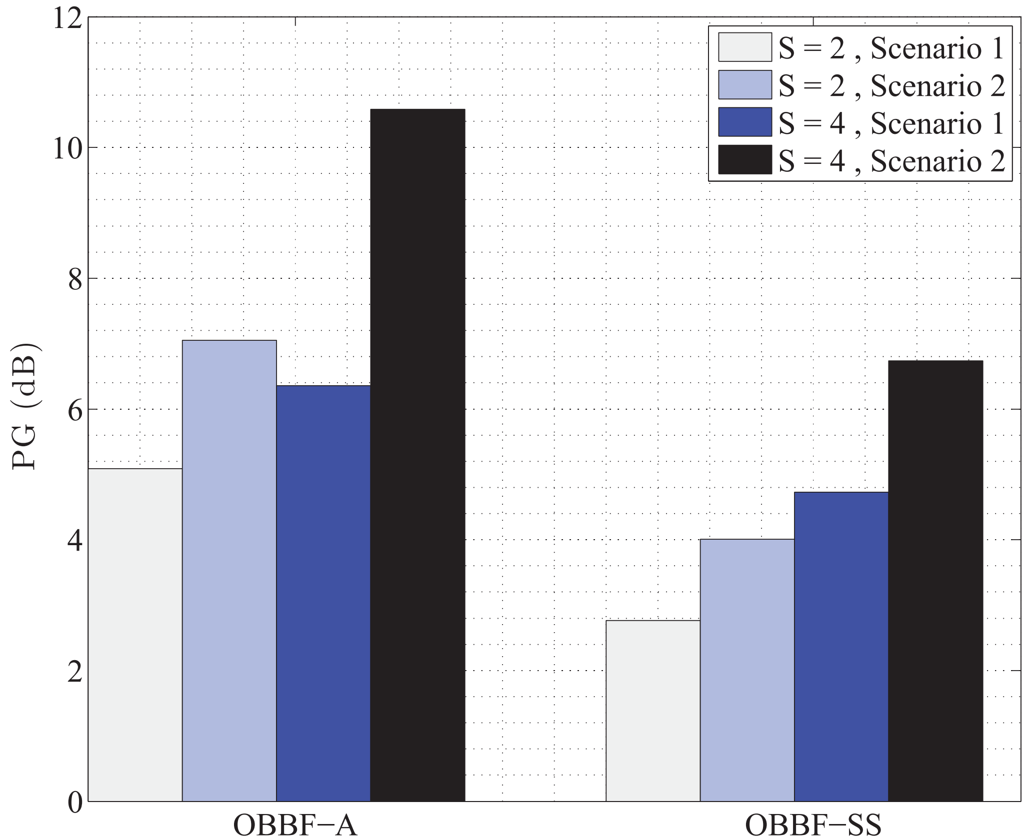

Figure 6.4: Precision Gain for OBBF-A and OBBF-SS relative to OBBF-ERC.

To have further insight into the results, we illustrate the beam patterns for the studied beamformers in Fig. 6.5 with $S = 4$, $E_b/N_o = 8$ dB. We can observe that OBBF-A and OBBF-SS provide high gain at 40° which is the desired user direction, whereas OBBF-ERC fails to do this. OBBF-A achieves this orientation by adapting BF coefficients and OBBF-SS by having the prior knowledge of this direction. However in the case of interference users present at $-75°$, $-35°$ and $60°$, only OBBF-A adapts the BF coefficients in a way to provide lower gain in these direction relative to 40°. Hence OBBF-A outperforms the rest in terms of prediction error by providing higher gain in the desired direction relative to the gains provided to interference sources.

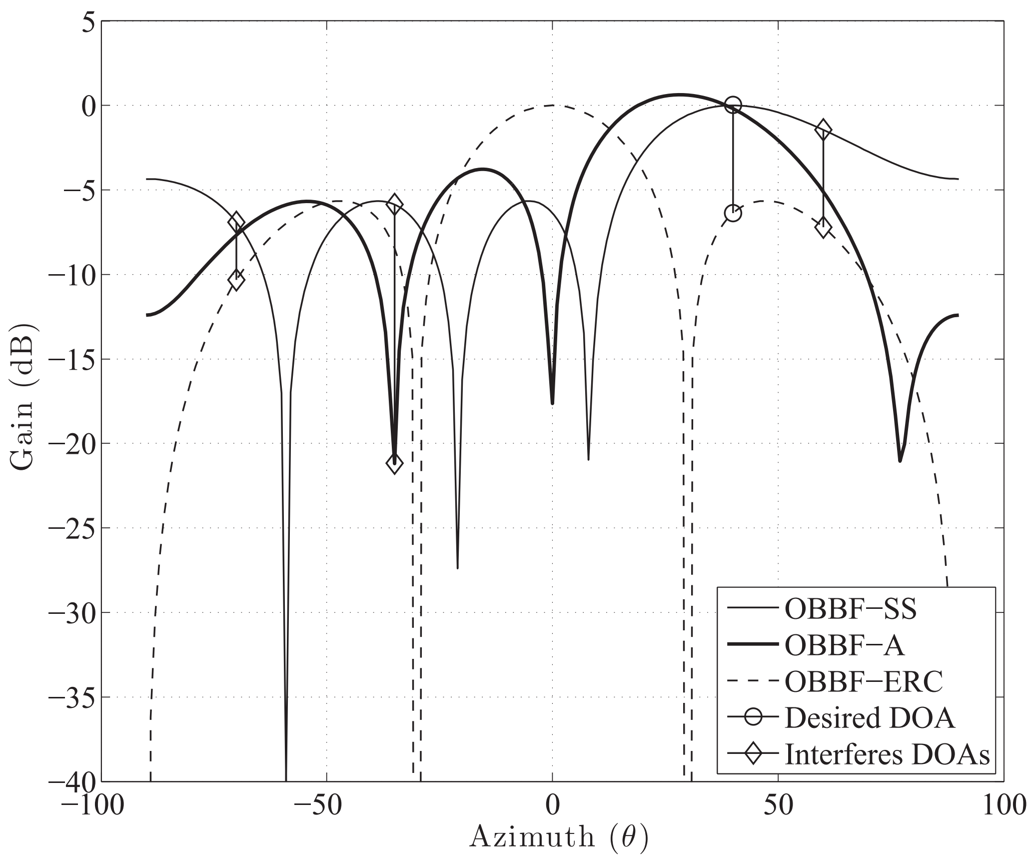

Figure 6.5: Beam patterns for studied schemes, antenna elements = 4 and $E_b/N_o = 8$ dB.

To elaborate on performance differences shown in Fig. 6.5, we analyse the Beamforming Gain (BFG) of the beamformers under study. Fig. 6.6 depicts the BFG provided by the respective beamformers for the aforementioned scenario. We can see that irrespective of the direction of the interference source, OBBF-A exhibits superior BFG. In other words, it suppresses interferes sources better than the rest of the beamformers. This is due to OBBF-A being desired direction as well as interference aware. BFG of OBBF-SS follows that of OBBF-A as it is only desired direction aware and not interference aware. OBBF-ERC has the lowest BFG in all directions as it is neither desired direction not interference aware.

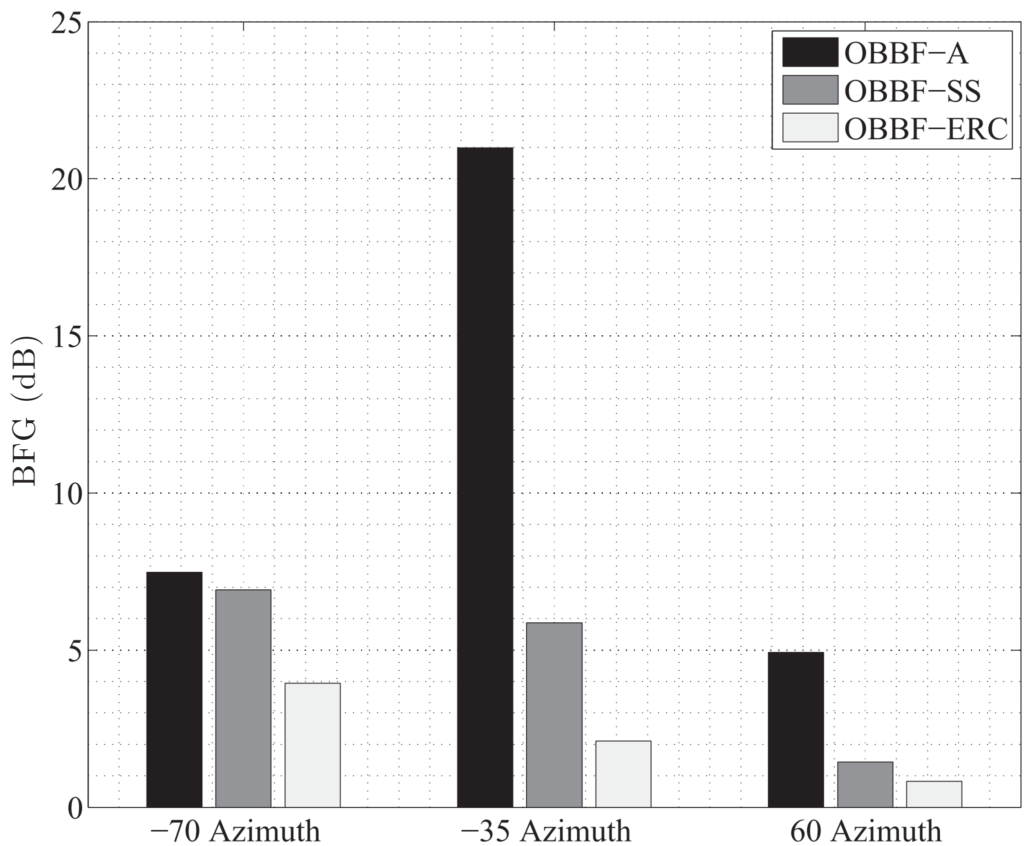

Figure 6.6: Beamforming Gain for studied schemes, antenna elements = 4 and $E_b/N_o = 8$ dB.

BFG further verifies the outcome of prediction error as well PG.

Fig. 6.7 shows the system performance in terms of BER versus desired user E_b/N_o with different antenna element configurations. We note that with increase in antenna elements or E_b/N_o, the BER achieved for the studied schemes improves. However, irrespective of the E_b/N_o or antenna element configuration, OBBF-ERC gives poor performance which is consistent with all the previous results. For the 2 antenna elements case, OBBF-A and OBBF-SS BER performance is comparable. This is a consequence of 1) higher prediction error as depicted in Fig. 6.3 and 2) with the $S = 2$, the ratio of interference to antenna elements is greater than

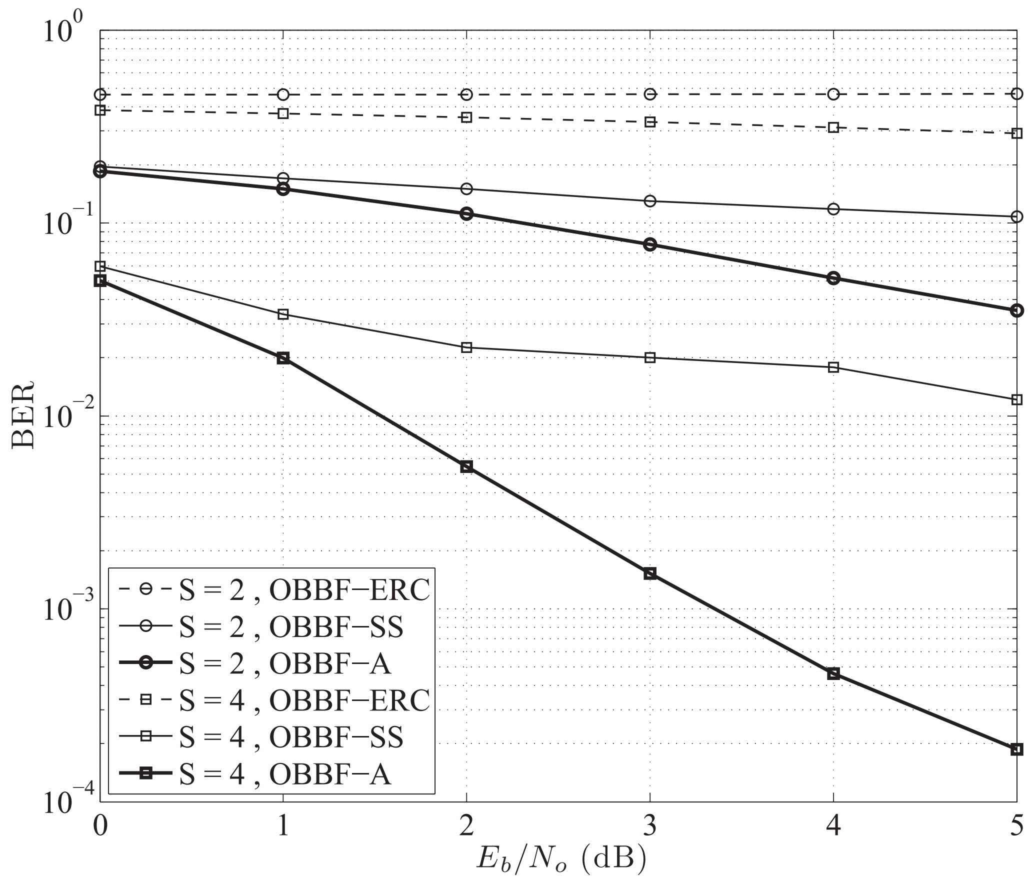

Figure 6.7: Bit Error Rate vs desired user E_b/N_o, antenna elements = 2 & 4.

1 which makes BF less effective. With $S = 4$ however, OBBF-A outperforms the competitors, especially at high E_b/N_o regime. On the contrary at very lower E_b/N_o values, the BER performance of OBBF-A and OBBF-SS is similar which is consistent with other results.

6.5 Conclusions

In this chapter we proposed OBBF-SS, a semi static hybrid space/ground BF approach. The OBBF-SS is far less complex than the adaptive solution and significantly reduces onboard and gateway complexity as well as feed link bandwidth requirements. We also employ LMS based full adaptive onboard BF and ERC BF techniques for a BICM-OFDM based HTSMS. We analysed their performance in terms of prediction error, beam pattern and Bit Error Rate (BER). We define Prediction Gain (PG) and Beamforming Gain (BFG) as the metrics to quantify BF performance. Simulation results show that OBBF-A is superior due to being interference aware. This however is achieved at the cost of higher complexity onboard the satellite. On the contrary, at low E_b/N_o regime as well as with higher interference users to antenna elements ratio, the performance of non-adaptive OBBF-SS is very much comparable to the full adaptive approach. Moreover, as compared to existing static BF approaches, OBBF-SS offers a practical and attractive alternative for satellite systems offering services such as TV broadcasting, broadband internet. As the non-adaptive scenario does not perform poorly, we can conclude that the full-adaptive process may not be required at all times in HTSMS scenario. Hence there exists space for semi-adaptive based BF solution that may have the potential to relax the onboard power requirements as well as perform far better than the non-adaptive approach. We exploit this observation in next chapter and proposed a novel semi-adaptive BF mechanism.

Chapter 7

Semi-Adaptive Beamforming for HTSMS

In this chapter we propose a novel semi-adaptive BF which switches between adaptive and non-adaptive processing depending on the input signal characteristics at the satellite antenna elements. We develop a novel switch based BF mechanism which is robust to both disturbance in the system as well as False Switching (FS). Subsequently, we compare the proposed semi-adaptive against full adaptive BF and quantify the performance advantages. Part of the work presented here is under review in *IEEE Transactions on Wireless Communications* 2010 [102].

7.1 Introduction

Full-adaptive processing whether implemented onboard the satellite or at the gateway has its associated complexities and issues. The proposed OBBF-SS in Chapter 6 offers a practical and attractive alternative for satellite systems offering broadcasting services. However this approach is not suitable for scenarios where beams need to be changed on a more frequent basis. For the HTSMS case, we observe in Chapter 6 that although adaptive BF is superior, semi-static performance is comparable in specific scenarios. From this we conclude that adaptive processing w.r.t BF may not be required at all times. Hence building on this, we here propose a novel semi-adaptive BF, referred to as OBBF-Semi Adaptive (OBBF-SA). The proposed technique is a switch-type onboard BF that enables adaptive and non-adaptive processing to coexist. For the OBBF-SA, we develop a novel and robust switching mechanism which is independent of disturbance in the system. We investigate the performance of this approach as compared to full adaptive BF in terms of both system performance as well computational gains.

7.2 Related Work and Algorithm Formulation

In HTSMS we implement BF onboard the satellite. State-of-the-art satellite systems employ GBBF-A as discussed earlier. The approach is preferable with respect to space BF as there are substantial overheads associated with onboard BF networks such as hardware mass, cost, power consumption and thermal control requirements. Despite the benefits, GBBF-A has issues such as requirement of large amount of transceiver hardware, redundant channels for feed signals and complex ground calibration system. In pursuit of addressing the trade-off, hybrid onboard/ground BF solutions [18, 19] have been proposed where some parts of the BF are done onboard and some at the gateway.

Splitting of BF between space and ground component of a satellite network as in [18, 19] reduces the computation needs onboard the satellite. However, a complex calibration system is still required at the gateway to compensate for propagation amplitude and phase dispersion effects. Moreover the topology is still sensitive to instabilities due to payload component changes in temperature and over its life time as well as similar gateway component changes.

We now examine the trade-off between ground and space BF from a different perspective. The main motivations behind aforementioned hybrid topologies are

1) To reduce the computational requirements for the space components and 2) to reduce the number of feeds transmitted to the gateway for ground processing. The more we move towards the space BF approach, the feed requirements reduce but complexity onboard the satellite increases. However noting our results from Chapter 6, we know that adaptive processing may not be required at all times. Hence by developing a comprehensive mechanism that can switch off and on the adaptive processing onboard the satellite as and when required can achieve both the objectives - 1) reduced complexity and power requirements onboard the satellite and 2) reduced signal space transmitted from space to gateway as BF takes place on the satellite end. Therefore, exploiting our results in Chapter 6, we devise a semi-adaptive BF framework which has reduced computational requirements without compromising on system performance.

We propose a novel switch-type semi-adaptive BF algorithm which switches between adaptive and non-adaptive processing depending on the input signal characteristics at the satellite antenna elements. *DiRienzo et al.* [103] develop a semi-adaptive smoothing algorithm for power spectrum estimation. Their work is extended by *Yang et al.* [104] which uses the same approach for spectrum estimation. As oppose to the aforementioned approaches, we develop a novel slope based switching mechanism which enables adaptive and non-adaptive processing to coexist. The proposed BF algorithm is independent of disturbance in the system and is robust to False Switching (FS).

In order to formulate the semi adaptive BF, we revisit LMS filtering. In LMS, the adaptation process is based on the energy of instantaneous errors. The weight update recursion is given by:

$$\mathbf{w}[k+1] = \mathbf{w}[k] + \mu e[k]\mathbf{x}[k] \quad . \tag{7.1}$$

Here $[k]$ presents the time indexing. The instantaneous error $e[k]$ can be presented as:

$$e[k] = d[k] - \mathbf{x}^T[k]\mathbf{w}[k] \quad , \tag{7.2}$$

where the desired user signal $d[k]$ is given by:

$$d[k] = \mathbf{x}^T[k]\mathbf{w}^*[k] + \delta[k] \ . \tag{7.3}$$

By substituting (7.3) into (7.2), we obtain:

$$\begin{aligned} e[k] =& \mathbf{x}^T[k](\mathbf{w}^*[k] - \mathbf{w}[k]) + \delta[k] \ , \\ =& \varepsilon[k] + \delta[k] \ , \end{aligned} \tag{7.4}$$

where $\varepsilon[k]$ and $\delta[k]$ can be referred to as the random error and the error floor respectively. For the conventional full-adaptive LMS, $e[k]$ is used in (7.1) to recursively adapt $\mathbf{w}[k]$ at every k leading to consistent reduction in $e[k]$. In an ideal case when $\delta[k] = 0$:

$$\lim_{k\to\infty} e[k] \to 0 \ . \tag{7.5}$$

With reference to spatial filtering, (7.5) refers to perfect interference mitigated state where low gains have been projected to the direction of interference sources while high gain towards the direction of the desired signal. In the ideal environment, state (7.5) would be achieved and $e[k] \to 0$. This can be an indicator used to switch-off the adaptivity of LMS process. Specific to the satellite payload, this can save valuable resources such as onboard computing power. However the error floor persists due to the presence of noise in the system and therefore the state (7.5) is not achieved. Moreover instantaneous $e[k]$ fluctuates around its mean and hence is not stable. Therefore in a practical system, $e[k]$ alone cannot be defined as an appropriate Beamforming Switching Metric (BSM). To solve this problem we need to derive a suitable BSM that can be used to switch BF from adaptive to non-adaptive state and vice versa. For an OFDM based system, we first analyse MSE obtained for the l^{th} OFDM symbol.

$$\omega_l = \frac{1}{N_p} . \sum_{n=1}^{Np} e_l^2(n) \ . \qquad l = 1, \ldots, L \ . \tag{7.6}$$

N_p and $\mathbf{e}$ in (7.6) represent the number of pilots and error vectors corresponding to the l^{th} OFDM symbol respectively. The variance of ω_l can be given as:

$$\Psi_{L-1} = \frac{1}{L-1}\sum_{l=1}^{L-1}(\omega_l - \bar{\omega})^2 + \acute{\delta} \ , \tag{7.7}$$

where $\bar{\omega}$ presents the block mean and $\acute{\delta}$ presents the variance floor due to disturbance in the system. The variance in (7.7) is computed over a window of $L-1$ OFDM symbols. This is defined as Monitoring Window (MW) whose size incrementally grows from 1 to $L-1$ as OFDM symbols are received. When the L^{th} OFDM symbol is received, the variance over $\parallel$ MW $\parallel = L$ as a function of (7.6) and (7.7) can be expressed as:

$$\Psi_L = \frac{1}{L}((L-1)\Psi_{L-1} + (\omega_l - \bar{\omega})^2 + \acute{\delta}) \ . \tag{7.8}$$

As $\parallel$ MW $\parallel \to \infty$, (7.8) can be expressed as:

$$\begin{aligned}
\lim_{L\to\infty}\Psi_L &= \frac{(L-1)\Psi_{L-1}}{L} + \frac{(\omega_l - \bar{\omega})^2 + \acute{\delta}}{L} \ . \\
\Psi_L &\approx \Psi_{L-1} + \frac{(\omega_l - \bar{\omega})^2 + \acute{\delta}}{L} \ . \\
\Psi_L &\approx \Psi_{L-1} \ .
\end{aligned} \tag{7.9}$$

In similar fashion to (7.8), Ψ_{L-1} can be further expressed as:

$$\Psi_{L-1} = \frac{1}{L-1}((L-2)\Psi_{L-2} + (\omega_{l-1} - \bar{\omega})^2 + \acute{\delta}) \ . \tag{7.10}$$

with

$$\lim_{L\to\infty}\Psi_{L-1} \approx \Psi_{L-2} \ . \tag{7.11}$$

Now if we compute the slope between (7.8) and (7.10), it can be formulated as:

$$\begin{aligned}
\nabla\Psi_L =& \Psi_L - \Psi_{L-1} \\
=& \left[\frac{1}{L}((L-1)\Psi_{L-1} + (\omega_l - \bar{\omega})^2 + \acute{\delta})\right] - \\
& \left[\frac{1}{L-1}((L-2)\Psi_{L-2} + (\omega_{l-1} - \bar{\omega})^2 + \acute{\delta})\right] \\
=& \frac{(L-1)^2\Psi_{L-1} - L(L-2)\Psi_{L-2} + (L-1)(\omega_l - \bar{\omega})^2 - L(\omega_{l-1} - \bar{\omega})^2}{L(L-1)}
\end{aligned} \tag{7.12}$$

Eq. 7.12 is simply the slope between two consecutive variance values $\Psi_L$and Ψ_{L-1}. We can also observe that the slope $\nabla\Psi$ is independent of the variance floor $\acute{\delta}$. Now as $\parallel$ MW $\parallel \rightarrow \infty$, (7.12) can be expressed as:

$$\begin{aligned}
\lim_{L\rightarrow\infty} \nabla\Psi_L = & \left[\frac{(L-1)^2\Psi_{L-1} - L(L-2)\Psi_{L-2}}{L(L-1)}\right] \\
& + \left[\frac{(L-1)(\omega_l - \bar{\omega})^2 - L(\omega_{l-1} - \bar{\omega})^2}{L(L-1)}\right] \\
\\
\approx & \left[\frac{L^2\Psi_{L-1} - L^2\Psi_{L-2}}{L^2}\right] \\
& + \left[\frac{L(\omega_l - \bar{\omega})^2 - L(\omega_{l-1} - \bar{\omega})^2}{L^2}\right] \\
\\
\approx & \Psi_{L-1} - \Psi_{L-2} + \frac{(\omega_l - \bar{\omega})^2 + (\omega_{l-1} - \bar{\omega})^2}{L} \ .
\end{aligned} \tag{7.13}$$

And using (7.9), (7.13) can be further simplified to:

$$\lim_{L\rightarrow\infty} \nabla\Psi_L \rightarrow 0 \ . \tag{7.14}$$

As $\nabla\Psi \rightarrow 0$ irrespective of the $\acute{\delta}$, ω_l and $\bar{\omega}$, hence it is not effected by the BF prediction error. Therefore, $\nabla\Psi$ can be effectively used as a BSM in the presence of disturbances in the system. Moreover as the $\nabla\Psi$ is measured over a MW, it is more reliable as compared to instantaneous error $e[k]$. However, we note that in (7.13) when $\parallel$ MW $\parallel = \infty$ ($L \rightarrow \infty$), the contribution of variance computed over L symbols towards the $\nabla\Psi_L$ is null.

$$\lim_{L\rightarrow\infty} \frac{(\omega_l - \bar{\omega})^2 + (\omega_{l-1} - \bar{\omega})^2}{L} \rightarrow 0 \ . \tag{7.15}$$

In other words when L is large, $\nabla\Psi$ is insensitive to changes in the characteristics of the input signal $\mathbf{x}$. With respect to BF, this condition makes the BSM immune to changes in user locations and hence BSM becomes incapable of turning back on the adaptive processing when needed. To solve this problem, we define a Moving

Monitoring Window (MMW) such that:

$$\parallel \text{MMW} \parallel = \rho \ . \qquad \rho \ll \infty \ . \tag{7.16}$$

Defining generically, MMW moves g symbols while performing continuous monitoring of $\nabla\Psi$. Now with the MMW, state (7.15) can be reformulated as:

$$\lim_{L\to\rho} \frac{(\omega_l - \bar{\omega})^2 + (\omega_{l-1} - \bar{\omega})^2}{L} \nrightarrow 0 \ . \tag{7.17}$$

Therefore the state (7.14) and (7.15) is not achieved as $\nabla\Psi$ will show variation if characteristics of $\mathbf{x}$ change. Moreover, as $L \nrightarrow \infty$, it implies $\nabla\Psi_L \nrightarrow 0$ and would vary within given bounds. Hence, for the case of i.i.d. complex Gaussian noise $\sim \mathcal{CN}(0, \sigma^2)$ in the system, we drive the bounds of the $\nabla\Psi$ in terms of σ^2 and ρ. The variance of the mean of $\nabla\Psi$ can given by:

$$\Omega = \text{Var}\left(\frac{1}{\rho}\sum_{l=1}^{\rho} \nabla\Psi_l\right) \ . \tag{7.18}$$

As all the variables have the same variance σ^2, division by ρ becomes a linear transformation. Hence (7.18) can be simplified to:

$$\Omega = \frac{\sigma^2}{\rho} \ . \tag{7.19}$$

We can observe that if the condition (7.16) is relaxed and $\rho \to \infty$, $\Omega \to 0$ which is consistent with (7.14). With respect to BF, imposing MMW will result into $\nabla\Psi$ varying within the bound derived in (7.19). This is given by:

$$\mid \nabla\Psi \mid \leq \mid \Omega \mid \ . \tag{7.20}$$

The state (7.20) is achieved when BF convergence has taken place and $\nabla\Psi$ becomes an effective BSM. It not only provides the switching functionality, it also takes into account any instantaneous changes in the received signal characteristics as well as system noise. However taking into account a practical BSM enabled BF system, there is a probability of False Switching (FS). Furthermore,

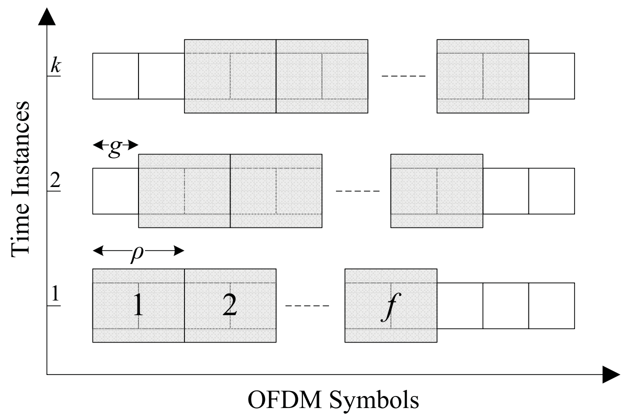

Figure 7.1: Moving Monitoring Block (MMB) schematics

the switching mechanism needs to be stable and robust. To ensure that the BSM does not trigger FS and to make it more stable, we monitor $\nabla\Psi$ over consecutive MMWs, each of size ρ rather than a single MMW. To enable this, we constitute a block, referred to as Moving Monitoring Block (MMB), of f consecutive MMWs which slides over g symbols. Illustration of MMB and its operation is depicted in Fig. 7.1. When all f MMWs meet the criteria as in (7.20), a Beamforming Triggering Flag (BTF), denoted by Λ, is set to 0 causing switch from adaptive to non-adaptive processing. If at any time after the switch has been made, all f MMWs violate the criteria in (7.20), adaptive BF is switched back on by setting Λ to 1. Provisioning of MMB ensures that the switching mechanism is robust and BSM does not trigger a false BF switch from adaptive to non-adaptive and vice versa. The pseudo-code representation of the proposed semi-adaptive algorithm is represented as Algorithm 2.

In order to verify the derived bounds and working of the proposed algorithm, Fig. 7.2 and 7.3 indicate $\nabla\Psi$ for the case of OFDM BF with MW and MMW. We can observe in Fig. 7.2 that for the case of MW where $L = \infty$, $\nabla\Psi$ is within the bounds derived in (7.19). However after around 200 OFDM symbols, $\nabla\Psi = 0$ which is consistent with (7.14). We can also see that as OFDM symbols increase,

Algorithm 2 Semi-Adaptive LMS Beamforming

Initialise: $(s, l, \mu, f, g, \rho, \text{MMB})$
Require: Λ (BTF) $\leftarrow 1$ for $l = 1$
$\sum_{s=1}^{s=S} w(s) = 1$ for $l = 1$
$\mu_{min} \leq \mu \leq \mu_{max}$ for every l

while $l \leq L$ **do**
  input $\mathbf{e}_l$ for every l
  Compute $\nabla\Psi$ and Ω over MMB
  if $\Lambda = 1$ **and** $|\nabla\Psi| \leq |\Omega|$ **then**
    $\Lambda \leftarrow 0$
    $\mathbf{w}[l+1] = \mathbf{w}[l]$
  else if $\Lambda = 1$ **and** $|\nabla\Psi| \geq |\Omega|$
    $\Lambda[l] = \Lambda[l-1]$
    Compute of $\mathbf{w}[l+1] \Rightarrow \mathbf{w}[l]$
  else if $\Lambda = 0$ **and** $|\nabla\Psi| \geq |\Omega|$
    $\Lambda \leftarrow 1$
    $\mathbf{w}[l+1] = \mathbf{w}[l] + \mu e[l]\mathbf{x}[l]$
  else
    $\Lambda[l] = \Lambda[l-1]$
    Compute of $\mathbf{w}[l+1] \Rightarrow \mathbf{w}[l]$
  end if
  Move MMB over g OFDM symbols
end while

no fluctuation is observed in $\nabla\Psi$, which is again consistent with observation in (7.15). Hence w.r.t BF, when the number of OFDM symbols are large, changes in interference profile or changes in the system would not be traceable. On the other hand for the MMW case with $\rho = 50$, $\nabla\Psi$ is within the bounds after $\approx$ 125 OFDM symbols. Interestingly we can also observe that $\nabla\Psi$ is not a constant value with increase in OFDM symbols and at all times its variation is within the bounds. This verifies (7.17) and that BSM with MMW will be able to track changes in the system. Hence for this particular scenario, we can potentially trigger the switch at the 150 symbol point. However if we employ MMB topology with for instance $f = 3$, the $\nabla\Psi$ monitoring will continue until 250 symbol and the switch can only take place when $l \geq 250$. The advantage of using the MMB

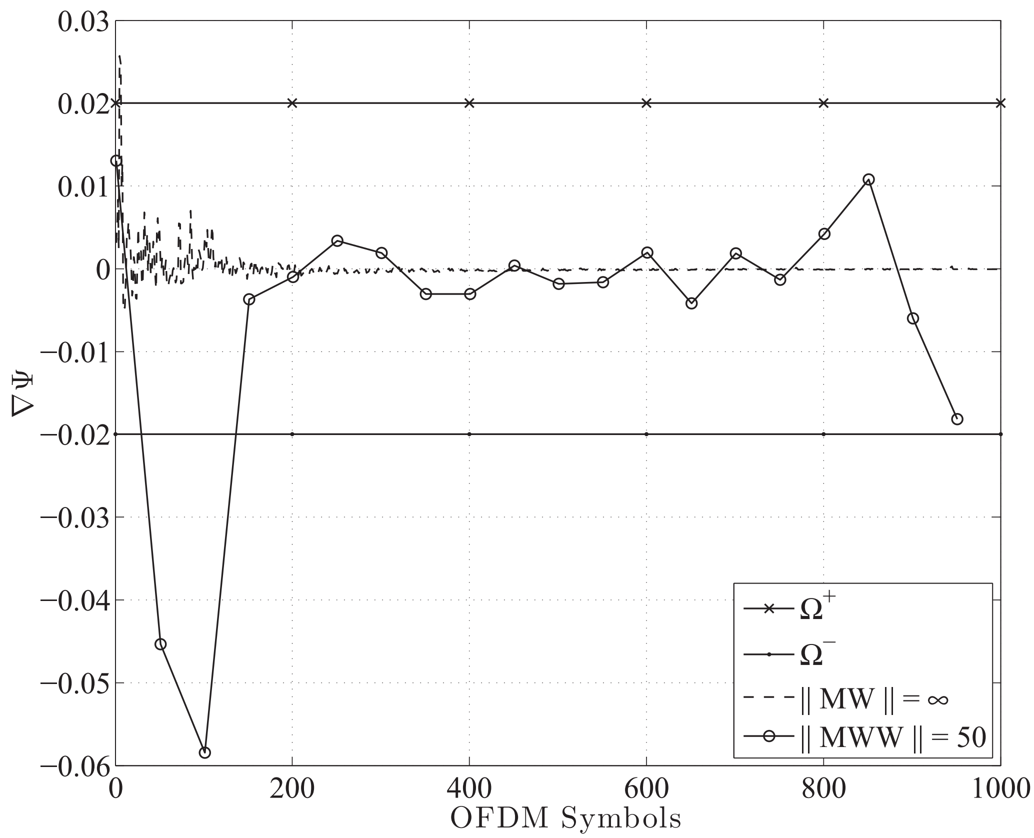

Figure 7.2: $\nabla\Psi$ vs OFDM symbols with $\sigma^2 = 1$, $\rho = 50$, $g = 10$, $N = 32$, $N_p = 5$ and antenna elements $= 4$.

approach is hence twofold. 1) It ensures that algorithm is stable and robust towards FS. 2) By defining parameter f, we can effectively control the number of symbols prior to which a switch cannot be triggered. The number of initial symbols which perform adaptive BF irrespective of $\nabla\Psi$ can be defined as:

$$L_{min} = \rho \times f \tag{7.21}$$

As we reduce σ^2 to 0.1, we can note from Fig. 7.3 the bounds are automatically adjusted to a much tighter value in accordance with (7.19). Moreover, $\nabla\Psi$ is operated within these bounds after $\approx$ 100 OFDM symbols and again at this point a switch can be triggered. However using the MMB approach with $f = 3$,

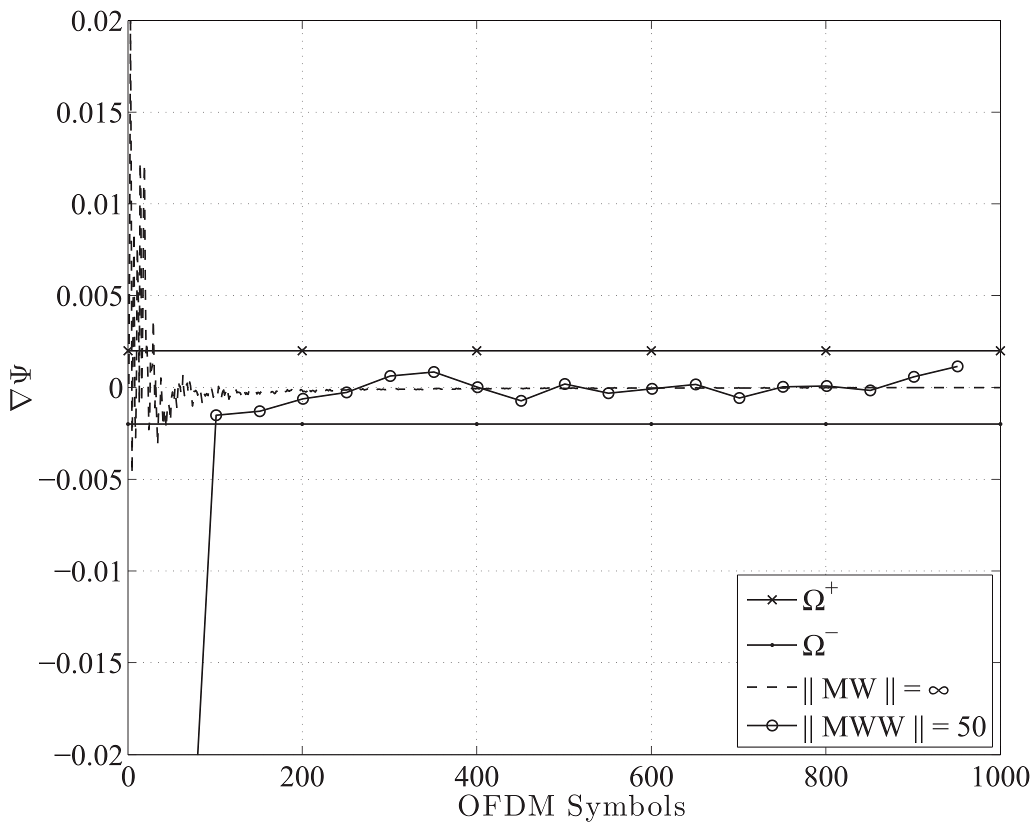

Figure 7.3: $\nabla\Psi$ vs OFDM symbols with $\sigma^2 = 0.1$, $\rho = 50$, $g = 10$, $N = 32$, $N_p = 5$ and antenna elements $= 4$.

the switch can be triggered at the 200 symbol point. Comparing the two figures, we can also conclude that with low noise variance, switching can be performed earlier than the case when noise is high. These figures in general verify our switching mechanism with BSM metric, and specifically the earlier derived bounds in (7.18)−(7.19) and states mentioned in (7.14), (7.15) and (7.17).

7.3 System Model

The HTSMS uplink scenario and the interference model is the same as depicted in Chapter 3, Fig. 3.3 and Fig. 3.4 respectively. A link between mobile and satellite is modelled as SIMO with one desired user and $J-1$ interference users. After the signal passes through the wireless channel, semi-adaptive Pre-FFT BF is applied at the satellite end to mitigate interference induced by BTS users. No time or frequency offsets exist in the system.

7.3.1 BICM-OFDM Transmitter Model

In Fig. 7.4 we show the transceiver architecture of the proposed BICM-OFDM based HTSMS and will be referred to throughout the chapter to follow the information flow in the system. Binary information bits $\{\mathbf{o}\}$ corresponding to the j^{th} user are generated at the user terminal end. Generation of bits $\{\mathbf{o}\}$ is followed by encoding them into $\{\mathbf{t}\}$ which are then interleaved into $\{\mathbf{c}\}$. The Interleaved bits $\{\mathbf{c}\}$ are then mapped into QPSK complex symbols and S/P converted to $\{\widetilde{\mathbf{x}}^q\}$. Pilots for the user considered $\{\widetilde{\mathbf{x}}^p\}$ are interspersed into data sequence $\{\widetilde{\mathbf{x}}^q\}$ at known pilot sub-carriers $\{\mathcal{I}\}$. The output of this process is an N sub-carriers OFDM symbol that can be expressed as:

$$\widetilde{\mathbf{x}}_j = [\widetilde{x}_j(0), \widetilde{x}_j(1), \ldots, \widetilde{x}_j(N-1)]^T \quad . \qquad j = 1, \ldots, J \ . \tag{7.22}$$

For the sake of brevity, we drop the subscript j that indicates user indexing. After formation of OFDM symbol, $\widetilde{\mathbf{x}}$ is converted to the time-domain by a N-point IFFT. This can be represented mathematically as:

$$\mathbf{x} = \mathbf{F}^H \widetilde{\mathbf{x}} \ , \tag{7.23}$$

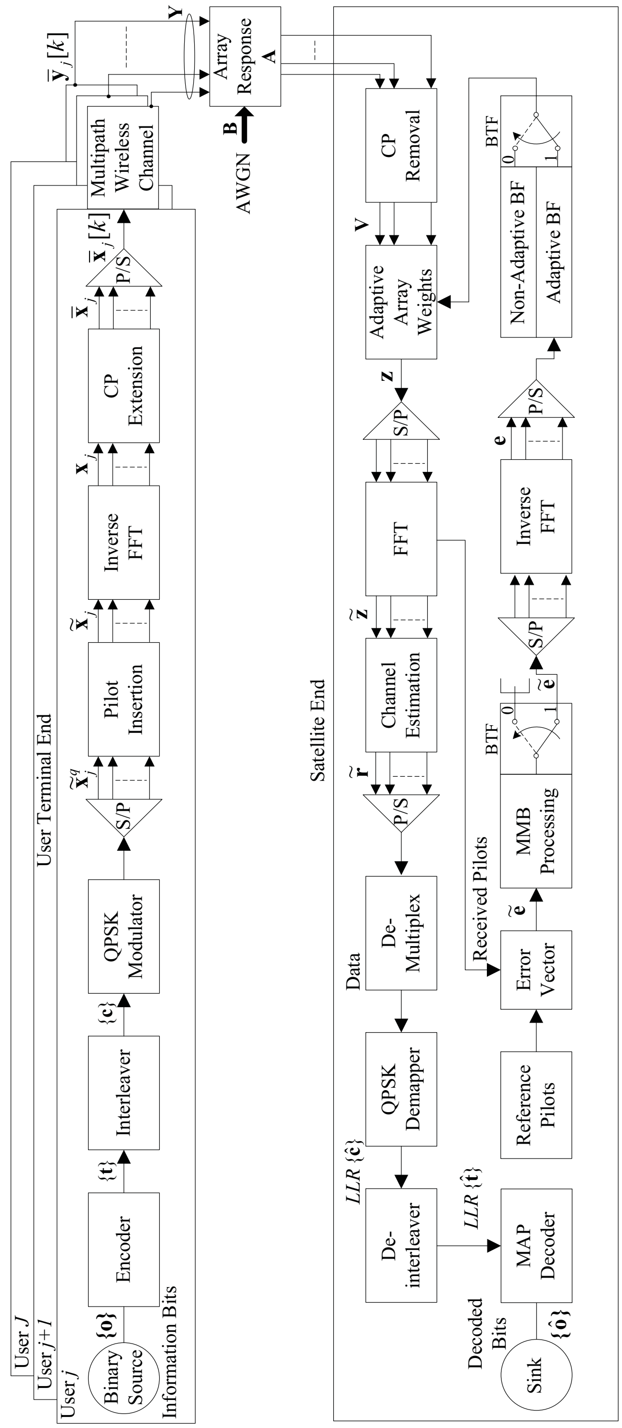

Figure 7.4: BICM-OFDM system model for the HTSMS with OBBF-SA at the satellite end

where

$$\mathbf{F} = \begin{bmatrix} 1 & 1 & \cdots & 1 \\ 1 & e^{-j2\pi(1)(1)/N} & \cdots & e^{-j2\pi(1)(N-1)/N} \\ \vdots & \vdots & \ddots & \vdots \\ 1 & e^{-j2\pi(N-1)(1)/N} & \cdots & e^{-j2\pi(N-1)(N-1)/N} \end{bmatrix} \ . \tag{7.24}$$

At the start of the every OFDM symbol, a CP of length G is appended and the output $\bar{\mathbf{x}} = [x(-G), x(-G+1), \ldots, x(N-1)]^T$ is serially transmitted over wireless channel, whose effect can be presented as:

$$\bar{\mathbf{y}}[k] = \bar{\mathbf{x}}[k] \otimes \mathbf{h}[k] \ . \tag{7.25}$$

7.3.2 BICM-OFDM Receiver with Semi-Adaptive BF

The signal from desired and interference sources is received at the satellite antenna elements (satellite end in Fig. 7.4). The ULA output after CP removal for the l^{th} OFDM symbol ($l = 1, \ldots, L$) for all the users can be presented as:

$$\mathbf{V} = \mathbf{A}\mathbf{Y}^H + \mathbf{B} \ , \tag{7.26}$$

where $\mathbf{Y}$, $\mathbf{B}$ and $\mathbf{V}$ represents the received signal, i.i.d complex Gaussian noise and ULA output respectively as defined earlier in Chapter 3, page 46. $\mathbf{A}$ is the ULA response, where $[\mathbf{A}]_{s,j}$ can be presented mathematically as:

$$a(s,j) = e^{(-j2\pi(s-1)d_a \sin(\theta_j)/\lambda)} \ . \tag{7.27}$$

The output of the ULA is processed by the beamformer to mitigate CCI. This is given by:

$$\mathbf{z} = \mathbf{w}^H \mathbf{V} \ . \tag{7.28}$$

Substituting (7.26) into (7.28), we get:

$$\mathbf{z} = \mathbf{w}^H (\mathbf{A}\mathbf{Y}^H + \mathbf{B}) \ , \tag{7.29}$$

$$\mathbf{z} = [z(0), z(1), \ldots, z(N-1)] \ ,$$

$$\mathbf{w} = [w(1), w(2), \ldots, w(S)]^T \ ,$$

where $\mathbf{z}$ is the weighted output of the beamformer and $\mathbf{w}$ are the applied BF complex weights. This is followed by S/P conversion and transformation of $\mathbf{z}$ to the frequency domain, which can be mathematically expressed as:

$$\widetilde{\mathbf{z}} = \mathbf{F}\mathbf{z}^H \ . \tag{7.30}$$

Using (7.30) and (7.29),

$$\widetilde{\mathbf{z}} = \mathbf{F}(\mathbf{w}^H\mathbf{A}\mathbf{Y}^H + \mathbf{w}^H\mathbf{B})^H \ . \tag{7.31}$$

The data sub-carriers in $\widetilde{\mathbf{z}}$ are de-multiplexed into $\widetilde{\mathbf{r}}^q$ which are then passed to the QPSK demapper as described in Chapter 5, page 111. The demapper outputs LLRs Γ for the v^{th} coded bits c_v in the desired user transmitted data sequence $\widetilde{\mathbf{x}}_d^q$ given received vector $\widetilde{\mathbf{r}}^q$, channel estimates $\widetilde{\mathbf{h}}^q$.

$$\Gamma(c_v(\tilde{x}_d^q(n))) = \ln \frac{\sum_{b \in U_v^+} P(\tilde{x}_d^q(n) = b \mid \tilde{r}^q(n), \tilde{h}^q(n))}{\sum_{b \in U_v^-} P(\tilde{x}_d^q(n) = b \mid \tilde{r}^q(n), \tilde{h}^q(n))} \ , \tag{7.32}$$

$$P(\tilde{x}_d^q(n) = b \mid \tilde{r}^q(n), \tilde{h}^q(n)) = \frac{1}{2\pi\sigma^2} \exp\left(-\frac{\|\tilde{r}^q(n) - \tilde{h}^q(n)\tilde{x}_d^q(n))\|^2}{2\sigma^2}\right) \ , \tag{7.33}$$

where U_v^- and U_v^+ represents the constellation set that contains all the symbols whose v^{th} bit is 0 and 1 respectively. The conditional probability given in (7.32) is computed using (7.33). The LLRs of the coded bits are de-interleaved and passed to the MAP decoder which outputs the decoded bits $\{\hat{\mathbf{o}}\}$. For the next OFDM symbol, new complex BF weights are computed as described in Chapter 3, page 47. This error vector at the input of the beamformer in frequency domain can be expressed as:

$$\widetilde{\mathbf{e}} = \widetilde{\mathbf{z}}^p - \widetilde{\mathbf{x}}_d^p \ . \tag{7.34}$$

As we employ Pre-FFT BF, $\widetilde{\mathbf{e}}$ is converted to the time-domain which can be presented mathematically as:

$$\mathbf{e} = \mathbf{F}^H\widetilde{\mathbf{e}} \ . \tag{7.35}$$

The time-domain error vector obtained in (7.35) is then used in the adaptive beamformer.

7.3.2.1 Full-Adaptive Beamformer

For the full-adaptive case, the BF weights are computed at every OFDM symbol (l) continuously until all OFDM symbols have been decoded. The LMS adaptation is given by:

$$\mathbf{w}[l+1] = \mathbf{w}[l] + 2\mu\mathbf{V}[l]\mathbf{e}[l] \ . \tag{7.36}$$

Using (7.35) and (7.36), we get:

$$\mathbf{w}[l+1] = \mathbf{w}[l] + 2\mu\mathbf{V}[l]\mathbf{F}^H\tilde{\mathbf{e}}[l] \ , \tag{7.37}$$

where $\mathbf{w}[l]$ and $\mathbf{w}[l+1]$ represent the beamformer's complex weights for $[l]$ and $[l+1]$ OFDM symbols. μ represents the positive step size which controls the rate of convergence such that [70]:

$$\mu_{min} \leq \mu \leq \mu_{max} \ , \tag{7.38}$$

with

$$\mu_{max} \leq \frac{2}{3\,\mathrm{tr}\,(\mathbf{R})} \ . \tag{7.39}$$

For the HTSMS, we employ LMS with optimised μ that adapts at each iteration according to (7.39).

7.3.2.2 Proposed Semi-Adaptive Beamformer

The semi-adaptive beamformer introduced in Section 7.2 uses $\tilde{\mathbf{e}}$ to compute the MSE ω as in (7.6) for every OFDM symbol. This is followed by calculation of Ψ and $\nabla\Psi$ using (7.8) and (7.12) respectively over a MMB which comprises of f consecutive MMWs each of size ρ. The MMB slides g OFDM symbols to perform continuous monitoring of $\nabla\Psi$. The value of g defines the frequency of potential triggers from adaptive to non-adaptive and vice versa. If g remains 1, it translates to a potential trigger every OFDM symbol whereas a large number corresponds to a slow triggering process. To enable continuous monitoring, $g \leq (f \times \rho)$.

When the receiver starts the BF process ($l = 1$), weights update takes place as in (7.35) $-$ (7.36). As the $\nabla\Psi$ monitoring continues, after certain number of OFDM symbols defined in (7.21) ($l \geq L_{min}$), criteria in (7.20) over a MMB is met which sets Λ to 0. This triggers non-adaptive BF is given by:

$$\mathbf{w}[l+1] = \mathbf{w}[l]. \tag{7.40}$$

In terms of the OFDM symbol, the point where the switch is triggered is denoted as L_s. Monitoring of $\nabla\Psi$ continues after this switch and if at any time criteria in (7.20) is violated over a MMB, Λ is set to 1 triggering back the adaptive BF processing given in (7.35)$-$(7.36).

7.3.2.3 Complexity Analysis of Semi-Adaptive against Full-Adaptive BF

The complexity for (7.36) in terms of addition and multiplication can be presented as:

$$\beta_A = LS(M + N(M + P)) \qquad \forall L \ . \tag{7.41}$$

The semi-adaptive algorithm has adaptive BF phase which has similar complexity function as depicted in (7.41). The monitoring phase of semi-adaptive algorithm constitutes of computation of 1) the variance function Ψ 2) the slope function $\nabla\Psi$ 3) computation of threshold Ω and 4) switching decision. For the MMB processing introduced in Section 7.2, these factors with the aim of minimising multiplication operations can be expressed as:

$$
\begin{aligned}
\beta_{SA} = & \overbrace{\beta_{A'}}^{AdaptiveBF} + \overbrace{\beta_{\Psi} + \beta_{\nabla\Psi} + \beta_s + \beta_{\Omega}}^{Monitoring} \quad . \\
= & \left[L_s S(M + N(M+P))\right] + \\
& \left[\left(\frac{L}{\rho}\right) \times \{4M + (\rho+2)\,P\}\right] + \\
& \left[2P + (f-2)\{M+P\} + \left(\frac{L-f\rho}{g}\right) P + \left(\frac{L-f\rho}{\rho}\right)\{M+P\}\right] + \\
& \left[\left(\frac{L-f\rho}{g} + 1\right) P\right] + \\
& \left[\gamma_s M\right] \quad .
\end{aligned}
\tag{7.42}
$$

Here γ_s is the number of times Ω in (7.19) needs to be evaluated due to change in system noise disturbance. If available SNR does not change, Ω will be computed once, as in our case. Proof of the expression is presented in Appendix B. Now splitting (7.42) into M and P components and simplifying it for the case of $\gamma_s = 1$:

$$\beta_A^m = M\left[LS(1+N)\right] \quad . \tag{7.43}$$

$$\beta_A^p = P\left[LSN\right] \quad . \tag{7.44}$$

$$\beta_{SA}^m = M\left[L_s S(1+N) + \frac{5L}{\rho} - 1\right] \quad . \tag{7.45}$$

$$\beta_{SA}^p = P\left[L_s SN + \frac{3L+\rho L}{\rho} + \frac{2(L-f\rho)}{g} + 1\right] \quad . \tag{7.46}$$

After obtaining composite computation expressions in (7.43)−(7.46), we define the potential gain of semi-adaptive beamformer as:

$$\hbar = \left(\frac{\beta_{SA}^m}{\beta_A^m + \beta_A^p} + \frac{\beta_{SA}^p}{\beta_A^m + \beta_A^p}\right) \quad , \tag{7.47}$$

where $\hbar$ can be looked as the relative filter computing power requirement of semi-adaptive algorithm if 1 unit is expended by the full-adaptive case.

***Lemma 1*:** M operations are a factor f_m complex than P.

As M operations are far more complex than P, we assign a factor f_m to P in (7.43) and (7.45) such that $M = f_m P$. Now substituting (7.43)$-$(7.45) into (7.47) and combining the M and P components, we get:

$$\hbar = \left(\frac{f_m \left[\frac{L_s(1+N)}{L} + \frac{5}{\rho S} - \frac{1}{LS} \right] + \left[\frac{L_s N}{L} + \frac{3+\rho}{\rho S} + \frac{2(L-f\rho)}{gLS} + \frac{1}{LS} \right]}{f_m \left[1+N \right] + \left[N \right]} \right) \quad . \tag{7.48}$$

***Lemma 2*:** M operations are far complex than P, hence assume $\frac{1}{fm} = 0$.

With *Lemma 2*, $\hbar$ in (7.48) can be reformulated as:

$$\begin{aligned} \hbar^{m_1} &= \frac{\frac{L_s(1+N)}{L} + \frac{5}{\rho S} - \frac{1}{LS}}{(1+N)} \quad . \\ &= \frac{L_s}{L} + \left(\frac{5}{\rho S(1+N)} - \frac{1}{LS(1+N)} \right) \quad . \end{aligned} \tag{7.49}$$

***Lemma 3*:** L is a large number, hence $\frac{1}{LS(1+N)} \approx 0$.

Using *Lemma 3*, (7.49) can be simplified to:

$$\hbar^{m_2} = \frac{L_s}{L} + \frac{5}{\rho S(1+N)} \quad , \tag{7.50}$$

where the factor $\frac{L_s}{L}$ and $\frac{5}{\rho S((1+N))}$ represent the relative computing power consumption in semi-adaptive beamformer due to BF and MMB operations respectively as compared to the full-adaptive beamformer.

***Lemma 4*:** $\rho S((1+N)) \gg 5$.

Finally with *Lemma 4*, $\hbar^{m_2}$ in (7.50) can be further approximated to:

$$\hbar^{'} \approx \frac{L_s}{L} \quad . \tag{7.51}$$

Here $\hbar^{'}$ will be the minimum computing power consumption of semi-adaptive beamformer as compared to full-adaptive BF. On the other hand, $\hbar$ in (7.48) is the maximum computing power requirement assuming switching takes place once.

7.4 Simulation and Discussions

A SIMO BICM-OFDM system with 32 sub-carriers (N) having 5 pilots per OFDM symbol (N_p) is modelled. 1×2 and 1×4 SIMO configurations are employed. In accordance with Fig. 3.4 (Chapter 3, page 42), one desired user was modelled at 40° while interference users were located at −70°,−35° and 60° azimuth respectively. Total number of symbols transmitted (L) are taken as 40,000. A rate-1/2 $(5, 7)_8$ convolution encoder and random interleaver/de-interleaver are employed in an AWGN channel condition. The power per interference user at the satellite end is set to −5 dBW. The input parameters for the proposed semi-adaptive algorithm are tabulated in Table 7.1:

Parameter	**Notation**	**Value**
‖ MMW ‖	ρ	50
Number of consecutive MMWs combined to form a MMB	f	10
Number of OFDM symbols MMB slides	g	50
BTF	Λ	1

Table 7.1: Input parameters for proposed semi-adaptive beamformer

7.4.1 Semi-Adaptive Switching

Using the aforementioned parameters, the proposed OBBF-SA is then compared to conventional full-adaptive LMS beamformer for HTSMS. Fig. 7.5 presents the plot of Real-time Beamforming Weights (RBFW) of one of the antenna elements in terms of their absolute value for $\sigma^2 = 1.0$ & 0.16. For the case of high disturbance level in the system ($\sigma^2 = 1.0$), we can clearly observe that the semi-adaptive algorithm switches off the adaptive processing when $l = 650$. Hence after 650

OFDM symbols, no new weights are computed and previous computed weights are applied to the received signal until all the data corresponding to the desired user has been decoded. For the case of $\sigma^2 = 0.16$, we can see that BF converges much quicker. Moreover, due to lower level of disturbance in the system, the switch takes place when $l = 500$. From this point onwards OBBF-SA halts computation of new weights and the current weights are used for all the remaining OFDM symbols. Hence we can see that with lower level of noise in the system, the proposed algorithm initiates the switch much earlier as compared to the case with high noise. Furthermore, using ρ and f in (7.21), we can calculate L_{min} as 500 OFDM symbols. This means that the semi-adaptive algorithm should not allow any switching for $l < L_{min}$ and hence $L_s \geq L_{min}$ irrespective of $\nabla\Psi$ and Ω. We can see that for both the cases in Fig. 7.5, the switch takes place after a minimum of 500 OFDM symbols have been received which verifies 7.21.

7.4.2 Complexity Gain

We will analyse the impact of the switching on overall performance later, but lets pause to see how much computational saving can be achieved by employing the proposed approach. With parameters tabulated in Table 7.1 and using (7.48)$-$(7.51), Fig. 7.6 presents the computational advantage in terms of computing power consumption of the proposed semi-adaptive beamformer relative to 1 unit computing power consumption of the full-adaptive case with $S = 4$. For the case $\sigma^2 = 1$, the switch from adaptive to non-adaptive is triggered when $L_s = 650$. The minimum relative computing power consumption (*lemma 4*) for the case is 0.0163 and if include the MMB processing as well, (*lemma 1 - 3*), the maximum computing power consumption goes upto 0.0177. This effectively means significant saving of resources as semi-adaptive algorithm switches off adaptive BF while using minimum energy during MMB processing. When the system noise reduces with $\sigma^2 = 0.16$, the switch is triggered earlier and $L_s = 500$.

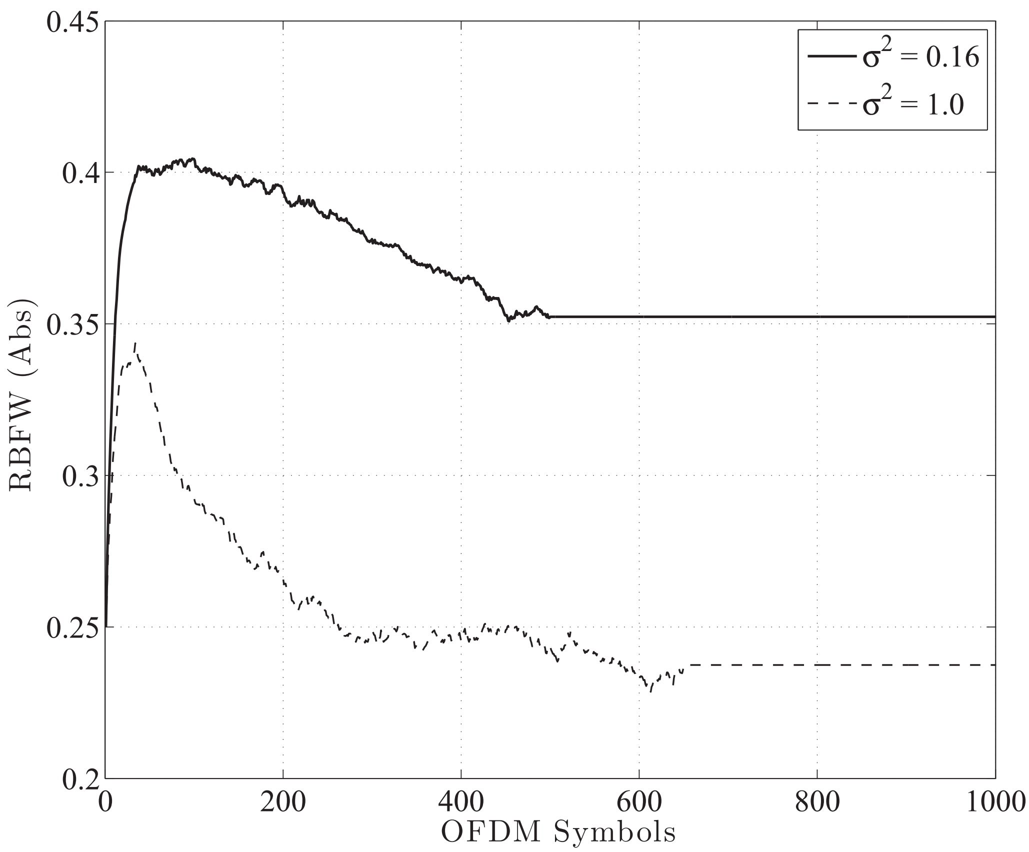

Figure 7.5: Beamforming convergence in terms of Real-time Beamforming Weights (Abs) of one of the antenna elements vs OFDM symbols with $\rho = 50$, $f = 10$, $g = 50$, $\sigma^2 = 1.0$ & 0.16 and antenna elements = 4.

This further reduces the computing power consumption of the semi-adaptive with minimum computing power consumption of 0.0125 and maximum of 0.0139. This gain in terms of % is presented in Fig. 7.7. With $L_s = 650$, the semi-adaptive requires 98.29% lesser filter computing power as compared to full-adaptive. Moreover, when $L_s = 500$, the gain increases to 98.67%. Hence irrespective of the noise level, the semi-adaptive is far less complex as compared to the full-adaptive case. This computer power saving is attributed to the freezing of computation of adaptive filtering associated with BF. This computer power saving relates to freezing

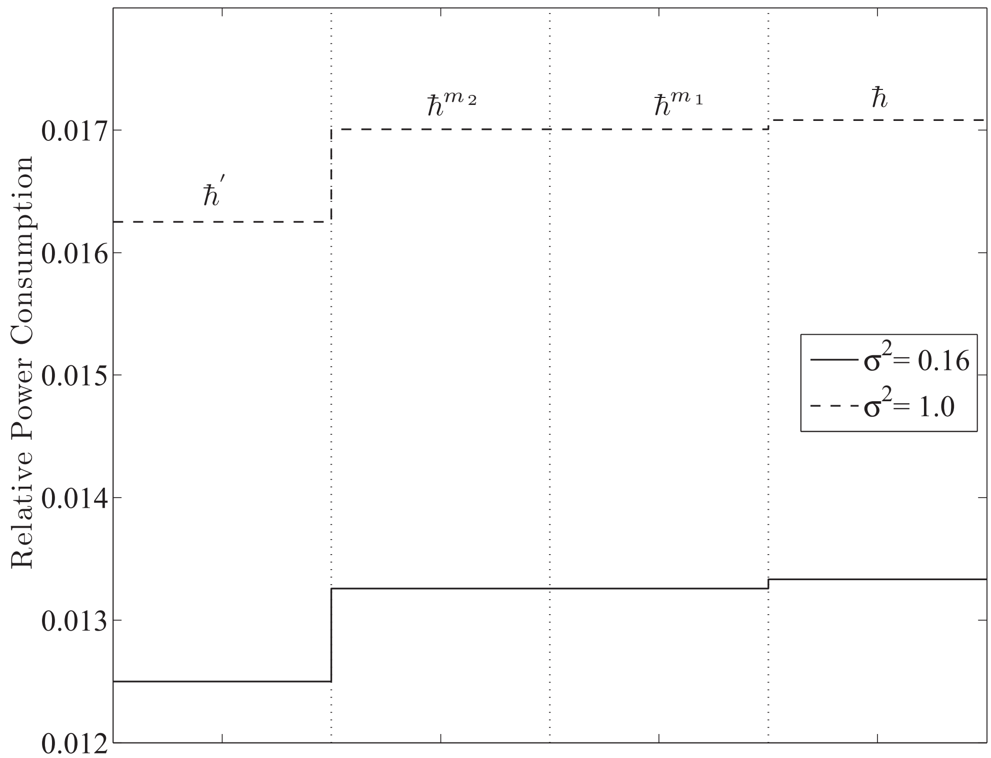

Figure 7.6: Computing power requirement of proposed semi-adaptive algorithm relative to 1 unit expended by full-adaptive beamformer with $\rho = 50$, $f = 10$, $g = 50$, $f_m = 100$, $\sigma^2 = 1.0(L_s = 650)$ & $0.16(L_s = 500)$ and antenna elements = 4.

up the computing facility for alternative use.

7.4.3 Performance

At first we study the beamformer's convergence in terms of received pilots against time. As oppose to results in Fig. 7.5, this analysis would tell us whether switching off the adaptive BF had any effect on the spatial filtering. Therefore in Fig. 7.8 we plot the magnitude of the received pilots $| \widetilde{\mathbf{z}}^p |$ corresponding to the desired

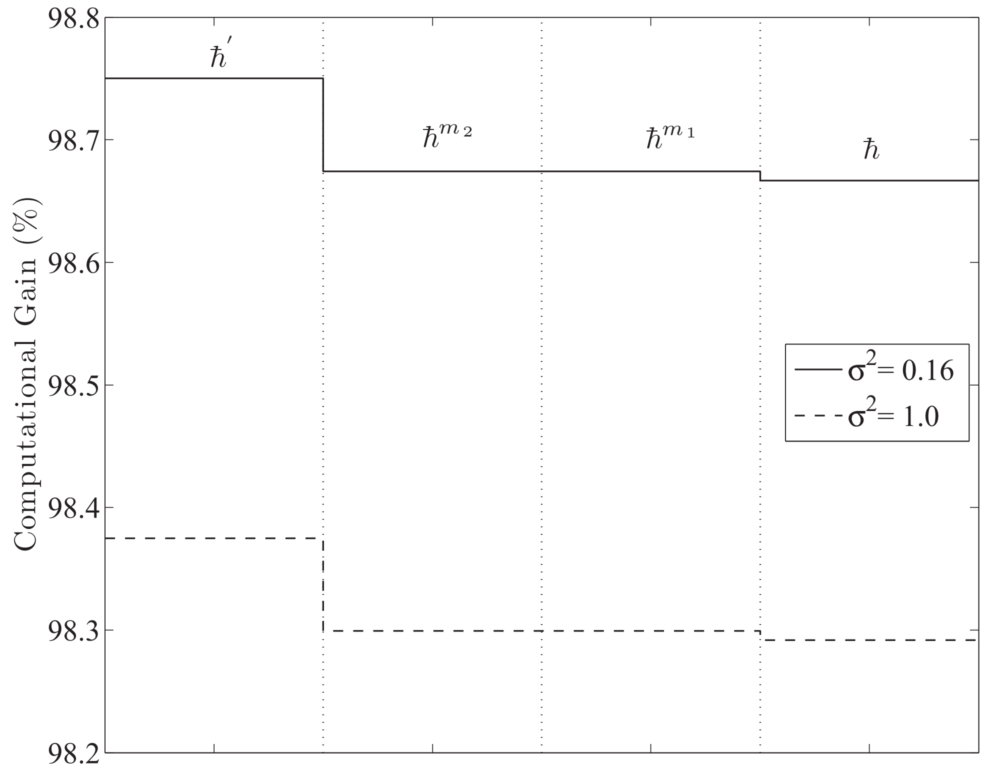

Figure 7.7: Computation gain of proposed semi-adaptive algorithm relative against full-adaptive beamformer with $\rho = 50$, $f = 10$, $g = 50$, $f_m = 100$, $\sigma^2 = 1.0(L_s = 650)$ & $0.16(L_s = 500)$ and antenna elements = 4.

user. We can see that irrespective of the σ^2, the received pilots converge towards the desired value and stay converged even after adaptive BF has been switched off. For the case of $\sigma^2 = 1$, $L_s = 650$ and even after the switch the received pilots remain converged. Similarly for the case of $\sigma^2 = 0.16$, the adaptive BF is switched off with $L_s = 500$ and even after this the received pilots remain converged. We do however observe that with less noise, the convergence is superior as compared to the case with higher noise.

Now we investigate the performance of the proposed algorithm. Fig. 7.9 presents

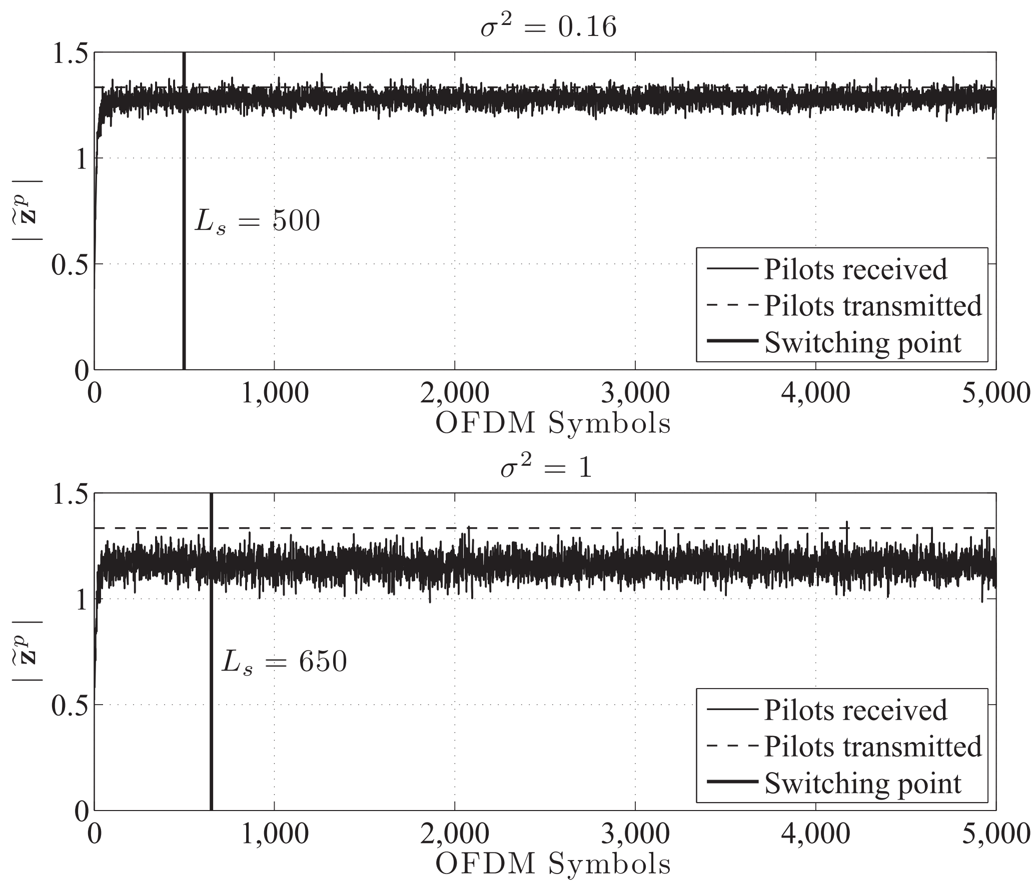

Figure 7.8: Absolute values of pilots received vs OFDM symbols with $\rho = 50$, $f = 10$, $g = 50$, $\sigma^2 = 1.0$ & 0.16 and antenna elements = 4

the short term prediction error performance of the proposed approach in terms of CMSE against OFDM symbols for 2 and 4 antenna element configuration. We note that the trend is similar to what has been observed for the case of full-adaptive BF in earlier chapters. With more antenna elements, we see faster convergence and lower CMSE achieved. As we receive more symbols, a decline in CMSE is observed until minimum possible CMSE is achieved.

After analysing the prediction error performance as a function of time for a single E_b/N_o value, we investigate how the proposed algorithm performs in terms of

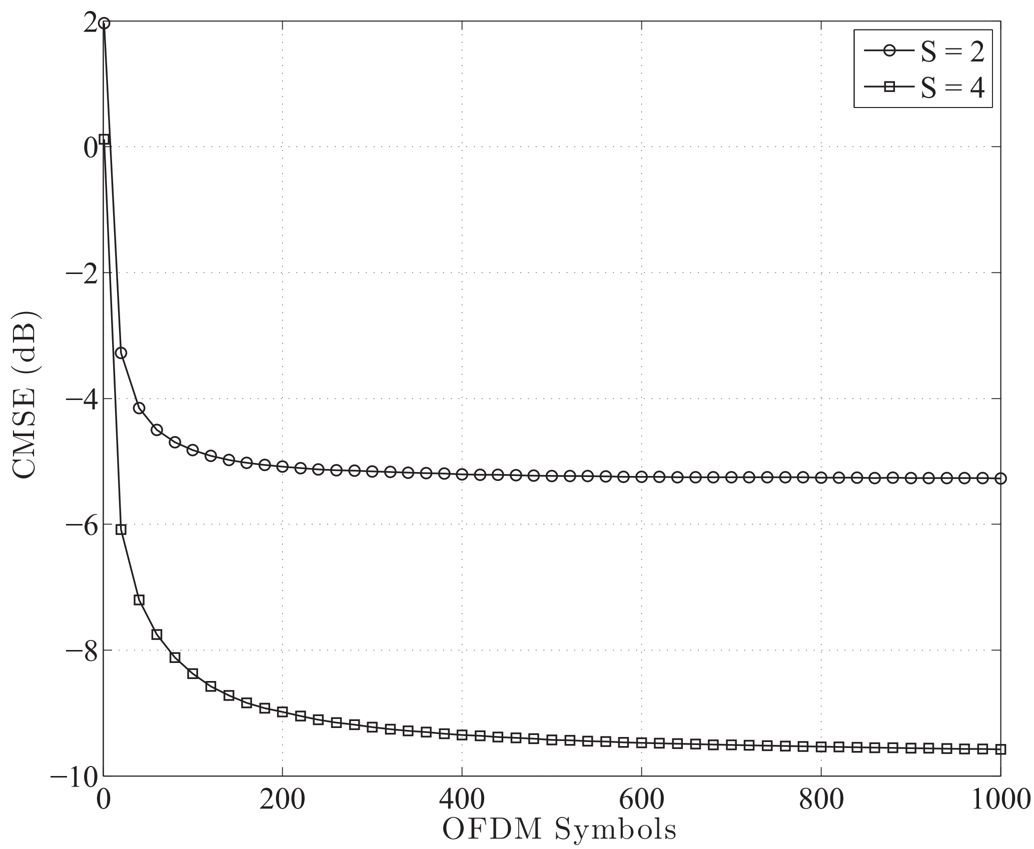

Figure 7.9: Beamforming convergence in terms of Cumulative Mean Squared Error vs OFDM symbols with $\rho = 50$, $f = 10$, $g = 50$, antenna elements = 2 & 4 and $E_b/N_o = 8$ dB.

its long term prediction error. For this, we plot in Fig. 7.10 the MSE of the proposed beamformer against E_b/N_o. What we observe is again a similar trend as to that in the case of the full-adaptive BF. With increase in antenna elements, the MSE reduces due to superior interference mitigation. Moreover as the level of disturbance reduces in the system, a lower MSE valuable is achieved. Hence irrespective of the number of antenna elements or the E_b/N_o value, the proposed algorithm shows promising results.

We have seen so far that the proposed algorithm performance is promising both in

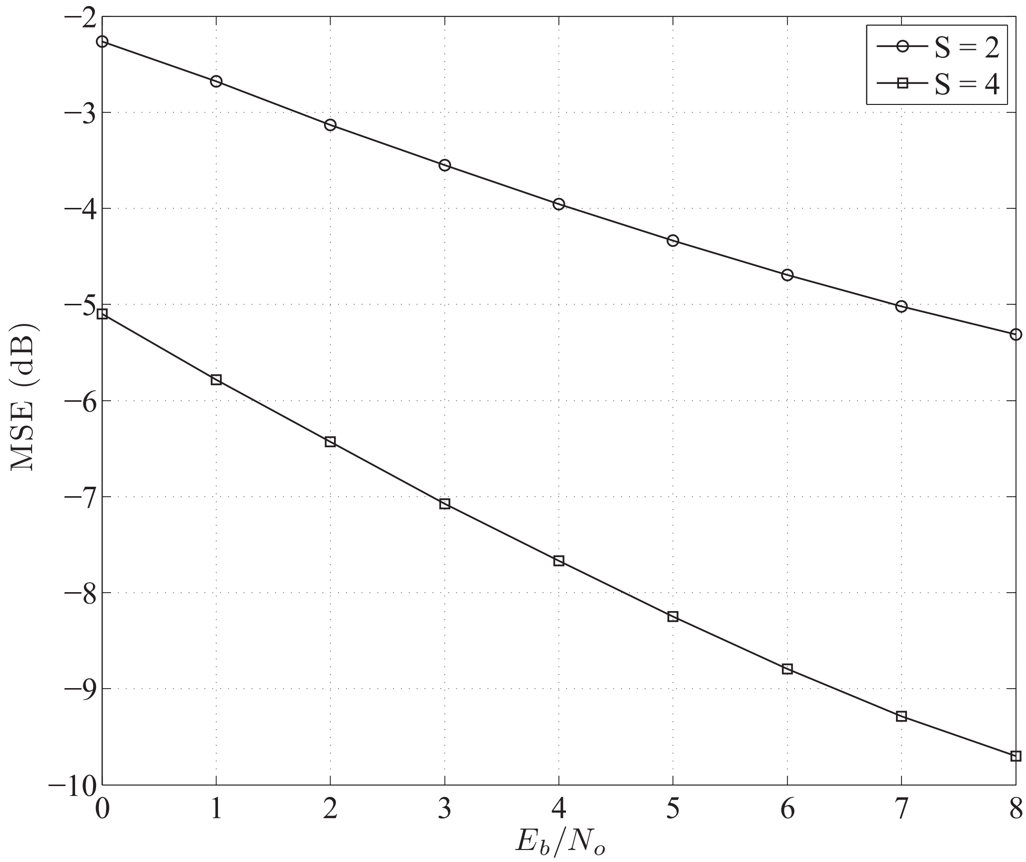

Figure 7.10: Beamforming prediction error in terms of Mean Squared Error vs E_b/N_o with $\rho = 50$, $f = 10$, $g = 50$ and antenna elements = 2 & 4.

terms of potential computation saving as well as BF performance. To gain complete insight into the performance of the proposed algorithm, we need to compare the results with the full-adaptive BF approach. Using the same parameters, we employ full-adaptive BF which is governed by (7.36)−(7.37) mentioned in Section 7.3.2.1. First we compare the MSE performance of adaptive and proposed semi-adaptive beamformer against E_b/N_o and the result is plotted in Fig. 7.11. For the case of $S = 2$, we see that irrespective of the E_b/N_o, the performance of both the schemes are almost identical. Hence there is no performance degradation for this particular case. When the number of antenna elements are increased

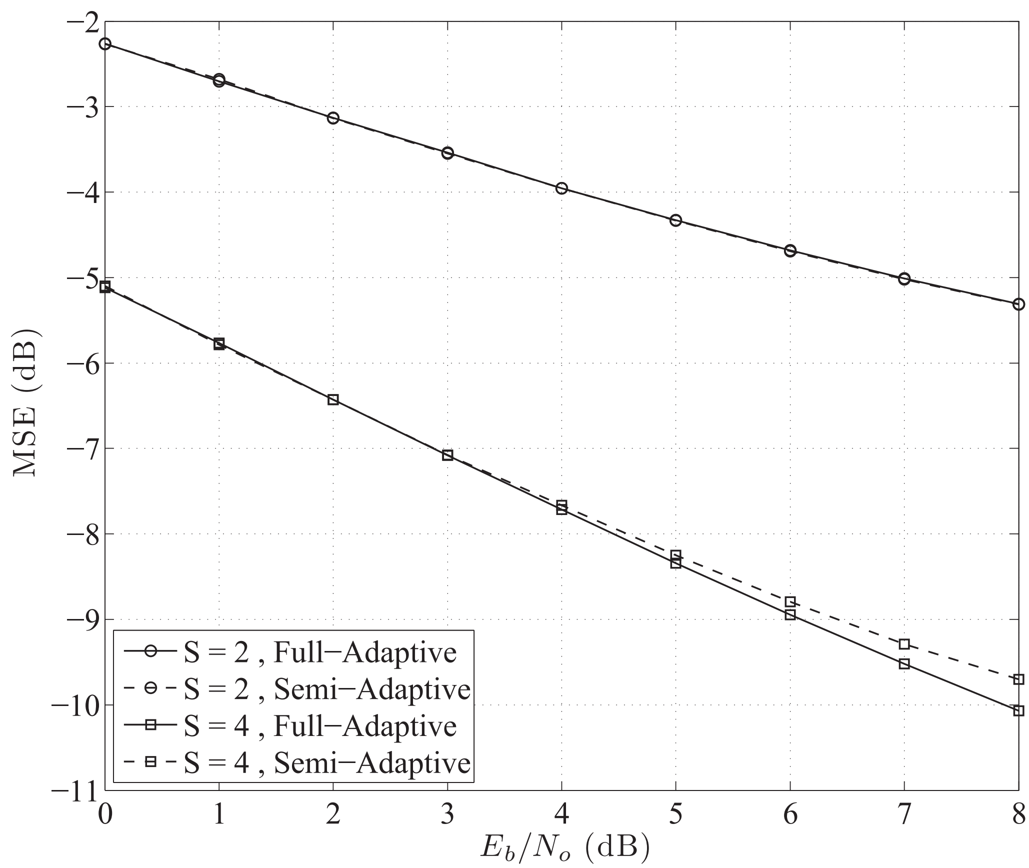

Figure 7.11: Beamforming prediction error in terms of Mean Squared Error vs E_b/N_o for full-adaptive and proposed semi-adaptive BF with $\rho = 50$, $f = 10$, $g = 50$ and antenna elements = 2 & 4.

to 4, we can observe that up to $E_b/N_o = 4$ dB, the MSE curves for both the schemes overlap. After this point, we observe a sightly better performance by the full-adaptive case. At 8 dB E_b/N_o, the semi-adaptive beamformer's performance is degraded by only 0.37 dB. Therefore, the proposed algorithm not only saves valuable computation resources, it does this elegantly by ensuring almost no degradation in performance.

The 0.37 dB is such a minimal degradation that it would inevitably have almost no effect on the BER performance. In order to verify this hypothesis, we compare

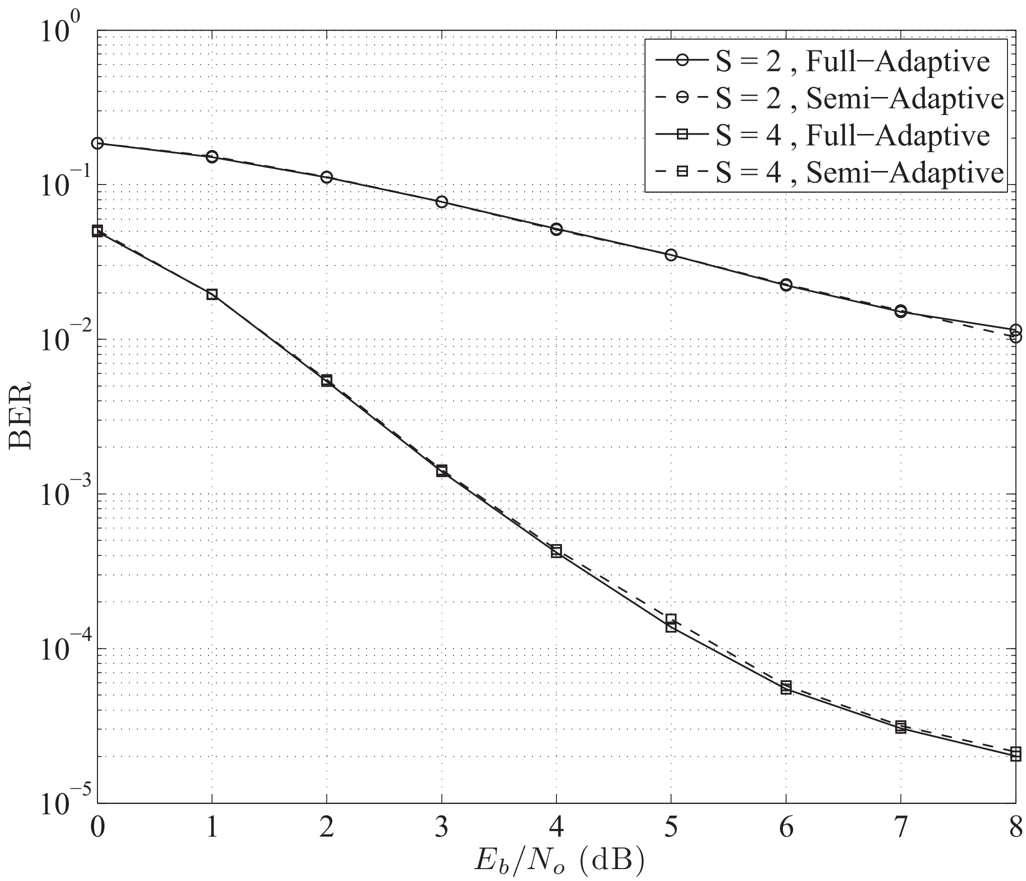

Figure 7.12: Bit Error Rate vs E_b/N_o for full-adaptive and proposed semi-adaptive BF with $\rho = 50$, $f = 10$, $g = 50$ and antenna elements = 2 & 4.

the system performance in terms of BER in Fig. 7.12. Interestingly we can see that irrespective of the available E_b/N_o or the antenna elements employed, the semi-adaptive performance is almost identical to the full-adaptive case. Moreover, the general trend observed is consistent with results recorded in earlier chapters i.e. improved BER with higher available E_b/N_o as well as with more antenna elements. This result is encouraging as it can pave the way for efficient adaptive processes on an "*if and when*" required basis.

7.5 Conclusions

Work in Chapter 6 suggested that adaptive BF may not be required at all times. Building on the observation in this chapter, we proposed a novel semi-adaptive BF employed onboard the satellite. The semi-adaptive BF is based on a novel switching mechanism that enables coexistence of adaptive and non-adaptive BF. The switching mechanism is based on a Beam Switching Metric (BSM) which triggers the adaptive to non-adaptive BF and vice versa. The BSM is monitored using MMB which takes into account any disturbance in the system. With more noise in the system, BSM delays the switching whereas for lower levels of noise, the switching is triggered sooner. The algorithm is also robust to False Switching (FS) due to the MMB processing. The design parameters f and g give more control over BF processing. Furthermore, the proposed algorithm has the capability of switching adaptive BF "*if and when*" required. On performance comparison with full-adaptive the proposed semi-adaptive approach can save up to 98% of filter computing power without any degradation in system performance. This clearly highlights the advantage of the proposed approach in terms of complexity reduction and its potential to huge computing power saving for onboard processing when considering BF onboard the satellite. The approach has all the ingredients that can pave the way for the evolution of onboard BF by significantly reducing the associated energy requirements. Apart from providing more flexibility onboard the satellite, onboard BF shifting from gateway to satellite is also a key enabler of 'green satellite' communication systems as the primary source of energy is solar. Such a step would also reduce the CO^2 footprint associated with satellite systems.

Chapter 8

Summary and Future Work

8.1 Conclusion

In this thesis we have studied BF for an OFDM based hybrid system of satellite and terrestrial networks. Specifically, we aim to propose a hybrid architecture where satellite and existing terrestrial networks work in conjunction to fulfil the aim of global coverage, enabling more capacity and reduced costs. We further intend to develop BF strategies with enhanced convergence, robustness, performance as well as reduced complexity for the hybrid architecture. The thesis presents the theoretical framework of the research validated through simulations and supported by relevant references, where deemed necessary. The scope of the work was limited to adaptive BF for HTSMS system for the uplink scenario only and the work does not address the downlink case. In this thesis we employ a 32 sub-carriers OFDM system with Cyclic Prefix and assume no time or frequency offsets in the system. For the interference model, we considered randomly distributed DOA corresponding to the desired and interferes signals. Total J users were considered in the system with one desired and $J-1$ interferes sources. For the study, we modelled multi-tap time selective wireless channel. The channel parameters were specific to terrestrial-satellite scenario and were measured as part of the EU project MAESTRO. The signal bandwidth and centre frequency were 5 MHz and 3 GHz respectively. At the satellite end, we assumed a Uniform Linear Array with S antenna elements having $\lambda/2$ inter-element spacing. Adaptive BF was performed at the satellite end and we assumed adequate processing capability onboard the satellite to support such operations.

Following the objective in Section 1.3, the achievements of the work can be concluded as follows:

HTSMS

In the quest of global connectivity and integration of satellite and terrestrial networks, we firstly proposed an OFDM based Hybrid Terrestrial-Satellite Mobile System (HTSMS). HTSMS aims to serve users in urban areas through terrestrial cellular Base Stations (BTSs) while satellite links provide service in rural areas in a seamless manner. The service provisioning by two different technologies should be transparent to the end-user, in the sense that the same mobile terminals should work with both terrestrial and satellite networks. In the system, terrestrial and satellite networks will reuse the spectrum dedicated to each other and hence increase the overall capacity. The reuse of spectrum induces Co-Channel Interference (CCI) by the terrestrial users at the uplink of the satellite and we employ adaptive BF onboard the satellite to mitigate it.

We investigate the system performance in realistic mobile satellite scenarios and also study the interaction between BF and CE. At first we found that although the beamformer tries to mitigate interference using pilots, it is unable to compensate for the channel distortions. Thus with interference in the system, channel estimation is essential on top of a beamformer in the presence of the satellite wireless channel. Secondly, we observed that an error floor existed in BER results independent of the channel condition or mobile speed. On investigation, we found that the system performance was sensitive to the convergence period or transient state of the beamformer and this was the reason behind the error floor. Even in the case of no interference, the error floor still persisted.

Preamble based Beamforming

From previous work we noted that during BF convergence, CE is forced to be carried out on non-interference free pilot sub-carriers. Accurate CE requires an interference free signal at its input. This however is not available until after BF convergence. Hence this concurrent processing of BF and CE leads to degradation in system performance. In order to enhance BF convergence as well as solving the concurrent BF and CE problem, we proposed a preamble based transmission strategies where the main idea was to disperse pilot sub-carriers from OFDM symbols to form a preamble at the beginning. We proposed FDP, PDP and RLP as three possible preamble based schemes and showed that such an approach could improve both BF convergence and CCI mitigation as well as system performance.

Iterative Turbo Beamforming

In light of the fact that BF was sensitive to reference signals, we proposed a novel ITBF algorithm that used both pilots and data in parallel to perform BF. The algorithm formed a distinctive three stage beamformer that was based on turbo-like principles. On performance comparison with the non-iterative approach, results showed that considerable gains in terms of BER could be achieved via ITBF.

Ground vs Onboard Beamforming

We followed up the work based on OBBF-A to investigate the applicability of onboard, gateway and hybrid BF solutions in more depth. We then proposed an onboard based non-adaptive BF mechanism called OBBF-SS. The methodology proposed incorporation of a BCC circuitry onboard the satellite which computes BF weights based on beam orientations transmitted from the gateway. In this way, beam patterns are less prone to amplitude and phase distributions. Moreover, OBBF-SS reduces feeder link bandwidth requirements. This made OBBF-SS a potential alternative to existing non-adaptive BF approaches especially for satellite systems offering broadcasting services. We then compared full-adaptive BF to non-adaptive OBBF-SS to establish performance advantages. We also formulated an OBBF-ERC scheme which was unaware of interference as well as desired user for the purpose of performance comparison. Results showed that overall full-adaptive BF was superior, however at low E_b/N_o as well as with lower antenna elements to user ratio, the performance of non-adaptive was comparable.

Semi-adaptive Beamforming

Based on our analysis of adaptive and non-adaptive BF as well as considering onboard complexity associated with the full-adaptive BF, we proposed a novel semi-adaptive BF algorithm. The proposed approach was based on a novel gradient based switching mechanism which enables co-existence of adaptive and non-adaptive BF. The switching mechanism was based on monitoring of the BSM metric via MMB processing. The algorithm was shown to be robust to both FS or spurious switching as well as changes in noise level in the system. On performance comparison with full-adaptive BF, results showed that the proposed algorithm could result into filter computing power reduction of up to 98% without any degradation in system performance. Such an approach has profound implications as it can significantly reduce the complexity requirements of onboard BF by reducing energy consumption. The approach can also be considered as strong enabler of onboard BF architectures.

8.2 Implications of Research

In this thesis we have proposed a Hybrid Terrestrial-Satellite Mobile System that combined advantages of both terrestrial and satellite networks. Hybrid architectures are already a reality with operation of systems such as of MSV. Hence the proposal of an OFDM based HTSMS with integrated terrestrial and satellite framework is an intuitive extension to the existing hybrid topologies and can be foreseen as a possible future Mobile Satellite System. In the study of the HTSMS, we incorporated an interference scenario with randomly distributed users and to mitigate the interference, proposed several flavours of onboard based adaptive BF. As adaptive BF requires high complexity, we have also proposed a novel semi-adaptive beamformer and have shown that in specific scenarios, the filter computing power consumption for interference mitigation process can be reduced upto 98%. Current generation of satellite systems have recently introduced adaptive ground based BF for interference mitigation as it enables simpler satellite payload design. However with advancements in technology and with the availability of more power onboard the satellite, a shift from complete ground based to Hybrid ground/onboard BF can be envisioned in near future. Within the hybrid framework, work is already in progress in the EU project "Hybrid Space-Ground Processing" under the flagship of SatNEx and European Space Agency (ESA). Following similar roadmap, the "Dream Payload" with full digital payload architecture encompassing features such as onboard digital processor with re-programmable components, transmit and receive digital beamforming, channel level control, demodulation/decoding may well be a reality within the next 10 years. The work carried out here would specifically apply to networks with digital satellite payloads.

The thesis focuses on adaptive BF onboard the satellite to mitigate interference with specific assumptions as stated in Section 8.1. When considering a real system, some of the assumptions need to be revisited to make the HTSMS model more practical. As the system is based on frequency reuse, hence it would be important to consider factors such as coverage area, frequency reuse pattern and the population statistics of the aimed coverage area. Furthermore, the interference model would have to be modified to account for such details. The OFDM frame structure would have to be specific to a standard such as 3GPP-LTE and parameters such as total number of sub-carriers, number of pilot sub-carriers and their arrangement would need to be retuned. Capability of Adaptive Coding and Modulation (ACM) would also be highly desirable as it would increase the system capacity depending on Channel State Information (CSI). Another important factor in a MSS system is management of inter-system users and thus employment of appropriate multiple access scheme and resource allocation strategy will also be necessary. In case the system does not have a centralised resource allocation, appropriate Multi-User Detection (MUD) techniques would need to be investigated to extract all the desired users in the system.

8.3 Future Work

As a consequence of the study, the following areas are identified for further improvement:

Downlink Beamforming

In the thesis we have only considered uplink interference mitigation using adaptive BF. However, to ensure functionality of a system as a whole we must also consider the downlink scenario. Hence further work needs to be done in the direction of downlink interference mitigation. The possible solutions include downlink transmit BF [22–24], joint transmit and receive BF [25], linear pre-coding techniques [72] (in both cooperative and non-cooperative scenarios) such as Maximum Ratio Combining [105] and Zero Forcing [106], Dirty Paper Coding [107], to name a few.

Scalability Issues

In our work we have assumed a maximum number of 9 antenna elements onboard the satellite. In an actual satellite system covering a large geographical area, the number of antenna elements would be much higher. With more antenna elements, not only the system becomes complex but the convergence of BF process would significantly reduce. Further works needs to be done in this direction to reduce the latency involved in BF process when large array of antenna elements is considered. Possible solutions include optimisation of number of antenna elements processed as a function of the interference scenario. Another solution as pursued in [108] is a proposal of a reduced-rank adaptive beamformer that the author proposes for a GEO satellite with high number of antenna elements. Scalability issues may also arise in case of large number of users. In such case, techniques such as one proposed in [38] for RADAR systems can be perused which only processes interference subspace and hence reduces the adaptive processing time.

Other Beamforming Algorithms

Throughout the thesis we have focused our efforts towards symbol-level LMS BF and some variants of LMS such as NLMS and VSS-LMS. Further performance improvement can be achieved by employing less complex Post-FFT approaches such as Multi-Stage Beamforming [68] and sub-carrier clustering based BF [67]. Furthermore, as OFDM transmission in actual systems take place in block form, hence the possibility of Least Squares (LS) BF needs to be be explored which has far less complexity to LMS and is also more viable for packet based transmission.

Improvements in ITBF

ITBF provides significant performance gains in terms of both BF prediction error as well and BER. This is attributed to its use of both pilots and data to perform BF following the turbo-principle. The following improvements are suggested within the ITBF framework:

1. As data is being utilised for BF, further work can be done to study the impact of reduction in pilot sub-carriers on BF. Reducing the pilots can potentially translate to increased data throughput while maintaining superior interference mitigation due to the use of soft data symbols.

2. The reliability of *extrinsic* information being exchanged between components of ITBF is susceptible to changes in the wireless channel. Therefore, more robust channel tracking mechanisms can be introduced within the iterative framework and the operability of ITBF validated for such scenarios.

Joint Iterative Beamforming and Channel Estimation

Just as BF, channel estimation can also be performed iteratively to enhance system performance as is done in [87]. Hence an intuitive extension to the iterative framework is the proposal of a joint iterative beamformer and channel estimator. Hence a turbo-like channel estimation can be introduced and combined with iterative BF. This will effectively result in a receiver that is both robust to interference as well as frequency and time selectivity.

Investigation of OBBF-SS

We have used OBBF-SS to establish performance comparison between adaptive and non-adaptive approaches for the MSS scenario. Work can be done to investigate advantages of OBBF-SS in terms of bandwidth saving as well as robustness to channel distortions as compared to conventional non-adaptive BF architectures.

Improvements in Semi-Adaptive Beamforming

The semi-adaptive algorithm significantly reduces the computational requirement of the interference mitigation process. In one of the scenario's studied, the proposed semi-adaptive algorithm exhibited filter computing power reduction of up to 98% without any performance degradation. Based on this result and the potential semi-adaptive approach exhibits, the following improvements are suggested:

1. Significant computational gains are achieved using the semi-adaptive approach as reported in Section 7.4.3. We have also analysed the complexity of the proposed algorithm and show that the MMB processing has very low filter computing power requirements. Further work needs to be done to analyse sensitivity of the semi-adaptive beamformer to parameters such f_m, L_s, ρ, g, f, to name a few.

2. As semi-adaptive reduces complexity, a comprehensive solution of iterative BF, channel estimation and semi-adaptive approach can be envisioned. A receiver that is efficient in use of resources by having switching capability and is robust due to iterative processing.

Ground and Hybridised Beamforming

Throughout the work, our study focused on adaptive BF onboard the satellite as a solution towards CCI mitigation. As ground and hybrid BF can have profound implications in the near future, further work can be pursued to investigate BF processing with gateway and hybrid space/gateway approaches. Furthermore, effort can be made to introduce the aforementioned proposed improvements to ground/hybrid topology.

Advanced Traffic Modelling

To improve the interference model, advanced traffic modelling of interference sources can be incorporated. Moreover, we can also redesign the interference model so that it is mapped to a particular geographical location and is also based on population statistics. Furthermore, investigation can be carried out on their impact on performance w.r.t the above proposed schemes.

Appendix A

Soft Input Soft-Output (SISO) Decoder

The Soft-Input-Soft-Output (SISO) decoder computes soft outputs based on the estimation of the probability of the information bit (denoted by u) is '1' to the probability that the information bit is '0'. This ratio is referred to as Log-Likelihood Ratio (LLR) which is an estimation of the *a posteriori probability* (APP) of the transmitted bit (denoted by x), given the observation of the received sequence of bits (denoted by r). Assuming a typical communication system composed of encoder, decoder, modulator, demodulator and an AWGN channel $\sim \mathcal{CN}(0, \sigma^2)$. For generality, we take the case of BPSK in which LLR for the assumed communication set up can be expressed as:

$$\Gamma(\hat{u}) = \Gamma(u|r) = \ln \frac{P(u=1|r)}{P(u=0|r)} = \ln \frac{P(x=+1|r)}{P(x=-1|r)} = \Gamma(x|r) \ . \tag{A.1}$$

The sign of the LLR value corresponds to the hard decision of the transmitted bit. A positive sign indicates transmission of bit '1', otherwise if it is negative, then bit '0' is assumed to be transmitted. The magnitude of Γ in (A.1) is reliability indicator of this decision and is a measure of certainty of "what was transmitted". The output of the demodulator in the soft form is thus based on the APP of the

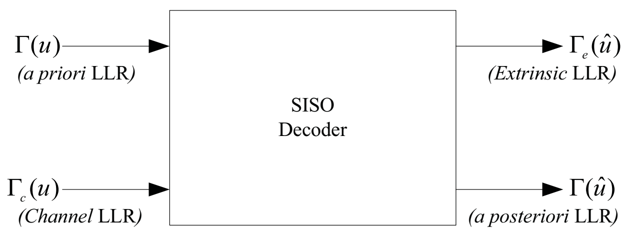

Figure A.1: Schematics of a SISO decoder

transmissible bit. From (A.1) and using *Bayes' rule*, we have:

$$\begin{aligned}\Gamma(x|r) &= \ln \frac{P(x=+1|r)}{P(x=-1|r)} \ , \\ &= \ln \frac{P(r|x=+1)\,P(x=+1)}{P(r|x=-1)\,P(x=-1)} \ , \\ &= \ln \frac{\frac{1}{\sqrt{2\pi}\sigma}\exp\left\{-\frac{1}{2}\left(\frac{r-1}{\sigma}\right)^2\right\}}{\frac{1}{\sqrt{2\pi}\sigma}\exp\left\{-\frac{1}{2}\left(\frac{r+1}{\sigma}\right)^2\right\}} + \ln \frac{P(r|x=+1)}{P(r|x=-1)} \ , \\ &= \frac{2}{\sigma^2} + \ln \frac{P(r|x=+1)}{P(r|x=-1)} \ , \\ &= \Gamma_c\, r + \Gamma(u) \ ,\end{aligned} \tag{A.2}$$

where $\Gamma_c = 2/\sigma^2$ is called the *channel reliability value* and the term $\Gamma(u)$ is the *a priori* LLR value corresponding to the bit u. The inclusion of encoder and decoder in the system yields benefits on decision making [109]. For the case of systematic code, the soft decoder output takes the following form:

$$\Gamma(\hat{u}) = \Gamma(x|r) = \Gamma_c\, r + \Gamma(u) + \Gamma_e(\hat{u}) \ . \tag{A.3}$$

The new term $\Gamma_e(\hat{u})$ w.r.t (A.2) is called the *extrinsic* LLR. It represents an extra estimation on the LLR of the information bits. It is independent of both the *a priori* and channel LLR values corresponding to the information bits. A schematic diagram of the LLR values used in a SISO decoder from (A.3) is shown in Fig. A.1. In the iterative decoding process, the *extrinsic* LLR is fed back to the input of another component decoder to serve as *a priori* information of the data bits for the next decoding iteration.

Appendix B

Proof of β_{SA}

Proof of β_{Ψ}:

Variance is computed once every MMW. With ρ as the length of MMW, the variance Ψ can be presenting generically as,

$$\Psi_{\rho} = \frac{(\rho - 1) \times \Psi_{\rho-1} + \left\{ w_{\rho} - \left(\frac{1}{l} \sum_{l=1}^{\rho} w_l \right) \right\}^2}{\rho} \tag{B.1}$$

The complexity of (B.1) lies at $4M + (\rho + 2)P$. For the computation of variance over all MMWs, we need to evaluate the total MMBs to be processed. As the MMB moves over g OFDM symbols after $\rho \times f$ symbols have elapsed, the total number of MMBs during transmission of L OFDM symbols can be presented as:

$$\mid \text{MMB} \mid = \frac{L - \rho f}{g} + 1 \tag{B.2}$$

The complexity associated with variance computation is critically influenced by the parameter g. With $g = a\rho$ corresponds to the less complex and practical case where length of g is scalar multiple of the length of MMW. This means that after MMB moves over g symbols, the variance for overlapping MMWs will remain unchanged. The Ψ would be computed for only a non-overlapping MMWs. Hence with $g = a\rho$, β_Ψ for the complete transmission can be presented as:

$$\begin{aligned}\beta_\Psi &= \left\{ f + \left(\frac{L-\rho f}{g}\right)\left(\frac{g}{\rho}\right)\right\} \times \{4M + (\rho+2)\,P\} \\ &= \left(\frac{L}{\rho}\right) \times \{4M + (\rho+2)\,P\}\end{aligned} \tag{B.3}$$

<u>*Proof of* $\beta_{\nabla\Psi}$</u>:

When considering the 1^{st} and f^{th} MMW of the 1^{st} MMB, only 1 adjacent Ψ value for slope calculation is available. Therefore, computation lies at P for each of them. For the rest of $f-2$ MMWs, operations lie at $M+P$ as 2 adjacent values are available. Furthermore, just as was the case of Ψ, there are overlapping MMWs for which slope is not required to be recomputed. After the MMB slides over g symbols, the last MMW of the MMB has only one Ψ for slope calculation whereas a have 2 adjacent Ψ values. Hence the computation for all possible MMB can be given as:

$$\beta_{\nabla\Psi} = [2P + (f-2)\{M+P\}] + \left[\left(\frac{L-f\rho}{g}\right)P + \left(\frac{L-f\rho}{\rho}\right)\{M+P\}\right] \tag{B.4}$$

<u>*Proof of* β_s and β_Ω</u>:

Switching can potentially take place once every MMB. Hence the number of MMB is the complexity factor and hence β_s can be given by:

$$\beta_s = \left(\frac{L-f\rho}{g} + 1\right)P \tag{B.5}$$

For the case of β_Ω, complexity is directly porportional to the number of times Ω needs to be re-evaluated due to change in system noise disturbance in accordance with (7.19). If available SNR does not change, Ω will be computed once, as in our case. Therefore, β_Ω can be expressed as:

$$\beta_\Omega = \gamma_s M \tag{B.6}$$

Here γ_s is the number of times Ω needs to be evaluated.

Bibliography

[1] B. G. Evans and K. Baughan, "Visions of 4G," *Electronics & Communication Engineering Journal*, vol. 12, no. 6, pp. 293 – 303, Dec. 2000.

[2] A. R. Bahai and B. R. Saltzberg, *Multi-Carrier Digital Communications: Theory and Applications of OFDM.* Plenum Publishing Corp., Oct. 1999.

[3] J. G. Foschini, "Layered space-time architecture for wireless communication in a fading environment when using multi element antennas," *Bell Labs Tech. J*, vol. 2, pp. 41 – 59, Autumn 1996.

[4] D. Gesbert, M. Shafi, D. shan Shiu, P. J. Smith, and A. Naguib, "From theory to practice: an overview of MIMO space-time coded wireless systems," *Selected Areas in Communications, IEEE Journal on*, vol. 21, no. 3, pp. 281 – 302, April 2003.

[5] A. J. Paulraj, D. A. Gore, R. U. Nabar, and H. Bolcskei, "An overview of MIMO communications - a key to gigabit wireless," *Proceedings of the IEEE*, vol. 92, no. 2, pp. 198 – 218, Feb. 2004.

[6] "SkyTerra Communications." [Online]. Available: http://www.skyterra.com/ (accessed on: 29 November 2010)

[7] P. D. Karabinis, "Systems and methods for terrestrial reuse of cellular satellite frequency spectrum," *U.S. Patent 6684057*, Jan. 2004.

[8] D. Zheng and P. D. Karabinis, "Adaptive beam-forming with interference supression in MSS with ATC," in *23rd ICSSC 2005, American Institute of Aeronautics and Astronautics*, Rome, Italy, Sep. 2005.

[9] P. D. Karabinis, S. Dutta, and W. W. Chapman, "Interference potential to MSS due to terrestrial reuse of satellite band frequencies," in *23rd ICSSC 2005, American Institute of Aeronautics and Astronautics*, Rome, Italy, Sep. 2005.

[10] B. D. V. Veen and K. M. Buckley, "Beamforming: A versatile approach to spatial filtering," *ASSP Magazine, IEEE*, vol. 5, no. 2, pp. 4 – 24, April 1988.

[11] Y. Fujino, T. Minowa, N. Hamamoto, H. Tsuji, and R. Suzuki, "Research and development plan for satellite/terrestrial integrated mobile communication system," in *27th ICSSC 2009, American Institute of Aeronautics and Astronautics*, Edinburgh, UK, June 2009.

[12] A. Miura, H. Watanabe, N. Hamamoto, Y. Fujino, and R. Suzuki, "On interference level in satellite uplink for satellite/terrestrial integrated mobile communication system," in *28th ICSSC 2010, American Institute of Aeronautics and Astronautics*, California, USA, Sep. 2010.

[13] "Inmarsat." [Online]. Available: http://www.inmarsat.com/ (accessed on: 29 November 2010)

[14] "ICO Global Communications." [Online]. Available: http://www.ico.com/ (accessed on: 29 November 2010)

[15] J. Walker, R. Menendez, D. Burr, and G. Dubellay, "Ground-based beamforming for satellite communications systems," *U.S. Patent 0051080 A1*, Feb. 2008.

[16] F. Makita and K. Smith, "Design and implementation of ICO system," in *17th ICSSC 1998, American Institute of Aeronautics and Astronautics*, Yokohama, Japan, Feb. 1998.

[17] V. Reinhardt, "Hybridized space/ground beam forming," *U.S. Patent 6571081 B1*, May 2003.

[18] P. Angeletti and N. Alagha, "Space/ground beamforming techniques for emerging hybrid satellite terrestrial networks," in *27th ICSSC 2009, American Institute of Aeronautics and Astronautics*, Edinburgh, UK, June 2009.

[19] A. Draganov and A. Weinberg, "Optimized beamforming for satellite communication," *U.S. Patent 0232227 A1*, Oct. 2007.

[20] W. Hreha and J. Walker, "Ground-based beamforming in communication satellites," *APSSC Quarterly Newsletter*, July 2006.

[21] T. C. Butash and J. R. Marshall, "Leveraging digital on-board processing to increase communications satellite flexibility and effective capacity," in *28th ICSSC 2010, American Institute of Aeronautics and Astronautics*, California, USA, Sep. 2010.

[22] L. Liu and H. Jafarkhani, "Successive transmit beamforming algorithms for multiple-antenna OFDM systems," *Wireless Communications, IEEE Transactions on*, vol. 6, no. 4, pp. 1512 – 1522, 2007.

[23] H. Lee, S. Park, and I. Lee;, "Transmit beamforming method based on maximum-norm combining for MIMO systems," *Wireless Communications, IEEE Transactions on*, vol. 8, no. 4, pp. 2067 – 2075, 2009.

[24] L. Liu and H. Jafarkhani, "Novel transmit beamforming schemes for time-selective fading multiantenna systems," *Signal Processing, IEEE Transactions on*, vol. 54, no. 12, pp. 4767 – 4781, 2006.

[25] V. Havary-Nassab, S. Shahbazpanahi, and A. Grami, "Joint receive-transmit beamforming for multi-antenna relaying schemes," *Signal Processing, IEEE Transactions on*, vol. 58, no. 9, pp. 4966 – 4972, 2010.

[26] "Digital Video Broadcasting Project." [Online]. Available: http://www.dvb.org/ (accessed on: 29 November 2010)

[27] M. Rohling, T. May, K. Bruninghaus, and R. Grunheid, "Broad-band OFDM radio transmission for multimedia applications," *Proceedings of the IEEE*, vol. 87, no. 10, pp. 1778 – 1789, Oct. 1999.

[28] 3GPP TSG RAN, "Physical layer aspects for evolved Universal Terrestrial Radio Access (UTRA)," Release 7, TS-25.814, V 7.1.0, 2006 – 08.

[29] IEEE 802.16-REVd/D5-2004, "IEEE standard for local and metropolitan area networks - part 16: Air interface for fixed broadband wireless access systems," May 2004.

[30] ETSI, "Broadband radio access networks (BRAN); HIPER-MAN; physical (PHY) layer," Standard TS 102 177, 2003.

[31] A. Goldsmith, *Wireless Communications.* Cambridge University Press., 2005.

[32] R. V. Nee and R. Prasad, *OFDM for Wireless Multimedia Communications*, 2nd ed. Artech House, 2000.

[33] S. Hara and R. Prasad, *Multicarrier Techniques for 4G Mobile Communications*, 3rd ed. Artech House, 2003.

[34] S. B. Weinstein and P. M. Ebert, "Data transmission by frequency-division multiplexing using the discrete fourier transform," *Communication Technology, IEEE Transactions on*, vol. 19, no. 5, pp. 628 – 634, Oct. 1971.

[35] B. Muquet, Z. Wang, G. Giannakis, M. de Courville, and P. Duhamel, "Cyclic prefixing or zero padding for wireless multicarrier transmissions?" *Communications, IEEE Transactions on*, vol. 50, no. 12, pp. 2136 – 2148, Dec. 2002.

[36] 3GPP TSG RAN, "Feasibility study for OFDM for UTRA enhancement," Release 6, TS-25.892, V 6.0.0, 2004 – 06.

[37] S. Haykin, *Array Signal Processing*. Prentice Hall, 1985.

[38] L. Scott and B. Mulgrew, "Sparse LCMV beamformer design for suppression of ground clutter in airborne radar," *Signal Processing, IEEE Transactions on*, vol. 43, no. 12, pp. 2843 – 2851, 1995.

[39] W. Knight, R. Pridham, and S. Kay, "Digital signal processing for SONAR," vol. 69, no. 11, pp. 1451 – 1506, Oct. 1981.

[40] A. Macovski, *Medical Imaging*. Prentice Hall, 1982.

[41] A. Readhead, "Radio astronomy by very-long-baseline interferometry," *Scientific American*, vol. 246, pp. 52 – 61, June 1982.

[42] B. Widrow, J. Glover, J. McCool, J. Kaunitz, C. Williams, R. Hearn, J. Zeidler, J. E. Dong, and R. Goodlin, "Adaptive noise cancelling: Principles and applications," *Proceedings of the IEEE*, vol. 63, no. 12, pp. 1692 – 1716, Feb. 1975.

[43] J. Litva and T. K.-Y. Lo, *Digital Beamforming in Wireless Communications*. Artech House Publishers, 1996.

[44] U. Madhow and M. Honig, "MMSE interference suppression for direct-sequence spread-spectrum CDMA," *Communications, IEEE Transactions on*, vol. 42, no. 12, pp. 3178 – 3188, March 1994.

[45] M.-H. Hsieh and C.-H. Wei, "Channel estimation for OFDM systems based on comb-type pilot arrangement in frequency selective fading channels," *Consumer Electronics, IEEE Transactions on*, vol. 44, no. 1, pp. 217 – 225, Feb. 1998.

[46] C. K. Kim, K. Lee, and Y. S. Cho, "Adaptive beamforming algorithm for OFDM systems with antenna arrays," *IEEE Transactions on Consumer Electronics*, vol. 46, no. 4, pp. 1052 – 1058, Nov. 2000.

[47] M. Okada and S. Komaki, "Pre-DFT combining space diversity assisted COFDM," *Vehicular Technology, IEEE Transactions on*, vol. 50, no. 2, pp. 487 – 496, March 2001.

[48] H. Matsuoka and H. Shoki, "Comparison of Pre-FFT and Post-FFT processing adaptive arrays for OFDM systems in the presence of co-channel interference," in *Proc. 14th IEEE on Personal, Indoor and Mobile Radio Communications PIMRC*, vol. 2, Sep. 2003, pp. 1603 – 1607.

[49] C. K. Kim, S. Choi, and Y. S. Cho;, "Adaptive beamforming for an OFDM system," *Vehicular Technology Conference, 1999 IEEE 49th*, vol. 1, pp. 484 – 488, March 1999.

[50] M. Lei, P. Zhang, H. Harada, and H. Wakana, "A combinational scheme of Pre-FFT adaptive beamforming and frequency-domain adaptive loading for OFDM," *Vehicular Technology Conference, 2004. VTC2004-Fall. 2004 IEEE 60th*, vol. 1, pp. 290 – 294, Sep. 2004.

[51] M. Lei and H. Harada, "Fast-convergence SMI adaptive beamforming based on frequency-to-time pilot transform for OFDM system," *Wireless Commu-*

nications, Networking and Mobile Computing, 2006. WiCOM 2006.International Conference on, pp. 1 – 5, Sep. 2006.

[52] M. Lei, P. Zhang, H. Harada, and H. Wakana, “Adaptive beamforming based on frequency-to-time pilot transform for OFDM,” *Vehicular Technology Conference, 2004. VTC2004-Fall. 2004 IEEE*, vol. 1, pp. 285 – 289, Sep. 2004.

[53] ——, “LMS adaptive beamforming based on Pre-FFT combining for ultra high-data-rate OFDM system,” in *Vehicular Technology Conference, 2004. VTC2004-Fall. 2004 IEEE 60th*, vol. 5, Sep. 2004, pp. 3664 – 3668.

[54] C.-H. Peng, K.-C. Huang, C.-Y. Chi, W.-K. Ma, and T.-H. Tsai, “A block-by-block blind Post-FFT beamforming algorithm for multiuser OFDM systems based on subcarrier averaging,” *Signal Processing Advances in Wireless Communications, 2007. SPAWC 2007. IEEE 8th Workshop on*, pp. 1 – 5, June 2007.

[55] V. Venkataraman, R. Cagley, and J. Shynk, “Adaptive beamforming for interference rejection in an OFDM system,” *Signals, Systems and Computers, 2003. Conference Record of the Thirty-Seventh Asilomar Conference on*, vol. 1, pp. 507 – 511, Nov. 2003.

[56] H. Liu and Q. Feng;, “A blind adaptive beamforming for OFDM system,” *Electrical and Computer Engineering, 2005. Canadian Conference on*, pp. 1208 – 1211, May 2005.

[57] Y.-F. Chen and C.-P. Li, “Adaptive beamforming schemes for interference cancellation in OFDM communication systems,” *Vehicular Technology Conference, 2004. VTC 2004-Spring. 2004 IEEE 59th*, vol. 1, pp. 103 – 107, May 2004.

[58] Y.-F. Chen and C.-S. Wang, “Adaptive antenna arrays for interference cancellation in OFDM communication systems with virtual carriers,” *Vehicular Technology, IEEE Transactions on*, vol. 56, no. 4, pp. 1837 – 1844, July 2007.

[59] C.-H. Peng, C.-C. Lin, Y.-H. Lin, and C.-Y. Chi, “Blind beamforming for CCI reduction by kurtosis maximization for OFDM systems in multipath,” *Intelligent Signal Processing and Communication Systems, 2005. ISPACS 2005. Proceedings of 2005 International Symposium on*, pp. 105 – 108, Dec. 2005.

[60] A. Khan, M. Imran, and B. Evans, “Adaptive beamforming for OFDM based hybrid mobile satellite system,” in *27th ICSSC 2009, American Institute of Aeronautics and Astronautics*, Edinburgh, UK, June 2009.

[61] “American Telephone and Telegraph.” [Online]. Available: http://www.att.com/ (accessed on: 29 November 2010)

[62] “Thuraya.” [Online]. Available: http://www.thuraya.com/ (accessed on: 29 November 2010)

[63] ETSI TS 102 585, “System specifications for satellite services to handheld devices (SH) below 3 GHz,” July 2007.

[64] ETSI EN 302 583, “DVB-SH waveform specification,” Jan. 2008.

[65] ETSI TS 102 584, “DVB-SH implementation guidelines,” Dec. 2008.

[66] U. Reimers, “DVB-The family of international standards for Digital Video Broadcasting,” in *Proceedings of the IEEE*, vol. 94, no. 1, Jan. 2006, pp. 173 – 182.

[67] Y. Sun and H. Matsuoka, “A novel adaptive antenna architecture - subcarrier clustering for high-speed OFDM systems in presence of rich co-channel

interference," *Vehicular Technology Conference, 2002. VTC Spring 2002. IEEE 55th*, vol. 3, pp. 1564 – 1568, Aug. 2002.

[68] S. Li, D. Huang, K. Letaief, and Z. Zhou, "Multi-stage beamforming for coded OFDM with multiple transmit and multiple receive antennas," *Wireless Communications, IEEE Transactions on*, vol. 6, no. 3, pp. 959 – 969, Mar. 2007.

[69] S. Coleri, M. Ergen, A. Puri, and B. A, "A study of channel estimation in OFDM systems," in *Vehicular Technology Conference, 2002. Proceedings. VTC 2002-Fall. 2002 IEEE 56th*, vol. 2, Dec. 2002, pp. 894 – 898.

[70] R. Kwong and E. Johnston, "A variable step size LMS algorithm," *Signal Processing, IEEE Transactions on*, vol. 40, no. 7, pp. 1633 – 1642, July 1992.

[71] D. N. C. Tse and P. Viswanath, *Fundamentals of Wireless Communication*. Cambridge, U.K: Cambridge Univ. Press, 2005.

[72] ETSI TR 102 662, "Satellite earth stations and systems (SES); Advanced satellite based scenarios and architectures for beyond 3G systems," Mar. 2010.

[73] J. Macias and A. Exposito, "Computation of running averages," *Circuits and Systems II: Express Briefs, IEEE Transactions on*, vol. 53, no. 10, pp. 1098 – 1102, 2006.

[74] K. Kwon and R. J. Kish, "A comparative study of technical trading strategies and return predictability: An extension of using NYSE and NASDAQ indices," *Q. Rev. Econ. Finance*, vol. 42, no. 3, pp. 611 — 631, 2002.

[75] Z. Yi and F. Liangzhong;, "Moving object detection based on running average background and temporal difference," *Intelligent Systems and Knowl-*

edge Engineering (ISKE), 2010 International Conference on, pp. 270 – 272, 2010.

[76] C. Cai, "Adaptive traffic signal control using approximate dynamic programming," Ph.D. dissertation, University College London, Oct. 2009.

[77] A. H. Khan, M. A. Imran, and B. G. Evans, "OFDM based adaptive beamforming for hybrid terrestrial-satellite mobile system with pilot reallocation," *Satellite and Space Communications, 2009. IWSSC 2009. International Workshop on*, pp. 201 – 205, Sep. 2009.

[78] A. Khan, M. Imran, and B. Evans, "Preamble based adaptive beamformer for hybrid terrestrial-satellite mobile system," in *28th ICSSC 2010, American Institute of Aeronautics and Astronautics*, California, USA, Sep. 2010.

[79] Y. Li and N. Sollenberger, "Adaptive antenna arrays for OFDM systems with cochannel interference," *Communications, IEEE Transactions on*, vol. 47, no. 2, pp. 217 – 229, Feb. 1999.

[80] T. Aboulnasr and K. Mayyas, "A robust variable step-size LMS-type algorithm: Analysis and simulations," *Signal Processing, IEEE Transactions on*, vol. 45, no. 3, pp. 631 – 639, March 1997.

[81] D. Slock, "On the convergence behavior of the LMS and the Normalized LMS algorithms," *Signal Processing, IEEE Transactions on*, vol. 41, no. 9, pp. 2811 – 2825, Sep. 1993.

[82] S. Douglas, "A family of Normalized LMS algorithms," *Signal Processing Letters, IEEE*, vol. 1, no. 3, pp. 49 – 51, Mar. 1994.

[83] J. Nagumo and A. Noda, "A learning method for system identification," *Automatic Control, IEEE Transactions on*, vol. 12, no. 3, pp. 282 – 287, June 1967.

[84] Z. Tang and G. Leus, "Pilot schemes for time-varying channel estimation in OFDM systems," in *Signal Processing Advances in Wireless Communications, 2007. SPAWC 2007. IEEE 8th Workshop on*, Jan. 2007, pp. 1 – 5.

[85] G. Auer and I. Cosovic, "On pilot grid design for an OFDM air interface," in *Wireless Communications and Networking Conference, 2007.WCNC 2007. IEEE*, March 2007, pp. 2172 – 2177.

[86] S. Coleri, M. Ergen, A. Puri, and A. Bahai, "Channel estimation techniques based on pilot arrangement in OFDM systems," *Broadcasting, IEEE Transactions on*, vol. 48, no. 3, pp. 223 – 229, Sep. 2002.

[87] M. Zhao, Z. Shi, and M. Reed, "Iterative turbo channel estimation for OFDM system over rapid dispersive fading channel," *Wireless Communications, IEEE Transactions on*, vol. 7, no. 8, pp. 3174 – 3184, Aug. 2008.

[88] M. Nicoli, M. Sala, O. Simeone, L. Sampietro, and C. Santacesaria, "Adaptive array processing for time-varying interference mitigation in IEEE 802.16 systems," in *Personal, Indoor and Mobile Radio Communications, 2006 IEEE 17th International Symposium on*, Sep. 2006, pp. 1 – 5.

[89] A. Khan, M. Imran, and B. Evans, "Iterative turbo beamforming for OFDM based hybrid terrestrial-satellite mobile system," *Communications, IET*, proposal under review.

[90] C. Berrou, A. Glavieux, and P. Titmajshima, "Near shannon limit error-correction coding and decoding: Turbo codes," *ICC, Geneva, Switzerland*, pp. 1064 – 1090, May 1993.

[91] L. Bahl, J. Cocke, F. Jelinek, and J. Raviv, "Optimal decoding of linear codes for minimizing symbol error rate (corresp.)," *Information Theory, IEEE Transactions on*, vol. 20, no. 2, pp. 284 – 287, March 1974.

[92] M. Sellathurai and S. Haykin, "A nonlinear iterative beamforming technique for wireless communications," *Signals, Systems, and Computers, 1999. Conference Record of the Thirty-Third Asilomar Conference on*, vol. 2, pp. 957 – 961, Oct. 1999.

[93] D. Mottier and L. Brunel, "A low complexity turbo adaptive interference cancellation using antenna arrays for W-CDMA," *Vehicular Technology Conference, 2001. VTC 2001 Fall. IEEE VTS 54th*, vol. 3, pp. 1644 – 1648, Oct. 2001.

[94] M. Reed and P. Alexander, "Iterative multiuser detection using antenna arrays and FEC on multipath channels," *Selected Areas in Communications, IEEE Journal on*, vol. 17, no. 12, pp. 2082 – 2089, Dec. 1999.

[95] T. Hunziker, T. Aono, and T. Ohira, "An iterative beamforming and decoding procedure for wireless networks with uncoordinated channel access," *Communications Letters, IEEE*, vol. 8, no. 4, pp. 256 – 258, April 2004.

[96] ——, "An iterative beamforming technique for OFDM-based wireless networks with uncoordinated channel access," *Communications, 2004 IEEE International Conference on*, vol. 5, pp. 2751 – 2756, June 2004.

[97] A. Pollok, W. Cowley, and N. Letzepis, "Symbol-wise beamforming for MIMO-OFDM transceivers in the presence of co-channel interference and spatial correlation," *Wireless Communications, IEEE Transactions on*, vol. 8, no. 12, pp. 5755 – 5760, Dec. 2009.

[98] M. Sandell and V. Ponnampalam, "Smooth beamforming for OFDM," *Wireless Communications, IEEE Transactions on*, vol. 8, no. 3, pp. 1133 – 1138, March 2009.

[99] A. Viterbi, "Error bounds for convolutional codes and an asymptotically

optimum decoding algorithm," *Information Theory, IEEE Transactions on*, vol. 13, no. 2, pp. 260 – 269, April 1967.

[100] A. Khan, M. Imran, and B. Evans, "Ground based and onboard based beamforming for hybrid terrestrial-satellite mobile system," in *28th ICSSC 2010, American Institute of Aeronautics and Astronautics*, California, USA, Sep. 2010.

[101] "Inside the Inmarsat-4 satellites." [Online]. Available: http://www.inmarsat.com/About/Our_satellites/ (accessed on: 29 November 2010)

[102] A. Khan, M. Imran, and B. Evans, "Semi-adaptive beamforming for OFDM based hybrid terrestrial-satellite mobile system," *Wireless Communications, IEEE Transactions on*, proposal under review.

[103] A. G. DiRienzo and I. G. Zurbenko, "Semi-adaptive non-parametric spectral estimation," *J. Comput. Graphical Stat.*, vol. 8, pp. 41 – 59, 1999.

[104] W. Yang and I. G. Zurbenko, "A semiadaptive smoothing algorithm in bispectrum estimation," *Signal Processing, IEEE Transactions on*, vol. 56, no. 11, pp. 5369 – 5375, Aug. 2008.

[105] T. Lo, "Maximum ratio transmission," *Communications, IEEE Transactions on*, vol. 47, no. 10, pp. 1458 – 1461, 1999.

[106] M. Schubert and H. Boche, "Solution of the multiuser downlink beamforming problem with individual SINR constraints," *Vehicular Technology, IEEE Transactions on*, vol. 53, no. 1, pp. 18 – 28, 2004.

[107] M. Costa, "Writing on dirty paper (corresp.)," *Information Theory, IEEE Transactions on*, vol. 29, no. 3, pp. 439– 441, 1983.

[108] J. Montesinos, O. Besson, and C. Guiraud, “Adaptive beamforming for large arrays in satellite communications,” *Antennas and Propagation Society International Symposium, 2008. AP-S 2008. IEEE*, pp. 1 – 4, 2008.

[109] B. Sklar, *Digital Communications fundamentials and applications*, 2nd ed. Prentice Hall PTR, 2001.